THE JOURNAL OF

PHYSICAL CHEMISTRY

Volume 74, Number 26 December 24, 1970

NOTES

COMMUNICATIONS TO THE EDITOR

AUTHOR INDEX

NOTICE TO AUTHORS

I. General Considerations

The Journal of Physical Chemistry is devoted to reporting both experimental and theoretical research dealing with fundamental aspects of physical chemistry. Space limitations necessitate giving preference to research articles dealing with previously unanswered basic questions in physical chemistry. Acceptable topics are those of general interest to physical chemists, especially work involving new concepts, techniques, and interpretations. Research that may lead to reexaminations of generally accepted views is, of course, welcome.

The Journal of Physical Chemistry publishes three types of manuscripts: *Articles*, *Notes*, and *Communications to the Editor*.

Authors reporting data should include, if possible, an interpretation of the data and its relevance to the theories of the properties of matter. However, the discussion should be concise and to the point and excessive speculation is to be discouraged. Papers reporting redeterminations of existing data will be acceptable only if there is reasonable justification for repetition: for example, if the more recent or more accurate data lead to new questions or to a reexamination of well known theories. Manuscripts that are essentially applications of chemical data or reviews of the literature are, in general, not suitable for publication in *The Journal of Physical Chemistry*. Detailed comparisons of methods of data analysis will be considered only if the paper also contains original data, or if such comparison leads to a genesis of new ideas.

Authors should include an introductory statement outlining the scientific rationale for the research. The statement should clearly specify the questions for which answers are sought and the connection of the present work with previous work in the field. All manuscripts are subject to critical review. It is to be understood that the final decision relating to a manuscript's suitability rests solely with the editorial staff.

Symposium papers are sometimes published as a group, but only after special arrangement with the editor.

Authors' attention is called to the "Handbook for Authors," available from the Special Issues Sales Department, American Chemical Society, 1155 Sixteenth St., N.W., Washington, D. C. 20036, in which pertinent material is to be found.

II. Types of Manuscripts

A. Articles should cover their subjects with thoroughness, clarity, and completeness. However, authors should also strive to make their *Articles* as concise as possible, avoiding unnecessary historical background. Abstracts to *Articles* should be brief—300 words is a maximum—and should serve to summarize the significant data and conclusions. The abstract should convey the essence of the *Article* to the reader.

B. Notes. Papers submitted in the category of *Notes* should report work that represents a complete and self-contained study of limited scope. *Notes* are a luxury in the present scientific literature; authors should not use a *Note* to report work that is part of a continuing study. *Notes* are not to be used for reporting preliminary results; reports of such work should be postponed until the work is completed or should be submitted as *Communications* if the results are of immediate or unusual interest to physical chemists. The same criteria of suitability for publication apply to *Notes* as to *Articles* (see General Considerations). The length of a *Note*, including tables, figures, and text, must not exceed 1.5 journal pages (1500 words or the equivalent). A *Note* should not be accompanied by an abstract.

C. Communications to the Editor are of two types, *Letters* and *Comments*. Both types are restricted to three-quarters of a page (750 words or the equivalent) including tables, figures, and text, and both types of *Communications* are subject to critical review, but special efforts will be made to expedite publication.

Letters should report preliminary results whose immediate availability to the scientific community is deemed important, and whose topic is timely enough to justify the double publication that usually results from the publication of a *Letter*.

Comments include significant remarks on the work of others. The editorial staff will generally permit the authors of the work being discussed to reply.

III. Introduction

All manuscripts submitted should contain brief introductory remarks describing the purpose of the work and giving sufficient background material to allow the reader to appreciate the state-of-knowledge at the time when the work was done. The introductory remarks in an *Article* should constitute the first section of the paper and should be labeled accordingly. In *Notes* and *Communications*, the introductory material should not be in such a separate section. To judge the appropriateness of the manuscript for *The Journal of Physical Chemistry*, the editorial staff will place considerable weight on the author's intentions as stated in the Introduction.

IV. Functions of Reviewers

The editorial staff requests the scientific advice of reviewers who are active in the area of research covered by the manuscript. The reviewers act only in an advisory capacity and the final decision concerning a manuscript is the responsibility of the editorial staff. The reviewers are asked to comment not only on the scientific content, but also on the manuscript's suitability for *The Journal of Physical Chemistry*. With respect to *Communications*, the reviewers are asked to comment specifically on the urgency of publication. All reviews are anonymous and the reviewing process is most effective if reviewers do not reveal their identities to the authors. An exception arises in connection with a manuscript submitted for publication in the form of a comment on the work of another author. Under such circumstances the first author will, in general, be allowed to review the communication and to write a rebuttal, if he so chooses. The rebuttal and the original communication may be published together in the same issue of the journal. Revised manuscripts are generally sent back to the original reviewers, who are asked to comment on the revisions. If only minor revisions are involved, the editorial staff examines the revised manuscript in light of the recommendations of the reviewers and without seeking further opinions. For the convenience of reviewers, authors are advised to indicate clearly, either in the manuscript or in a covering letter, the specific revisions that have been made.

V. Submission of Manuscripts

All manuscripts must be submitted at least in duplicate and preferably in triplicate to expedite handling. Manuscripts must be typewritten, double-spaced copy, on $8^1/_2 \times 11$ in. paper. Legal sized paper is not acceptable. Authors should be certain that copies of the manuscript are clearly reproduced and readable. **Authors submitting figures must include the original drawings or photographs thereof, plus two xerographic copies for review purposes. These reproductions of the figures should be on $8^1/_2 \times 11$ in. paper.** Graphs must be in black ink on white or blue paper. Lettering at the sides of graphs may be penciled in and will be typeset. Figures and tables should be held to a minimum consistent with adequate presentation of information. All original data which the author deems pertinent must be submitted along with the manuscript. For example, a paper reporting a crystal structure should include structure factor tables for use by the reviewers.

Footnotes and references to the literature should be numbered consecutively within the paper; the number should also be placed in parentheses in the left margin opposite the line in which the reference first appears. A complete list of references should appear at the end of the paper. Initials of the authors referred to in the citations should be included in the complete reference at the back of the paper. Nomenclature should conform to that used in *Chemical Abstracts* and mathematical characters should be underlined for italics, Greek letters should be annotated, and subscripts and superscripts clearly marked.

Papers should not depend for their usefulness on unpublished material, and excessive reference to material in press is discouraged. References not readily available (*e.g.*, private technical reports, preprints, or articles in press) that are necessary for a complete review of the paper must be included with the manuscript for use by the reviewers.

VI. Revised Manuscripts

A manuscript sent back to an author for revision should be returned to the editor within 6 months; otherwise it will be considered withdrawn and treated as a new manuscript when and if it is returned. Revised manuscripts returned to the editor must be submitted in duplicate and all changes should be made by typewriter. **Unless the changes are very minor, all pages affected by revision must be retyped.** If revisions are so extensive that a new typescript of the manuscript is necessary, it is requested that a copy of the original manuscript be submitted along with the revised one.

VII. Supplementary Material

By arrangement with the National Auxiliary Publications Service (NAPS) of the American Society for Information Science (ASIS), supplementary material, such as extensive tables, graphs, spectra, and calculations, can be distributed in the form of microfiche copies or photoprints readable without optical aids. This material should accompany the manuscript for review by the editors and reviewers. Upon acceptance, it will be sent by the editor to NAPS where it is assigned a document number. A deposit fee of $12.50 (for 60 manuscript pages or less) is required and should be included with the material sent to the editor. The check must be made payable to CCMIC–NAPS. Further details may be obtained from NAPS, c/o CCM Information Corp., 909 3rd Ave., New York, N. Y. 10022.

VIII. Proofs and Reprints

Galley proofs, original manuscript, cut copy, and reprint order form are sent by the printer directly to the author who submitted the manuscript. The attention of the authors is directed to the instructions which accompany the proof, especially the requirement that all corrections, revisions, and additions be entered on the proof and not on the manuscript. Proofs should be checked against the manuscript (in particular all tables, equations, and formulas, since this is not done by the editor) and returned as soon as possible. No paper is released for printing until the author's proof has been received. Alterations in an article after it has been set in type are made at the author's expense, and it is understood that by entering such alterations on proofs the author agrees to defray the cost thereof. The filled-out reprint form must be returned with the proof, and if a price quotation is required by the author's organization a request for it should accompany the proof. Since reprinting is generally done from the journal press forms, all orders must be filed before press time. None can be accepted later, unless a previous request has been made to hold the type. Reprint shipments are made a month or more after publication, and bills are issued by the printer subsequent to shipment. Neither the editors nor the Washington office keeps any supply of reprints. Therefore, only the authors can be expected to meet requests for single copies of papers.

A page charge is assessed to cover in part the cost of publication. Although payment is expected, it is not a condition for publication. Articles are accepted or rejected only on the basis of merit, and the editor's decision to publish the paper is made before the charge is assessed. The charge per journal page is $50.

THE JOURNAL OF
PHYSICAL CHEMISTRY

Registered in U. S. Patent Office

VOLUME 74, NUMBER 26 DECEMBER 24, 1970

Electrolyte Effects on the Hydrolysis of Acetals and Ortho Esters[1]

by C. A. Bunton and J. D. Reinheimer[2]

Department of Chemistry, University of California, Santa Barbara, California 93106 *(Received August 28, 1970)*

For hydrolysis in aqueous hydrochloric acid the relative reactivities are 1,1-diethoxyethane, 1; 2,2-diethoxypropane, 2200; triethyl orthoformate, 680; and triethyl orthoacetate, 19,000. The kinetic solvent isotope effect for triethyl orthoacetate $k_{H_2O}/k_{D_2O} = 0.54$ is intermediate between the values for tetraethyl orthocarbonate and triethyl orthoformate. Salt effects upon the rates of acid hydrolysis and the activity coefficients of the substrates have been used to calculate the salt effects upon the activity coefficients of the transition state relative to an anilinium ion and the tri-*p*-anisyl carbonium ion, and the activity coefficients of the transition state and the anilinium ion are very similar. The salt effects on the transition states relative to those of the anilinium ion generally decrease in the sequence orthoacetate > orthoformate > ketal > acetal. These results suggest that the structures of the transition states are close to those of the conjugate acids and are consistent with a mechanistic change from A1 to A-SE2 in going from acetal to ortho ester.

Acetals, ketals, and ortho esters are structurally similar compounds whose hydronium ion catalyzed hydrolysis follows the general reaction scheme shown below, although the timing of the bond making and breaking steps is uncertain.[3]

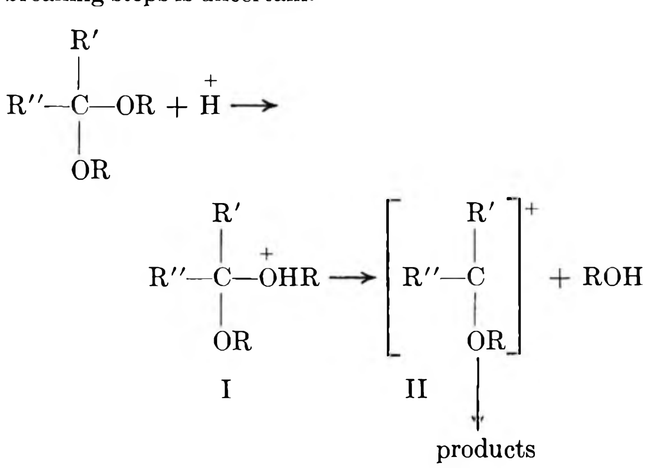

(R′, R″ = alkyl, aryl, OR)

It is generally accepted that in water, or in mixtures of water and aprotic solvents, the oxocarbonium ion (II) reacts rapidly to generate the products. If it is assumed that the oxonium ion (I) is in equilibrium with the reactants and decomposes slowly to products by formation of (II)[4,5] an A1 mechanism could reasonably be written. However hydrolyses of some aliphatic ortho esters are general acid catalyzed,[3,6-8] and in addition the electronic effects of substituents are not those expected for an A1 mechanism involving a carbonium-ion-like transition state. Recently evidence has been found for buffer catalysis of some acetal and ketal

(1) Support of this work by the National Science Foundation is gratefully acknowledged. This investigation was supported by BioMedical Support Grant FR 07099-03 from the General Research Support Branch, Division of Research Resources, Bureau of Health Professions, Educational and Man Power Training, National Institutes of Health. Acknowledgment is made to the donors of the Petroleum Research Fund, administered by the American Chemical Society, for support of travel and research.

(2) On research leave from the Department of Chemistry, The College of Wooster, Wooster, Ohio 44691.

(3) For a general review, see E. H. Cordes, *Progr. Phys. Org. Chem.*, **4**, 1 (1967).

(4) S. Winstein and R. E. Buckles, *J. Amer. Chem. Soc.*, **65**, 613 (1943).

(5) C. K. Ingold, "Structure and Mechanism in Organic Chemistry," Cornell University Press, Ithaca, N. Y., 1953, p 344.

(6) J. N. Brønsted and W. F. K. Wynne-Jones, *Trans. Faraday Soc.*, **25**, 59 (1929).

(7) R. H. DeWolfe and R. M. Roberts, *J. Amer. Chem. Soc.*, **76**, 4379 (1954).

(8) A. J. Kresge and R. J. Preto, *ibid.*, **87**, 4593 (1965).

hydrolyses,[9-11] and it has been suggested that these compounds and some ortho esters react by an A-S_E2 mechanism with concerted proton attack on oxygen and carbon-oxygen bond breaking.[3,8,12] Some of the latter evidence depended on basicity estimates[12] (*cf.* ref 13) which were consistent with A1 mechanisms for hydrolysis of aliphatic acetals and ketals, and the question arises as to whether there is a sharp mechanistic break in going from ortho ester to acetal hydrolysis. For example, general acid catalysis is observed in the hydrolysis of ethyl orthoformate in aqueous dioxane, but not in water.[6,7]

Recently, the α-D deuterium isotope effect has been measured for hydrolysis of triethyl orthoformate and some acetals.[14] For propionaldehyde diethyl acetal $k_H/k_D = 1.17$, indicating CO bond breaking in the transition state,[15] whereas lower values were found for hydrolyses of triethyl orthoformate and benzaldehyde- and *p*-methoxybenzaldehyde diethyl acetal indicating less CO bond stretching in the transition states for these reactions (however for the hydrolysis of *p*-nitrobenzaldehyde diethyl acetal $k_H/k_D = 1.15$).[14]

Correlations between reaction rate and acidity function support an A1 mechanism for hydrolyses of unreactive acetals,[16-19] but generally ortho esters and ketals are too reactive for their hydrolyses to be studied in moderately concentrated acid (*cf.* ref 20).

Long and McIntyre found that the salt effects upon the acid hydrolysis of dimethoxymethane could be explained in part in terms of the effects of the salts on the activity coefficient of the substrate.[21] For the hydrolysis of carboxylic, and other esters, salt effects are specific, and depend on mechanism.[22] Therefore we have examined the kinetic salt effects upon the hydrolyses of 1,1-diethoxyethane, 2,2-diethoxypropane, and triethyl orthoformate and orthoacetate in the presence of dilute aqueous mineral acid and compared these salt effects with those upon ionization of *p*-nitroaniline and tri-*p*-anisyl carbinol,[22,23] in order to extend the investigation of Long and McIntyre to more reactive substrates, and in the hope that we would see a relation between salt effect and mechanism. An additional question centers on the validity of the assumption that salt effects can be compensated for by maintaining constant ionic strength with some arbitrarily chosen electrolyte. This question is of considerable importance when the pH is controlled by buffers and evidence is sought for a small catalysis by a general acid, especially when mixed solvents are used.

Experimental Section

Materials. 1,1-Diethoxyethane (acetal) and triethyl orthoformate were purified by shaking them with dilute NaOH, then with water, and then drying them (Na_2SO_4). Triethyl orthoacetate was obtained from Dr. R. H. DeWolfe. These samples were distilled through a Nester-Faust Teflon spinning-band column. 2,2-Diethoxypropane (ketal) was prepared from acetone and triethyl orthoformate in ethanolic HCl;[24] after isolation it was purified by distillation through a Teflon spinning-band column.

The nmr spectra were examined at 60 or 100 MHz (Jeolco C60H, Varian A60, or Varian HA100) and showed the absence of impurities.

Kinetics. The reactions were followed using dilute aqueous hydrochloric acid in a Durrum stopped flow apparatus at 25.0°. The acid-salt solution was in one syringe and the substrate-salt solution in the other, so that there were no mixing effects. The hydrolyses of ethyl orthoacetate and orthoformate were followed at 2200 Å, that of 2,2-diethoxyethane (acetal) was followed at 2800 Å, and that of 2,2-diethoxypropane (diethyl ketal) was followed at 2650 Å. A simple program was used with the Hewlett-Packard 9100 A desk computer to convert transmittance into absorbance and the first-order rate constants, k_ψ, sec^{-1}, were then calculated graphically. In the presence of added salts duplicate rate constants agreed to within 10%, but in the absence of added salts they agreed to within 5%. The greatest uncertainties were with the more concentrated salt solutions.

The hydrolyses of 1,1-diethoxyethane, 2,2-diethoxypropane, and triethyl orthoformate have been shown to be first order with respect to hydrogen ion concentration in dilute acid,[3,6,17] and in the present work with triethyl orthoacetate we confirmed the first-order dependence of C_{H^+}. The acid concentration was varied between 6×10^{-4} and 6×10^{-3} *M*, and the values of $k_{H^+} = k_\psi/C_{H^+}$ changed by <10%.

With each substrate the composition of the product was checked by nmr and uv spectrometry on the solution after complete reaction. With ethyl orthoacetate there is the possibility of formation of a diethyl ketene

(9) T. H. Fife and L. K. Jao, *J. Amer. Chem. Soc.*, **90**, 4081 (1968).
(10) R. H. DeWolfe, K. M. Ivanetich, and N. F. Perry, *J. Org. Chem.*, **34**, 848 (1969).
(11) E. Anderson and B. Capon, *J. Chem. Soc. B*, 1033 (1969).
(12) C. A. Bunton and R. H. DeWolfe, *J. Org. Chem.*, **30**, 1371 (1965).
(13) T. Pletcher and E. H. Cordes, *ibid.*, **32**, 2294 (1967).
(14) E. H. Cordes and T. C. Pletcher, *ibid.*, **32**, 2294 (1970); H. Bull, T. C. Pletcher, and E. H. Cordes, *Chem. Commun.*, 527 (1970).
(15) V. J. Shiner, M. W. Rapp, M. Wolfsberg, and E. A. Halevi, *J. Amer. Chem. Soc.*, **90**, 7171 (1968).
(16) F. A. Long and M. A. Paul, *Chem. Rev.*, **57**, 935 (1957).
(17) M. M. Kreevoy, *J. Amer. Chem. Soc.*, **78**, 4236 (1956).
(18) J. F. Bunnett, *ibid.*, **83**, 4956 (1961), and accompanying papers.
(19) J. F. Bunnett and F. R. Olsen, *Can. J. Chem.*, **44**, 1899, 1917 (1967).
(20) M. Price, J. Adams, C. Lagenauer, and E. H. Cordes, *J. Org. Chem.*, **34**, 22 (1969).
(21) F. A. Long and D. McIntyre, *J. Amer. Chem. Soc.*, **76**, 3243 (1954).
(22) C. A. Bunton, J. H. Crabtree, and L. Robinson, *ibid.*, **90**, 1258 (1968).
(23) M. A. Paul, *ibid.*, **76**, 3236 (1954).
(24) H. E. Carswell and H. Adams, *ibid.*, **50**, 235 (1928).

acetal (III), either directly, or from an oxocarbonium ion, and the first possibility would provide a simple explanation for the general acid catalysis which is observed in orthoacetate hydrolysis. However, ketene

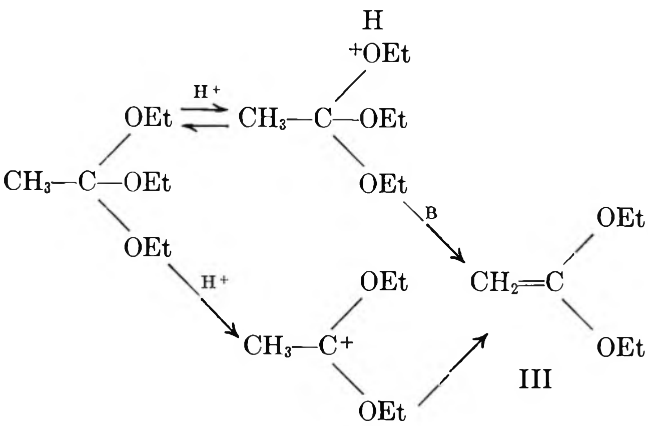

acetal was excluded as a major contributor by carrying out the hydrolysis in D_2O in which it would have been hydrolyzed[25] and showing by 100-mHz nmr spectrometry that the methyl group of the ethyl acetate product was not deuterated. These experiments would have detected 2% of deuterium in the product. In order to avoid any changes in the hydrogen ion concentration we used only uni-univalent salts of strong acids and bases and could use only those which did not absorb at the wavelengths used.

Distribution Experiments. The activity coefficients were determined by distribution,[26] using a water-jacketed separatory funnel at 25.0°, which was shaken for 5 min in a wrist action shaker. A stock solution (5 ml) of 2,2-diethoxyethane in Spectrograde cyclohexane was treated with 3 drops of 0.01 *M* NaOH and then shaken with the aqueous salt solution (pH 7–8). The aqueous layer was separated and centrifuged, its absorbance was measured after *acidification*, and the difference in absorbance gave the concentration of acetal.

The same general method was used with 2,2-diethoxypropane, except that the concentration of acetone, after hydrolysis of the ketal, was determined by converting it into its 2,4-dinitrophenylhydrazone. The extinction coefficient of acetone in water is too low for uv spectroscopy to be a useful method in these distribution experiments. We initially attempted to use a literature method,[27] but we were unable to obtain consistent results and therefore used the following procedure. After distribution of the ketal between cyclohexane and the aqueous salt solution 1 ml of the aqueous solution was made up to 10 ml with purified MeOH,[27] and 1 ml of this solution was treated with 1 ml of a saturated solution of recrystallized 2,4-dinitrophenylhydrazine in purified MeOH and 1 drop of concentrated HCl. The mixture, in a tightly stoppered 10-ml flask, was treated for 20 min in a 65° bath. The solution was then treated with methanolic KOH (25 g of KOH + 50 ml of water and made up to 250 ml with MeOH). The absorbance at 5300 Å was then measured using 2,4-dinitrophenylhydrazine as a blank.

The activity coefficients of triethyl orthoformate were determined by distributing it between cyclohexane and the aqueous salt solution. The aqueous layer was then acidified and the ethyl formate was determined spectrophotometrically. Calibration curves were prepared for each salt concentration, and the wavelength was varied between 2040 and 2100 Å. The same general method was used with triethyl orthoacetate, except that the absorbance of ethyl acetate was determined at 2140–2240 Å, depending on the salt.

The errors in the distribution experiments are largest for high concentrations of those salts which strongly "salt-out" the substrates, because the absorbances of the aqueous layer were low. The errors in the activity coefficients are also large at low salt concentrations, because the activity coefficients depend on two similar distribution coefficients.

The activity coefficients in 1 *M* salt solutions were obtained by interpolation. The activity coefficient of *p*-nitroaniline in tetramethylammonium chloride was not in the literature and was determined using standard methods,[26] as was $-\Delta H_0'$ for this salt.

Results

Kinetics. The kinetic salt effects upon the acid hydrolyses are shown in Table I. Similar salt orders were found for all the substrates, with $LiClO_4 \sim NaClO_4 > LiCl \sim NaCl \sim KCl > CH_3SO_3Na > (CH_3)_4NCl$. The salt effects are not specific for each substrate, although their magnitudes decrease in the sequence ketal ~ acetal > orthoformate ~ orthoacetate.

The second-order rate constants are given in Table II, together with the value for hydrolysis of triethyl orthoacetate in D_2O, because the only values of the deuterium solvent isotope effects available for ortho esters involved either measurements in buffers or in aqueous organic solvents[3,28] (for triphenyl orthoformate the solvent isotope effect is very different for reactions in aqueous dioxane and in water with added solubilizing agent).[20]

The directly determined value of $k_{H_2O}/k_{D_2O} = 0.54$ for the hydrolysis of triethyl orthoacetate is in the range which has traditionally been associated with specific hydronium ion catalyzed hydrolyses,[29,30] although the hydrolysis is catalyzed by general acids.

Distribution Experiments. Salts have specific effects upon the activity coefficients, f_X, of the acetals, ketals,

(25) A. Kaanperc and H. Touminen, *Suom. Kemistilehti. B*, **340**, 271 (1967).
(26) F. A. Long and W. F. McDevit, *Chem. Rev.*, **51**, 119 (1952).
(27) S. Siggia, "Quantitative Organic Analysis *via* Functional Groups," Wiley, New York, N. Y., 1963, p 124.
(28) W. F. K. Wynne-Jones, *Trans. Faraday Soc.*, **34**, 245 (1938).
(29) R. P. Bell, "Acid-Base Catalysis," Oxford University Press, London, Chapter IV.
(30) K. B. Wiberg, *Chem Rev.*, **55**, 713 (1955).

Table I: Salt Effects upon Acid Hydrolysis[a]

Salt	C_{salt}, M	$CH_3CH(OEt)_2$[b]	$(CH_3)_2C(OEt)_2$[c]	$HC(OEt)_3$[d]	$CH_3C(OEt)_3$[e]
LiCl	0.80	2.22	1.87	1.56	1.43
LiCl	1.60	4.31	2.83	2.54	2.23
LiCl	2.40	7.77	5.20	4.00	3.51
LiCl	3.20	15.1		7.17	4.79
NaCl	0.80	2.45	2.00	1.57	1.39
NaCl	1.60	5.19	3.07	2.34	2.15
NaCl	2.40	8.50	4.97	3.63	3.53
NaCl	3.20	13.3		5.66	4.23
KCl	0.80	2.16	1.65	1.42	1.47
KCl	1.60	4.17	3.00	2.12	2.08
KCl	2.40	6.12	4.33	2.95	2.71
KCl	3.20	8.22		3.45	3.37
$(CH_3)_4NCl$	0.80	1.59	1.37	0.97	1.13
$(CH_3)_4NCl$	1.60	1.81	1.70	1.29	1.55
$(CH_3)_4NCl$	2.40	2.00	1.90	1.65	1.70
$(CH_3)_4NCl$	3.20	2.40		1.85	
$LiClO_4$	0.80	2.56	2.13	2.02	1.85
$LiClO_4$	1.60	5.33	4.80	3.90	2.85
$LiClO_4$	3.20	30.7		16.3	
$NaClO_4$	0.80	2.52	2.83	1.93	2.17
$NaClO_4$	1.60	5.44	6.33	3.36	3.46
$NaClO_4$	2.40	10.1	9.10	6.68	5.40
$NaClO_4$	3.20	21.6		13.5	6.45
CH_3SO_3Na	0.80	1.95	1.50	1.35	1.13
CH_3SO_3Na	1.60	2.25	2.17	1.89	1.55
CH_3SO_3Na	2.40	3.46	2.67	2.69	1.70
CH_3SO_3Na	3.20	4.68		5.50	

[a] Values of k_s/k_0 in aqueous acid at 25.0°. [b] In 0.120–0.122 M HCl $k_{H^+} = 1.39$ l. mol^{-1} sec^{-1}. [c] In 0.00242 M HCl $k_{H^+} = 3.00 \times 10^3$ l. mol^{-1} sec^{-1}. [d] In 0.0120 M HCl $k_{H^+} = 9.40 \times 10^2$ l. mol^{-1} sec^{-1}. [e] In 6×10^{-4} to 6×10^{-3} M HCl $k_{H^+} = 2.66 \times 10^4$ l. mol^{-1} sec^{-1}.

Table II: Second-Order Rate Constants for the Hydrogen Ion Catalyzed Hydrolysis[a]

Substrate	k_{H^+}, l. mol^{-1} sec^{-1}	Rel rates
$CH_3CH(OEt)_2$	1.39[b]	1
$(CH_3)_2C(OEt)_2$	3.00×10^3[c]	2,200
$HC(OEt)_3$	9.40×10^2[d]	680
$CH_3C(OEt)_3$	2.66×10^4[e]	19,000
$CH_3C(OEt)_3$	4.97×10^4[f]	
$C(OEt)_4$		66[g]

[a] In water at 25.0°. [b] In 0.121 and 1.125 M HCl. [c] In 0.00242 M HCl. [d] In 0.012 M HCl. [e] 6×10^{-4} to 6×10^{-3} M HCl. [f] M DCl in D_2O. [g] Calcd from rate measurements in buffers, at 20° (ref 28).

Table III: Salt Effects upon Activity Coefficients[a]

Salt	C_s, M	Substrate: $CH_3CH(OEt)_2$	$(CH_3)_2C(OEt)_2$	$HC(OEt)_3$	$CH_3C(OEt)_3$
LiCl	0.80	1.22	1.42	1.20	1.35
LiCl	1.60	1.55	1.83	1.40	1.58
LiCl	2.40	2.38	2.38		
LiCl	3.20			1.84	3.22
NaCl	0.80	1.42	1.32	1.63	1.46
NaCl	1.60	2.10	2.30	2.38	2.68
NaCl	2.40	3.46	3.30		
NaCl	3.20			4.66	5.60
KCl	0.80	1.48	1.33	1.59	1.42
KCl	1.60	2.85	2.46	2.19	2.52
KCl	2.40	4.20	4.20		
KCl	3.20			4.18	6.30
$(CH_3)_4NCl$	0.80	1.21	1.28	1.54	1.42
$(CH_3)_4NCl$	1.60	1.56	1.75	1.90	2.00
$(CH_3)_4NCl$	2.40	2.19	2.05		
$(CH_3)_4NCl$	3.20			4.10	3.70
$LiClO_4$	0.40	0.94			
$LiClO_4$	0.80	0.87	1.00	1.16	1.29
$LiClO_4$	1.60	0.83	0.95	1.30	1.11
$LiClO_4$	2.40	0.83	0.96		
$LiClO_4$	3.20			1.37	1.31
$NaClO_4$	0.80	1.02	1.15	1.47	1.22
$NaClO_4$	1.60	1.18	1.77	1.85	1.47
$NaClO_4$	2.40	1.54	2.38		
$NaClO_4$	3.20			2.92	2.70
CH_3SO_3Na	0.80	1.40	1.42	1.76	1.61
CH_3SO_3Na	1.60	2.71	2.80	3.08	2.71
CH_3SO_3Na	2.40	4.20	4.10		
CH_3SO_3Na	3.20			6.50	6.00

[a] Values of the activity coefficients f_X; a dilute aqueous solution at 25.0° is taken as the standard state.

and ortho esters (Table III). For anions f_X increases in the sequence $ClO_4^- < Cl^- \sim CH_3SO_3^-$, and for cations the sequence is $Li^+ < (CH_3)_4N^+ < Na^+ \sim K^+$. In general it is the bulky, low-charge density ions which "salt-in" polar nonelectrolytes,[26] and the position of lithium is anomalous, possibly because it can interact with the ethereal oxygen atoms, either directly or through water molecules which are strongly polarized by the lithium ion.[31] There are only minor differences between the salt effects upon f_X for the various substrates.

The activity coefficient of *p*-nitroaniline in aqueous tetramethylammonium chloride fitted the equation $\log f = -0.20C_s$ (a dilute solution in water is taken as the standard state). The activity coefficients are very close to those found earlier using tetramethylammonium bromide.[23] Using 0.12 M HCl and 1.0 M $(CH_3)_4NCl$, $-\Delta H_0' = -0.04$ and this salt effect is slightly smaller than that of the bromide.[23]

Discussion

Substrate Reactivities. The second-order rate constants for the hydronium ion catalyzed hydrolysis confirm the conclusion reached earlier that the potentially strong electron-releasing power of an alkoxy group is not utilized in formation of the transition state for ortho ester hydrolysis.[3,12] The rate constants for reaction in water (Table II) confirm the earlier results, which depended on experiments in aqueous buffers for ortho

(31) H. S. Frank and M. G. Evans, *J. Chem. Phys.*, 13, 507 (1945); G. R. Choppin and K. Buijs, *ibid.*, 39, 2042 (1963).

esters and in aqueous organic solvents for acetals and ketals and show that introduction of an α-methyl group into acetal increases the rate by 2×10^3, whereas the effect for an orthoformate is approximately tenfold less. (Tetraethyl orthocarbonate is actually less reactive than triethyl orthoacetate.[3,28])

There is a large rate enhancement in going from a formal to an acetal and to a ketal,[32] and various explanations have been cited, including hyperconjugation.[33] Steric effects may also be important in helping the carbon at the reaction center to go from a tetrahedral towards a trigonal configuration.[34] Such effects should be more important in acetal and ketal than in ortho ester hydrolysis, because of the decreasing carbonium ion character of the transition state for ortho ester hydrolysis, and in addition, the greater bulk of a methyl than an alkoxy group[35] should make this effect most important in ketal hydrolysis and 2,2-diethoxypropane is more reactive than triethyl orthoformate (Table II).

In the original discussion of the scheme for a hypothetical A1 reaction in which $k_{-1} \gg k_2$ consideration of the second-order rate constants and the probable basic-

$$S + H_3\overset{+}{O} \underset{k_{-1}}{\overset{k_1}{\rightleftharpoons}} \overset{+}{S}H^+ + H_2O$$

$$\overset{+}{S}H \xrightarrow{k_2} \text{products}$$

ity of the substrate showed that it was reasonable to assume that $k_{-1} \gg k_2$ for hydrolysis of aliphatic acetals, but the calculation was not made for the much more reactive ketals.[12]

If we take $pK_a \sim -5.2$ for 2,2-diethoxypropane[13] and $k_{H^+} = 3 \times 10^3$ l. mol^{-1} sec^{-1} (Table III), $k_2 \sim 5 \times 10^8$ sec^{-1} if the ketal and its conjugate acid are to be in equilibrium, but then $k_{-1} \gg 5 \times 10^8$ sec^{-1}, and would be close to the limiting value for a proton transfer from an acid to water.[36]

Deuterium Solvent Isotope Effects. It is generally assumed that acid-catalyzed reactions for which $k_{H_2O}/k_{D_2O} > 1$ involve slow proton transfers, whereas when $k_{H_2O}/k_{D_2O} < 1$ a preequilibrium proton transfer is involved. The magnitude of the solvent isotope effect appears to be different for A1 and A2 hydrolyses, and for many acetal, ketal, and ortho ester hydrolyses the values are in the range typical of A1 hydrolyses,[3,37–39] although for the hydronium ion catalyzed hydrolysis of benzaldehyde methyl phenyl acetal $k_{H_2O}/k_{D_2O} = 1.02$,[11] and for tetraethyl orthocarbonate $k_{H_2O}/k_{D_2O} = 0.71$.[28] In some hydrolyses values of k_{H_2O}/k_{D_2O} less than unity have been observed for the hydrogen ion catalyzed hydrolyses even though buffer catalysis was observed (ref 7, 8, and 11 and Table II).

For a reaction involving slow proton transfer the overall isotope effect is a combination of a primary effect $k_{H_2O}/k_{D_2O} < 1$, and a secondary effect arising from the changes in the hydrogen bonding of protons as another proton is transferred to the substrate.[38,39] We do not

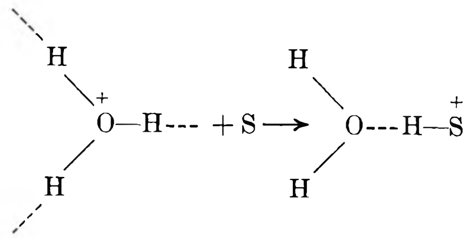

know the relation between extent of the proton transfer in the transition state and loss of zero point energy,[39,40] but if slight, or almost complete, proton transfers involve very little loss of zero point energy, the primary isotope effect for proton transfers from a hydronium ion could be partially offset by a secondary effect.[38] In orthoformate and orthobenzoate hydrolysis where in strong acid $k_{H_2O}/k_{D_2O} \sim 0.44$, instead of *ca.* 0.34 for acetal or ketal hydrolysis, proton transfer may not be complete, but too large for observation of general acid catalysis. For the dioxolane hydrolyses studied by Fife[9] and by DeWolfe[10] and their coworkers the values of $k_{H_2O}/k_{D_2O} = 0.43$ and 0.38 are surprisingly low for reactions in which general acid catalysis was found (but in solvents of higher dioxane content than those used for the study of the isotope effect).[10]

For the hydrogen ion catalyzed hydrolysis of benzaldehyde methyl phenyl acetal in water $k_{H_2O}/k_{D_2O} = 1.02$, which is considerably larger than those observed for most acetal and ketal hydrolyses.[11] These results indicate that proton transfer is incomplete in the hydronium ion catalyzed hydrolysis of the benzaldehyde compound and is consistent with the low α value for this reaction catalyzed by weak acids.[11,41]

The changes in k_{H_2O}/k_{D_2O} with changes in structure for hydrolysis in strong acids are understandable in terms either of a mechanistic charge from A1 to A-SE2, or an A-SE2 mechanism in which the relative importance of OH bond making and OR bond breaking changes.

The values of $k_{H_2O}/k_{D_2O} = 1.4$ for the weak acid-catalyzed hydrolysis of tetraethyl orthocarbonate[28] and 2.11

(32) M. M. Kreevoy and R. W. Taft, *J. Amer. Chem. Soc.*, **77**, 5590 (1955).

(33) J. E. Leffler and E. Grunwald, "Rates and Equilibria of Organic Reactions," Wiley, New York, N. Y., 1963, pp 231–235.

(34) H. C. Brown, *Chem. Soc. Spec. Publ.*, **16**, 140 (1962).

(35) J. March, "Advanced Organic Chemistry," McGraw-Hill, New York, N. Y., 1968, p 107.

(36) M. Eigen, *Angew. Chem., Int. Ed. Eng.*, **3**, 1 (1964); R. P. Bell, "The Proton in Chemistry," Cornell University Press, Ithaca, N. Y., 1959, p 118.

(37) J. G. Pritchard and F. A. Long, *J. Amer. Chem. Soc.*, **78**, 6008 (1956); **80**, 4162 (1958); M. Kilpatrick, *ibid.*, **85**, 1036 (1963).

(38) C. A. Bunton and V. J. Shiner, *ibid.*, **83**, 3207 (1961).

(39) R. L. Schowen, *Progr. Phys. Org. Chem.*, in press.

(40) R. A. More O'Ferral and J. Kuoba, *J. Chem. Soc. B*, 985 (1967); W. J. Albery, *Trans. Faraday Soc.*, **63**, 200 (1967).

(41) In a number of reactions in which a proton is transferred between electronegative atoms in the rate-limiting step the primary isotope effect is very small.[3,36] In view of the deuterium solvent isotope effects for hydrolysis of ethyl orthocarbonate[28] and benzaldehyde methyl phenyl ketal,[11] it seems that zero point energy can be lost in proton transfer to oxygen.

for benzaldehyde methyl phenyl acetal[11] are understandable in these terms because the secondary isotope effect, which is so important with the hydronium ion catalyzed reaction, should now be very small. With a monobasic general acid only one hydrogen atom changes its nature when the transition state is formed, whereas with H_3O^+ the two hydrogens which are not directly involved in the transfer nevertheless change their hydrogen bonding to water.

Deuterium isotope effects are similar for A-SE2 orthoacetate hydrolysis and A2 hydrolyses, with values of k_{H_2O}/k_{D_2O} larger than those characteristic of A1 hydrolyses in which the transition state has appreciable carbonium ion character, simply because any factor which maintains acidic protons in the transition state increases k_{H_2O}/k_{D_2O},[38] and in much the same way entropies of activation are generally more negative for both A2 and A-SE2 than for A1 reactions.[42] In addition electronic effects are not clear cut for A2 reactions[43] and may be similar to those characteristic of A-SE2 reactions. In some cases A2 mechanisms have been assumed simply because the evidence was inconsistent with A1 mechanisms, but at least for hydrolyses of ortho esters and related compounds there seems to be no compelling evidence for A2 mechanisms; for example all the evidence cited for an A2 mechanism in the hydronium ion catalyzed hydrolysis of phenyl-1,3-oxathidanes[44] is consistent with an A-SE2 mechanism, which also is reasonable for the mercuric ion catalyzed hydrolysis.

Kinetic Salt Effects. Although the salt order is similar for all the substrates the kinetic salt effects decrease in the general sequence of increasing carbonium ion stability: 1,1-diethoxyethane > 2,2-diethoxypropane > triethyl orthoformate > triethyl orthoacetate (Table I).

Added salts affect the protonation of a primary amine, and a triarylcarbinol, ROH, differently.[22] Bulky anions, *e.g.*, ClO_4^-, stabilize a triaryl methyl cation relative to a nitroanilinium ion, but at least for univalent salts the charge density of the cation does not appear to be important. We therefore compare kinetic salt effects upon acetal and ortho ester hydrolysis with those upon the protonation of primary amines and triaryl carbinols.

The α-deuterium isotope effects observed by Cordes and his coworkers suggest that the transition state for the hydrolysis of triethyl orthoformate and the more reactive benzaldehyde acetals involves very little CO bond breaking, but that there is more bond breaking in the transition state of the hydrolysis of propionaldehyde diethyl acetal,[14] *i.e.*, the latter has more A1 characteristics than the former. If the transition state for an acetal or ortho ester hydrolysis is close to that of an oxocarbonium ion(II) in which the positive charge is delocalized over several alkoxy groups we might expect electrolyte effects upon its activity coefficient to be more similar to that upon a triaryl methyl cation than upon an anilinium ion, because in the triaryl methyl cation the charge is also extensively delocalized, and hydrogen bonding is unimportant (ionizations of nitric and nitrous acids to NO_2^+ and NO^+ follow ionization of triaryl carbinols rather than amine protonations[45]).

For the acid hydrolysis

$$\frac{k_s}{k_0 f_X} = a_{H^+}/f^*$$

(where f_X and f^* are the activity coefficients of the substrate and the transition state, respectively). For amine protonation

$$\Delta h_0' f_B = a_{H^+}/f_{HB^+}$$

and for carbinol ionization

$$\frac{\Delta h_R a_{H_2O}}{f_{ROH}} = a_{H^+}/f_{R^+}$$

(where Δ signifies the change in the parameter brought about by addition of the salt, and h_0' and h_R are acidity functions for primary amine protonation and carbinol ionization).

The values of $\Delta h_0'$ and Δh_R were measured for 1 *M* salts and for the kinetic salt effects we use rate constants interpolated to 1 *M* salt.

For all four substrates we have tabulated values of f^*/f_{R^+} and f^*/f_{HB^+}, and for the ketal, orthoformate, and orthoacetate we tabulate f^*/f^*_{Ac}, where f^*_{Ac} is the activity coefficient of the transition state for acetal hydrolysis (Tables IV–VI).

All the salts destabilize the transition states relative to the tri-*p*-anisyl cation (Table IV), in the sequence acetal < ketal < orthoformate < orthoacetate.

Table IV: Salt Effects upon the Relative Activity Coefficients of the Transition State and the Trianisyl Methyl Cation[a]

Substrate	Salt: LiCl	NaCl	$LiClO_4$	$NaClO_4$	CH_3SO_3Na
$CH_3CH(OEt)_2$	2.4	2.2	2.7	3.7	1.5
$(CH_3)_2C(OEt)_2$	3.0	3.0	3.2	3.6	1.75
$HC(OEt)_3$	2.9	3.4	4.5	5.6	1.85
$CH_3C(OEt)_3$	3.9	3.7	5.1	5.3	1.75

[a] Values of f^*/f_{R^+} at 25.0° in 1 *M* salt. The tri-*p*-anisyl methyl cation is taken as reference.

(42) L. L. Schaleger and F. A. Long, *Advan. Phys. Org. Chem.*, **1**, 1 (1963); M. A. Matesich, *J. Org. Chem.*, **32**, 1258 (1967).

(43) (a) C. K. Ingold, *J. Chem. Soc.*, 1032 (1930); R. W. Taft, *J. Amer. Chem. Soc.*, **74**, 2729, 3120 (1952); (b) M. Charton, *ibid.*, **91**, 615 (1969), and accompanying papers.

(44) N. D. De and L. R. Fedor, *ibid.*, **90**, 7266 (1968).

(45) F. H. Westheimer and M. S. Kharasch, *ibid.*, **68**, 1871 (1946); N. C. Deno, H. E. Berkheimer, W. L. Evans, and H. J. Peterson, *ibid.*, **81**, 2344 (1959); M. A. Lowen. M. A. Murray, and G. Williams, *J. Chem. Soc.*, 3318 (1950); K. Singer and P. A. Vamplew, *ibid.*, 3971 (1956).

Table V: Salt Effects upon the Relative Activity Coefficients of the Transition State and an Anilium Ion[a]

	Salt						
Substrate	LiCl	NaCl	KCl	$(CH_3)_4NCl$	$LiClO_4$	$NaClO_4$	CH_3SO_3Na
$CH_3CH(OEt)_2$	0.81	0.82	0.97	1.16	0.75	0.93	1.11
$(CH_3)_2C(OEt)_2$	1.00	1.12	1.25	1.54	0.89	0.90	1.25
$HC(OEt)_3$	0.97	1.30	1.39	1.80	1.24	1.39	1.33
$CH_3C(OEt)_3$	1.23	1.49	1.52	1.76	1.41	1.32	1.25

[a] Values of f^*/f_{HB^+} at 25.0° in 1 *M* salt. The *p*-nitroanilinium ion is taken as reference.

Table VI: Salt Effects upon the Transition State[a]

	Salt						
Substrate	LiCl	NaCl	KCl	$(CH_3)_4NCl$	$LiClO_4$	$NaClO_4$	CH_3SO_3Na
$(CH_3)_2C(OEt)_2$	1.23	1.36	1.29	1.32	1.19	1.97	1.13
$HC(OEt)_3$	1.19	1.59	1.43	1.53	1.65	1.49	1.20
$CH_3C(OEt)_3$	1.52	1.81	1.57	1.52	1.87	1.42	1.13

[a] Values of f^*/f^*_{AC} at 25.0° in 1 *M* salt. The transition state for hydrolysis of $CH_3CH(OEt)_2$ is taken as reference.

For the hydrolysis of dimethoxymethane Long and McIntyre obtained the following values of f^*/f_{HB^+}[21] for 1 *M* salts: LiCl 0.78, NaCl 1.00, KCl 0.86, which are reasonably close to our values for hydrolysis of diethoxyethane (Table V). Unfortunately we could not extend the comparisons between the two sets of data, because several of the salts used by Long and McIntyre absorbed in the ultraviolet and therefore could not be used with our stopped-flow spectrophotometer. However the evidence confirms that for hydrolysis of simple acetals $f^*/f_{HB^+} \sim 1$ for all the salts examined.

Comparison of the salt effects upon f^*/f_{R^+} and f^*/f_{HB^+} suggest that the carboniumlike character of the transition follows the sequence acetal > ketal > orthoformate > orthoacetate, which is consistent with the α-deuterium isotope effects found by Cordes and his coworkers using acetals and triethyl orthoformate.[14]

Salts could affect the proton transfer from a hydronium ion to an ortho ester by changing the structure of water.[31] Proton transfer is faster in ice than in water,[46] and a salt which breaks up the "icelike" clusters of water should hinder this process, although it need not necessarily inhibit an equilibrium proton transfer (*cf.* ref 47).

In general it is the bulky "structure-breaking" ions which increase f^*/f_{HB^+} for ortho ester hydrolysis (Table V) and the "structure-breaking" effect increases with decreasing charge density of the ions (except for very low charge density ions).[48]

Small high charge density cations, such as lithium, increase acidity as measured by acidity functions, by reducing the affinity of water molecules for protons and by destabilizing the indicator base,[16,23,49] and they are effective catalysts of acid hydrolyses. However although lithium ions have very strong effects upon the properties of water they have only small effects on f^*/f_{HB^+} (Table V), and f^*/f_{HB^+} increases in the sequence $Li^+ < Na^+ < K^+ < (CH_3)_4N^+$. This cation effect contrasts sharply with the large anion and small cation effects observed in carboxylic ester hydrolysis[22] where formation of the transition state involves complete proton transfer and extensive carbon oxygen bond making and breaking.[50]

The present results show that comparison between salt effects upon the rate of a given reaction and a model kinetic or equilibrium system can provide mechanistic information, and we hope to be able to find additional evidence for our hypothesis that large specific cationic effects are characteristic of slow proton transfers to electronegative atoms, noting that although anionic effects are large upon the measured reaction rate constants (Table I), they are reduced when we take into account the effects upon the activity of the initial state.

Studies of reaction rates in moderately concentrated acids have value as mechanistic tools,[16,18,19,51] and kinetic salt effects may be useful for those reactions which are too fast to be examined in other than very dilute acid, even though kinetic salt effects have at present to be treated empirically. The relatively large salt effects which we observe suggest that adventitious salt

(46) N. H. Grant, D. E. Clark, and H. E. Alburn, *J. Amer. Chem. Soc.*, **83**, 4476 (1961); T. C. Bruice and A. R. Butler, *ibid.*, **86**, 4104 (1964); R. E. Pincock, *Accounts Chem. Res.*, **2**, 97 (1969).

(47) M. M. Kreevoy and J. M. Williams, *J. Amer. Chem. Soc.*, **90**, 6809 (1968), and references cited.

(48) R. K. McMullan and G. A. Jeffrey, *J. Chem. Phys.*, **31**, 1231 (1959).

(49) C. L. Perrin, *J. Amer. Chem. Soc.*, **86**, 256 (1964).

(50) C. K. Ingold, "Structure and Mechanism in Organic Chemistry," Cornell University Press, Ithaca, N. Y., 1953, Chapter XIV.

(51) E. M. Arnett and S. W. Mach, *J. Amer. Chem. Soc.*, **88**, 1177 (1966); R. H. Boyd in "Solute-Solvent Interactions," J. F. Coetzle and C. D. Ritchie, Ed., Marcel Dekker, New York, N. Y., 1969, Chapter 3.

effects could be a source of apparent buffer catalysis in those reactions in which general acids or bases are only weakly catalytic, especially when large amounts of an added salt are used to maintain ionic strength.

The Mechanism of Hydrolysis of Diazoacetate Ion

by Maurice M. Kreevoy* and Dennis E. Konasewich

School of Chemistry, University of Minnesota, Minneapolis, Minnesota 55455 (*Received March 6, 1970*)

The hydrolysis of potassium diazoacetate to potassium glycolate uses an A-1 mechanism in strongly basic solution but switches to an A-SE2 mechanism in less basic or acidic solution. These conclusions are supported by the form of the rate law and the variation in solvent isotope effect with solution basicity. The competitive isotope effects, κ_H/κ_T, for H^+, CH_3COOH, and H_2O as acids are 8.1, 12.4, and 3.0, respectively. The Swain–Schaad relations correctly predict the relative magnitudes of κ_H/κ_T and κ_D/κ_T when H^+ is the acid, and a κ_H/κ_D of 4.2 is estimated. Comparison of κ_H/κ_D for H^+ and H_2O with the solvent isotope effects permits the calculation of α_i values, analogous to the Brønsted α, for H^+ and H_2O. They are 0.30 and 0.89, suggesting that the Brønsted plot will be curved. Upper limits of about 10^7 and 10^5 sec^{-1}, respectively, can be inferred for the rate constants for the spontaneous loss of N_2, and the loss of H^+ to H_2O, from $^+N_2CH_2COO^-$. The upper limit for the acid dissociation constant of this ion is about 1 *M*.

Some time ago Bell,[1] reinterpreting data of King and Bolinger,[2] on the aqueous solution hydrolysis of the diazoacetate ion, advanced a novel mechanistic hypothesis. The steps suggested by Bell are shown in eq 2–4. (The overall reaction is summarized in eq 1.)

$$N_2CHCOO^- + H_2O \longrightarrow N_2 + HOCH_2COO^- \quad (1)$$

$$N_2CHCOO^- + H_2O \underset{k_{-H_2O}}{\overset{k_{H_2O}}{\rightleftarrows}} {}^+N_2CH_2COO^- + OH^- \quad (2)$$

$$N_2CHCOO^- + H^+ \underset{k_{-H}}{\overset{k_H}{\rightleftarrows}} {}^+N_2CH_2COO^- \quad (3)$$

$$^+N_2CH_2COO^- \xrightarrow{k_2} \underset{\text{fast steps}}{\overset{\text{series of}}{\longrightarrow}} HOCH_2COO^- + N_2 \quad (4)$$

Using the steady-state approximation these steps lead to the rate law shown in eq 5

$$-\frac{d(N_2CHCOO^-)}{dt} = \frac{\{k_H(H^+) + k_{H_2O}\}(N_2CHCOO^-)}{k_{-H} + k_2 + k_{-H_2O}(OH^-)} \quad (5)$$

It was then postulated that k_{-H} was small compared to k_2 and that $k_{-H_2O}(OH^-)$ was small compared to k_2 at low base concentrations, but that at high base concentrations $k_{-H_2O}(OH^-)$ substantially exceeded k_2. After making suitable cancellations it becomes apparent that the qualitative upshot of this is an A-1 scheme at high basicities and an A-SE2 scheme at lower basicities or in acid solution.

This mechanism is unique and interesting in several ways. In spite of a great deal of work on acid-catalyzed reactions in general[3] and A-SE2 reactions in particular[4] there seem to be no well-studied examples of this sort of cross over. There are also very few well-established examples of A-1 reactions in which the reversible protonation is on carbon. If the Bell mechanism is correct, there also seemed to be an opportunity to get some useful information about the longevity of an aliphatic diazonium ion in dilute aqueous solution. Furthermore, there is reason to believe that proton transfer reactions which have rate constants which are large but substantially short of the diffusion-governed limit may be particularly useful in revealing the structure of proton transfer transition states.[5] The present paper describes progress toward these objectives.

Results

All the rates were measured at 25.0 ± 0.1° and, as expected, accurately conformed to a pseudo-first-order rate law within a given experiment, since all concentrations except that of the substrate were constant.[6] The

* To whom correspondence should be addressed.

(1) R. P. Bell, "The Proton in Chemistry," Cornell University Press, Ithaca, N. Y., 1959, Chapter IX.

(2) C. V. King and E. D. Bolinger, *J. Amer. Chem. Soc.*, **58**, 1533 (1936).

(3) A. V. Willi, "Sauerkatalytische Reactionen der organischen Chemie," Friedr. Vieweg und Sohn, Braunschweig, Germany, 1965.

(4) J. M. Williams, Jr., and M. M. Kreevoy, *Advan. Phys. Org. Chem.*, **6**, 63 (1968).

(5) R. A. Marcus, *J. Phys. Chem.*, **72**, 891 (1968).

(6) A. A. Frost and R. G. Pearson, "Kinetics and Mechanism," Wiley, New York, N. Y., 1961, p 29.

pseudo-first-order rate constants, k_1, are $\{-d(N_2CHCOO^-)/dt\}(N_2CHCOO^-)^{-1}$. Repetitions and multiple repetitions of a number of experiments showed that k_1 values could be replicated with deviations not usually exceeding 3% in the pH range 14–11, and not usually exceeding 10% in the pH range 11–7. Results in D_2O were comparable.

Rate Constants in Aqueous Base. Values of k_1 determined at 26 different base concentrations are shown in Table I. Comparable results for D_2O are shown in Table II. In all solutions less than 0.1 M in NaOH the ionic strength, μ, was brought to 0.105 M by addition of KCl.

Table I: Rate Constants in H_2O

$(H^+)\gamma_+\gamma_-$, M^a	k_1, sec^{-1}
1.02×10^{-14}	1.26×10^{-7}
1.71×10^{-14}	2.00×10^{-7}
2.49×10^{-14}	3.52×10^{-7}
5.20×10^{-14}	7.13×10^{-7}
9.80×10^{-14}	1.45×10^{-6}
1.22×10^{-13}	1.80×10^{-6}
3.91×10^{-13}	5.10×10^{-6}
9.54×10^{-13}	1.08×10^{-5}
1.23×10^{-12}	1.30×10^{-5}
2.04×10^{-12}	1.64×10^{-5}
5.10×10^{-12}	2.28×10^{-5}
1.04×10^{-11}	2.93×10^{-5}
1.33×10^{-11}	3.03×10^{-5}
5.40×10^{-11}	3.97×10^{-5}
7.60×10^{-11}	4.20×10^{-5}
9.26×10^{-10}	1.26×10^{-4}
7.69×10^{-9}	5.60×10^{-4}
1.34×10^{-8}	9.57×10^{-4}
2.04×10^{-8}	1.17×10^{-3}
2.05×10^{-8}	1.42×10^{-3}
2.54×10^{-8}	2.00×10^{-3}
2.84×10^{-8}	1.88×10^{-3}
3.14×10^{-8}	2.05×10^{-3}
3.38×10^{-8}	2.38×10^{-3}
3.96×10^{-8}	2.47×10^{-3}
5.40×10^{-8}	3.77×10^{-3}

[a] Assuming K_w is 1.00×10^{-14} M^2; ref 32 and references cited therein.

Table II: Rate Constants in D_2O

$(D^+)\gamma_+\gamma_-$, M^a	k_1^D, sec$^{-1\,b}$
1.7×10^{-15}	1.08×10^{-7}
3.4×10^{-15}	1.87×10^{-7}
8.7×10^{-15}	4.15×10^{-7}
2.75×10^{-14}	1.28×10^{-6}
4.35×10^{-14}	1.77×10^{-6}
8.57×10^{-14}	3.17×10^{-6}
1.09×10^{-13}	3.65×10^{-6}
1.27×10^{-13}	4.30×10^{-6}
1.79×10^{-13}	4.78×10^{-6}
2.28×10^{-13}	5.03×10^{-6}
2.85×10^{-13}	5.47×10^{-6}
5.75×10^{-13}	7.55×10^{-6}
5.78×10^{-13}	7.72×10^{-6}
7.70×10^{-13}	8.05×10^{-6}
1.25×10^{-12}	8.62×10^{-6}
1.48×10^{-10}	3.03×10^{-5}
1.23×10^{-9}	7.27×10^{-5}
3.20×10^{-9}	1.33×10^{-4}
1.05×10^{-8}	3.02×10^{-4}
1.95×10^{-8}	4.93×10^{-4}
3.80×10^{-8}	1.02×10^{-3}
7.57×10^{-8}	2.17×10^{-3}

[a] Assuming K_w^D is 1.36×10^{-15} M^2; ref 32 and references cited therein. [b] Corrected for adventitious H.

Table III: Rate Constants in Phenol–Phenate Buffer Solutions

$10^2(C_6H_5OH)$, M	$10^2(C_6H_5O^-)$, M	$10^{11}(H^+)\gamma_+\gamma_-$, M	10^3k_1, sec^{-1}
5.0	6.1	0.91	1.25
4.5	5.4	0.93	1.22
4.0	4.6	0.98	0.98
2.5	2.8	1.00	0.92
1.0	1.1	1.04	0.69
4.4	5.6	0.88	1.53
5.0	5.0	1.11	1.56
6.2	3.8	1.79	2.22
7.3	2.7	3.05	2.92
7.6	2.4	3.52	2.54
8.3	1.7	5.52	3.56
8.9	1.1	9.06	3.66

Rates in the Presence of General Acids and Bases. In phenol–sodium phenate buffer solutions k_1 values were determined at a number of pH's and phenol concentrations. All the k_1 values were substantially above those observed in unbuffered solution at the same pH, but they are not a linear function of the general acid concentration. A satisfactory rate law, permitting the evaluation of general acid catalytic coefficients, can only be obtained by considering the reaction mechanism. Consequently, their evaluation is postponed to the Discussion section. The k_1 values are shown in Table III. The first five data in Table III are of the precision already described. The subsequent seven, however, were the result of early experiments with phenol and may be less reliable because the problem with bubbles, described in the Experimental section, was being encountered for the first time. In all of these experiments μ was maintained at 0.105 by addition of KCl where necessary. The pH was determined potentiometrically, and the evaluation of $(H^+)\gamma_+\gamma_-$ is described in the Discussion section.

When 0.1 M sodium acetate was added to reaction mixtures at pH values around 8, k_1 values observed were higher by a factor of about 10 than those obtained in the absence of sodium acetate. These results are shown in

Table IV: Rate Constants in Aqueous 0.105 *M* Sodium Acetate Solutions at 25°

$10^5(CH_3COOH)$, *M*	$10^3(H^+)\gamma_+\gamma_-$, *M*	10^2k_1,[a] sec^{-1}	No. of experi-ments
2.93	0.53	0.751	3
4.52	0.80	1.13	3
7.10	1.27	1.81	2
11.3	2.01	2.71	3

[a] Mean value.

Table IV. Their interpretation is also postponed until the Discussion section.

Product Composition. The competitive isotope effect, κ_H/κ_T, is defined as $(H/T)_{prod} \times (T/H)_{solv}$.[4] In the present case only one of the two hydrogens of the glycolate ion has had an opportunity to be tritiated, so $(T/H)_{prod}$ is the counting rate per half mole of calcium salt, while $(T/H)_{solv}$ is the counting rate per half mole of water. Experiments were carried out at various pH's; in one set of experiments acetic acid was present and in one the solvent was tritiated D_2O instead of H_2O. In H_2O, with the pH about 1.5, six experiments were carried out, leading to an average deviation from the mean of 4% and a probable error of the mean of 2%. Under each of the other sets of conditions only two or three experiments were carried out. The values reported are the means, and their uncertainties are similar to the average deviation from the mean for experiments in H_2O at a pH of 1.5, about 4%. The results are summarized in Table V, along with the uncertainties described above.

Table V: Results of Isotopic Competition

pH or pD	Acid or base	$(H/T)_{prod} \times (T/H)_{solv}$[a,b]
1.5	HCl	8.14 ± 0.10
5.5	HCl	8.1 ± 0.3
5.5	CH_3COOH	11.2 ± 0.5
10.4	NaOH	3.02 ± 0.12
1.1[c]	DCl	1.98 ± 0.08[c]

[a] $(T/H)_{prod}$ is the counting rate per half mole of product $(HOCH_2COO^-)_2Ca^{2+}$. [b] $(T/H)_{solv}$ is the counting rate per half mole of water, taking account of the fact that water has two positions which may be labeled. [c] These experiments were carried out in nearly pure D_2O, and the product ratio given is $(D/T)_{prod} \times (T/D)_{solv}$. A small correction has been made for adventitious H in the D_2O (ref 29).

Discussion

Activity Coefficients. The Bell mechanism, in the A-SE2 region, requires that each acid generate its own transition state in combination with N_2CHCOO^-. In the case that the acid is the aquated proton the transition state will be neutral regardless of its structure or the number of water molecules involved. For a reaction having such a transition state the Brønsted–Bjerrum rate law[7] requires that the product of the concentrations be multiplied by $\gamma_{H^+}\gamma_{N_2CHCOO^-}/\gamma_{\pm}$. Empirical observation supports the assumption that activity coefficient products, $\gamma_{A^+}\gamma_{B^-}$, in aqueous solution, at concentrations not much above 0.1 *M* do not vary with the structure of the ions by more than a few per cent in most cases.[8] Similarly, activity coefficients for neutral species, such as the transition state, do not vary widely from unity.[8] Furthermore, in ratios such as $\gamma_{H^+}\gamma_{N_2CHCOO^-}/\gamma_{\pm}$, where the same structural elements occur in the substances whose activity coefficients are in the numerator as those whose activity coefficients are in the denominator, such deviations from these rules as do occur tend to cancel.[9] In view of this it seems reasonable to replace $\gamma_{H^+}\gamma_{N_2CHCOO^-}/\gamma_{\pm}$ with $\gamma_+\gamma_-$, where the activity coefficients of all positive species are equated to γ_+ and those of all negative species are equated to γ_-.

Transition states formed from N_2CHCOO^- plus a neutral acid require activity coefficient ratios of the form. $\gamma_{N_2CHCOO^-}\gamma_{HA}/\gamma_{\pm}^-$, and those formed solely from N_2CHCOO^- and water require ratios of the form, $\gamma_{N_2CHCOO^-}/\gamma_{\pm}^-$. With the approximations outlined these all reduce to unity. Reexamining eq 5 in the light of these approximations it is seen that all the quantities in parentheses assume the significance of concentrations if (H^+) is replaced with $(H^+)\gamma_+\gamma_-$.

The quantity $(H^+)\gamma_+\gamma_-$, in unbuffered aqueous base, is conveniently given by $k_W/(OH^-)$, where K_W is the autoprotolysis constant of water. In unbuffered solutions near neutral, or in buffer solutions, where pH was the directly measured variable, antilog (pH) was multiplied by γ_- to get $(H^+)\gamma_+\gamma_-$. It was taken from eq 6 and had a value of 0.79

$$-\log \gamma_- = \frac{0.5092\sqrt{\mu}}{1 - \sqrt{\mu}} - 0.2\mu \tag{6}$$

Evaluation of Rate Constants. In the absence of incompletely dissociated acids and bases, neglecting k_{-H}, k_1 should be given by eq 7. The concentration-independent parameters of eq 7, k_H, k_{H_2O}, and k_{-H_2O}/k_2 have been evaluated by minimizing the sum of the squares of the fractional discrepancies between the observed k_1 values and those calculated with a given set of parameters. Computation was done using a Control Data Corp.

$$k_1 = \frac{k_H(H^+)\gamma_+\gamma_- + k_{H_2O}}{1 + k_{-H_2O}(OH^-)/k_2} \tag{7}$$

(7) S. Glasstone, K. J. Laidler, and H. Eyring, "The Theory of Rate Processes," McGraw-Hill, New York, N. Y., 1941, pp 404, 405.

(8) R. A. Robinson and R. H. Stokes, "Electrolyte Solutions," Butterworths, Washington, D. C., and London, 1955, Appendix 8.10.

(9) L. Zucker and L. P. Hammett, *J. Amer. Chem. Soc.*, 61, 2791 (1939).

6600 computer.[10] The values obtained are given in Table VI. The value of k_H is almost independent of the other two parameters, because k_1 is almost perfectly proportional to $(H^+)\gamma_+\gamma_-$ at the lower pH's. Thus its uncertainty is just that following from the uncertainty in the measurements. However, k_{H_2O} and the ratio k_{-H_2O}/k_2 are correlated, so that a higher value of the former can be better tolerated if it is accompanied by a lower value of the latter. The uncertainties given in Table VI along with the values are probable errors, with the proviso that the other parameters are free to be adjusted to optimize the fit.[11]

Table VI: Values of Kinetic Parameters in H_2O and D_2O at 25°

Parameter	Units	Value and uncertainty[a]
k_H	M^{-1} sec^{-1}	$6.49 \pm 0.08 \times 10^4$
		1.9×10^6 [b]
k_{H_2O}	Sec^{-1}	$3.79 \pm 0.05 \times 10^{-5}$
		5×10^{-5} [b]
k_{-H_2O}/k_2	M^{-1}	$2.68 \pm 0.15 \times 10^2$
		6×10^2 [b]
k_D	M^{-1} sec^{-1}	$2.80 \pm 0.05 \times 10^4$
k_{D_2O}	Sec^{-1}	$1.03 \pm 0.02 \times 10^{-5}$
k_{-D_2O}/k_2^{D} [c]	M^{-1}	$1.39 \pm 0.08 \times 10^2$
$k_{C_6H_5OH}$	M^{-1} sec^{-1}	$6.2 \pm 1.0 \times 10^{-2}$
		6.7×10^{-2} [b]
k_{CH_3COOH}	M^{-1} sec^{-1}	$2.55 \pm 0.11 \times 10^2$

[a] Probable error, taking correlation between the parameters into account. [b] Values of Bell[1] as derived from the data of King and Bolinger[2] and converted into the present units and treatment of electrolyte effects. [c] The rate constant for eq 4, when the intermediate is $^+N_2CD_2COO^-$, is k_2^D.

The comparable parameters and uncertainties were evaluated from the data for D_2O, and these are also shown in Table VI. It may be noted that k_{-H_2O}/k_2 rests mainly on data obtained in solutions where exchange is more rapid than hydrolysis (*i.e.*, $k_{-H_2O}(OH^-)$ is larger than k_2). In D_2O, therefore, the decomposing species is mostly $^+N_2CD_2COO^-$. The rate constant for this decomposition is distinguished from that for $^+N_2CH_2COO^-$ by the superscript "D."

Graphical comparison of observed values of k_1 with those given by eq 7, with optimized parameters, is shown in Figure 1. It amply demonstrates the adequacy of the Bell mechanism. Calculated and observed values generally do not diverge by more than the imprecision of the measurements. The only significant exceptions to this occur in D_2O, at pD between 8 and 10. These measurements are the slowest made using the CO_2 compensation technique and may involve systematic error. The numerical agreement of the parameters with those of Bell,[2] which are also shown in Table VI, is as good as could be expected in view of the limited range of data with which he was working. In particular the large divergence in the values of k_H is traceable to the fact that the King and Bolinger results do not extend to pH values below 10, at which point the H^+-catalyzed path still contributes less than 20% of the total rate. Discrepancies between the values of k_1 given by eq 7 with the reported parameters, and values of k_1, reported by King and Bolinger for comparable solutions average about 5%. This is not outside the combined experimental imprecision.

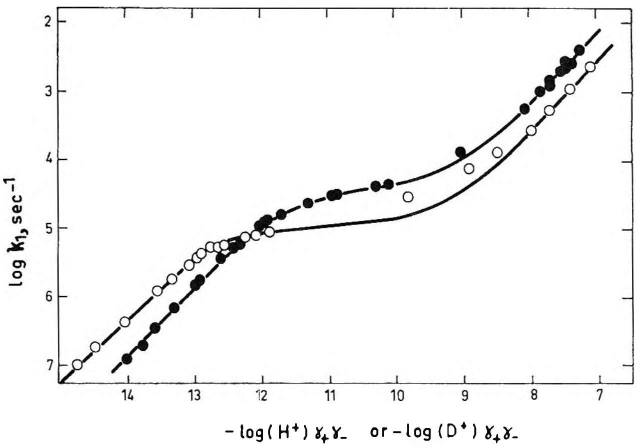

Figure 1. Log k_1 as a function of log $(H^+)\gamma_+\gamma_-$ or log $(D^+)\gamma_+\gamma_-$: closed circles represent values obtained in H_2O; open circles those for D_2O. The circles do not represent uncertainties. The solid curves are calculated from eq 7, using the parameters given in Table VI.

Under the conditions of most of our experiments $(^+N_2CH_2COO^-)$ never reaches its equilibrium value, $(^+N_2CH_2COO^-)_{equil}$. Nevertheless $(^+N_2CH_2COO^-)_{equil}$ is given equally by the mass action expression for protonation of substrate by any acid, including H_2O, H^+, and the general acid, HA, as shown in eq 8. When eq 8 is specialized for the cases of H^+ and H_2O, the two results combined, and K_W substituted for $(H^+)(OH^-)$-

$$(^+N_2CH_2COO^-)_{equil} = (N_2CHCOO^-)(HA)k_{HA}/(A^-)k_{-HA} \quad (8)$$

$\gamma_+\gamma_-$ the quantity K_Wk_H/k_{H_2O} is obtained for k_{-H}/k_{-H_2O}. Since k_{-H_2O}/k_2 is $2.7 \times 10^2\ M^{-1}$, k_{-H}/k_2 is about 5×10^{-3}. This value of k_{-H}/k_2 fully justifies the neglect of k_{-H} is evaluating the other parameters of eq 7.

The decomposition of $^+N_2CH_2COO^-$ to give products is shown as a unimolecular reaction in eq 4. There is no direct way to determine the role of water in this reaction, but hydroxide ion participation is excluded by the form of the rate law. Such participation would lead to a pH-independent term in the rate law for high basicities. This would be manifested by systematic positive deviations from eq 7 in the most basic solutions. Figure 1 shows no sign of such deviations, although rates

(10) The program was written by Dr. Masato Nakashima.

(11) J. Topping, "Errors of Observation and Their Treatment," 3rd ed, Chapman and Hall, London, 1962, p 109.

were studied at OH^- concentrations as high as 1 *M*. This suggests that the decomposition to give products requires no nucleophilic reagent. That is, in basic solution, the reaction is of the A-1 type. An attractive route for the decomposition of $^+N_2CH_2COO^-$ is *via* the lactone, $\overline{OCH_2CO}$.[12] This speculation is supported by the report that alanine reacts with HNO_2 to give lactic acid with an excess of retention over inversion of configuration.[13]

In the presence of a general acid, HA, and its conjugate base, A^-, the mechanistic scheme shown in eq 1–4 must be expanded to include protonation of N_2CHCOO^- by HA, with a rate constant, k_{HA}, and deprotonation of $^+N_2CH_2COO^-$ by A^-, with a rate constant, k_{-HA}. Incorporation of these terms in eq 7 gives eq 9. Equation 9 was used to evaluate k_{HA} as

$$k_1 = \frac{k_{H_2O} + k_H(H^+)\gamma_+\gamma_- + k_{HA}(HA)}{1 + \{k_{-H_2O}(OH^-) + k_{-HA}(A^-)\}/k_2} \qquad (9)$$

follows. When eq 8, as specialized for H_2O, is combined with its general form, a relation is obtained between k_{-H_2O} and k_{-HA}, shown in eq 10. This leads directly to the general equation for k_{-HA}/k_2, shown as eq 11. A minimum value of k_{HA} was obtained by neglecting $k_{-HA}(A^-)/k_2$ in eq 9. This value was then used to evaluate k_{-HA}/k_2, and k_{HA} was reevaluated using the resultant

$$k_{-HA}/k_{-H_2O} = K_W k_{HA}/k_{H_2O}K_{HA} \qquad (10)$$

$$k_{-HA}/k_2 = (k_{-H_2O}/k_2)(K_W k_{HA}/k_{H_2O}K_{HA}) \qquad (11)$$

values of $k_{-HA}(A^-)/k_2$. This process was repeated until further repetition no longer changed k_{HA}. This was evaluated by the method of least squares with the constraint that k_1 must have the value given by eq 7 when (HA) is zero. In the evaluation of k_{HA} for phenol only the first five pieces of data from Table III were used because they are thought to be more reliable than the rest. The final values of k_{HA} are given in Table VI, along with their probable errors. The dissociation constants used in eq 11 were 1.75×10^{-5} for acetic acid[14] and 1.12×10^{-10} for phenol.[15]

Equation 12 shows the more conventionally expected rate law for a general acid catalyzed reaction. Figure 2

$$k_1 = k_H(H^+) + k_{H_2O} + k_{HA}(HA) \qquad (12)$$

shows that eq 9 accurately describes the points thought to be most reliable, for phenol, and eq 12 does not. Although the points, plotted according to eq 12, are approximately colinear, the line misses the origin by many times the experimental error. On the other hand, if all the data are considered, the scatter is such that it is hard to choose between eq 9 and 12. These observations are at least consistent with the preferred method of evaluating k_{HA} and the mechanism underlying it.

The acetic acid work was all done at a single acetate concentration, and, therefore, provides no test of the relative validity of eq 9 and 12. In view of the other

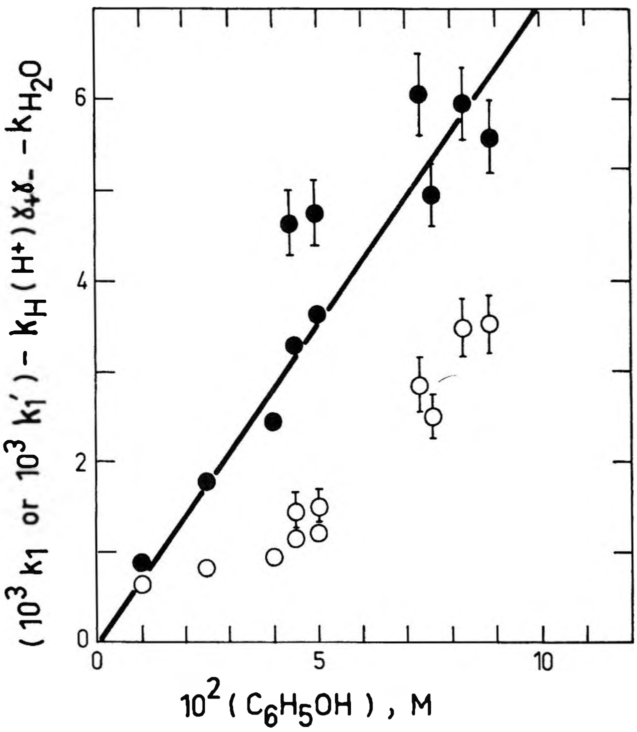

Figure 2. Tests of eq 9 and 12 for phenol. For the closed circles k_1 is multiplied by $1 + \{k_{-H_2O}(OH^-) + k_{-C_6H_5OH}(C_6H_5O^-)\}/k_2$, required by eq 9, to get k_1'. For the open circles it is not. The line is the least-squares line through the closed circles having no bars, forced through the origin. The vertical bars represent the probable experimental error in cases where this substantially exceeds the height of the circles.

evidence eq 9 has been applied, and the resulting rate constant, k_{CH_3COOH}, is given in Table VI.

In the presence of a buffer system the crossover from A-1 to A-SE2 can occur at pH's well below those at which it occurs with H^+ and OH^- only, depending on the concentration of basic buffer constituent and its rate constant for proton abstraction from $^+N_2CH_2COO^-$. In such a system, if the conventional experiments testing for general acid catalysis are carried out, with the buffer ratio (pH) held constant and a series of increasing buffer concentrations studied, a curve with steadily decreasing slope will be observed. Such observations have been reported by Gold and Waterman,[16] and attributed to association between the anion and the acid. While such association may be real, deprotonation by the conjugate base of the acid offers an attractive alternative explanation.

(12) R. A. More-O'Ferrall, *Advan. Phys. Org. Chem.*, **5**, 331 (1967).

(13) P. Brewster, F. Heron, E. D. Hughes, C. K. Iingold, and P. A. D. Rao, *Nature*, **166**, 178 (1950).

(14) G. Kortum, W. Vogel, and K. Andrussow, "Dissociation Constants of Organic Acids in Aqueous Solutions," Butterworths, Washington, D. C., and London, 1961, p 292.

(15) P. D. Bolton, F. M. Hall, and I. H. Reece, *Spectrochim. Acta*, **22**, 1153 (1966).

(16) V. Gold and D. C. A. Waterman, *J. Chem. Soc.*, 839 (1968).

One might attempt to apply the Brønsted catalysis law[17] to k_H, k_{CH_3COOH}, $k_{C_6H_5OH}$, and k_{H_2O}. In fact, a plot of log k_{HA} against log K_{HA} for these four acids is not linear. An examination of other catalytic coefficients, which will be described elsewhere, confirms that the relation between K_{HA} and K_{HA} for this system is more complicated than anticipated by the Brønsted catalysis law.

Kinetic Isotope Effects. A number of kinetic isotope effects can be obtained from the results in Table VI, and they are all consistent with the proposed mechanism. The ratio k_H/k_D is 2.32 ± 0.07 and k_{H_2O}/k_{D_2O} is 3.68 ± 0.12. Neither of these is a pure primary isotope effect.[18] Both are quite consistent with rate-determining proton transfers. The quantity $k_H k_2/k_{-H}$, in the present mechanistic scheme, is the rate constant for an A-1 hydrolysis. The ratio of this quantity to its deuterio analog, 0.28, is within the usual limits of solvent isotope effects on such rate constants.[19] The quantity k_H/k_{-H} is the equilibrium constant for protonation of the substrate by H^+. Since there are no strong hydrogen bonds in the protonated substrate,[20] the ratio of this quantity to its deuterio analog might be expected to be about l^3, which is 0.33.[4] (The fractionation factor for the hydronium ion is l.) If the ratio of k_2 to k_2^D is assumed to be about unity[21,22] (recalling that k_2 is the rate constant for an internal displacement rather than a carbonium ion forming reaction), then 0.28 is also the value of the ratio of equilibrium constants $k_H k_{-D}/k_D k_{-H}$. Considering the experimental uncertainties and the theoretical approximations this agreement is entirely satisfactory. On the other hand, if the decomposition of $^+N_2CH_2COO^-$ is assumed to give a carbonium ion, k_2/k_2^D would be expected to be around 1.2.[23] This would lead to the quite unacceptable value of 0.24 for $k_H k_{-D}/k_D k_{-H}$.

Limits on Rate Constants. Neither k_{-H} nor k_2 nor k_{H_2O} can be individually evaluated from the present results. However, it may be noted that k_{-H_2O} is the rate constant for a second-order reaction, and, therefore, cannot have a value higher than that for a diffusion-limited reaction, that is, about 10^{10} M^{-1} sec^{-1}.[24] This imposes an upper limit of about 10^7 sec^{-1} on k_2, 10^5 sec^{-1} on k_{-H}, and about 1 M on the acid dissociation constant for the protonated substrate. The last value indicates that $^+N_2CHCOO^-$ is a stronger base for protonation on carbon than might have been anticipated. The rather unanticipated stability of $^+N_2CH_2COO^-$ has been previously commented on by More-O'Ferrall.[12]

κ_H/κ_D Values and Primary Hydrogen Isotope Effects. The value of k_{-H}/k_2 obtained above implies that no more than 1 part in 200 of the $^+N_2CH_2COO^-$ which is formed in aqueous HCl at pH values below 7 reverts to starting material. Under the same conditions over 99% of the $^+N_2CH_2COO^-$ should result from reaction of the aquated proton with the substrate. Thus the quantity $(H/T)_{prod} \times (T/H)_{solv}$ should be the fractionation factor for the transferring proton in the transition state formed by the aquated proton and the substrate,[4] previously dubbed κ_H/κ_T.[25,26] If our interpretation of the kinetics is correct, κ_H/κ_T should be invariant under pH changes at pH values below 7, and it can be seen that this is so, within the experimental uncertainty.

The comparable quantity obtained in D_2O is κ_D/κ_T. The semiempirical "low temperature" Swain–Schaad relations[27] predict that κ_D/κ_T is $(\kappa_H/\kappa_T)^{0.307}$, or 1.90. The disagreement between this and the experimental value, 1.98, is less than the combined probable errors. A purely experimental value of κ_H/κ_D is given by $(\kappa_H/\kappa_T)/(\kappa_D/\kappa_T)$, and has the value 4.1 ± 0.2. Alternatively, assuming the Swain–Schaad relations hold exactly, (κ_H/κ_D) is $(\kappa_H/\kappa_T)^{0.693}$, which has a value of 4.28 ± 0.05. The difference between these two values is not significant for most purposes, and 4.2 will be adopted as the value for the remainder of this discussion. These results constitute further evidence of the usefulness and reasonable accuracy of the Swain–Schaad relations.[28,29]

With the pH around 10, in the absence of buffer, H_2O is the most important acid, and most $^+N_2CH_2$-COO^- formed goes on to product. Nevertheless, to get $(\kappa_H/\kappa_T)_{H_2O}$ corrections must be made both for reversion and for H^+ acting as the acid. The latter correction is straightforwardly made if it is noted that the product obtained is actually the sum of that generated by H_2O and H^+. Since the tracer quantity of tritium does not measurably influence the rate constants this leads to eq 13. The correction for reversion

$$\left(\frac{T}{H}\right)_{prod} = \frac{(H/T)_{solv}\{k_H(H^+)(\kappa_H/\kappa_T) + k_{H_2O}(\kappa_H/\kappa_T)_{H_2O}\}}{k_H(H^+) + k_{H_2O}} \quad (13)$$

can be made by noting that each $^+N_2CH_2COO^-$ that

(17) J. N. Brønsted, *Chem. Rev.*, **5**, 231 (1928).

(18) C. A. Bunton and V. J. Shiner, Jr., *J. Amer. Chem. Soc.*, **83**, 3214 (1961).

(19) Reference 3, Chapter IV.

(20) C. A. Bunton and V. J. Shiner, *J. Amer. Chem. Soc.*, **83**, 3207 (1961).

(21) J. A. Llewellyn, R. E. Robertson, and J. M. W. Scott, *Can. J. Chem.*, **38**, 222 (1960).

(22) K. T. Leffek, J. A. Llewellyn, and R. E. Robertson, *ibid.*, **38**, 1505 (1960).

(23) V. J. Shiner, M. W. Rapp, E. Halevi, and M. Wolfsberg, *J. Amer. Chem. Soc.*, **90**, 7171 (1968).

(24) M. Eigen and L. DeMaeyer, "Investigation of Rates and Mechanisms of Reactions," Vol. VIII, part II, S. L. Friess, E. S. Lewis, and A. Weissberger, Ed., Wiley-Interscience, New York, N. Y., 1963, p 1031.

(25) M. M. Kreevoy and R. A. Kretchmer, *J. Amer. Chem. Soc.*, **86**, 2435 (1964).

(26) M. M. Kreevoy, P. J. Steinwand, and W. V. Kayser, *ibid.*, **88**, 124 (1966).

(27) C. G. Swain, E. C. Stivers, J. F. Reuwer, Jr., and L. J. Schaad, *ibid.*, **80**, 5885 (1958).

(28) E. S. Lewis and J. K. Robinson, *ibid.*, **90**, 4337 (1968).

(29) M. M. Kreevoy and R. Eliason, *J. Phys. Chem.*, **72**, 1313 (1968).

is formed has a probability of going forward to product given by $k_2/\{k_2 + k_{-H_2O}(OH^-)\}$ and a probability of going back given by $k_{-H_2O}/\{k_2 + k_{-H_2O}(OH^-)\}$. Each time $^+N_2CH_2COO^-$ is formed it has another opportunity to be tritiated. To simplify the algebra abstraction of T was neglected in comparison with abstraction of H. (The isotope effect is actually about 3.) Successively smaller amounts of product have had 2, 3, etc., chances to be tritiated, and no more than three chances have been considered because inclusion of more chances did not change the results significantly. In this way eq 14 was obtained.[30] The corrected value of $(H/T)_{prod}$, $(H/T)_{prod}^{cor}$, was used in eq 13 to obtain $(\kappa_H/\kappa_T)_{H_2O}$. Neither correction was as large as 5%,

$$(H/T)_{prod}^{corr} = \left(\frac{H}{T}\right)_{prod}\left(\frac{A^2 - 3A + 3}{A^2 - AB - 3A + 3B + 3}\right) \quad (14)$$

$$A \equiv k_2/\{k_2 + k_{-H_2O}(OH^-)\}$$

$$B \equiv {}^1/_2k_{-H_2O}(OH^-)/\{{}^1/_2k_{-H_2O}(OH^-) + k_2\}$$

and they were compensatory, so that the final values were close to the experimental values.

In the same way, three values of $(\kappa_H/\kappa_T)_{CH_3COOH}$ were obtained with acetic acid-acetate buffers. $(H/T)_{prod}$ was corrected for acetate ion induced reversion using eq 14 with $k_{-CH_3COOH}(CH_3COO^-)$ in the place of $k_{-H_2O}(OH^-)$, and $(\kappa_H/\kappa_T)_{CH_3COOH}$ was obtained using an equation analogous to eq 13 to correct for the residual H^+-catalyzed reaction. Table VII gives all the κ_H/κ_T values currently available for this reaction.

Table VII: Isotope Effects and Isotopic α's for Various Acids

HA	k_{HA}/k_{DA}	$(\kappa_H/\kappa_T)_{HA}$	$(\kappa_H/\kappa_D)_{DA}$	α_i
H^+	2.3	8.1	4.2[a]	0.30
CH_3COOH		12.4	5.7[b]	
H_2O	3.7	3.0	2.2[b]	0.89

[a] Obtained as described in the text. [b] Obtained from the Swain–Schaad relations and $(\kappa_H/\kappa_T)_{HA}$.

For comparison with the kinetically determined k_{HA}/k_{DA}, values of $(\kappa_H/\kappa_D)_{HA}$ have been calculated using the Swain–Schaad relations. As anticipated,[4] for H^+ κ_H/κ_D is larger than k_H/k_D. This discrepancy has two causes.[4] The transferring proton originates in the H_3O^+ unit of $H^+(aq)$, so κ_H/κ_D must be multiplied by the H_3O^+ fractionation factor, l (0.69), to get the primary hydrogen isotope effect, $(k_H/k_D)_I$, which has the value 2.9 in this case. The solvent isotope effect also is modified by a secondary isotope effect, $(k_H/k_D)_{II}$, caused by the partial transformation of the other two protons of the H_3O^+ unit into water protons. Equation 15 gives $(k_H/k_D)_{II}$, which has a value of 0.80. Equation 16 shows its use to calculate a value of 0.30 for an "isotopic α," α_i[4,31]

$$k_H/k_D = (k_H/k_D)_I \times (k_H/k_D)_{II} \quad (15)$$

$$\alpha_i = \frac{\log (k_H/k_D)_{II}}{2 \log l} \quad (16)$$

For water there is no reason to regard κ_H/κ_D as different from $(k_H/k_D)_I$, but it still differs substantially from k_{H_2O}/k_{D_2O}. This is understandable if it is recalled that the isotopic ratio of autoprotolysis constants for water, K_{H_2O}/K_{D_2O}, is 7.35[32] while l^{-3} is 3.05. Since $OH^-(aq)$ is the only thing, other than $H^+(aq)$, formed when water ionizes as an acid, the product over all the fractionation factors of $OH^-(aq)$ is $1/(l^3 \times 7.35)$, or 0.415. In the transition state in which H_2O acts as an acid, $OH^-(aq)$, with its characteristic fractionation factors, must be partially formed from water, so that k_{H_2O}/k_{D_2O}, which includes all the solvent isotope effects, is expected to be larger than $(k_{H_2O}/k_{D_2O})_I$, which measures only the isotope effect on the transferring proton. An equation exactly analogous to eq 15 can be used to obtain a value of 1.70 for $(k_{H_2O}/k_{D_2O})_{II}$, the secondary isotope effect attending proton transfer from water.

To interpret $(k_{H_2O}/k_{D_2O})_{II}$ in terms of an α_i, models and individual fractionation factors are required for $OH^-(aq)$ and for the transition state. Neither of these is yet definitively available. However, the trihydrated model for $OH^-(aq)$[33,34] seems reasonable. This leads to two kinds of positions which potentially have nonunity fractionation factors: the three strongly hydrogen-bonded protons of the inner solvation shell, and the unique proton of OH^-. In the absence of experimental evidence we have arbitrarily neglected the latter, which makes ϕ_{OH}, the fractionation factor for each of the three hydrogen-bonding protons, 0.75. This treatment is, at least, self-consistent, as the model chosen for $OH^-(aq)$ is very similar to that now generally accepted for $H^+(aq)$, and the resultant ϕ_{OH} is similar to l. Following these same general ideas, if in the transition state, OH^- is being generated directly adjacent to the substrate,[35] it will have two isotopically sensitive positions. Then $(k_{H_2O}/k_{D_2O})_{II}$ should be between 1 and $(1/\phi_{OH})^2$, 1.81. The experimental value does fall within these limits. If eq 17, which is analogous to 16 is used to evaluate α_i for H_2O, it is 0.89.

(30) A complete derivation of eq 15 is given in the Ph.D. thesis of Dr. D. E. Konasewich, University of Minnesota, Dec 1969, pp 123, 124.

(31) A. J. Kresge, *Pure Appl. Chem.*, 8, 243 (1964).

(32) L. Pentz and E. R. Thornton, *J. Amer. Chem. Soc.*, 89, 6931 (1967); also other papers cited therein.

(33) T. Ackermann, *Z. Phys. Chem.* (Frankfurt am Main), 27, 34 (1961).

(34) B. R. Agarwal and R. M. Diamond, *J. Phys. Chem.*, 67, 2785 (1963).

(35) M. M. Kreevoy and J. M. Williams, Jr., *J. Amer. Chem. Soc.*, 90, 6809 (1968).

$$\alpha_i = \frac{\log (k_{H_2O}/k_{D_2O})_{II}}{-2 \log \phi_{OH}} \quad (17)$$

A detailed discussion of the relations between α, α_i, acidity, and isotope effects will not be undertaken at this time, because of the paucity of results. However, it may be noted that these results seem to foreshadow district curvature in a plot of log k_{HA} against log K_{HA} for general acids of strength between that of H_2O and H^+, and primary isotope effects passing through a maximum. These predictions are being tested, and results will be reported in subsequent publications.

Experimental Section

Materials and Solutions. Potassium diazoacetate was prepared by the method of Muller.[36] Its purity, determined gasometrically, was at least 90%. The impurities included a trace of KOH and some polymer. Water used was deionized by means of ion-exchange resins and freed of CO_2 by boiling. Carbonate-free NaOH (Merck, reagent grade) was made up by pipetting a 50% solution away from the insoluble Na_2CO_3 and diluting it with carbonate-free water. It was standardized in the usual way against potassium hydrogen phthalate (Mallinckrodt, analytical reagent). Phenol (Mallinckrodt, analytical reagent) had mp 38–40° (reported[37] mp 40.70–40.95°). It was assumed to be pure, and its solutions were made up gravimetrically. The concentration of acetic acid (DuPont, reagent grade) solutions was determined by titration with standard NaOH. Sodium deuterioxide in D_2O was prepared by slow addition of sodium to D_2O in a flask cooled by an ice–water bath. The head space was continuously purged with N_2 during addition to prevent the accumulation of D_2. After preparation this solution was handled like concentrated NaOH. Deuterium oxide was obtained from Bio-Rad Laboratories and had a nominal isotopic purity of 99.87%. Tritiated water was purchased from International Chemical and Nuclear Corp.

Rates. When the pH was greater than 10, rates were measured by standard spectrophotometric technique[38] in a Beckman DU spectrophotometer. The cell compartment was maintained at 25.0 ± 0.1° by water from a constant temperature water bath circulating through jackets. The temperature of the reaction mixtures was verified by measurements in the cells. Reactions were followed for at least one half-life. For the slower reactions infinite time optical densities were obtained by adding a drop of concentrated HCl to the spectrophotometer cell containing the reaction mixture.

In unbuffered solutions at pH values below 10 severe problems in pH control would be encountered, due to CO_2 absorption and desorption, if rates were measured by conventional techniques. In the present work these were overcome by carrying out the reaction in a water-jacketed vessel outside of the spectrophotometer in which the pH was maintained at a constant value ±0.01 by a Radiometer pH-stat. From the reaction mixture, solution was continuously pumped through a flow-through cell in the Beckman DU spectrophotometer, and the progress of the reaction was monitored by following the decrease in substrate absorption. The pH was measured precisely with a Radiometer scale expander before and after each reaction and the average was taken as the pH of the reaction. The values before and after did not differ by more than 0.01 units. The function of the pH-stat in this method is just to compensate for CO_2 lost or gained—the reaction itself does not consume or produce acid. As many as three successive kinetic experiments could be carried out in the same solution in this way, simply by adding more substrate after the first batch was more than 99.9% exhausted. Such experiments gave k_1 values differing by no more than a few per cent, and randomly, showing that general acid catalysis by carbonic acid is insignificant. Rates measured in this way had half-lives between 20 sec and 300 min.

For HCl and acetic acid catalyzed reactions the substrate concentration was monitored by means of the strong diazoacetate bond at 258 mμ. Phenol and phenolate absorb strongly at that wavelength, however, so the much weaker absorption at 350 mμ had to be used. At that wavelength about 3×10^{-3} M of substrate were required to get changes of over 0.1 in absorbance. As a result bubbles of nitrogen formed on the cell windows and had to be dislodged periodically. This difficulty was not encountered when the shorter wavelength was used, because the initial substrate concentration was at least an order of magnitude lower.

In the case of the D_2O data a small correction was applied to each observed value of k_1 because of the adventitious presence of 0.01 to 0.03 atom fraction of H in the reaction mixtures. The fraction H was determined by the method of Kreevoy and Straub.[39] In the pD range 12–14, the equations of Purlee[40] were assumed to govern the relation between k_1^x and the atom fraction H; in the range 9–7 the relation of Gold[41] was assumed, with an α of 0.3; at pD ~10, the relation was assumed to be linear. (The rate constant in water with an atom fraction deuterium of x is k_1^x.) The differences between k_1^x and k_1^D never exceeded 5% and were, more typically, 2–3%. The significance and evaluation of $(H^+)\gamma_+\gamma_-$ and $(D^+)\gamma_+\gamma_-$ are described in the Discussion section.

Product Collection. In product collection experiments involving HCl, 50 ml of tritiated water was brought to the appropriate acid concentration by the addition of HCl. For experiments at pH 5.5 this was

(36) K. Muller, *Ber.*, **41**, 3136 (1908).

(37) H. G. Boit, "Beilsteins Handbuch der organischen Chemie," 3rd Suppl., Vol. VI, part 2, Springer-Verlag, Berlin, 1965, p 508.

(38) M. M. Kreevoy, *J. Amer. Chem. Soc.*, **81**, 1099 (1959).

(39) M. M. Kreevoy and T. S. Straub, *Anal. Chem.*, **41**, 214 (1969).

(40) E. L. Purlee, *J. Amer. Chem. Soc.*, **81**, 263 (1959).

(41) V. Gold, *Trans. Faraday Soc.*, **56**, 255 (1960).

done with the pH-stat. From these solutions 5 ml was then removed for later determination of tritium and (in the case of the D_2O experiments) hydrogen.[39] About 0.2 g of substrate was added to the rest, and several minutes were allowed for reaction, with the temperature maintained at 25.0 ± 0.1° by means of a water jacket around the reaction vessel.

The kinetic experiments indicate that the reaction proper is over in a fraction of a second under these conditions. The reaction period was allowed to ensure that all the substrate had dissolved. After the reaction was complete an equivalent quantity of $CaCl_2$ was added, and the reaction mixture was neutralized with KOH. The tritiated water was removed by evaporation and 200 ml of untritiated water was added to remove most of the exchangeable tritium. Most of this water was also removed by evaporation. The $(HOCH_2COO^-)_2Ca^{2+}$ was recrystallized from water twice and each time washed with ethanol. Further recrystallization was shown not to change the radioactivity of the product. It was then heated at 110° for 12 hr to remove volatile solvents. Nonradioactive material prepared in this way was subjected to elemental analysis to establish its purity.

Anal. Calcd for $C_4H_6O_6Ca$: C, 25.21; H, 3.17; Ca, 21.00. Found: C, 24.96; H, 2.95; Ca, 20.84.

For experiments involving acetic acid the procedure was the same, except that an appropriate amount of acetic acid was first added by pipet, and the solution was then brought to the desired pH by adding NaOH with the pH-stat. For experiments in unbuffered solution at pH 10.4, half-lives were about 300 min. These reaction mixtures were brought to the desired pH after the addition of the substrate and thereafter maintained at that pH for the duration of the experiment by means of the pH-stat. A reaction period of about 3000 min was allowed for these experiments. After the completion of the reaction period, products from experiments involving acetic acid, and those from the high pH experiments, were treated exactly like those from the HCl experiments.

Solutions for counting contained 10 ml of the dioxane "cocktail,"[42] 1 ml of 0.1 *M* HCl (to solubilize the calcium salt) and about 5 mg of calcium salt. Each experiment required the counting of three such solutions: one made up with the radioactive calcium glycolate and nonradioactive water; one made up with nonradioactive calcium glycolate and radioactive water; and a blank, for the determination of background. The concentration of calcium glycolate and HCl in the three solutions did not differ by more than 2%. The samples were counted in a Beckman liquid scintillator (Model LS 200 B) for two 50-min intervals. External standard counting efficiencies were determined for each sample, and observed counting rates were corrected for these counting efficiencies if they were between 0.85 and 1.15. If the counting efficiency was outside of these limits, the result was discarded.

Acknowledgments. This work was supported, in part, by the National Science Foundation through GP-7915. The paper was written while M. M. Kreevoy was a participant in the Cultural Exchange Program between the U. S. National Academy of Science and the Yugoslav Council of Academies. He wishes to thank the Institute "Rudjer Bošković" and Professor D. E. Sunko for their hospitality. D. E. Konasewich wishes to thank E. I. du Pont de Nemours, Inc., Mobil Oil Inc., and General Mills, Inc., for fellowships held at various times.

(42) A. R. Friedman and E. Leete, *J. Amer. Chem. Soc.*, **85**, 2141 (1963).

Intramolecular Proton Transfer Reactions in Excited Fluorescent Compounds

by David L. Williams and Adam Heller*

The Exploratory Research Laboratory, Bayside Research Center of General Telephone & Electronics Laboratories Inc., Bayside, New York 11360 *(Received July 17, 1970)*

Intramolecular hydrogen transfer reactions in excited fluorescent molecules lead to unusually large Stokes shifts. The photochemical stability of compounds undergoing such reactions is also improved. As a result fluorescent materials of desirable properties are obtained. In crystalline 2-(2′-hydroxyphenyl)benzothiazole and in its derivatives, a proton is transferred in the excited state from an oxygen to a nitrogen atom. The compound and its derivatives have typical Stokes shifts of 7000 cm^{-1} and quantum yields to 0.57. The photochemical stability of the compounds is greatly improved relative to N-methylated and other derivatives in which no hydrogen transfer can take place.

Introduction

Many crystalline "azole" compounds having the general structure

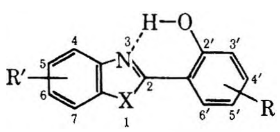

are bright, uv-stable fluorescers where X = S, O, or NH giving, respectively, benzothiazoles, benzoxazoles, or benzimidazoles. We have prepared over twenty of these azole derivatives and studied their solution properties and solid-state spectral characteristics. The compounds are generally colorless, but yield visible fluorescence with long-wavelength uv excitation, the particular spectral characteristics being dependent on the nature and position of the various substituents, R and R′. It is our purpose to present a concerted model of the behavior of these azoles subsequent to excitation and, in particular, to elucidate the role played by the intramolecular hydrogen bond in stabilizing the molecules toward ultraviolet degradation.

Experimental Section

1. Materials. All azoles were prepared by essentially the same procedure, a one-step condensation reaction between a salicylic acid derivative and *o*-aminothiophenol (or derivative). The chemicals, obtained from chemical suppliers, were mixed in equimolar amounts in hot toluene. An equimolar amount of PCl_3 was added dropwise, and the solution was refluxed for 2 hr. The crystals formed on cooling were washed, filtered, and recrystallized from acetic acid. Yields for most azoles were about 50%. For **15**, the *N*-methyl derivative (see Table I for identification of compounds), 10 ml of a 1:1 molar mixture of 2-(2′-hydroxphenyl)-benzothiazole and dimethyl sulfate were heated in an oil bath at 115° for 30 min. The clear, light-amber solution that resulted was cooled and about 75 ml of dry ether was added, and then 30 ml of distilled water. This solution was then made basic with sodium hydroxide. The deuterated azoles were made from the parent compounds by exchange and recrystallization from deuterated acetic acid.

Pure crystalline powders were used in most measurements. When plastic solutions were used, liquid solutions in partially polymerized methyl methacrylate containing 10% butyl phthalate were prepared. Polymerization was completed by adding 0.2% of benzoyl peroxide and heating in a sealed, evacuated ampoule at 60° for 3 hr.

2. Stability Studies. The crystalline samples, homogeneously dispersed over a support material, were placed in quartz tubes which were set in a circular holder that slowly rotated around a Hanovia 977B-1 1000-W mercury–xenon arc lamp. Between the lamp and the samples was a circular quartz cooling jacket through which distilled water was pumped. The entire system was encased in an aluminum tank in which air was continuously drawn for cooling and removing ozone. This arrangement ensured that all samples were equally and uniformly irradiated despite minor fluctuations in lamp output or inhomogeneities in radiation distribution. Operating conditions for the nominal 1000-W lamp were 28 A and 14 V, leading to an actual input power of 392 W. Approximately 30% of the lamp output occurs below 4000 Å, and the lamp is assumed to be 20% efficient. This leads to a 23.5-W output of ultraviolet radiation, or 0.075 W/cm^2 on the samples which were at a distance of 5 cm from the arc.

3. Fluorescence Spectra. Spectra of the crystalline solid powders were recorded with a Jarrell-Ash 0.5-m Ebert scanning spectrometer fitted with a 1180 lines/mm grating blazed at 5000 Å. The excitation source was a Hanovia 977B-1 1000-W mercury–xenon arc lamp coupled with a Schoeffel Instrument Company miniature quartz prism monochromator; excitation was usually at 3663 Å. Fluorescence was detected by an ITT FW130 focusing photomultiplier (S-20 response) operated at a potential of 1600 V. Prior to striking

* To whom correspondence should be addressed.

Table I: Emission Characteristics of Azoles

Compd		λ_{max}, mμ	Quantum efficiency, %	Relative photochem. stability[a]
	I. X = S Benzothiazoles			
1	2′-OH	517	30.7	10
1D	2′-OD	516	21.0	
2	2′-OH, 5′-OCH_3	575	13.5	36
2D	2′-OD, 5′-OCH_3	576	8.3	
3	2′-OH, 3′-OCH_3	529	21.8	43
4	2′-OH, 5′-NH_2	543	37.6	
5	2′-OH, 5′-Br	523	2.2	50
6	2′-OH, 5′-Cl	527	25.4	45
7	2′-OH, 3′-NO_2	537	~1	0
8	2′-OH, 3′-Cl, 5′-Cl	536	36.5	30
9	2′-OH, 5′-NO_2	518	6.5	0
10	2′-OH, 3′-NO_2, 5′-NO_2, 5-NO_2	Thermochromic and photochromic		
11	2′-OH, 5′-OCH_3, 5-Cl	533	5.8	
12	2′-OH, 5′-CH_3	532	57	97
13	2′-OH, 3′-$C(CH_3)_3$, 6′-CH_3	523	36.9	8.5
14	2′-OH, 3′-biphenyl	550	28.9	55
15	2′-O^-, N^+-CH_3	604	5.4	0
16	No substituent	No fluorescence		
17	3′-OH	No fluorescence		
18	4′-OH	No fluorescence		
19	2′-OCH_3	No fluorescence		
	II. X = O Benzoxazoles			
20	2′-OH	506	42.0	38
20D	2′-OD	503	34.0	
	III. X = NH Benzimidazole			
21	2′-OH	462	3.5	

[a] Per cent residual brightness after 26 hr of illumination at 0.075 W/cm^2 of ultraviolet radiation.

the photomultiplier, the emission was chopped at 200 Hz, and the modulated signal was amplified by an Electronics, Missiles, and Communications, Inc. Model RJB Lock-In amplifier and was recorded. The spectral response of the system was determined by using a standarized NBS tungsten filament lamp of known output. A computer program was written which corrected the spectra and plotted out the true fluorescence emission curves. The empirical curve was processed with a Calma VIP 480 digitizer.

The fluorescence spectra were obtained in an apparatus allowing front surface excitation. The exciting radiation was diffused to a hemispherical reflecting surface with a hole (for viewing the sample) in its center. The sample was placed in the focal point of the hemisphere. In measurements down to liquid nitrogen temperatures cold nitrogen, obtained by boiling off the liquid, was passed through the quartz chamber in which the sample was held. For measurement of spectra at lower temperatures a special liquid helium Dewar with windows at 90° was used. Helium boiling off the liquid was used for cooling.

4. Quantum Efficiencies. Quantum efficiencies of the solid powders were determined by reference to a known NBS standard luminescent compound, magnesium tungstate, and to sodium silicate whose efficiency is wavelength independent from 2537 to 3550 Å. This, coupled with measurements of relative excitation intensities at 3550 and 3663 Å, enabled a determination of quantum efficiency of the crystalline azoles at 3663 Å based on a value of 43.4% for sodium silicate.

5. Excitation and Infrared Spectra. The excitation spectra of the powders were taken on a Hitachi MPF-2A fluorescence spectrophotometer. The infrared spectra were taken on a Perkin-Elmer 627.

6. Decay Rates. A capillary (1 mm i.d.) lamp filled with 20 atm of hydrogen, and a 0.5-cm gap between the electrodes was used to obtain pulses of light for the excitation of fluorescence. The decay time of the pulse to $1/e$ of the peak intensity was about 1 nsec, but the light pulse had a "tail" of about 8 nsec, limiting the range of our measurements to decay times longer than 10^{-8} sec. The lamp was pulsed at 10^3 cps. The light was filtered by a filter combination limiting the radiation reaching the sample to the ultraviolet. The emitted light from the sample was focused on a fast photomultiplier (less than 1-nsec rise time) directly connected to a fast Tektronics sampling scope, Model 556 with a 1S1 sampler. The rise time of the sampling scope system was less than 100 psec.

Results and Discussion

1. Proton Transfer. The phenomenon of proton transfer in excited states has been firmly established by studies on the thermochromic and photochromic properties of anils of *o*-hydroxybenzaldehydes,[1-6] all having the basic substructure

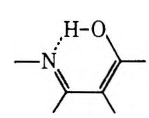

Cohen and Flavian[1] proposed such a transfer process for the luminescence of solutions of two azoles, 2-(2′-hydroxyphenyl)benzothiazole (**1**) and 2-(2′-hydroxyphenyl)benzoxazole (**20**).

The stable ground-state configuration of the benzothiazole shown above has the proton predominantly on the oxygen, whereas the "stable" excited singlet configuration, S′*, has the proton on the nitrogen. The molecule initially formed in the excited state, S*, can be regarded simply as a vibrationally excited form of

(1) M. D. Cohen and S. Flavian, *J. Chem. Soc. B*, 317 (1967).
(2) M. D. Cohen and G. M. J. Schmidt, *J. Phys. Chem.*, **66**, 2442 (1962).
(3) M. D. Cohen, *J. Pure Appl. Chem.*, **9**, 567 (1964).
(4) R. S. Becker and W. F. Richey, *J. Amer. Chem. Soc.*, **89**, 1298 (1967).
(5) W. F. Richey and R. S. Becker, *J. Chem. Phys.*, **49**, 2092 (1968).
(6) R. Potashnik and M. Ottolenghi, *ibid.*, **51**, 3671 (1969).

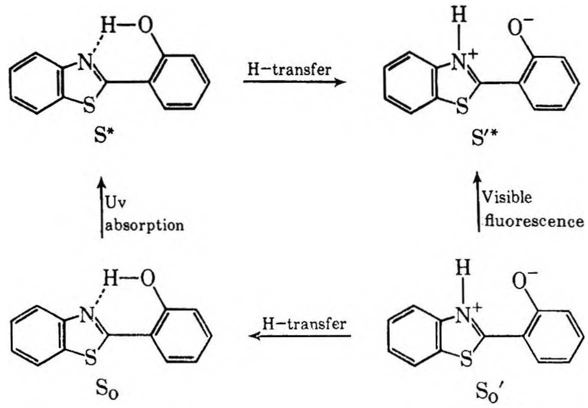

Basic Mechanism for Fluorescence of **1**

S′*. Vibrational relaxation by loss of the excess vibrational energy to the environment is rapid. The same type of argument can be made for the ground state wherein S'_0 is viewed as a vibrationally excited form of S_0.

The transfer of the proton in the excited state is evidenced by a large Stokes shift for the azoles (~7400 cm^{-1}). The change in the electronic distribution effecting the transfer has been demonstrated by studies of pH changes in excited states.[7-10] For excited singlets, phenols become considerably stronger acids and *N*-heterocyclics become stronger bases; changes for excited triplets are several orders of magnitude less.[10]

2. Uv Stability. Instability toward ultraviolet radiation is simply a measure of the probability of photochemical bond breaking upon excitation by uv light. If, in fact, excess energy is localized in one of a few vibrational modes for a finite length of time, the particular bond may be expected to rupture. However, if the process is reversible, no permanent degradation occurs; such a reversibility is built into an intramolecular hydrogen bond. An internal mechanism is thus provided to stabilize a molecule against uv degradation.

Recent discussions of photochemical reactions[11,12] have indicated that excess electronic energy is preferentially coupled into stretching vibrations with high vibrational energies, in particular, the stretching modes involving hydrogen with carbon, nitrogen, and oxygen. It has been theorized that acceptance of electronic energy may incipiently involve only one stretching vibration of a hydrogen atom, and also that proximity to the center of electronic excitation is a factor influencing energy transfer.[12] Furthermore, the larger the anharmonicity[13] of the vibration or the displacement of nuclei upon excitation,[14] the greater the Franck–Condon overlap, and thus the larger the probability of a stretching mode being activated.

In light of these ideas, it should be expected that excess electronic energy would flow, at least initially, into the stretching vibration of an intramolecularly bonded proton between an oxygen and nitrogen in molecules such as the azoles under discussion. For an $n \rightarrow \pi^*$ transition, the proton is close to the center of electronic excitation, and a vibration between two different locations would be expected to be exceedingly anharmonic. Furthermore, because of the changes of the acidities of the phenol and the nitrogen, the hydrogen nuclei change their equilibrium position upon excitation. Hence, stability toward ultraviolet radiation can be incorporated into a molecule by a judicious choice of potential energy acceptors.

3. Spectral Characteristics of Crystalline Azoles. Table I lists the various azoles studied, their fluorescence wavelength maxima, quantum efficiencies, and relative photochemical stability. The actual stability figures are given in terms of per cent residual brightness after 26-hr illumination at 0.075 W/cm² uv radiation. This would correspond to 1600 days using a 15-W black light at a distance of 36 in.

The fluorescence spectra of all the azoles are similar; that for 2-(2′-hydroxyphenyl)benzothiazole (**1**) is given in Figure 1. An important point is the lack of any observable fluorescence emission for **16**, **17**, **18**, and **19** (see Table I), none of which has a hydroxyl group in the 2′ position. **17** and **18** have no hydroxyl group and **19** has a 2′-methoxy group. From these observations, it appears that a hydroxyl group in the 2′ position is a necessary requirement for fluorescence.

There is an indication in almost all the azole spectra that there are actually two broad overlapping bands, the second band being located some 800–1000 cm^{-1} to the red relative to the first. This is best manifested in the spectrum of **3** shown in Figure 2. Certain derivatives, namely, **7**, **9**, and **14**, show almost no indication of a second peak. The origin of this second peak will be indicated later.

The oxazole, 2-(2′-hydroxyphenyl)benzoxazole (**20**), has a higher quantum efficiency and greater uv stability than **1**, its thiazole counterpart. Its fluorescence emission, shown in Figure 3, is more structured than that of the thiazoles, having four bands instead of two.

The spectrum of the imidazole, 2-(2′-hydroxyphenyl)-benzimidazole (**21**), is given in Figure 4. It is an unsymmetrical single peak shifted well into the blue from either **1** or **20**. It is a relatively weak emitter.

An excitation spectrum of **1** is given in Figure 5. It is representative of the excitation spectra of all the azoles listed in Table I, having a maximum at approximately 3750 Å.

(7) A. Weller, *Z. Elektrochem.*, **60**, 1144 (1956).
(8) A. Weller, *ibid.*, **61**, 956 (1957).
(9) N. Mataga, Y. Kaifu, and M. Koizumi, *Bull. Chem. Soc. Jap.*, **29**, 373 (1956).
(10) G. Jackson and G. Porter, *Proc. Roy. Soc., Ser. A*, **260**, 13 (1961).
(11) N. C. Yang, S. P. Elliott, and B. Kim, *J. Amer. Chem. Soc.*, **91**, 7551 (1969).
(12) A. Heller, *Mol. Photochem.*, **1**, 257 (1969).
(13) W. Siebrand and D. F. Williams, *J. Chem. Phys.*, **49**, 1860 (1968).
(14) R. Englman and J. Jortner, *J. Luminescence*, **1,2**, 134 (1970).

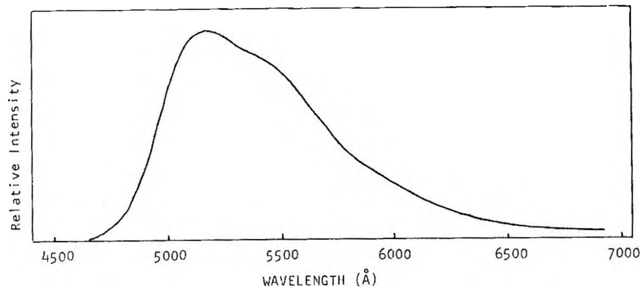

Figure 1. Fluorescence spectrum of 2-(2′-hydroxyphenyl)benzothiazole (**1**).

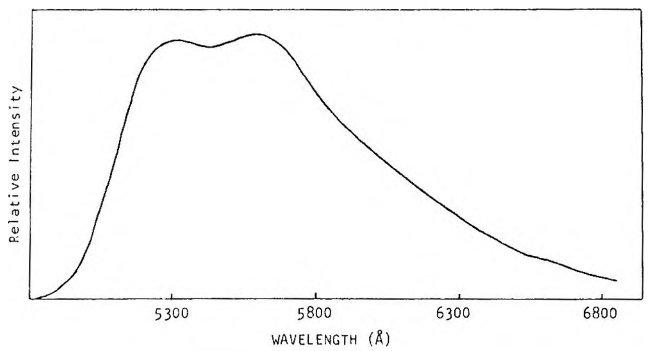

Figure 2. Fluorescence spectrum of 2-(2′-hydroxy-3′-methoxyphenyl)benzothiazole (**3**).

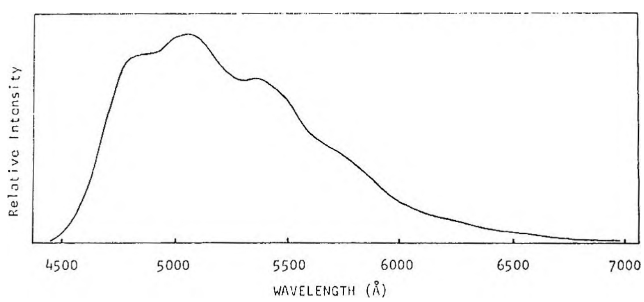

Figure 3. Fluorescence spectrum of 2-(2′-hydroxyphenyl)benzoxazole (**20**).

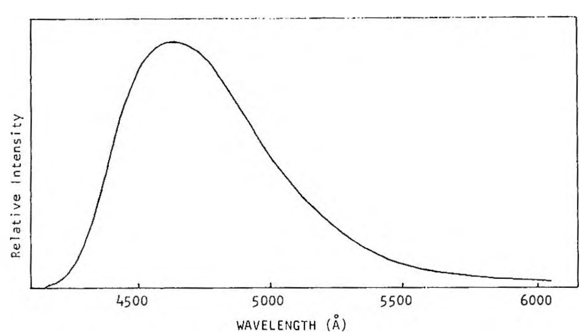

Figure 4. Fluorescence spectrum of 2-(2′-hydroxyphenyl)benzimidazole (**21**).

4. Decay Characteristics. The emission of each compound investigated decays with a rate exceeding 10^8 sec^{-1}, the fastest rate that we could measure on our apparatus. There was no evidence for any slower component (phosphorescence) at either room or liquid nitrogen temperatures in the crystalline materials. Solutions of the compounds in plastics, in which phosphorescence is usually observable at room temperature, did not show phosphorescence.

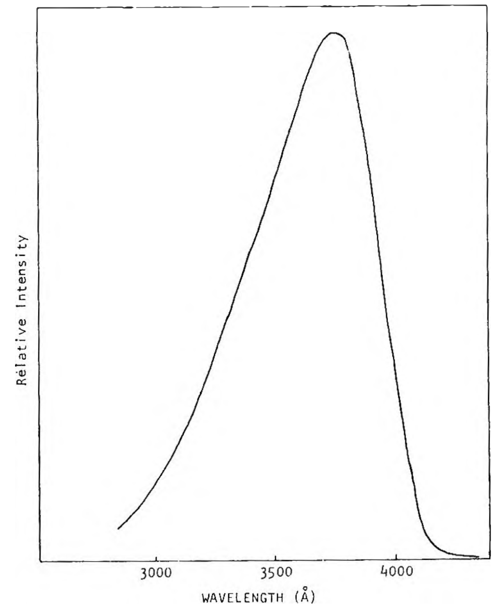

Figure 5. Excitation spectrum of 2-(2′-hydroxyphenyl)benzothiazole (**1**).

5. Mechanisms of Fluorescence and Uv Stabilization. The combination of large Stokes shift and unsymmetrical fluorescence band shape are consistent with the basic proton transfer mechanism illustrated previously. Also, the lack of fluorescence in molecules lacking a hydroxyl group in the 2′ position confirms the importance of a proton being associated with the nitrogen as part of the luminescence mechanism.

To further illustrate the function of the intramolecularly bonded proton, an *N*-methyl derivative of **1** was prepared.

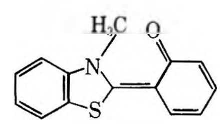

6-[3-Methyl-2(3*H*)-benzothiazolylidene]cyclohexa-2,4-dienone

This compound, **15**, exists in two distinct forms (*vide infra*), a yellow modification stabilized by water and a dry-stable orange modification. The yellow, wet-stabilized form fluoresces yellow-green, and the orange, dry-stabilized form, fluoresces orange. However, neither form is stable toward uv radiation, both degrading very rapidly. This is a further indication that the facile transfer of a proton from oxygen to nitrogen is the key to stability. It is, however, not absolutely essential for luminescence. Lacking any substituent on the nitrogen in the excited state, the molecules do not fluoresce. The fluorescence of the *N*-methyl derivative

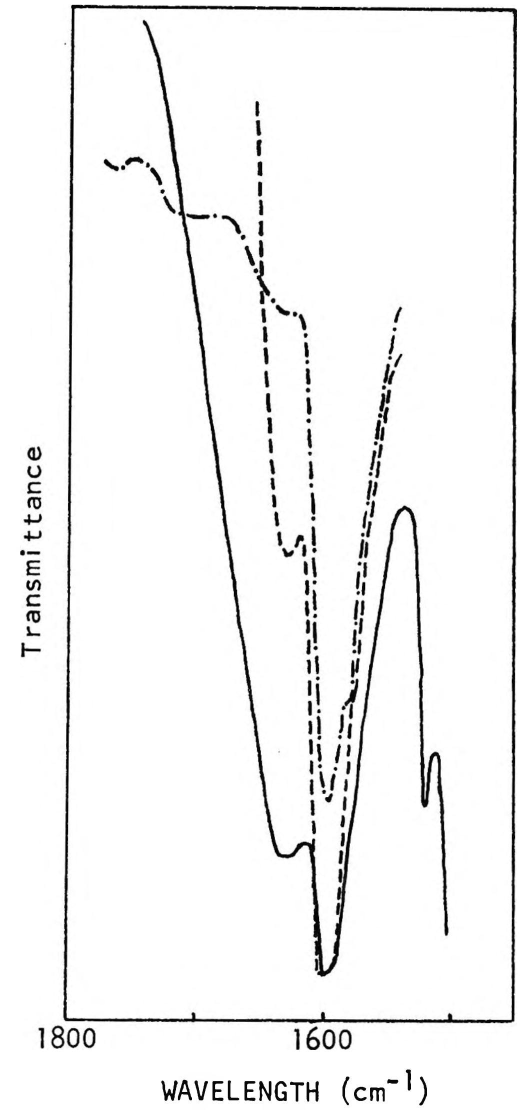

Figure 6. Infrared spectra of the two modifications of **15**: (a)———, recrystallized from water; (b)- - - - -, same as (a) after having dried in spectrometer; (c)-·-·-·-, recrystallized from anhydrous CH_3CN.

demonstrates that the substituent on nitrogen need not be hydrogen.

The configuration having the proton bonded to the nitrogen may be written either as an ionic entity (the previously designated S′ state) or in the form

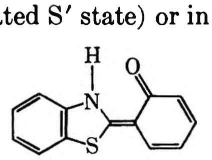

S′ Quinoid (Q′)

which may be thought of as either a tautomer of the ionic form S′, or if there is a slight change in molecular configuration, as a distinct quinoid species derived from S′. In addition, with the molecule in the S′ form, there is the possibility of rotation about the C_2–$C_1{}'$ bond yielding a "trans" species labeled S″. This S″ state will also have a corresponding quinoid form

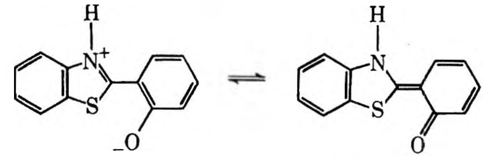

S″ S″ Quinoid (Q″)

Evidence for the existence of a quinoid species is derived from the properties of **15**, the *N*-methyl derivative. Its two modifications, the wet-stabilized yellow form and the dry-stabilized orange form are completely interconvertible. Infrared spectra were taken of each form, and the results are given in Figure 6. The yellow modification has a strong band at 1635 cm^{-1} which is assigned to a C=O stretch. Upon drying, the band becomes greatly reduced in intensity and the compound turns orange. A very dry, recrystallized sample of the orange modification shows no band at 1635 cm^{-1}. (An intense band at 1605 cm^{-1} is found in both the yellow and orange modifications and is assigned to the aromatic phenyl-ring vibrations.) The structures and mechanism proposed to explain the behavior of **15** are shown in Figure 7.

Separation of charge is facilitated by a medium of high dielectric constant, and thus the yellow modification is assigned the "trans" configuration with the quinoid form predominating. The dry, orange modification is assigned the "cis" configuration with the ionic form predominating. The possible close approach of the positive and negative charges in the "cis" ionic form is the stabilizing factor for the orange modification.

The reason the ionic and quinoid forms are distinct entities and not simply resonance forms of each other can be seen with the aid of molecular models. The ionic form is planar. However, even though the quinoid form can be planar, it is less strained in a slightly bent configuration, the bend occurring along an axis formed by CH_3, N, and S.

To further confirm the above hypothesis, the following two compounds were prepared and studied

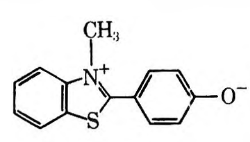

15a

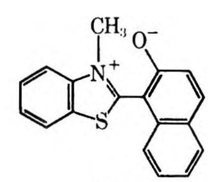

15b

15a cannot have "cis" and "trans" forms. The possible configurations are shown in Figure 8. The crystals show a very slight change in color upon drying under vacuum, going from a yellow-orange to a yellow-brown. However, this change is far less dramatic than for **15** itself. The infrared spectrum shows a strong maximum at 1600 cm^{-1} attributable to the aromatic ring and a very weak shoulder at 1630 cm^{-1} when the compound is very dry. The shoulder is more pronounced

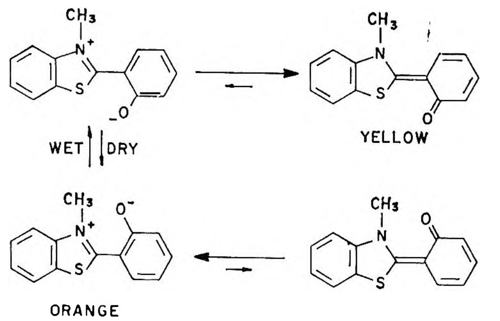

Figure 7. Structures and mechanism of **15**.

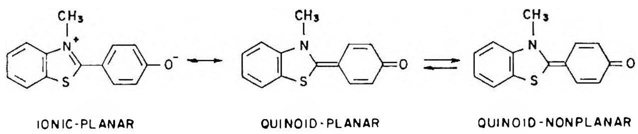

Figure 8. Structures of **15a**.

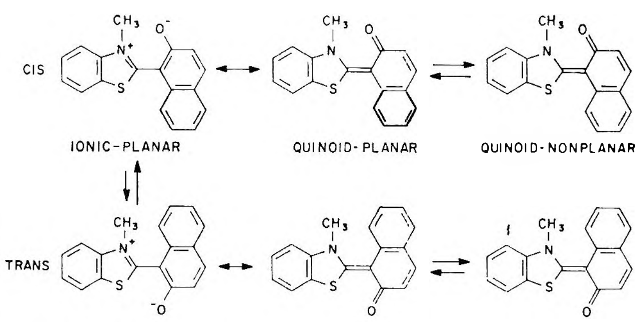

Figure 9. Possible configurations for **15b**.

when the compound is wet. Both have intense bands at 1250 cm^{-1}, the region where aromatic ethers and phenols absorb (C–O). This would seem to indicate that there is very little quinoid form present, most probably that which can be detected being a small amount of the nonplanar configuration in equilibrium with the ionic form.

The possible forms for **15b** are shown in Figure 9. The "trans" forms are all improbable for steric reasons, and indeed, only an orange-red modification is found, similar in color to the orange, dry form of **15**. There is a strong band at 1619 cm^{-1} which is ascribed to aromatic ring vibrations and not C=O stretching. Also, at 1250 cm^{-1} there is a very intense absorption, most probably due to C–O. Evidence therefore, indicates the dominant form to be the "cis" ionic configuration.

With the above information, it is possible to construct a more comprehensive picture of the processes occurring in the azole compounds. This is presented in Figure 10. The ground-state molecule, S_0, absorbs a photon in the ultraviolet and assumes an excited state, S*, having essentially the same molecular configuration as S_0. In this state, the hydroxyl proton is more acidic and shifts to reside predominantly on the nitrogen. This is the excited molecule S′*. For most

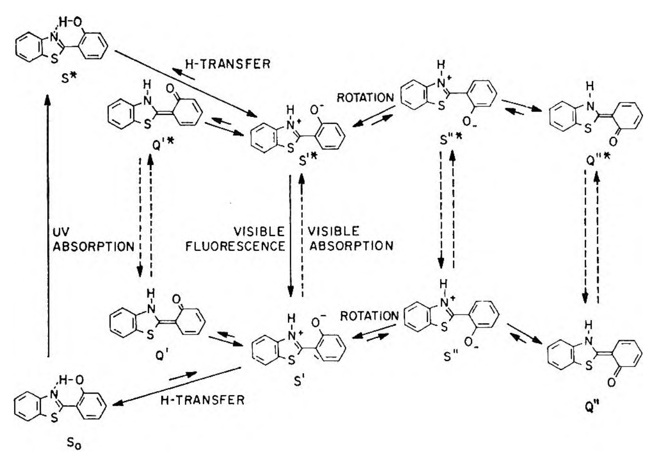

Figure 10. Reaction sequence and species involved in the luminescence of 2-(2′-hydroxylphenyl)benzothiazole and related azoles. The transitions indicated by solid lines have been established; those indicated by broken lines are tentative.

of the azoles, it is this state which emits the visible fluorescence, decaying to the ground-electronic state S′ with the proton remaining on the nitrogen. However, in the ground state, the configuration with the proton situated on the oxygen is the stable form, and the molecule thermally relaxes back to S_0, thereby completing the cycle.

As has been shown, there are other configurations possible, and depending on activation energies and stabilizing influences, either intramolecular or intermolecular, the azole system may follow a different route. There is the possibility of a rotation about the C_2–C_1' bond to form a "trans" state although the barrier for this would be expected to be considerable in the solid state. However, stabilizing factors could make the process energetically favorable, and solid-state isomerism has been postulated for related systems.[2] Such isomerism is postulated to explain the behavior of **15**, the *N*-methyl compound.

The S′* state may also assume the nonplanar quinoid form, again as postulated as part of the mechanism for **15**. The stability of this form or the activation energy for its formation are difficult to assess.

The processes of Figure 10 may be depicted in terms of potential energy curves as is shown in Figure 11. The diagram was constructed with the following points in mind. First, the shapes of the absorption and the emission spectra suggest that the excited-state minima are located vertically above their corresponding ground-state minima. Second, the energy differences between the ground states and the excited states are shown to correspond to the large Stokes shift between the ultraviolet absorption and the visible emission spectra. Insufficient information is available to calculate actual barrier heights. However, the data do allow some qualitative conclusions to be reached. The greatest uncertainty is the size of the barrier between S* and S′* (and also between S′ and S_0), and an attempt to

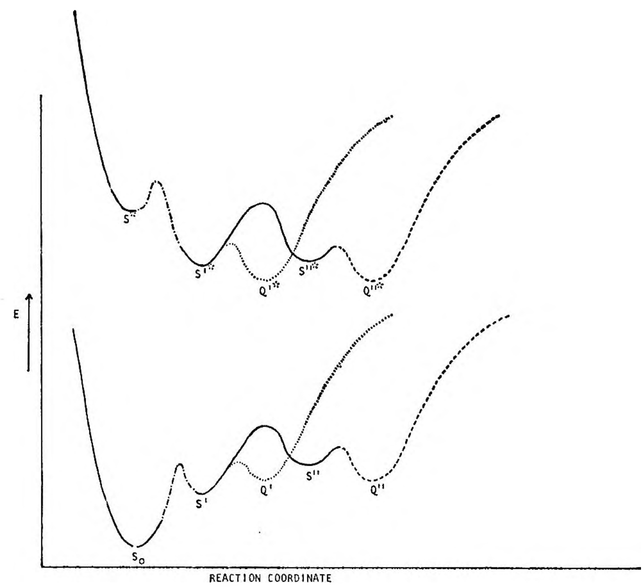

Figure 11. Potential energy diagram for the various states involved in the luminescence of azoles.

define the barrier led to a study of deuteration and temperature effects on fluorescence.

6. Deuteration and Temperature Effects. Deuteration of the 2′-hydroxy group produces compounds with lower quantum yields of fluorescence implying that either the rate of crossing from S* to S′* is reduced, or there is an increase in radiationless relaxation from one of the excited-state forms. Since such an increase is contrary to the usual deuterium effects, we must assume that there is a measurable barrier between S* and S′*, and that the difference in zero-point energy between -O-H and -O-D vibrations reduces the crossover process.

Fluorescence spectra of **1** and **1D** were obtained at 7°K, and there was a decrease in the overall quantum yield of both, but only of about 35%. In addition, the ratio of the two peaks for each compound (at 5470 and 5170 Å) changes so that the peak that is major at room temperature (5170 Å) is reduced by about 43% at 7°K, and the secondary peak becomes dominant. This indicates that temperature changes are affecting the populations of the S″* and/or the quinoid states relative to that of the S′ state.

7. Barrier Heights. If the barrier between S* and S′* were of sufficient magnitude that differences in zero-point energies were responsible for the deuteration effect, there should have been a drastic reduction in quantum yield at 7°K, at least for the deuterated compound. Nevertheless, deuteration does reduce the fluorescence output. Based on the facts available, we conclude that there is a potential-energy minimum and that the transfer from S* to S′* is a tunneling effect. This is consistent with viewing the S* form as a vibrationally excited state of S′*.

From the S′ states, it is possible to go to "trans"

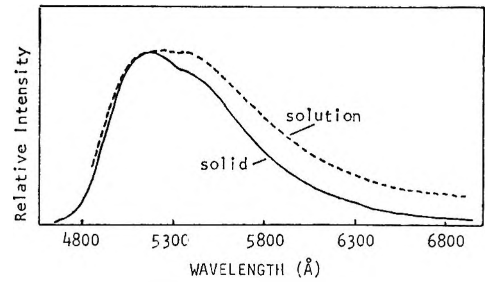

Figure 12. Normalized fluorescence spectra of **1** for the solid and 0.04 *M* solution in $CHCl_3$.

states (solid line ——) or nonplanar quinoid states (dotted line ....). As mentioned previously, the barriers to the trans quinoid states, Q′ and Q′*, would be expected to be high in the solid state, although they should be considerably reduced in solution. The spectrum of a 0.04 *M* solution of I in chloroform superimposed on the spectrum of solid **1** is shown in Figure 12. As can be seen, there is considerably more red emission in the solution spectrum. The presence of the second band in many of the fluorescence spectra can be attributed to emission from a state other than S′*, and it appears that this band is enhanced in solution as well as at low temperatures.

The barrier from the S″* state (dashed line ---) is expected to be of the same order as that between S′* and Q′*. The actual energy level of the S″* state (or S″ state) can presumably be lowered by the addition of water or some other high-dielectric medium as discussed for **15** since the S″ states involve a separation of charge.

8. Thermochromic and Photochromic Azoles. Azole **10**, 2-(2′-hydroxy-3′,5′-dinitrophenyl)-5-nitrobenzothiazole is a yellow compound which is both thermochromic and photochromic (unlike the anils of Cohen, *et al.*, whose thermochromicity and photochromicity are mutually exclusive). Upon irradiation with ultraviolet light, **10** fluoresces green, but gradually turns into a brown, nonfluorescent form. Also, **7** and **9**, the 3′-nitro and 5′-nitro derivatives, show some thermochromism and photochromism. The presence of the nitro groups on the phenyl ring considerably enhances the acidity of the phenol, thus enhancing the stability of the forms in which the proton is situated on the nitrogen. This undoubtedly stabilizes the S′ state with respect to the S_0 state. The colored nature of **10** indicates that its ground state most likely is predominantly an S′- or Q′-type molecule, that is, a molecule with the proton bonded to nitrogen. The thermochromic–photochromic state is stable. This denotes a measurable barrier between the colored state and the ground state, leading one to suggest that the thermochromic–photochromic molecule is a "trans" species. This is supported by the fact that regeneration of the ground state is best accomplished by first treatment with a base (ammonia) followed by treatment with an acid (hydrochloric). For cis–trans isomerization, the molecules must be in the ionic form. Hence, the need for a base signifies that the thermochromic–photochromic state is the trans quinoid species, Q″.

9. Triplets. Thus far, no mention has been made of the possible role played by triplet states in these systems. The decay time of less than 10^{-8} sec is evidence that luminescence originates from nothing but singlet states. Such a result is consistent with the studies of Richey and Becker,[6] who estimated the decay time for the related anil salicylideneaniline at 20 ± 10 nsec.

Intersystem crossing from the excited singlet, S′*, would produce a vibrationally excited triplet. The stable form of the triplet in all likelihood is with the proton on the oxygen. Such a species, as we have seen previously, does not luminesce, and therefore decays by a radiationless process.

The Influence of Solvent and Temperature upon the Fluorescence of Indole Derivatives[1]

by Edward P. Kirby* and Robert F. Steiner

Laboratory of Physical Biochemistry, Naval Medical Research Institute, National Naval Medical Center, Bethesda, Maryland 20014 *(Received July 20, 1970)*

The temperature dependence of fluorescence quantum yield for indole in water can be rationalized in terms of two nonradiative deexcitation processes. One of these is temperature independent and the other is temperature dependent. The temperature-dependent process may be associated with electron ejection from the excited indole. When D_2O is used as the solvent, or nonaqueous solvents are added to H_2O solutions, the magnitude of the temperature-dependent process is decreased. Indole derivatives which have a lower quantum yield than indole generally exhibit a decreased apparent activation energy, but this may be due to the introduction of a second, unresolved, temperature-dependent deexcitation process with a lower activation energy.

Introduction

Although a considerable volume of data has been accumulated on the luminescence properties of indole, tryptophan, and their derivatives, no definitive picture of the mechanisms responsible for the dependence of emission characteristics upon environment and chemical structure is currently available. For an indole derivative under a particular set of conditions, the quantum yield and excited lifetime of fluorescence are primarily dependent upon the competition between the direct emission of radiation by the excited state and various radiationless deexcitation processes. The nature and relative significance of these deactivation processes are still the subjects of considerable controversy. Intersystem crossing is generally conceded to account for a portion of the radiationless deactivation observed, but this mechanism would not be expected to exhibit the profound temperature and solvent dependence observed in indole and its derivatives. Several other deactivation mechanisms have been proposed, including "tunneling" from the excited to the ground state,[2a] electron ejection to the solvent,[2b] proton or hydrogen transfer,[3,4] and intramolecular electron transfer to a quenching group.[5]

The characteristics of the emission spectrum, the quantum yield, and the fluorescent lifetime of the indole derivatives have all been shown to be very dependent on the solvent.[3,6] Walker, Bednar, and Lumry[2b,7] have postulated that a stoichiometric complex is formed by the excited indole with molecules of a polar solvent. They have introduced the term "exciplex" for such complexes. They also investigated the temperature dependence of the fluorescent lifetime for several indole derivatives in water and have observed that at least one temperature-dependent deactivation process is present.[8] A

* To whom correspondence should be sent at Department of Biochemistry, University of Washington, Seattle, Wash. 98105.

(1) From Bureau of Medicine and Surgery, Navy Department, Research Task MR005.06-0005. The opinions in this paper are those of the authors and do not necessarily reflect the views of the Navy Department or the naval service at large.

(2) (a) J. Eisinger and G. Navon, *J. Chem. Phys.*, **50**, 2069 (1969). (b) M. S. Walker, T. W. Bednar, and R. Lumry, *ibid.*, **47**, 1020 (1967).

(3) R. W. Cowgill, *Biochim. Biophys. Acta*, **133**, 6 (1967).

(4) L. Stryer, *J. Amer. Chem. Soc.*, **88**, 5708 (1966).

(5) R. F. Steiner and E. P. Kirby, *J. Phys. Chem.*, **73**, 4130 (1969).

(6) B. L. Van Duuren, *J. Org. Chem.*, **26**, 2954 (1961).

(7) M. S. Walker, T. W. Bednar, and R. Lumry, *J. Chem. Phys.*, **45**, 3455 (1966).

large temperature dependence of the quantum yield has also been observed by other workers.[2a,9–11] Stryer[4] and Eisinger and Navon[2a] have observed that the quantum yield for indole derivatives is significantly higher in D_2O than in H_2O and have attributed this to the decreased efficiency of the quenching processes in D_2O.

This paper will deal with the effects of temperature and solvent composition on the quantum yields and excited lifetimes of several indole derivatives. Emphasis will be placed on the bearing of these results upon the nature and relative magnitudes of the various radiationless deexcitation processes.

Experimental Section

Methods. Measurements of the spectral distribution and relative intensity of fluorescence were made using an Aminco spectrofluorometer, which was equipped with a spectral compensation unit. The latter served to correct for the wavelength dependence of instrumental response and yielded energy corrected spectra. For the calculation of quantum yields the procedures recommended by Parker were followed.[12] Tryptophan in water was used as a reference material. A value of 0.14 at 25° was assumed for the absolute quantum yield of tryptophan, in accordance with recent determinations.[13–15] The relative quantum yields were corrected for the "inner filter" effect arising from absorption of the incident beam.[16] Concentrations were generally maintained sufficiently low so that this correction was small (< 20%).

The temperature dependence of fluorescence intensity was determined by measurements of relative intensity at a single emission wavelength, which ordinarily was chosen to correspond to the maximum in the emission spectrum. No broadening or shift in the fluorescence peak was observed upon changing the temperature. The solvent was generally 0.05 M potassium acetate, pH 5.0 (or in D_2O apparent pD = 5.0). A hollow cell holder was used, through which water from a constant-temperature bath was circulated. In this way the temperature could be controlled to within ±0.2° between 5° and 70°. The observed intensities at ambient temperature were compared with those from a control solution, which was maintained at room temperature. The control solution was generally indole in 1:1 propylene glycol:H_2O. This showed a very low temperature dependence of its own and was not subject to evaporation losses.

Measurements of the excited lifetime of fluorescence were made using the TRW system (TRW Instruments, El Segundo, California). The principles of operation and the details of the experimental procedure have been described elsewhere.[17]

Determinations of absorbance were made with a Gilford spectrophotometer or a Cary 14 recording spectrophotometer.

Materials. The following indole derivatives were purchased from Sigma: indole, indole-3-acetic acid, indole-3-acetic acid ethyl ester, tryptamine, tryptophan, and tryptophan ethyl ester. Acetyl tryptophan, acetyl tryptophan methyl ester, acetyl tryptophan amide, glycyl tryptophan, tryptophyl glycine, tryptophyl glycine amide, and carbobenzoxy tryptophan (cbz-typtophan) were purchased from Cyclo. 3-Methyl indole was obtained from Aldrich.

Analytical grade formamide and "spectroquality" methanol, propylene glycol, dioxane, and cyclohexane were purchased from Matheson Coleman and Bell. Deuterium oxide was from Aldrich and dimethyl sulfoxide (Spectrograde) was from Crown Zellerbach. Glass-distilled water was used for the preparation of all aqueous solutions. The inorganic reagents used were analytical grade.

Calculations. If all quenching processes are first order with respect to the excited state, then for any fluorescent species, the quantum yield, Q, may be represented by

$$Q = k_f/(k_f + \sum_i k_i) \tag{1}$$

where k_f is the first-order rate constant for the direct emission of fluorescent radiation by the excited state, and the set of k_i are the first-order rate constants for the various deactivation processes.

The observed fluorescent lifetime, τ, is given by

$$\tau = 1/(k_f + \sum_i k_i) \tag{2}$$

so that

$$k_f = Q/\tau \tag{3}$$

Equation 1 may be rewritten as

$$Q^{-1} = 1 + k_f^{-1} \sum_i k_i \tag{4}$$

If the reasonable assumption is made that k_f is independent of temperature (at least in the region between 0 and 70°), then the temperature dependence of the quantum yield may be expressed by

$$Q^{-1} - 1 = k_f^{-1} \sum_i f_i \exp(-E_i/RT) \tag{5}$$

(8) M. S. Walker, T. W. Bednar, and R. Lumry in "Molecular Luminescence," E. C. Lim, Ed., Benjamin, New York, N. Y., 1969, pp 135–152.

(9) J. A. Gally and G. M. Edelman, *Biochim. Biophys. Acta*, **60**, 499 (1962).

(10) K. K. Turoverov, *Opt. Spectrosc.*, **26**, 310 (1969).

(11) G. M. Barenboim, A. V. Sokolenko, and K. K. Turoverov, *Tsitologiya*, **10**, 636 (1968).

(12) C. A. Parker, "Photoluminescence of Solutions," Elsevier, New York, N. Y., 1968.

(13) J. Eisinger, *Photochem. Photobiol.*, **9**, 247 (1969).

(14) R. F. Chen, *Anal. Letters*, **1**, 35 (1967).

(15) H. C. Børresen, *Acta Chem. Scand.*, **21**, 920 (1967).

(16) R. F. Steiner, J. Roth, and J. Robbins, *J. Biol. Chem.*, **241**, 560 (1966).

(17) R. F. Chen, G. G. Vurek, and N. Alexander, *Science*, **156**, 949 (1967).

where f_i is the frequency factor for the ith deactivation process and involves the entropic component of the corresponding free energy of activation, E_i is the activation energy for the ith deactivation process, R is the gas constant, and T is the absolute temperature.

If only one deexcitation process is significant,

$$Q^{-1} - 1 = \frac{f}{k_f} \exp(-E/RT) \qquad (6)$$

in which case ln $(Q^{-1} - 1)$ should vary linearly with $1/T$. E may be computed directly from the slope of this line.

If two or more deactivation processes with significantly different activation energies are present, then curvature will be apparent in plots of ln $(Q^{-1} - 1)$ *vs.* $1/T$. In this case, interpretation of the data is considerably more difficult.

A second special case, however, is of interest. If only two deactivation processes are important, one of which is temperature independent ($E_0 = 0$) and the other temperature dependent ($E_1 > 0$), then eq 5 reduces to

$$Q^{-1} - 1 = \frac{f_0}{k_f} + \frac{f_1}{k_f} \exp(-E/RT) \qquad (7)$$

$$= \alpha_0 + \alpha_1 \exp(-E_1/RT)$$

In this paper, estimation of the parameters α_0, α_1, and E_1, has been done in two different ways.

Procedure 1. Differentiating eq 7 with respect to $1/T$

$$\frac{\partial Q^{-1}}{\partial(1/T)} = -\left(\frac{\alpha_1 E_1}{R}\right)\exp(-E_1/RT) \qquad (8)$$

$$\ln\left(-\frac{\partial Q^{-1}}{\partial(1/T)}\right) = \ln\left(\frac{\alpha_1 E_1}{R}\right) - \left(\frac{E_1}{RT}\right) \qquad (9)$$

In this case $\partial Q^{-1}/\partial(1/T)$ may be estimated by drawing tangents to a plot of Q^{-1} *vs.* $1/T$ at various values of $1/T$. Then a logarithmic plot of $\partial Q^{-1}/\partial(1/T)$ *vs.* $1/T$ should be linear with a slope equal to E_1/R. The difficulty with this procedure lies in the inaccuracy involved in drawing the tangents to the curve. Alternatively, the Q^{-1} *vs.* $1/T$ data may be fitted to a polynomial function and the derivative taken directly, but because the data are basically exponential, often polynomial fits are very unsatisfactory.

Once E_1 has been determined, eq 7 indicates that a plot of $(Q^{-1} - 1)$ *vs.* $\exp(-E_1/RT)$ should yield a straight line whose slope is equal to α_1 and whose intercept is α_0.

Procedure 2. Equation 7 may be rewritten as

$$\ln[(Q^{-1} - 1) - \alpha_0] = \ln \alpha_1 - \left(\frac{E_1}{RT}\right) \qquad (10)$$

and an empirical value of α_0 selected such that plots of ln $[(Q^{-1} - 1) - \alpha_0]$ *vs.* $1/T$ are linear. Much of the calculation for this paper was done by a computer program which used a search technique to determine the value of α_0 which gave the best straight line fit to the data.

Calculation of the parameters α_0, α_1, and E_1 by the two different procedures generally agreed very well. However, the possibility for systematic errors in the estimation of these parameters is very great and certain qualifications must be made in considering the results.

1. If more than one temperature-independent process were to exist, eq 7 would still fit the data, as α_0 actually represents the sum of all temperature-independent processes.

2. Turoverov[10] has demonstrated that the value of E_1 which is calculated is independent of the value selected for the absolute quantum yield at 25°. The accuracy of the estimates of α_0 and α_1, however, is very dependent upon the selection of the correct value of Q_{25}. For values of α_0 of approximately 1, a 10% error in the estimate of Q_{25} can introduce an error of about 20% in the estimate of α_0.

3. It should be noted that even if the data can be fitted very well by eq 7, this is not conclusive evidence for the existence of only one temperature-dependent quenching process. If a second temperature-dependent process were also important, the resulting data could in many cases still be fitted by eq 7. This is a result of the inherent scatter in the data and the limited temperature range (275–345°K) available for aqueous solutions.

Results

Indole in Water. The temperature dependence of the quantum yield of indole in water (0.05 M KOAc, pH 5) is quite large, as shown in Figure 1a. A fivefold change in quantum yield is observed between 5 and 50°. No broadening of the emission spectrum or shift in the λ_{max} of emission is observed upon raising the temperature, suggesting that the excited state itself is not altered. Increased temperature apparently affects only the rates of the various deexcitation processes. When ln $(Q^{-1} - 1)$ is plotted *vs.* $1/T$, according to eq 6, considerable curvature is apparent (Figure 1b), indicating that the data cannot be rationalized on the basis of a single temperature-dependent quenching process. It is worth mentioning that this deviation from linearity might well have been obscured by scatter of the data if measurements had been confined to temperatures above 25°.

If the assumption is made that a temperature-independent process is also quenching the fluorescence, the data can be fitted quite well. Both procedure 1 (Figures 2a and 2b) and procedure 2 (Figure 2c) give essentially the same result for a given set of data (E_1 = 13.0 and 12.9 kcal/mol, respectively, for the data of Figure 2), but the values of E_1 obtained from different experiments generally vary by 10–15%. The data given in Table I are the averages of several experiments.

The magnitude of the temperature-independent process, relative to the fluorescence, is given by α_0. The

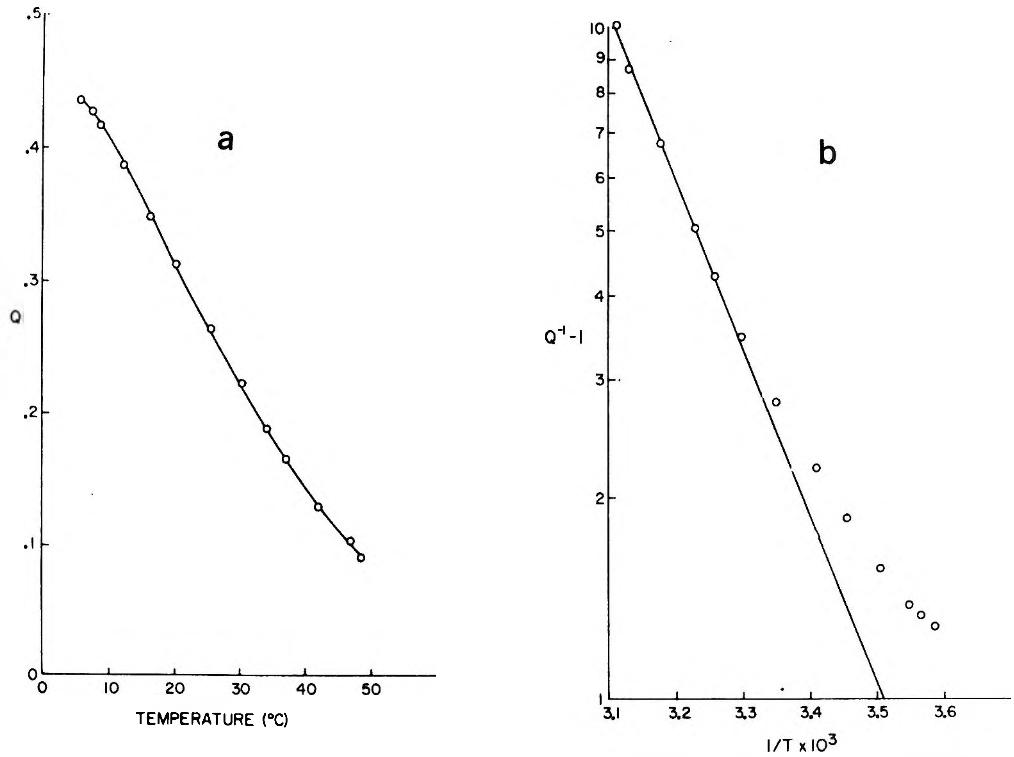

Figure 1. (a) Temperature dependence of fluorescence quantum yield for indole (5×10^{-5} M) in water (0.05 M KOAc, pH 5); (b) logarithmic plot of ($Q^{-1} - 1$) *vs.* $1/T$ for indole in water.

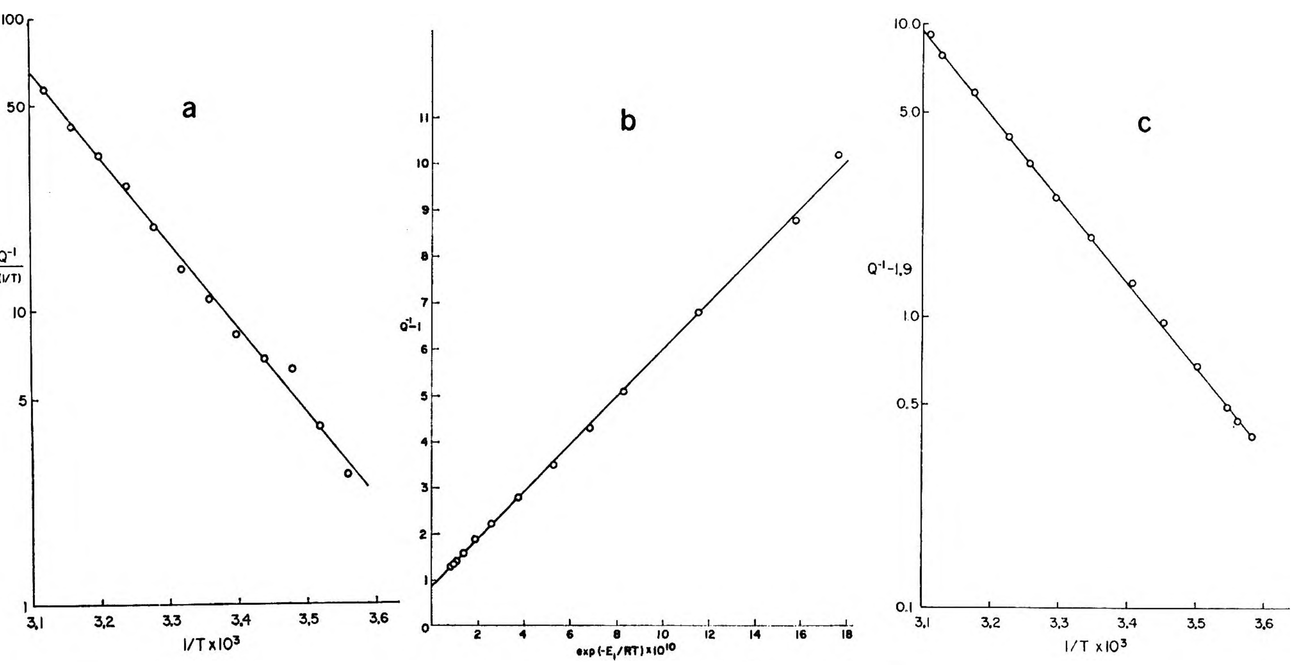

Figure 2. For indole in water: (a) logarithmic plot of $\partial Q^{-1}/\partial(1/T)$ *vs.* $1/T$; (b) plot of $Q^{-1} - 1$ *vs.* $\exp(-E/RT)$ for E = 12.9 kcal/mol; (c) logarithmic plot of ($Q^{-1} - 1.9$) *vs.* $1/T$.

values of α_0 cited in Table I should be regarded as only approximate because of the possibility of systematic errors involved in estimating this parameter. For indole in water, α_0 is approximately 1.0 (Table I), suggesting that, for an excited indole molecule, emission of fluorescence and radiationless deexcitation by the temperature-independent process are about equally probable. The activation energy for the temperature-dependent process is approximately 12.5 kcal/mol. The relative magnitude of this temperature-dependent process at 25° (given by $\alpha_1 \exp(-E_1/298R)$) is about 1.6. These data indicate that when indole molecules in water

Table I

	Solvent	Q_{25}[a]	τ (nsec)[a]	k_f ($\times 10^{-7}$)	α_0[b]	$\alpha_1 \exp(-E_1/298R)$	E_1[c] (kcal/mol)	Literature values of E_1
Indole	H_2O	0.28	4.0	7.0	1.0	1.6	12.5	8.5,[8] 12.0,[10] 9.9[11]
	D_2O	0.39	5.8	6.7	0.9	0.7	12.4	10.4[8]
3-Methyl indole	H_2O	0.34	9.4	3.6	0.4	1.5	12.9	12.5[8]
	D_2O	0.50	12.6	4.0	0.4	0.6	11.6	
Indole-3-acetate	H_2O	0.33	8.7	3.8	0.6	1.4	12.8	10.1[11]
	D_2O	0.40	11.0	3.6	0.8	0.7	13.3	
Tryptamine	H_2O	0.30	6.0	5.0	0.8	1.5	8.9	
	D_2O	0.46	8.0	5.7	0.7	0.5	9.6	
Acetyl tryptophan	H_2O	0.23	4.8	4.8	1.3	2.0	9.1	10.0,[10] 9.4[11]
	D_2O	0.30	5.8	5.2	1.3	1.0	9.1	
Cbz-tryptophan	H_2O	0.19	3.7	5.1	0.9	3.4	9.4	
	D_2O	0.23	5.4	4.3	1.0	2.4	8.6	
Acetyl tryptophan amide	H_2O	0.15	2.6	5.8	1.6	4.2	6.6	
	D_2O	0.18	3.3	5.5	1.6	3.0	5.8	
Tryptophan	H_2O	0.14	2.8	5.0	0.6	5.5	6.6	7,[2a] 8.1,[9] 8.45,[10] 8.1[11]
	D_2O	0.29	5.8	5.0	0.9	1.4	8.4	
Indole-3-acetic acid ethyl ester	H_2O	0.13	2.4	5.4	1.6	5.1	7.1	
	D_2O	0.15	2.6	5.8	1.6	4.1	6.4	

[a] Estimated accuracy = ±15%. [b] Estimated precision = ±20%. [c] Estimated accuracy = ±1.5 kcal/mol. (All values are based upon an assumed value of 0.14 for Q_{25} for tryptophan.[13-15])

at 25° are excited, 28% re-emit this excitation energy as fluorescence, approximately 28% are quenched by some temperature-independent process, and the remaining 44% lose their excitation energy by some temperature-dependent mechanism.

As mentioned earlier, the self-consistency of this kind of analysis does not provide a proof of the uniqueness or correctness of the model. If other quenching processes were present but did not differ greatly from these in their activation energies, they could not be resolved because of the scatter and limited range of the data. The important result is that at least two processes are necessary to explain the observed temperature dependence data.

Isotope Effects on Indole Fluorescence. In D_2O, the quantum yield and fluorescent lifetime of indole at 25° are increased by about 40% (Table I), in agreement with the findings of Stryer[4] and Walker, *et al.*[8] Since both the quantum yield and the fluorescent lifetime are increased to the same extent, eq 4 indicates that the value of k_f for indole is not affected by substitution of D_2O for H_2O. Furthermore, no change is observed in the emission spectrum.

The magnitude of the temperature-independent quenching process and the activation energy of the temperature-dependent process are also essentially unchanged, within experimental error, from the values observed in H_2O (Table I). The principal effect of the substitution of D_2O for H_2O is to reduce the magnitude of f_1, the frequency factor for the temperature-dependent process. This is perhaps best illustrated in Figure

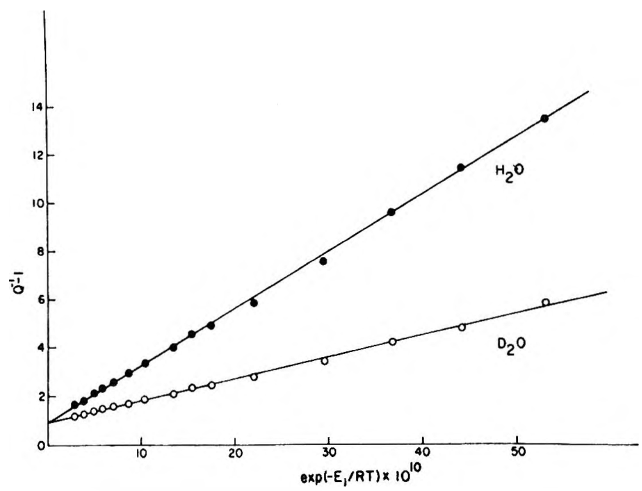

Figure 3. Effect of D_2O substitution on temperature dependence of indole fluorescence. For E_1 = 12.5 kcal/mol; ●, indole in H_2O; ○, indole in D_2O.

3. For a single experiment in which the temperature dependence of quantum yield for indole was run simultaneously in H_2O and D_2O, the data were seen to give straight lines when $Q^{-1} - 1$ was plotted against exp($-E_1/RT$), as predicted from eq 7. The two lines intersect on the y axis, indicating that α_0 is the same in both solvents. The only parameter which differs is the slope, which is proportional to f_1, the frequency factor for the temperature-dependent process.

The Effect of External Quenchers. Figure 4a illustrates the behavior of indole in the presence of an exter-

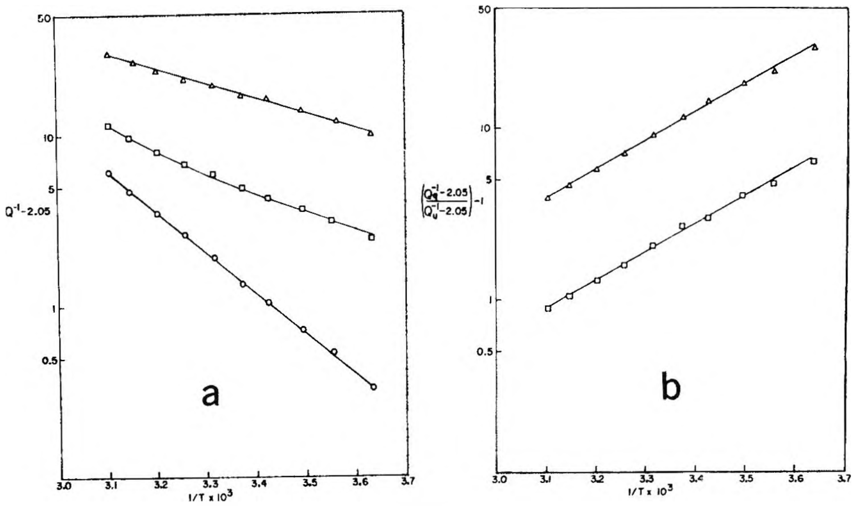

Figure 4. (a) Effect of histidine on temperature dependence of indole fluorescence: O, without histidine; □, 0.1 M histidine; Δ, 0.25 M histidine. (b) Logarithmic plot of $[(Q_q^{-1} - 1) - \alpha_0]/[(Q_u^{-1} - 1) - \alpha_0]$ *vs.* $1/T$ for indole in the presence of histidine: □, 0.1 M histidine; Δ, 0.25 M histidine.

nal quencher, such as histidine. For this experiment a value of α_0 equal to 1.05 was found to give the best linear fit to a logarithmic plot of $(Q^{-1} - 1) - \alpha_0$ *vs.* $1/T$. In the presence of 0.1 M histidine, the plot was curvilinear. At sufficiently high concentrations of quencher, the plots again became linear with slopes corresponding formally to a much lower activation energy. The results obtained with histidine are very similar to those obtained with various other quenching agents.

The presence of a second molecule which quenches the fluorescence of indole by interaction with the excited state introduces an additional term into eq 7

$$(Q_u^{-1} - 1) - \alpha_0 = \alpha_1 \exp(-E_1/RT) \quad \text{(no quencher)} \quad (7)$$

$$(Q_q^{-1} - 1) - \alpha_0 = \alpha_1 \exp(-E_1/RT + \alpha_2 \exp(-E_2/RT) \quad \text{(quencher present)} \quad (11)$$

Combining and rearranging these equations

$$\left(\frac{(Q_q^{-1} - 1) - \alpha_0}{(Q_u^{-1} - 1) - \alpha_0}\right) - 1 = \frac{\alpha_2}{\alpha_1} \exp\left(\frac{E_1 - E_2}{RT}\right) = \frac{\alpha_2}{\alpha_1} \exp(\Delta E/RT) \quad (12)$$

A logarithmic plot of the left-hand side of eq 12 *vs.* $1/T$ should yield a straight line whose slope is independent of the concentration of quencher and is proportional to ΔE, the algebraic difference between the activation energies for the two processes.

When the data from Figure 4a are graphed according to eq 12 (Figure 4b), the plots are indeed linear and parallel. From the slopes of these lines and the value of E_1 obtained in the absence of quencher, E_2 is calculated to be 3.3 kcal/mol. The values of E_2 for the external quenching process were quite small for all the quenchers examined, being of the order of 3 kcal/mol. The reaction of quencher with the excited state of indole may well be diffusion controlled[5] and so the apparent activation energy of approximately 3 kcal/mol for the external quenching process may only reflect a decrease in the viscosity of water with increased temperature.

From Figure 4a it may be seen that the presence of an external quenching process with high efficiency can mask the normal temperature-dependent quenching process and lead to a temperature-dependence profile which simulates the behavior expected for a single quenching process of intermediate activation energy. This is a consequence of the limited resolving capacity of this method of analysis, arising from the restricted available temperature range.

Indole Derivatives. Table I summarizes the relevant parameters for a series of indole and tryptophan derivatives in aqueous solution. The values of α_0, α_1, and E_1 were determined by both procedures 1 and 2. In general, calculations done by the two procedures agreed quite well with each other.

In the cases of derivatives with quantum yields at 25° less than 0.2 the estimation of α_0 is rather inexact (especially by procedure 2), because the value of α_0 is small in comparison with Q^{-1} and $\alpha_1 \exp(-E_1/298R)$. Moreover, if two or more temperature-dependent quenching processes are present, as is likely for the more highly quenched derivatives, α_0 may well be affected by artifacts introduced by the analysis procedure.

Because of the errors involved in determining Q and τ, the values of k_f listed in Table I are probably accurate to only ±20%. The value of k_f is apparently constant for the tryptophan derivatives[18] and probably constant, within the limits of error, for all of the indole derivatives studied. At least there is no apparent sys-

(18) I. Weinryb and R. F. Steiner, *Biochemistry*, 7, 2488 (1968).

tematic dependence of k_f on the type of substituent on the 3 position of the indole ring.

The values of α_0 are generally on the order of 1, although an apparent increase in magnitude is seen with decreasing quantum yield. As mentioned above, it is somewhat difficult to determine whether this increase is real or an artifact of the method used.

Both the quantum yield and the apparent activation energy for the temperature-dependent quenching process (or processes) are very dependent on the chemical structure of the indole derivative (Table I). As the quantum yield decreases, generally the apparent activation energy of quenching also decreases, but the overall importance of the temperature-dependent quenching process [as measured by $\alpha_1 \exp(-E_1/298R)$] increases. Most likely this represents the increasing importance of one or more additional temperature-dependent quenching processes. As mentioned earlier, the inaccuracies in the data and the limited temperature range prevent any additional processes from being resolved, so that the values of parameters such as E_1 should be considered as only apparent. The marked decrease in E_1 for the more quenched derivatives, however, does indicate that whatever new quenching process is important, its activation energy must be considerably less than 12 kcal/mol.

As mentioned above, D_2O apparently does not affect k_f. For the derivatives examined, the replacement of H_2O by D_2O also did not profoundly alter either E_1, or the magnitude of α_0 (Table 1), although minor, but significant, changes may be masked by experimental error. It appears that the primary effect is to reduce f_1, the frequency factor for activated quenching. Eisinger and Navon[2a] have reported a similar conclusion in the case of tryptophan. Since, in general, the magnitude of the temperature-independent process is not affected by D_2O substitution, the most sensitive index of the extent of the D_2O effect is the ratio

$$R_{H/D} = \frac{[(Q^{-1} - 1) - \alpha_0]H_2O}{[(Q^{-1} - 1) - \alpha_0]D_2O} \quad (13)$$

so that

$$R_{H/D} = \frac{[\alpha_1 \exp(-E_1/RT)]H_2O}{[\alpha_1 \exp(-E_1/RT)]D_2O} \quad (14)$$

When the activation energies are equal in H_2O and D_2O, R is then equal to the ratio of the frequency factors of the temperature-dependent process in the two solvents. In this manner, R is composed only of the parameters most sensitive to D_2O substitution.

Unfortunately, if more than one temperature-dependent process is present, the value of α_0 can be altered by artifacts in the analysis procedure. For this reason, a more cautious estimate of the D_2O effect is the ratio suggested by Eisinger and Navon[2a]

$$r_{H/D} = \frac{(Q^{-1} - 1)D_2O}{(Q^{-1} - 1)H_2O} \quad (15)$$

Table II lists values of both $R_{H/D}$ and $r_{H/D}$ for several different indole derivatives.

Table II

	$Q_{25}(H_2O)^a$	$r_{H/D}$	$R_{H/D}$
3-Methyl indole	0.34	1.94	2.57
Indole-3-acetate	0.33	1.35	2.04
Indole	0.28	1.65	2.38
Acetyl tryptophan	0.23	1.44	1.99
Cbz-tryptophan	0.19	1.27	1.43
Acetyl tryptophan amide	0.15	1.25	1.38
Indole-3-acetic acid ethyl ester	0.13	1.18	1.25
Glycyl tryptophan	0.07	1.15	1.17
Tryptamine	0.30	1.98	3.19
Tryptophan	0.14	2.51	3.58
Tryptophyl glycine	0.11	1.6	1.8
Tryptophyl glycine amide	0.05	1.4	1.5
Tryptophan ethyl ester	0.024	1.1	1.1

[a] Estimated accuracy = ±15%. (Values are based on an assumed value of 0.14 for Q_{25} for tryptophan.)

The derivatives listed in Table II are divided into two groups on the basis of whether or not they possess a protonated α-amino group, in proximity to the indole ring. Within either group, with the exception of the data for tryptamine and tryptophan, the magnitude of the deuterium isotope effect generally decreases with decreasing quantum yield. For derivatives of similar quantum yield, the presence of a protonated α-amino group close to the indole ring greatly enhances the D_2O effect.

Indole in Nonaqueous Solvents. Figure 5 shows the temperature dependence of quantum yield for indole in methanol and in dioxane. It is apparent that the temperature dependence in these solvents is much less than in water (Figure 1a). Table III lists the quantum yields, fluorescence lifetimes, and activation energies for indole in a series of solvents of varying polarity. Because of the low-temperature dependence of quantum yield in the nonaqueous solvents, it was not possible to analyze the data in terms of two different processes. Reasonable fits could be obtained with any value of α_1 chosen (in the range between 0 and $Q^{-1} - 1$). The data were fitted to eq 6 purely for the purposes of tabulation, and the activation energies reported should be considered as apparent values which indicate only the low-temperature dependence of fluorescence under these conditions.

Although the quantum yield and fluorescent lifetime show a more or less monotonic change with decreasing solvent polarity, the temperature dependence in all nonaqueous solvents was very much less than in H_2O. While the origin of this anomalous behavior in H_2O pre-

Table III

	Solvent	Q_{25}[a]	τ[a]	E_{app}[b]
Indole	Formamide	0.23	2.6	3.3
	Methanol	0.32	3.4	0.9
	Propylene glycol	0.38	3.9	1.6
	Dioxane	0.42	4.6	1.5
	Cyclohexane	0.41	5.2	0.3
3-Methyl indole	Methanol	0.29	5.2	0.0
	Propylene glycol	0.46	8.0	1.0
Indole acetic acid ethyl ester	Methanol	0.13	2.1	3.4
	Propylene glycol	0.17	2.6	4.1
	Dioxane	0.40	4.6	2.1
Acetyl tryptophan methyl ester	Methanol	0.10	1.7	2.8
	Propylene glycol	0.18	3.7	6.1
	Dioxane	0.28	3.8	3.1

[a] Estimated accuracy = ±15%. [b] From eq 6. These should be regarded as apparent values only (see text).

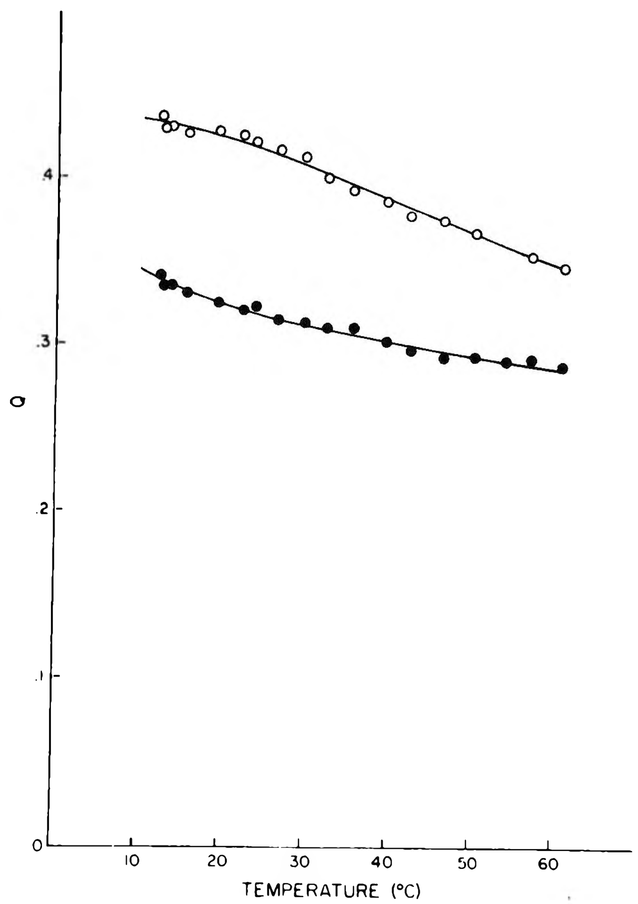

Figure 5. Temperature dependence of indole fluorescence in nonaqueous solvents: ●, methanol; ○, dioxane.

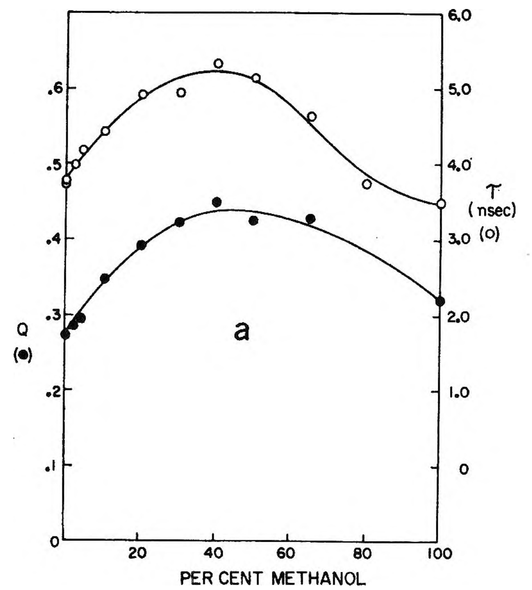

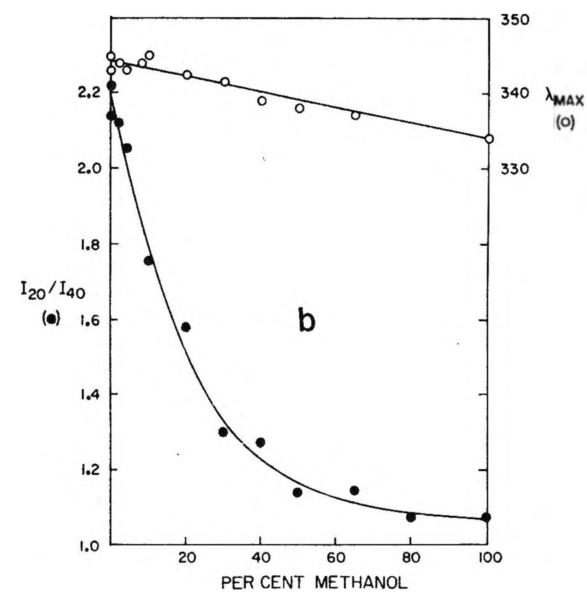

Figure 6. Effect of addition of methanol on the fluorescence properties of aqueous indole solutions; (a) ○, fluorescent lifetime (τ); ○, quantum yield (Q); (b) ○, wavelength of maximum emission (λ_{max}); ●, temperature dependence of fluorescence (intensity at 20°/intensity at 40°).

sumably lies in the unique solvent properties of water, an explanation in terms of a definite mechanism will be postponed to the Discussion.

The fluorescence properties of indole were also examined in mixtures of water plus a second solvent. The results for mixtures of water and methanol are shown in Figure 6. The wavelength of maximum emission decreases almost linearly as the percentage of methanol is increased. The quantum yield and fluorescent lifetime initially increase upon adding methanol, approaching a maximum value at approximately 40% methanol. Associated with this increase in Q and τ is a large decrease in the temperature dependence of the quantum yield (Figure 6b). The apparent explanation for these results is that the addition of methanol decreases the probability of deactivation of the excited state by the temperature-dependent process. Figure 7 demonstrates that if the activation energy of the temperature-dependent process is assumed to be the same in 8% methanol as that in water, the data yield straight lines, extrapolating to the same value of α_0. The frequency factor, f_1, for the temperature-dependent process is only about 70% of that in water. Apparently, addition of methanol causes a decrease in the probability of deactivation by the temperature-dependent process but does not affect the activation energy of this process or alter the probability of the temperature-independent process. At concentrations of methanol below 20%, significantly better fits are not obtained by assuming all three parameters, α_1, α_0, and E_1, can vary. This is not to deny that addition of methanol could cause changes in all three parameters, but since the data can be fitted very well with a change in only one parameter, namely α_1, this simpler assumption is used to rationalize the data.

At concentrations of methanol above 40–50%, the quantum yield and fluorescent lifetime decrease. At these higher concentrations of methanol the temperature dependence is essentially the same as in pure methanol. The difference in the temperature dependence from that observed in water can no longer be explained on the basis of a simple decrease in α_1, but the low-temperature dependence prevents accurate analysis in terms of α_0, α_1, and E_1.

Essentially the same results are obtained with mixtures of water and several other solvents. Addition of the second solvent causes an abrupt decrease in the temperature dependence of fluorescence (see Figure 8). The influence of solvent composition on the temperature dependence was qualitatively rather similar for all of the solvents tested, irrespective of their polarity.

Table III also cites the fluorescence parameters in nonaqueous solvents of several indole derivatives which display extensive intramolecular quenching in water. To avoid ambiguities arising from possible changes in the state of ionization, derivatives were selected which did not contain an ionizable site.

When these indole derivatives are dissolved in nonaqueous solvents, the quantum yields and fluorescent lifetimes are significantly higher than in water.[3] As shown in Table III, however, the quantum yields for some of the derivatives, such as indole acetic acid ethyl ester and acetyl tryptophan methyl ester are still quite low, suggesting that intramolecular quenching by the substituent group may still play an important role. The temperature dependence of fluorescence is low, preventing accurate analysis of the data in terms of more than one quenching process. The temperature dependence is somewhat greater than that observed for indole in nonaqueous solvents, indicating that the apparent E may be that for the intramolecular quenching process, rather than that for the temperature-dependent process found for indole in water.

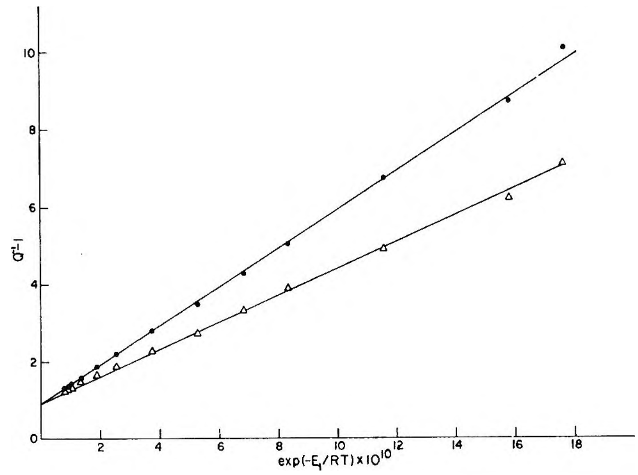

Figure 7. Effect of the addition of methanol on the temperature dependence of indole fluorescence. For E_1 = 12.9 kcal/mol: ●, indole in H_2O; △, indole in 8% methanol.

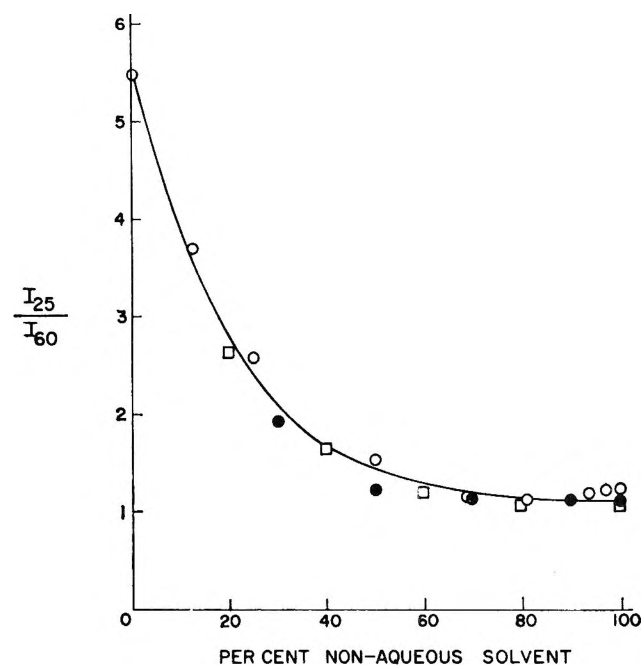

Figure 8. Effect of the addition of nonaqueous solvents on the temperature dependence of aqueous indole solutions: ○, dioxane; ●, dimethyl sulfoxide; □, propylene glycol.

Discussion

It is clear from the preceding results that the characteristics of the solvent and the chemical structure of the derivative strongly influence the radiationless processes which deactivate the first excited singlet state of indole and its derivatives. The temperature dependence of quantum yield can give some indications of the nature of these processes. If no group capable of intramolecular quenching is present, as in the case of indole or 3-methyl indole, the thermal dependence of quantum yield in water can be accounted for in terms of two kinds of processes. The first process, or collection of processes, is temperature independent and occurs with a rate constant similar in magnitude to the rate constant for direct emission of fluorescence. The second process is temperature dependent with a high activation energy and is approximately 1.5 times as efficient as fluorescent emission at 25°.

The replacement of H_2O by D_2O increases the quantum yield and fluorescence lifetime of indole, primarily by decreasing the probability of deexcitation by the temperature-dependent quenching process. The activation energy for the temperature-dependent process, the probability of the temperature-independent process, and k_f are not profoundly changed. This agrees with the findings of Eisinger and Navon,[2a] Stryer,[4] and Walker, Bednar, and Lumry.[8]

A similar effect is seen upon the addition of nonaqueous solvents to solutions of indole. The increased quantum yield and fluorescence lifetime can be accounted for by a decrease in the frequency factor for the temperature-dependent process.

Since the changes in Q, τ, and α_1 which are observed upon adding a less polar solvent are quite similar for the addition of solvents which differ greatly in their polarity (Figure 8), the effects cannot be primarily due to an alteration of the dielectric constant of the medium. It is possible that the modification of the structure of the water lattice upon dilution with a second solvent is the dominant factor. In particular, the partial or complete elimination of the hydrogen-bonded regions of localized order in proximity to the nonpolar indole ring may alter the interaction of the indole and the solvent.

To summarize the processes leading to the deexcitation of the first excited singlet state of indole

(a) $In^* \xrightarrow{k_f} In + h\nu$ (fluorescence)

(b) $In^* \xrightarrow{k_0} In$ (temperature-independent process)

(c) $In^* \xrightarrow{k_1} In$ (temperature-dependent process)

The identity of neither of the two radiationless deactivation processes can be assigned with certainty at present. Stryer[4] has suggested that the nonradiative processes are associated with changes in the protonation of the excited state, but the data of Walker, *et al.*,[8] seem to indicate that this is not likely. A strong possibility for the temperature-independent process is, of course, intersystem crossing to the lowest triplet state. Eisinger and Navon[2a] have suggested that the temperature-dependent deactivation process is "tunneling" to the ground state. An alternative assignment is that the temperature-dependent process is associated with electron ejection to the solvent. It has been demonstrated that solvated electrons are produced upon irradiation of indole and its derivatives[19,20] and since this mechanism involves a large separation of charge, a high activation energy would be expected. Our data indicate that approximately 45% of the indole molecules which are excited in water at 25° lose their excitation energy by this temperature-dependent process, but Hopkins and Lumry[20] report that the quantum yield for solvated electrons is only about 0.15. It may be that the temperature-dependent process which we are observing indirectly is not the actual ejection of an electron, but some preliminary step.

The behavior of the indole derivatives in water presents a fairly self-consistent pattern. The value of k_f does not vary to any great extent or in any obvious manner for the 3-substituted indole derivatives, and the magnitude of the temperature-independent process does not appear to be appreciably affected by substitution. The quantum yield and apparent activation energy are, however, greatly influenced by the type of substituent on the indole ring. In general, the derivatives with lower quantum yields have lower apparent activation energies.

Two possible models may be proposed to explain the observations on the temperature dependence of quantum yield of the more highly quenched derivatives. (1) There is only one temperature-dependent quenching process which is important in the derivatives. This is the same process that occurs in unsubstituted indole but is modified by the presence of the quenching group. (2) A second temperature-dependent quenching process of lower activation energy is present, resulting from the interaction of the quenching group with the excited indole. The limited resolution attainable over the accessible temperature range results in the simulation of a single activation energy.

If the primary temperature-dependent quenching process is "tunneling" to the ground state, it would be very difficult to distinguish between these two models experimentally. If the primary temperature-dependent process is associated with electron ejection, however, model 1 predicts that the yield of solvated electrons should be greater from the more highly quenched derivatives. If, on the other hand, model 2 is correct, the primary deactivation process would be partially suppressed as a consequence of the competitive occurrence of the second process, and possibly by the direct influence of the quenching group as well. In this case, the yield of solvated electrons would decrease with decreasing quantum yield.

The few data which are presently available are most consistent with model 2. According to Grossweiner and Joschek[19] the yield of solvated electrons from tryptophan is substantially less than that from such relatively unquenched derivatives as indole-3-acetate. Hopkins and Lumry[20] have also reported that the yield of electrons is considerably less from the more highly quenched derivatives.

While a final decision on the validity of model 2 should

(19) L. I. Grossweiner and H. Joschek, *Advan. Chem. Ser.*, 50, 279 (1965).

(20) T. R. Hopkins and R. Lumry, *Biophys. J.*, 9, A216 (1969).

at present be deferred, it is possible to speculate as to the identity of the second temperature-dependent deactivation process. Since the quenching substituents of indole for the series of derivatives considered here correspond to parent compounds which are effective as electron scavengers, and since electron scavengers as a class are effective quenchers of the fluorescence of indole derivatives,[5] one possible mechanism for intramolecular quenching is electron capture by the quenching group, perhaps involving direct contact of the side chain with the indole ring.

The substitution of D_2O for H_2O suppresses the primary quenching process to a significant extent. This is responsible for the large isotope effect observed for indole and probably for those indole derivatives in which extensive intramolecular quenching does not occur. In addition, the presence of a charged α-amino group in immediate proximity to the indole ring appears to enhance the isotope effect. This is not the case if the amino group is separated from the indole ring by one or more residues, as in gly-trp. One possible explanation is that the charged α-amino group serves as a proton donor and that proton quenching of the excited indole is an important factor in such cases. Apart from this, the intramolecular quenching processes for this series of derivatives do not appear to show much isotopic dependence. Consequently, the magnitude of the isotope effect generally decreases with decreasing quantum yield.

Finally, the persistence of intramolecular quenching, although to a diminished extent, in nonpolar media deserves comment. If model 2 is correct, it would be expected that the primary quenching process would be largely suppressed under these conditions, while the strictly internal quenching may persist, although modified by the different medium.[21]

Acknowledgment. The authors recognize the able technical assistance of Mr. Theodore Lutins, Mr. Richard Kolinski, and Mr. Ross Bolger. We also thank Dr. Rufus Lumry and Dr. Gary Pool for some very helpful discussions. This work was partially supported by ONR Grant No. NR108-815.

(21) Note Added in Proof. The values cited in Tables I, II, and III are based upon an assumed value of 0.14 for Q_{25} for tryptophan in H_2O.[13-15] Should this value be revised, the values of Q, α_0, and α_1 would be altered, but not E_1.

Methylene Produced by Vacuum-Ultraviolet Photolysis. II. Propane and Cyclopropane

by A. K. Dhingra and R. D. Koob

Department of Chemistry, North Dakota State University, Fargo, North Dakota 58102 *(Received June 29, 1970)*

Propane, argon, and oxygen are used as additives to investigate the reactions of methylene produced by the vacuum-ultraviolet photolysis of propane (123.6 nm and 147.0 nm), cyclopropane, and *cis*- and *trans*-1,2-dimethylcyclopropane (~165 nm). With the exception of propane at 147.0 nm, insertion of $CH_2(^1A_1)$ into propane to yield butanes accounts for at least 60% of the total methylene yield. Similarly, with the above exception, no $CH_2(^3\Sigma_g^-)$ appears to arise from the primary photodecomposition of the source molecule. The relative yield of insertion product obtained in the photolysis of propane shows a definite wavelength dependence. However, the relative rate of reaction of methylene with argon in competition with propane is wavelength independent. The rate of reaction of methylene with argon relative to propane found for our systems is similar to that found in other steady-state systems, but is different by an order of magnitude from recent flash photolysis results. Contrary to a suggestion of other workers, it does not appear necessary to postulate a trimethylene diradical in the primary process in the photolysis of cyclopropane.

Introduction

Recently, we have reported studies of methylene produced by the vacuum-ultraviolet photolysis of propane at 123.6 nm.[1] We noted at that time the similarity between the reactions of methylene produced from this source and methylene produced from the more conventional sources, ketene and diazomethane. These studies have since been extended to propane at 147 nm and cyclopropane at approximately 165 nm. The results of these studies are presented here.

(1) R. D. Koob, *J. Phys. Chem.*, 73, 3168 (1969).

Experimental Section

Materials. Propane and cyclopropane were obtained from Air Products and Chemicals, Inc. Propane was research grade. *cis*- and *trans*-1,2-dimethylcyclopropane were obtained from Chemical Samples Co. and were used without further purification. Glc examination of these substituted cyclopropanes showed no butane or butene impurities. Both propane and cyclopropane were purified by gas chromatography until impurity levels were below 10 ppm. For cyclopropane this required at least two successive purification cycles. The hydrocarbons were then dried over Drierite and vacuum distilled to storage bulbs. Argon used was Air Products Ultra High Purity grade. Oxygen was Linde CP. Both were used without further purification.

Lamps and Cells. Rare gas resonance lamps, similar to those described by Ausloos and Lias,[2] were used for the photolysis. All lamps were filled on a mercury-free vacuum line capable of achieving pressures less than 1×10^{-6} Torr (Veeco discharge gauge). For the propane photolysis, lamps were gettered with titanium gettering assemblies and were greater than 98% chromatically pure in the region between 105 and 200 nm (McPherson 0.3-m vacuum monochromator). LiF windows were used for both krypton and xenon lamps. For the cyclopropane work, a water impurity was intentionally left in a krypton filled lamp. This lamp gave an intense water emission spectrum, Figure 1.

Two lamp–cell configurations were used to study propane photolysis. The first was a "T" shaped lamp with windows at each end of the crossbar. The windows looked into individual sample cells. After a short break-in period, the ratio of light intensity entering each of the two cells was constant. Thus, one cell with constant sample conditions was used as an external standard to which runs made in the other cell could be compared. The second lamp–cell configuration consisted of an LiF window clamped between two O-ring joints and sealed vacuum tight. One such joint formed the discharge area of the lamp and the second was attached to a stopcock and served as a sample cell. This configuration was used for sample pressures greater than 1 atm.

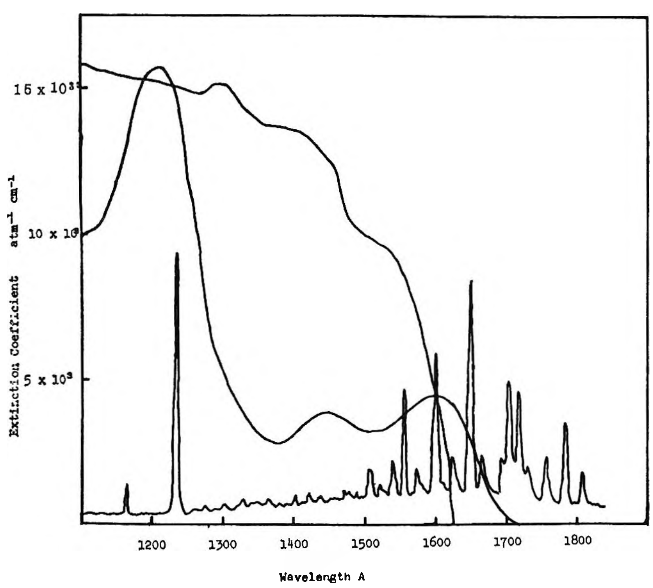

Figure 1. The many-line spectrum is the water emission spectrum in this region. The absorption spectrum of propane begins around 162 nm. The absorption spectrum of cyclopropane begins near 171 nm. The overlay shows the importance of the water 165-nm line when cyclopropane is photolyzed through a propane filter.

Propane–cyclopropane mixtures were irradiated in a two-compartment cell. The first compartment had a path length of approximately 1.5 cm and was filled with 200 Torr of propane. The second compartment was filled with a propane–cyclopropane mixture. Such an arrangement assured that only the cyclopropane component of the mixture was actually undergoing photolysis. A "water" lamp was used in these experiments. The nature of the light absorbed by the cyclopropane can be deduced from Figure 1. Here the absorption spectra of propane and cyclopropane overlay the emission spectrum of the "water" lamp. Only those wavelengths which lie between the onset of the cyclopropane absorption and the onset of the propane absorption contribute to the photolysis.

Oxygen was added to all reaction mixtures in amounts equal to 10% of the total hydrocarbon pressure. The oxygen is intended to serve as a free radical scavenger. Absence of products in the five and six carbon range indicate that it is performing this function.

In all experiments, photolysis was carried to less than 0.1% conversion of parent to product. All analyses were done by gas chromatography (FID) on a 20-ft, 20% (w/w) squalane column maintained at room temperature.

Results

Table I lists the observed isobutane to normal butane ratio for all systems examined. The values of this ratio obtained by Halberstadt and McNesby[3] in a propane–ketene–oxygen system and by Johnson, Hase, and Simons[4] in a propane–diazomethane–oxygen system are also included. Within experimental error these values are equal. Correcting for the number of hydrogens of each type in propane we obtain $3k_2/k_1 = 1.2$. (Reactions 1 and 2 are found in the Discussion section below).

Figure 2 is a plot of the product ratio $[C_2H_6]/[C_4H_{10}]$ *vs.* the reactant mixture ratio $(Ar)/(C_3H_8)$. Experimentally, these numbers were obtained in two ways:

(2) P. Ausloos and S. G. Lias, *Radiat. Res. Rev.*, **1**, 75 (1968).

(3) M. L. Halberstadt and J. R. McNesby, *J. Amer. Chem. Soc.*, **89**, 3417 (1967).

(4) R. L. Johnson, W. L. Hase, and J. W. Simons, *J. Chem. Phys.*, **52**, 3911 (1970).

Table I: Relative Rates of Insertion of Methylene into Primary and Secondary Bonds of Propane as a Function of the Source of the Methylene

Source of CH_2	$i\text{-}C_4H_{10}^a$ / $n\text{-}C_4H_{10}$	$3k_2/k_1$	Ref
C_3H_8, 123.6 nm[b]	0.40	1.20	c
C_3H_8, 147.0 nm[b]	0.38	1.14	c
$c\text{-}C_3H_6$, 165 nm	0.39	1.17	c
CH_2CO, 313.0 nm	0.43	1.29	d
CH_2N_2, 366.0 nm	0.40	1.20	e
CH_2N_2, 435.8 nm	0.39	1.17	e
	Av	1.2	

[a] Averaged values. [b] A ratio of excess argon over propane as great as 160:1 has no effect on these values within experimental error. Similarly they are independent of total sample pressure to at least 5 atm. [c] This work. [d] Reference 3. [e] Reference 4.

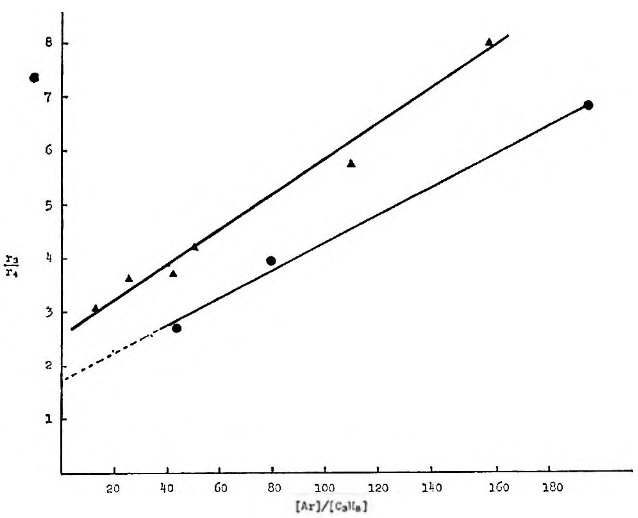

Figure 2. Curve A, ●, argon–propane–oxygen mixtures photolyzed at 123.6 nm. Curve B, ▲, argon: propane–oxygen mixtures photolyzed at 147.0 nm. $r_3/r_4 = [C_2H_6]/[C_4H_{10}]$.

(a) by holding $[(C_3H_8)]$ constant and varying the argon–propane ratio by increasing the total pressure with argon; (b) by holding the total pressure constant at one atmosphere and varying the argon–propane ratio. Above 400 Torr total pressure, the two methods are indistinguishable within experimental error as far as average results are concerned. However, there is considerably less scatter in the data using the latter method. The ethane–butane ratio was obtained at two wavelengths 123.6 nm (curve A) and 147 nm (curve B). Above 400 Torr the ratio $[C_2H_6]/[C_4H_{10}]$ is the same as the ratio of the rate of production of the two products since neither undergoes further decomposition. Only one reaction contributes to the formation of C_2H_6.[5] $[C_2H_6]/[C_4H_{10}]$ is independent of pressure above 400 Torr to pressures as high as 5 atm. This is true for photolysis at both 123.6 nm and 147 nm. However, $[C_2H_6]/[C_4H_{10}]$ is wavelength dependent. At 123.6 nm

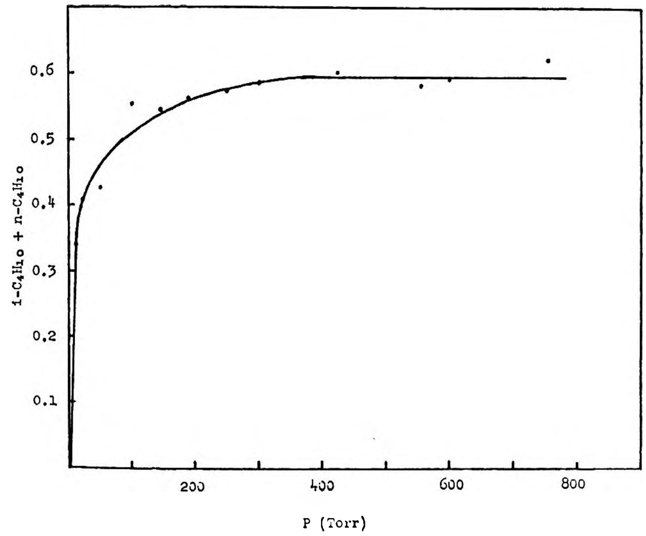

Figure 3. Butane relative to ethylene as a function of total sample pressure in propane:cyclopropane:oxygen mixtures (100:10:1). The ratio of iso- to n-butane is constant over the pressure range 10–760 Torr.

the high-pressure value of this ratio is 0.6 while at 147.0 nm it decreases to 0.39.

Figure 3 demonstrates the dependence of butane yield on total pressure in the system propane–cyclopropane–oxygen. The butane yield is measured relative to the yield of ethylene. While enough energy is given cyclopropane in the photon absorption step that the product ethylene may undergo further decomposition, the most probable decomposition ($C_2H_2 + H_2$) does not appear to occur at pressures greater than 10 Torr. The ethylene–acetylene ratio was found to be constant throughout the pressure range of Figure 3. Note at pressures greater than 300 Torr that the butane–ethylene ratio becomes constant and equal to 0.59 ± 0.03.

Table II: Relative Yields of *cis-* and *trans-*Butene-2 from the Photolysis of *cis-* and *trans-*1,2-Dimethylcyclopropane

Parent	Butane/butene-2 P = 100 Torr	*cis-*butene-2 / total butene-2	*trans-*butene-2 / total butene-2
*cis-*1,2-Dimethylcyclopropane	0.55	1.0	0.0
*trans-*1,2-Dimethylcyclopropane	0.54	0.0	1.0

Two experiments related to cyclopropane photolysis were the irradiation of *cis-*1,2-dimethylcyclopropane (*cis-*DMCP) and *trans-*1,2-dimethylcyclopropane (*trans-*

(5) (a) P. Ausloos, S. G. Lias, and I. B. Sandoval, *Discuss. Faraday Soc.*, **36**, 66 (1963); (b) H. Okabe and J. McNesby, *J. Chem. Phys.*, **37**, 1340 (1962).

DMCP) under the same condition of excess propane and an oxygen scavenger as used for cyclopropane. Runs with the substituted cyclopropanes were made at 100 Torr total pressure. Butene-2 is produced in the photolysis of both *cis*- and *trans*-DMCP and accounts for about 10% of the total product in the scavenged system. However, when *cis*-DMCP is photolyzed only *cis*-butene is observed and when *trans*-DMCP is photolyzed only *trans*-butene-2 is observed, Table II. In both cases the butane: butene-2 ratio, analogous to the butane: ethylene ratio in cyclopropane, is approximately 0.6.

Discussion

Relative Rates of Methylene Insertion into Primary and Secondary Carbon–Hydrogen Bonds of Propane. Methylene may insert in either a primary or secondary carbon–hydrogen bond of propane according to reactions 1 and 2 to yield *n*- and isobutane, respectively.

$$^1CH_2 + C_3H_8 \xrightarrow{k_1} n\text{-}C_4H_{10} \quad (1)$$

$$^1CH_2 + C_3H_8 \xrightarrow{k_2} i\text{-}C_4H_{10} \quad (2)$$

Examination of Table I makes it clear that the relative yields of iso- to *n*-butane derived from the insertion of methylene into propane are completely independent of the source of the methylene. This observation is useful for two reasons. First, it provides a link between the methylene produced in the vacuum-ultraviolet (vuv) photolysis of alkanes and the methylene produced by the more usual photolyses of ketene and diazomethane. That portion of the methylene produced in the vuv photolysis which reacts with propane to produce butanes is indistinguishable from the methylene produced in the photolysis of ketene and diazomethane which inserts in propane to form butanes. This observation is chemical evidence for this fraction of the methylene produced in the vuv photolysis being in the $^1A_1$ state. Second, the complete lack of a dependence of $i\text{-}C_4H_{10}/n\text{-}C_4H_{10}$ on wavelength, source molecule, an excess of a nonreactive (moderator) gas, or total pressure (above 10 Torr) provides an interesting opportunity to speculate about the nature of this reaction. The independence of the insertion rate ratio of previous history of the methylene can be interpreted either as a complete lack of energy dependence of the reaction, *i.e.*, no activation energy to insertion, or that the methylenes which insert are all energetically similar regardless of source. The observation that insertion favors the secondary carbon–hydrogen bond in propane argues against the first possibility in that steric factors would appear to favor the primary position. We feel that $3k_2/k_1$ is *significantly* larger than the statistically expected unity and that insertion must occur with some activation energy. On the other hand, the rate at which insertion product, butane, dissociates is dependent upon the source of the methylene from which it is formed.[4] This would indicate that all methylenes which do insert are not energetically identical in all respects. To be consistent with all experimental observations to date, it is necessary to postulate that while the amount of energy available to methylene to surmount the activation barrier to insertion is independent of the source of that methylene, excess energy (source dependent) must be stored in the methylene and that energy becomes available to the insertion product. Lack of intimate detail on both the insertion process and energy transfer between internal modes prevents a more extensive discussion at this time.

Dilutions as high as 160/1 of argon over propane cause no change in k_2/k_1 from the undiluted system. Thus, it would appear that $^1CH_2$ is *translationally* equilibrated before insertion.

Reactions of Singlet Methylene Produced by Vuv Photolysis. The following mechanism represents possible reactions of methylene produced in the photolysis of propane.

$$C_3H_8 = {}^1CH_2 + C_2H_6 \qquad \phi_s^pI \quad (3a)$$

$$= {}^xCH_2 + C_2H_6 \qquad \phi_x^pI \quad (3b)$$

$$^1CH_2 + C_3H_8 = C_4H_{10} \qquad k_4 \quad (4)$$

$$^1CH_2 + C_3H_8 = {}^3CH_2 + C_3H_8 \quad k_5 \quad (5)$$

$$^1CH_2 + Ar = {}^3CH_2 + Ar \qquad k_6 \quad (6)$$

$$^3CH_2 + O_2 = \text{product} \qquad k_7 \quad (7)$$

$$^xCH_2 + \text{reactant} = \text{not butane} \quad (8)$$

Reaction 3 has been established as a primary process in the photolysis of propane and as the only source of ethane in this system when radicals are removed by a suitable additive.[5] At pressures where secondary decomposition of this ethane is negligible, the yield of ethane may be taken as the yield of total methylene produced in the photolysis. (ϕ_x^p is the quantum yield of methylene other than that in the $^1A_1$ state. ϕ_s^p is the quantum yield of methylene in the $^1A_1$ state. I is the intensity of the absorbed light.)

Reaction 4 is the insertion of $^1CH_2$ into propane. This composite reaction can readily be separated into its components by the data of the previous section. We treat it as a single reaction for convenience.

Reaction 5 is included to allow for depletion of $^1CH_2$ by pathways other than collisional conversion by an inert gas, reaction 6. It was assumed by Eder, Carr, and Koenst that the rates of reactions 5 and 6 were of the same order of magnitude.[6] As will be discussed in more detail later, if all important reactions of $^1CH_2$ are expressed in the above mechanism, then ϕ_x^p must be greater than zero or k_5 must be considerably larger than k_6. That reaction 7 will be the only important reaction

(6) T. W. Eder, R. W. Carr, Jr., and J. W. Koenst, *Chem. Phys. Lett.*, 3, 520 (1969).

of triplet methylene in the presence of oxygen has been shown by Russell and Rowland.[7] Further, McKnight, Lee, and Rowland find that singlet product yields in a CH_2CO–butene-2 photolysis system do not decrease as O_2 is added from 0.03 to 20.0%.[8] On this basis we have not included any reaction of $^1CH_2$ with O_2 in the above mechanism.

Reaction 8 allows for reactions of methylene in states other than $^1A_1$ or $^3\Sigma_g$. The product of any such reactions yielding butane would be counted as belonging to $CH_2(^1A_1)$ reaction. Thus, products of reaction 8 are indicated to be other than butane.

A steady-state treatment of the above mechanism leads to the following general expression.

$$\frac{r_3}{r_4} = \frac{(\phi s + \phi x)}{\phi s}\left[1 + \frac{k_5}{k_4} + \frac{k_6(\mathrm{Ar})}{k_4(\mathrm{C_3H_8})}\right] \qquad (9)$$

The rate of production of ethane is r_3 (all methylenes) and r_4 is the rate of production of butane (methylene reacting *via* insertion). Any reactions of singlet methylene with propane other than those proposed in the mechanism, *e.g.*, H abstraction, would only add another rate constant to the second term of eq 9. On the other hand, any reaction not in the mechanism which involved a precursor to singlet methylene would show as a concentration dependence in the second term. The importance of this last observation to determining the primary process in cyclopropane will be discussed in a subsequent section.

When cyclopropane is used as the source of methylene (cyclopropane–propane mixture), reaction 3 is replaced by eq 10a and 10b.

$$c\text{-}C_3H_6 = {}^1CH_2 + C_2H_4 \qquad \phi_s{}^cI \qquad (10a)$$

$$= {}^xCH_2 + C_2H_4 \qquad \phi_x{}^cI \qquad (10b)$$

As long as the concentration of cyclopropane remains low relative to propane, the remaining equations of the mechanism are unchanged. Cyclopropane is a useful source of methylene. Reaction 10 is the most important primary process in the photolysis of cyclopropane.[9,10] C_2H_4 does not appear to undergo secondary decomposition at pressures as low as 10 Torr. This is in contrast to the behavior of ethane from propane.[1] We are currently exploiting this aspect of the cyclopropane system in an attempt to obtain an estimate of the energy carried by methylene produced by vuv photolysis when it inserts into propane.

Other sources of methylene such as *cis*- and *trans*-1,2-dimethylcyclopropane may also be substituted for reaction 3 provided concentrations relative to propane are kept low.

The relative yield of butane to methylene cofragment in each of the molecules studied is always less than or equal to 0.6. This means that at least 0.4 of the methylene produced in the photolysis does not insert into propane. There are several possible explanations for this observation. The primary photochemical process may not produce all $^1A_1$ methylenes. For example, $^3\Sigma_g$-methylene is known not to insert.[11,12] Higher energy singlet states are energetically available[13] and their reactions are not well known. Another reaction with a component of the reaction system may compete with the insertion reaction. The simplest system is that of propane and oxygen. Since the yield of singlet products has been found to be independent of oxygen concentration,[8] propane would have to compete with insertion through another reaction mode such as reaction 5. Of course, this competition would not show a concentration dependence in the systems containing only propane. One should be able to differentiate between two such competing reactions in mixed cyclopropane–propane systems. This has not proved feasible, however, since the reaction products of methylene and cyclopropane have remained obscure.[9] Finally, it is possible that fragments smaller than methylene, *e.g.*, CH, are produced in the reaction yielding that product taken by us to be the methylene cofragment. Such fragments are energetically possible only in the propane photolysis at 123.6 nm. Since similar yields of singlet (as butane) are seen in the cyclopropane and other propane systems, this alternative is rejected.

Of the two reasonable alternatives, direct production of CH_2 in states other than $^1A_1$ and competing reactions of propane with $^1CH_2$, the former can be investigated indirectly using *cis*- or *trans*-1,2-dimethylcyclopropane.

Methylene addition to *cis*- and *trans*-2-butene has long been used as a diagnostic for determining the presence of singlet and triplet methylene.[14] Singlet adds to the double bond with retention of geometry and triplet addition is thought to lead to a certain amount of randomization of geometric isomers in the addition

(7) R. L. Russell and F. S. Rowland, *J. Amer. Chem. Soc.*, **90**, 1671 (1968).

(8) C. McKnight, E. K. C. Lee, and F. S. Rowland, *Ber. Bunsenges. Phys. Chem.*, **72**, 236 (1968).

(9) A. A. Scala and P. Ausloos, *J. Chem. Phys.*, **49**, 2282 (1968).

(10) C. L. Currie, J. H. Okabe, and J. R. McNesby, *J. Phys. Chem.*, **67**, 1494 (1963).

(11) P. S. T. Lee, R. L. Russell, and F. S. Rowland, *Chem. Commun.*, **1970**, 18 (1970).

(12) W. Braun, A. M. Bass, and M. Pilling, *J. Chem. Phys.*, **52**, 5131 (1970).

(13) G. Herzberg, "Molecular Spectra and Molecular Structure. III. Electronic Spectra and the Electronic Structure of Polyatomic Molecules," Van Nostrand Company, Princeton, N. J., 1967.

(14) (a) T. W. Eder and R. W. Carr, *J. Phys. Chem.*, **73**, 2074 (1969); (b) D. F. Ring and B. S. Rabinovitch, *ibid.*, **72**, 191 (1968); (c) R. Hoffmann, *J. Amer. Chem. Soc.*, **90**, 1474 (1968); (d) C. McKnight, P. S. T. Lee, and F. S. Rowland, *ibid.*, **89**, 6802 (1967); (e) R. W. Carr, Jr., and C. B. Kistiakowsky, *J. Phys. Chem.*, **70**, 118 (1966); (f) R. F. W. Bader and J. I. Generosa, *Can. J. Chem.*, **43**, 1631 (1965); (g) J. A. Bell, *J. Amer. Chem. Soc.*, **87**, 4996 (1965); (h) H. M. Frey, *Progr. React. Kinet.*, **2**, 131 (1964); (i) W. Kirmse, "Carbene Chemistry," Academic Press, New York, N. Y., 1964; (j) J. Bell, *Progr. Phys. Org. Chem.*, **2**, 1 (1964); (k) R. C. Woodwarth and P. S. Skell, *J. Amer. Chem. Soc.*, **81**, 3383 (1959); **78**, 4496 (1956).

product. Presumably the randomization occurs due to bond rotation during the time the triplet intermediate (trimethylene derivative) is crossing the spin-imposed barrier to bond formation. Using similar arguments for the reverse reaction

$$cis\text{-DMCP} \xrightarrow{h\nu} CH_2 + \diagdown\!\!=\!\!\diagup \qquad (11)$$

and presuming that if triplet methylene were formed directly from the decomposition of the parent molecule, the incipient butene would also be in a triplet state, we attempted to measure the amount of triplet arising from the primary fragmentation by noting the amount of randomization of the butene produced. As is apparent from Table II, there is no randomization of geometric isomers when either *cis*- or *trans*-1,2-dimethylcyclopropane is photolyzed to give methylene plus butene-2. Thus, if triplet methylene is produced directly in the fragmentation reaction, no triplet cofragment is formed. As there is no reason to expect violation of the spin conservation rule, we conclude that no triplet methylene is produced directly by this fragmentation. We note further that the yield of butane relative to butene-2 is similar to the butane–ethylene ratio in the cyclopropane photolysis and the butane–ethane ratio in the 123.6-nm photolysis of propane. It is reasonable, then, to presume that triplet methylene is not produced directly by the fragmentation of cyclopropane or propane (123.6 nm). The failure to observe equal yields of butane and methylene cofragment in each of these systems must then be the result of an unexpectedly high rate for reaction 3b, the production of higher electronic states of methylene (singlet) in the primary process, or the removal of singlet methylene by a reaction not specified in the mechanism given above. These alternatives will be discussed further after the following section.

If, for the photolysis of propane, ϕ_x^p in eq 9 is assumed to equal zero, as we assumed in our previous communication,[1] plotting the Ar–C_3H_8 ratio *vs.* ethane (total methylene yield) over butane (singlet methylene surviving to insert) yields $1 + k_5/k_4$ as the intercept and k_6/k_4 as the slope. This treatment gives $k_6/k_4 = 0.024 \pm 0.006$ and $k_5/k_4 = 0.7$ for propane photolyzed at 123.6 nm and $k_6/k_4 = 0.033 \pm 0.003$ and $k_5/k_4 = 1.5$ for propane photolyzed at 147 nm.

If one does not assume a value for $(\phi_s + \phi_x)/\phi_s$, the sets of rate constant ratios presented above cannot be uniquely determined. Algebraic manipulation of eq 9, however, yields the expression

$$k_6/(k_4 + k_5) = \text{slope/intercept} \qquad (12)$$

where the intercept and slope are of the lines of Figure 2. From this relationship, $k_6/(k_4 + k_5) = 0.014$ and 0.013 for the 123.6-nm for the 147-nm photolyses, respectively. These values are easily within experimental error of one another and show that the rate of reaction of singlet methylene with argon relative to sum of the rates of reaction of singlet methylene with propane is constant at different wavelengths. Thus, while it is clear that the competition between propane and argon for $^1CH_2$ is independent of wavelength, it is not clear whether *observable* singlet methylene is reduced at lower photolysis energies by a different partitioning of the reactions of methylene with propane or by a change in the initial fraction of total methylene produced in a form that can eventually insert.

Braun, Bass, and Pilling have recently published the results of a flash photolysis examination of the singlet to triplet conversion of methylene from diazomethane and ketene.[12] The pertinent results from this study are listed in eq 13–15. (Units of the rate constants are cm^3 molecule^{-1} sec^{-1}.)

$$^1CH_2 + Ar \longrightarrow {}^3CH_2 + Ar \qquad (6.7 \pm 1.3) \times 10^{-13} \quad (13)$$

$$^1CH_2 + CH_4 \longrightarrow C_2H_6^* \longrightarrow CH_3 + CH_3 \qquad (1.9 \pm 0.5) \times 10^{-12} \quad (14)$$

$$^1CH_2 + CH_4 \longrightarrow {}^3CH_2 + CH_4 \qquad (1.6 \pm 0.5) \times 10^{-12} \quad (15)$$

The similarity of rates for the insertion of methylene into a CH bond of methane and for methaae-induced intersystem crossing is reminescent of our results for the relative importance of these two reaction rates with propane. However, $k_{13}/(k_{14} + k_{15})$ is equal to 0.18. This is approximately a factor of 10 larger than the ratio of reactivity of argon to propane with methylene observed by us. Our value is consistent with other estimates of the relative rate of reactivity of methylene toward inert gas *vs.* hydrocarbon molecules.[6,15] In fact, changing k_{14} and k_{15} to values characteristic of methane rather than propane, using the data of Halberstadt and McNesby,[3] indicates a value of 0.02 for $k_{13}/(k_{14} + k_{15})$ rather than 0.18 as found by Braun, *et al.*[12] The inherent differences between the steady-state systems and the more direct flash photolysis make an analysis of this discrepancy difficult.

Table III summarizes the available values for the rate of collisional conversion of singlet to triplet methylene by argon relative to the rate of reaction of singlet methylene with a hydrocarbon species. The large discrepancy between the flash photolysis data and the steady-state data prevents us from using the flash photolysis data to decide whether the observation that only 0.6 of the total methylene produced in the photolysis of propane and cyclopropane appears as insertion product results from approximately equal values of k_4 and k_6 or whether it results from ϕ_x being greater than zero. Additional work must be done to identify the fate of the remaining methylene. Similarly, until more is known about the nature of the methylene and its

(15) R. A. Cox and K. F. Preston, *Can. J. Chem.*, 47, 3345 (1969).

Table III: Rate of Reaction of $^1CH_2$ with Ar Relative to Rate of the Reactions of $^1CH_2$ with Hydrocarbons in Various Systems

System		$\frac{k_6}{k_4 + k_5}$ [a]	$\frac{k_6}{k_4}$	$\frac{k_6}{k'}$ [b]	Ref
Ar, C_3H_8, O_2, 123.6 nm		0.014	0.024[c]		*f*
Ar, C_3H_8, O_2, 147 nm		0.013	0.033[c]		*f*
Ar, C_3H_8, CH_2CO, O_2, 366, 334, 313, 205 nm			0.025[d]		*g*
Ar, CH_2CO, O_2, 280, 249 nm				0.014	*h*
Ar, CH_2CO, O_2	Flash	0.18[e]	0.35[e]		*i*
	Far and vac.				
Ar, CH_2N_2, O_2	Uv				

[a] The denominator contains all possible reactions of $^1CH_2$ with propane. [b] k' is the rate constant for the reaction, $^1CH_2 + CH_2CO \rightarrow C_2H_4 + CO$. [c] Assumes $\phi_X = 0$, some value of ϕ_X must be assumed to evaluate k_6/k_4 from our data. [d] Assumes $k_5 \approx k_6$. [e] Substituting CH_4 for C_3H_8 in each of the reactions. [f] This work. [g] Reference 6. [h] Reference 15. [i] Reference 12.

reactions in steady-state systems of this type, the wavelength dependence observed in the photolysis of propane cannot be satisfactorily explained.

Implications for Primary Processes in the Photolysis of Cyclopropane. While Currie, Okabe, and McNesby postulate reaction 10 as the source of methylene and ethylene in the photolysis of cyclopropane,[10] Scala and Ausloos, in a more recent study,[12] suggest the following reaction sequence as the source of these products[9]

$$c\text{-}C_3H_6 = (CH_2)_3^* \quad (16)$$

$$(CH_2)_3^* = CH_2 + C_2H_4 \quad (17)$$

where $(CH_2)_3^*$ is a trimethylene intermediate. At least two pieces of evidence are available from our work to indicate that, at least for the production of methylene and ethylene, there is no need to postulate the trimethylene intermediate.

First, Figure 3 shows that the yield of singlet methylene produced in the photolysis of cyclopropane is independent of pressure above 300 Torr in a propane–cyclopropane mixture. If singlet trimethylene could undergo collisional conversion to triplet trimethylene by collision with propane, the yield of singlet methylene should show an inverse pressure dependence at higher pressures. Thus, collisional conversion of singlet to triplet trimethylene is not competitive with reaction 17 if the trimethylene is indeed produced.

Secondly, *cis*- and *trans*-1,2-dimethylcyclopropane yield only *cis*- and *trans*-butene-2, respectively. Thus, rotation about a bond in the (proposed) diradical structure is not competitive with decomposition to give methylene and the olefin. Presumably, the substituted cyclopropanes are similar to cyclopropane itself. Since there appears to be no direct method of detecting the proposed trimethylene intermediates chemically, we suggest that if it exists it must be very short lived. The primary process proposed by Currie, *et al.*, reaction 10, adequately describes the production of methylene and ethylene from the photolysis of cyclopropane.

Acknowledgment. We are indebted to the National Science Foundation and the Petroleum Research Fund, administered by the American Chemical Society, each for partial support of this research.

Radiolysis of Aqueous Solutions of Methyl Chloride. The Concentration Dependence for Scavenging Electrons within Spurs[1]

by Turgut I. Balkas, J. H. Fendler, and Robert H. Schuler*

Mellon Institute Radiation Research Laboratories and Department of Chemistry, Carnegie-Mellon University, Pittsburgh, Pennsylvania 15213 and Chemistry Department, Middle East Technical University, Ankara, Turkey
(Received July 24, 1970)

The radiolysis of 0.01 *M* aqueous solutions of methyl chloride produces chloride ion with a yield of 2.75 ± 0.07 which appears to result, for the most part, from reaction with electrons that escape spur recombination. This reaction occurs with a rate constant of $1 \times 10^9\ M^{-1}\ sec^{-1}$ as indicated by both competitive and optical pulse radiolysis measurements. At higher concentrations the yield increases. In presence of OH scavenger the observed increases in yield are interpreted as the result of scavenging electrons within the spurs and are in accord with the predictions of Schwarz on the spur-diffusion model. Extrapolation of the results at 0.01 *M* CH_3Cl to zero solute concentration gives the yield of electrons which escape spur recombination in pure water as 2.63 ± 0.07. The concentration dependence for competitive scavenging from the spur, together with the above mentioned rate constant, establishes the time dependence for reaction of electrons within the spurs. Such reaction occurs mostly in the time region of 10^{-10} to 10^{-8} sec after solvation. Pulse conductivity studies show that secondary reactions do not occur on the 10^{-5} to 10^{-2} sec time scale and that the yield is independent of dose down to doses of the order of a few rads. Methyl chloride appears to be an excellent reference solute for pulse conductivity work.

It is now generally accepted that the yield of hydrated electrons which escape from the spurs in neutral water is ~2.7.[2] Most recently a value of 2.76 was obtained by Bielski and Allen[3] by examining the initial yield for oxidation of ferrous ion and of peroxide from ethanol solutions, of 2.76 by Asmus and Fendler from a determination of the fluoride yield from SF_6 solutions,[4] and 2.66 by Fricke and coworkers from measurements of H_2O_2 production in solutions containing hydrogen and oxygen.[2] All of these results were obtained in near neutral solutions and at sufficiently low solute concentrations ($<10^{-3}$ *M*) that scavenging within the spurs should not contribute significantly to the yield. It is known that at low pH's and high solute concentrations scavenging of electrons which normally do not escape from the spur in pure water leads to an increase in the observed yield and detailed calculations of the effects expected have been carried out by Schwarz.[5] In many of the early experimental attempts to examine this effect, as has already been commented on quite extensively by Czapski,[6] true initial yields were not measured and only very limited data with which to compare the results of model calculations are presently available. SF_6 has proven to be an excellent scavenger of electrons in aqueous solution[4] and can be examined at low doses and over a wide pH range. Unfortunately its low solubility precludes examination of scavenging in the high concentration region. We wish to report here the results of studies on aqueous CH_3Cl solutions which have been carried out over the concentration range of 0.006 to 0.8 *M*. It is demonstrated by competitive studies with known electron scavengers that methyl chloride reacts reasonably rapidly with solvated electrons. Chloride ion is produced and can be readily and conveniently analyzed for by the use of an ion-selective electrode. At the lower concentrations this system appears to be extremely simple in that one chloride ion is produced for each electron scavenged, with little or no contribution from either hydrogen atom or hydroxyl radical reactions. Above 0.1 *M* CH_3Cl, secondary reactions of OH radicals produce a small additional amount of chloride but can be eliminated by the addition of a low concentration of OH scavenger. Studies of the concentration dependence of chloride production in systems containing an appropriate radical scavenger show a small increase in yield with increased methyl chloride concentration and it appears that this increase can be attributed to electron scavenging within the spurs. Because chloride ion is an unreactive product, secondary reactions should be unimportant and this system appears to be an excellent one with which to probe the spur reactions. The results from auxiliary optical and conductometric pulse radiolysis experiments are also reported as well as data obtained in an exten-

* To whom correspondence should be directed.

(1) Supported in part by the U. S. Atomic Energy Commission.

(2) For references to earlier studies see K. Sehested, H. Corfitzen, and H. Fricke, *J. Phys. Chem.*, **74**, 211 (1970).

(3) B. H. J. Bielski and A. O. Allen, *Int. J. Radiat. Phys. Chem.*, **1**, 153 (1969).

(4) K.-D. Asmus and J. H. Fendler, *J. Phys. Chem.*, **72**, 4285 (1968).

(5) H. A. Schwarz, *ibid.*, **73**, 1928 (1969).

(6) G. Czapski, Advances in Chemistry Series, No. 81, American Chemical Society, Washington, D. C., 1968, p 106.

sion of the previous study of SF_6 to more dilute solutions.

Experimental Section

For the steady-state experiments methyl chloride, nitrous oxide, and sulfur hexafluoride were purified on a vacuum line by trap-to-trap distillation at Dry Ice temperature. Reagent grade acetone, methanol, isopropyl alcohol, sulfuric acid, perchloric acid, sodium hydroxide, sodium nitrate, and sodium formate were used without further purification. For the pulsed optical and conductivity experiments Matheson methyl chloride was taken directly from a lecture bottle and bubbled through the appropriate solution to saturate it at atmospheric pressure.

Except for the studies in acid solutions and the competitive studies with SF_6, all steady-state irradiations were carried out in phosphate buffered solutions at pH ~6.5 (buffer concentration $\sim 10^{-3}$ *M*). The desired amounts of methyl chloride and other solutes were added to degassed solutions of triply distilled water and sealed in vessels having less than 10% vapor volume. The solubility coefficient of methyl chloride is 2.5,[7] so that essentially all (*i.e.*, >96%) of the methyl chloride was in solution. The concentrations of other gaseous solutes were determined from their solubility coefficients in the manner previously described.[4] At high methyl chloride concentrations, degassing was by the usual thaw-freeze-pump method (4 cycles) at liquid nitrogen temperature. At methyl chloride concentrations below 10^{-2} *M* degassing was at −34° (frozen 1,2-dichloroethane bath) to remove as much dissolved CO_2 as possible.

Most of the irradiations were carried out inside a cylindrical ^{60}Co source at an absorbed dose rate of 5.2×10^{18} eV g^{-1} hr^{-1}. Absorbed doses were determined by reference to the Fricke dosimeter. Yields are calculated on the basis of the energy absorbed in the water. The yields based on the total energy absorbed will be lower by a factor (1 + 0.045 *M*) if one assumes that the methyl chloride is lost from the sample at the time of measurement. Where chloride was to be determined, doses in the range 10^{18}–10^{19} eV/g were used. These doses are sufficient to build up $\sim 10^{-4}$ *M* H_2O_2 and also appreciable oxygen which will tend to suppress secondary hydrogen atom and hydroxyl radical reactions. Certain additional experiments were carried out at dose rates of 10^{18} and 7×10^{19} eV g^{-1} hr^{-1}.

In the studies on SF_6 solutions, both in the presence and absence of methyl chloride, the fluoride ion concentration was determined with an Orion 94-09 fluoride electrode as previously described.[4] The chloride ion concentration produced from methyl chloride was similarly determined with a chloride electrode. The electrode potential relative to the reference electrode was determined with an Orion Model 801 digital pH meter capable of measuring the emf to 0.1 mV. Three different electrode systems were used. Initially an Orion Model 94-17A chloride electrode was used in conjunction with a Model 90-02 double junction reference calomel electrode using a 10% KNO_3 solution as the junction electrolyte. This electrode could not be used with perchloric acid solutions because of problems caused by precipitation of $KClO_4$. For certain experiments the 94-17A electrode was used directly in conjunction with a Model 90-01 reference electrode. Although the junction fluid contained chloride ions, leakage was minimal and satisfactory results could be obtained in measuring times of a few minutes. For the more recent measurements an Orion Model 96-17-00 combination chloride electrode was used. Although all three electron systems gave comparable results, the combination electrode proved most satisfactory because of the very small volume of solution (~0.1 cc) required for measurement.

The measured potentials were compared with those of standard solutions at the same ionic strength and pH. For all three electrode systems a plot of emf *vs.* log *C* obeyed the Nernst relation over the range of 10^{-4} to 2×10^{-3} *M* and had a slope of 59.1 mV per decade. The emf measurements were made with a reproducibility of ±0.2 mV and the overall absolute accuracy of the concentration measurements is estimated to be ~2%. It is noted that the sensitivity of the chloride electrode is less by two orders of magnitude than that of the fluoride electrode so that quantitative measurements are presently restricted to concentrations above 10^{-4} *M* though chloride ion can be detected at a level $\sim 10^{-6}$ *M*. Tests of the hydrolysis of 10^{-2} *M* methyl chloride solutions showed no measurable hydrolysis in the pH range of 2–12; *i.e.*, after standing 3 days the chloride ion concentration was $< 10^{-6}$ *M*. A neutral solution 0.7 *M* in CH_3Cl was stable over the normal period required for preparation and measurement (several hours) but showed a small amount of hydrolysis ($\sim 10^{-5}$ *M*) upon standing several days.

Several determinations of the yields of CH_4 and C_2H_6 were made by analyzing 1 cc of the irradiated solution gas chromatographically on a 5-meter silicone grease column. The sample handling system was similar to that previously described.[8]

The production of HCl on the 10^{-6} to 10^{-2} sec time scale was examined in conductometric pulse radiolysis experiments similar to those described by Beck[9] and previously used in studies of various aromatic systems[10] and SF_6 solutions.[11] The conductometric cell con-

(7) "Landolt-Börnstein Tabellen," 6, II, 2b, Springer-Verlag, Berlin, 1962, pp 1–32.

(8) J. M. Warman and S. J. Rzad, *J. Chem. Phys.*, **52**, 485 (1970).

(9) G. Beck, *Int. J. Radiat. Phys. Chem.*, **1**, 361 (1969).

(10) K.-D. Asmus, G. Beck, A. Henglein, and A. Wigger, *Ber. Bunsenges. Phys. Chem.*, **70**, 869 (1966); J. Lilie, G. Beck, and A. Henglein, *ibid.*, **72**, 529 (1966); J. Lilie and A. Henglein, *ibid.*, **73**, 170 (1969); W. Grünbein and A. Henglein, *ibid.*, **73**, 376 (1969).

sisted of two 9-mm square platinum plates separated by $\sim$9 mm inside a 1-cm square flowthrough Pyrex cell. The cell constant, determined by a conventional ac bridge method, was 0.7 cm^{-1} which implies an effective cell length of 1.3 cm. The outside of the cell was grounded by a coating of Aquadag. Without this coating, charge from the electron pulse built up in the glass vessel and leaked back through the measuring system for a period $\sim$10 μsec. Conductometric changes corresponding to the production of HCl in concentrations $\sim 10^{-7}$ M or greater could be measured within 3 μsec after the termination of the pulse. Pulse currents of up to 25 mA were delivered for periods of 0.5 to 10 μsec at 2.8 MeV from a Van de Graaff accelerator with the doses absorbed being from 2×10^{15} to 4×10^{18} eV/g (30–60,000 rads) per pulse. The beam diameter on entering the cell was $\sim$5 mm and approximately 60% of the beam current was collected from the cell itself. Signals corresponding to the conductometric change and beam current pulse were displayed simultaneously on a Tektronix Dual Trace oscilloscope and photographed.

For the conductometric studies, a flow system was used with triply distilled water which was first degassed by bubbling with nitrogen. The solution was then saturated at a known partial pressure of methyl chloride. At atmospheric pressure the solubility of methyl chloride is 0.1 M. Buffers could, of course, not be used here. However, even at the highest doses used the build-up of hydrogen ion was only $\sim 10^{-4}$ M, a concentration insufficient to compete significantly for reaction with electrons in solutions saturated with methyl chloride at atmospheric pressure. The absolute yield of HCl on the microsecond time scale was determined by reference to measurements on tetranitromethane.[9]

The rate of reaction of electrons with CH_3Cl was determined both by competition against SF_6 and by directly following the electron decay at 620 mμ in a conventional optical pulse radiolysis experiment.[12] The rate of reaction is sufficiently high ($\sim 10^9$ M^{-1} sec^{-1} *vide infra*) that direct examination on the μsec time scale requires a concentration of less than 10^{-3} M. An apparatus was developed for appropriately diluting a solution saturated at atmospheric pressure. Because of the high volatility of the methyl chloride, however, the concentrations of the resultant solutions have considerable uncertainty and the results obtained must be regarded as being of only limited significance.

Results and Discussion

The Rate Constant for $e_{aq}^- + CH_3Cl$. Competitive studies between SF_6 and CH_3Cl, in which F^- was measured as a function of SF_6 concentration at 1.2×10^{-2} M CH_3Cl, show the linear dependence of $1/G(F^-)$ *vs.* $1/[SF_6]$ expected from a simple competition between the two solutes for reaction with electrons (see Figure 2 in ref 4).

$$e_{aq}^- + CH_3Cl \longrightarrow Cl^- + \cdot CH_3 \quad (1)$$

$$e_{aq}^- + SF_6 \longrightarrow F^- + \cdot SF_5 \longrightarrow \quad (2)$$

This reciprocal plot extrapolates to an intercept which corresponds to $G(F^-)_0 = 16.5$, the value of $G(F^-)$ obtained from SF_6 in the absence of CH_3Cl, as it should if complications are absent. Taking the rate constant for reaction 2 as 1.65×10^{10} M^{-1} sec[-14] the rate constant for reaction of electrons with methyl chloride was determined to be 1.1×10^9 M^{-1} sec^{-1} from the slope and intercept of this plot.

Optical pulse radiolysis experiments were carried out at pH 10 for solutions 2.5×10^{-4} and 1.0×10^{-3} M in methyl chloride and gave half periods for electron decay, respectively, of 3.1 and 0.85 μsec. These values correspond to an average rate constant in reaction 1 of 0.8 $\times$ 10^9 M^{-1} sec^{-1}. In these experiments, however, because of volatility losses the methyl chloride concentrations are not well known and this estimate of the rate constant can only be regarded as a lower limit and a general confirmation of the value measured in the competitive experiments where the samples are sealed and the solute concentrations more accurately known.

Steady-State Experiments. Yield–dose plots for the formation of chloride ion at three CH_3Cl concentrations are given in Figure 1. It is seen that even though Cl^- production is somewhat dependent on the CH_3Cl concentration, at each concentration it is linear with dose over the range 2 to 15×10^{18} eV/g. Buffering of the CH_3Cl solutions is essential at these doses since otherwise the hydrogen ion produced by the irradiation builds up to $\sim 10^{-3}$ M and competes with the methyl chloride for the electrons. Data taken in unbuffered solutions show lower yields and a decrease with dose as expected. Measurements on 9×10^{-3} M CH_3Cl solutions at dose rates of 10^{18} and 7×10^{19} eV g^{-1} hr^{-1} gave respective yields of 2.70 and 2.65 and demonstrate that there is no significant dependence on dose rate over this range.

The yield of chloride ion from 18 measurements made on solutions in the range (6–9) $\times 10^{-3}$ M CH_3Cl was 2.75 $\pm$ 0.07. This value can be compared with the yield of electrons scavenged by SF_6 of 2.76 $\pm$ 0.05 measured at the same effective concentration. It seems evident that at this concentration the CH_3Cl is reacting only with electrons. To substantiate that Cl^- is not produced by OH attack an experiment was carried out at 2×10^{-3} M CH_3Cl and 5×10^{-2} M N_2O. For this solution >99% of the electrons are expected to be scavenged by the N_2O to produce OH radicals. No chloride was detected [$G(Cl^-) < 0.1$] so that OH attack cannot contribute significantly to chloride ion formation, at least at the lower CH_3Cl concentrations. The

(11) K.-D. Asmus, W. Grünbein, and J. H. Fendler, *J. Amer. Chem. Soc.*, **92**, 2625 (1970).

(12) M. S. Matheson and L. M. Dorfman, "Pulse Radiolysis," The M.I.T. Press, Cambridge, Mass., 1969.

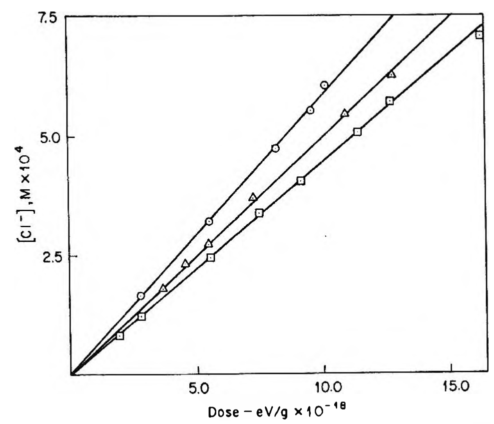

Figure 1. Formation of Cl^- as a function of dose for aqueous solutions: □, 9×10^{-3} *M*; △, 7×10^{-2} *M*; and ⊙, 2.5×10^{-1} *M* in methyl chloride at pH 6.5.

presence of hydrogen ion similarly reduces the chloride ion yield. For a solution 10^{-2} *M* in both H^+ and CH_3Cl $G(Cl^-)$ was found to be 0.2 as expected if one considers the 20-fold greater rate constant for reaction of electrons with H^+. Production of chloride ion *via* hydrogen atom attack on the CH_3Cl is apparently unimportant[13] compared to the other competing processes. Experiments at 0.007 and 0.013 *M* CH_3Cl in which 0.1 *M* CH_3OH was added to scavenge both H atoms and OH radicals gave Cl^- yields of 2.73 and 2.71 in agreement with the results obtained at this concentration in the absence of methanol (see also Table I). It seems, therefore, that at a concentration of 10^{-2} *M* or less, CH_3Cl is a specific scavenger for solvated electrons.

Table I: Effect of Methanol on Chloride Ion Yield

	$G(Cl^-)$			
$[CH_3OH]$	~0.01 *M* CH_3Cl	0.3 *M* CH_3Cl	0.5 *M* CH_3Cl	0.8 *M* CH_3Cl
	2.75	3.51	3.90	4.90
0.001	2.78		3.62	
0.01	2.73	3.47	3.59	3.73
0.1	2.71	3.64[a]	3.75	3.92
0.5			3.78	

[a] $G(Cl^-) = 3.49$ in the presence of 0.1 *M* $HCOO^-$.

Electron transfer from radicals such as $CH_3C(OH)CH_3$ was also shown not to be a source of Cl^- in an experiment in which electrons were scavenged by 2 *M* acetone and hydrogen atom and hydroxyl radicals were scavenged by 0.1 *M* isopropyl alcohol. At a CH_3Cl concentration of 7×10^{-2}, $G(Cl^-)$ was <0.1.

Two measurements of $G(Cl^-)$ at pH 12, where hydrogen atoms are converted to electrons, gave values of 3.15 and 3.19. Correcting $G_{e_{aq}^-} + G_H$ (= 0.45) by an additional 0.1 for scavenging from the spurs at this pH, the expected yield of reduction is 2.63 + 0.45 + 0.1 = 3.2. There is little, if any, effect of pH on the total yield of reducing radicals over the pH range of 4–12.

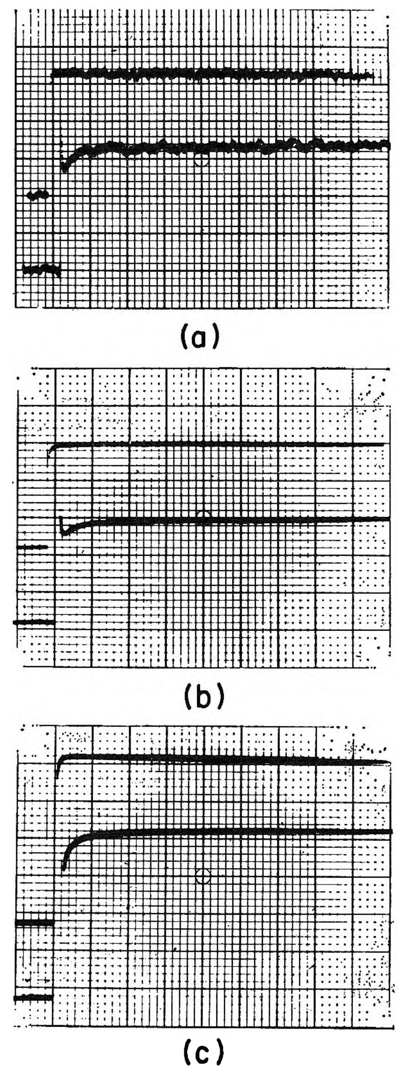

Figure 2. Oscilloscopic patterns of conductivity changes for methyl chloride saturated solutions at doses of (a) 10^{16}, (b) 10^{17}, and (c) 10^{18} eV/g. Isopropyl alcohol (0.1 *M*) and methanol (0.1 *M*) have been added to (a) and (c), respectively, but patterns obtained without added alcohol are comparable. In each case the time scale of the upper trace is 200 μsec/cm and lower trace 20 μsec/cm. Base lines on the left have been displayed by appropriate pretriggering of the oscilloscopic traces.

Determination of $G(CH_4)$ and $G(C_2H_6)$ at 10^{-1} *M* CH_3Cl gave yields of 0.2 and 0.3. Only 25% of the methyl radicals are accounted for so that they mostly react with other radicals or impurities either initially present or produced by the radiation. It is pointed out that at the doses used peroxide and oxygen must have built up to concentrations ~10^{-4} *M* (see Figure 1). Addition of 0.1 *M* CH_3OH eliminated the formation of methane and ethane.

Pulse Conductivity Experiments. Examination of the

(13) P. Neta, R. W. Fessenden, and R. H. Schuler, to be published, have found that k_{H+CH_3Cl} is only 9×10^4 M^{-1} sec^{-1}.

conductivity change in the pulse irradiation of a pH 6 methyl chloride saturated solution shows that, as expected, the reaction is complete within several microseconds. Presumably at pH values below 7 the observed change is the result of the formation of one molecule of HCl for each electron captured by the CH_3Cl; *i.e.*, the H^+ ion which is produced as a complement of the electron will remain unneutralized in acid solutions. Typical oscilloscopic traces observed at low to moderately high doses are illustrated in Figure 2. The observed effect plateaus quickly and remains flat out to several milliseconds.

The conductivity change was determined as a function of dose with and without added methanol and isopropyl alcohol. The alcohols have no apparent effect on the observed change. A yield–dose plot is given in Figure 3 along with comparison data taken on tetranitromethane and benzyl chloride solutions. Irradiation of an acetone–isopropyl alcohol solution gave a blank ~2% of the change found with methyl chloride. Since the net change in conductivity in this latter case should be nil, *i.e.*

$$e^- + (CH_3)_2CO \longrightarrow (CH_3)_2\dot{C}O^-$$
$$H^+ + (CH_3)_2CO^- \longrightarrow (CH_3)_2\dot{C}OH$$

this blank (corresponding to a G ~0.06) must result either from an ionic producing impurity or some chemical product such as $H\dot{O}_2$ which would be ionized at pH's near neutral. In the absence of other ionized products, conductivity should provide an extremely sensitive method for examining for the formation of small amounts of $HO_2\cdot$ ($\rightleftharpoons O_2\cdot^- + H^+$). This blank is sufficiently small that its effect will be lost in the other errors and it has been disregarded in the following since it is not clear to what extent it should be applied.

For methyl chloride the conductivity change is proportional to dose for doses up to ~4×10^{17} eV/g. At higher doses the apparent yield drops off somewhat as is illustrated in Figure 4 although there is no obvious chemical reason for such a drop. In the steady-state experiments the yield is independent of dose to considerably higher doses. While the dose rate here is up to a factor of 10^8 greater than in the steady-state experiments the total amount of product is less. For an absorbed dose of 2×10^{18} eV/g, where the observed drop is ~25%, the amount of hydrogen ion produced in the pulse is only 10^{-4} M so that the $e_{aq}^- + H^+$ reaction should account for only a few per cent of the scavenging at 0.1 M CH_3Cl. While the radical concentration is relatively high the data for solutions with and without added isopropyl alcohol (and also methanol) overlap so that reactions of $H\cdot$ and $\cdot OH$ cannot be important. It seems likely that the observed drop is an experimental artifact. In particular it is noted that at the highest doses used the cell current was of the order of 1 mA so that electrode polarization problems are undoubtedly important. In Figure 4 the drop in apparent yield in the region of 10^{18} eV/g is roughly proportional to the dose from which one can conclude that at doses less than 2×10^{17} the effect for methyl chloride can only be a few per cent or less. The absolute noise level in these experiments is extremely low (corresponding to dose levels of $<10^{13}$ eV/g) so that measurements can be made at extremely low doses with roughly the same percentage accuracy as at high doses. The lowest point in Figure 4 (which is the point just above the origin in Figure 3) corresponds to a dose of only 30 rads where the amount of product produced was only 10^{-7} M. Measurable changes were observed for doses an

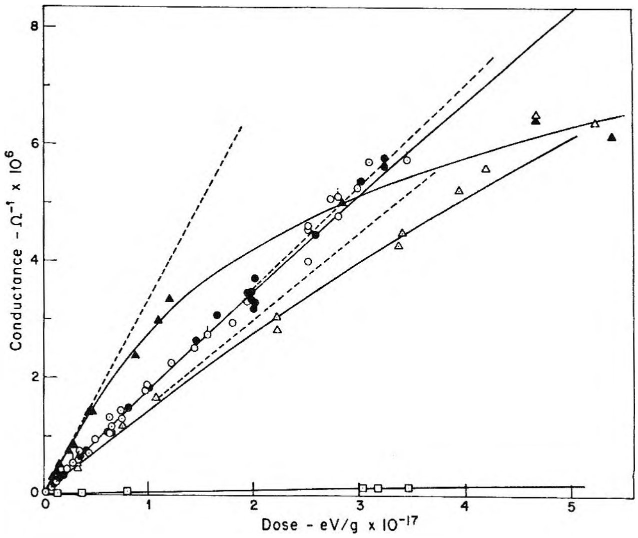

Figure 3. Conductivity change as a function of dose for saturated methyl chloride solutions (●) containing in addition 0.1 M methanol (○) and isopropyl alcohol (ȯ). Results are also given for 6×10^{-4} M tetranitromethane containing 0.1 M isopropyl alcohol (▲), saturated benzyl chloride (△), and 0.1 M acetone-0.1 M isopropyl alcohol (⊡). Solid curves through the points correspond to a yield which decreases linearly with dose and which extrapolates to an initial yield at zero dose given by the dashed lines.

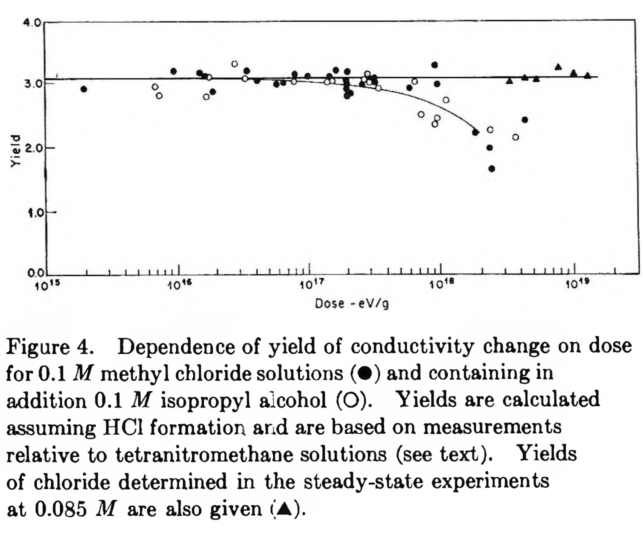

Figure 4. Dependence of yield of conductivity change on dose for 0.1 M methyl chloride solutions (●) and containing in addition 0.1 M isopropyl alcohol (O). Yields are calculated assuming HCl formation and are based on measurements relative to tetranitromethane solutions (see text). Yields of chloride determined in the steady-state experiments at 0.085 M are also given (▲).

order of magnitude lower where integration of the electron pulse (only 10^{-11} coulombs) became the most significant problem. Since differential conductances are measured, one must be careful at such low doses to bias the initial solution slightly on the acid side of neutral so that the H^+ ion will not be lost in neutralization.

A least-mean-squares treatment of the data for methyl chloride without added alcohol gives an initial slope of 320 ± 3 mhos/C of electron beam current collected in the cell where the indicated error is the probable error in the intercept of a linear plot of yield as a function of dose. The arithmetic average of the yields for all 50 data points given in Figure 3 (equally weighting all yields determined over the range 10^{15}–4×10^{17} eV/g where the decrease with dose is less than a few per cent) gives a value of 321 mhos/coulomb. An estimate of the absolute yield can be made if one knows the average dose rate per unit current within the cell volume. If the 2.8 MeV of energy is effectively dissipated over a volume of 3.0 cm^3 then an absolute yield of 3.2 can be given for HCl production (taking HCl = 425 mhos/equiv). This value is, however, subject to considerable uncertainty and should be regarded as being good to only ±25%. Beck has suggested[9] that tetranitromethane and benzyl chloride are appropriate reference standards and in the case of nitromethane has compared the conductance change to the optical absorption of the nitroform anion. Both of these substances are somewhat difficult to work with and, as is seen in Figure 3, exhibit appreciable decreases with dose. In addition, the yields from benzyl chloride solutions are poorly reproducible because of hydrolysis which builds up background H^+ and as a result cannot be regarded as reliable references. Extrapolation of the yield to zero dose for both sets of data given in Figure 3 gives initial slopes of 601 ± 10 mhos/coulomb for tetranitromethane (containing 0.1 *M* 2-propanol) and 262 ± 10 mhos/coulomb for benzyl chloride. The initial yield of nitroform produced in the former system has been determined to be 6.3 ($= G_{e_{aq}^-} + G_H + G_{OH}$).[14] Assuming this to be accurate and correcting the extrapolated conductivity changes given above for the difference in equivalent conductances ($\Lambda_{H^+} + \Lambda_{C(NO_2)_3^-} = 386$ mhos/equiv)[9] a yield of 3.05 ± 0.06 is obtained for the methyl chloride system and 2.5 ± 0.1 for benzyl chloride. This latter value is about 10% lower than expected but does confirm, in a general way, the reliability of the referencing of the measurements to tetranitromethane. Both the absolute and relative determinations give the yield from conductivity measurements for doses up to 2×10^{17} eV/g as approximately 3 and it would seem reasonable to identify the actual yield with the value of 3.14 determined in the steady-state experiments for a methyl chloride solution saturated at atmospheric pressure (*i.e.*, at 0.1 *M* CH_3Cl; see eq III below) even though the latter measurements were made at an order of magnitude higher absorbed dose. With this assumption it is suggested that methyl chloride solutions represent an excellent standard for pulse conductivity measurements.

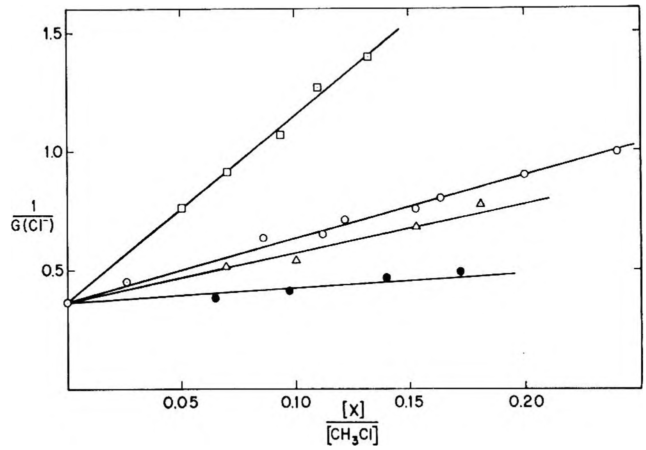

Figure 5. Competition plots of results from methyl chloride solutions to which a concentration [X] of (□) hydrogen ion (at pH 3, methyl chloride varied), (○) nitrous oxide, (△) acetone, and (●) nitrate ion had been added (0.01 *M* methyl chloride, second solute varied).

Competitive Experiments. The simplicity of the radiation chemistry of methyl chloride in dilute solution argues for its use for determining the rate constants for the reaction of electrons in competitive experiments. Figure 5 illustrates results obtained with H^+, N_2O, $(CH_3)_2CO$, and NO_3^-. The study with H^+ was carried out at a constant pH of 3 (varying the CH_3Cl concentration) because at lower pH's oxidation of Cl^- by electron transfer to OH complicated the competition and gave low Cl^- yields. In the other cases the concentration of the second solute was varied at constant [CH_3Cl]. Assuming that the rate constant for reaction 1 is 1.1×10^9 M^{-1} sec^{-1} as given by the competitive experiments with SF_6, the rate constants determined for the first three solutes form the slopes of Figure 3 are $k_{e+H^+} = 2.4 \times 10^{10}$, $k_{e+N_2O} = 8.3 \times 10^9$, and $k_{e+(CH_3)_2CO} = 6.3 \times 10^9$ M^{-1} sec^{-1} and are in good agreement with literature values.[15] The data on NO_3^-, if taken at face value, give an apparent rate constant of 1.8×10^9 M^{-1} sec^{-1} for $k_{e+NO_3^-}$ which is a factor of 8 lower than reported values.[15] Determination of this rate constant by similar competition experiments with SF_6 gives a value of 7.6×10^9 M^{-1} sec^{-1}.[16] Apparently chloride is produced by secondary reactions in the nitrate system. This result indicates that one must use care in interpreting the results of competitive experiments with CH_3Cl.

Concentration Dependence. The concentration de-

(14) K.-D. Asmus and A. Henglein, *Ber. Bunsenges. Phys. Chem.*, **68**, 348 (1964).

(15) M. Anbar and P. Neta, *Int. J. Appl. Radiat. Isotopes*, **18**, 493 (1967).

(16) K.-D. Asmus and J. H. Fendler, *J. Phys. Chem.*, **73**, 1583 (1969).

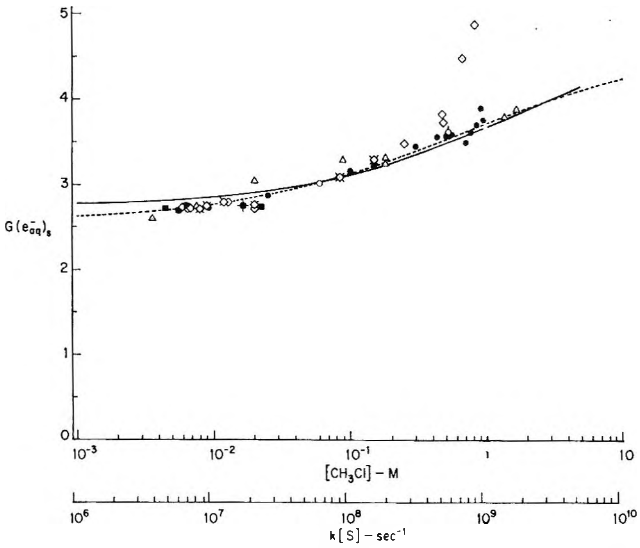

Figure 6. Dependence of chloride ion yield on methyl chloride concentration: no additives (◇; ⯐ from yield-dose plots), 10^{-3} (ȯ), 10^{-2} (●) and 10^{-1} (○) M methanol. Results from SF_6 solutions (■; ✚ from ref 4) and from nitrous oxide solutions (△ from ref 18) are also given. Solid curve represents *a priori* predictions of Schwarz (see ref 19). Dashed curve is empirical correlation $G(Cl^-) = 2.55 + 2.23(\sqrt{1.3[CH_3Cl]})/(1 + \sqrt{1.3[CH_3Cl]})$.

pendence of $G(Cl^-)$ is given in Figure 6. Also given in the figure are data on $G(F^-)/6$ obtained from solutions $\sim 10^{-4}$ M in SF_6 during the course of this study along with the value previously reported at 10^{-3} M.[4] It is seen that at CH_3Cl concentrations above 10^{-2} M, $G(Cl^-)$ increases appreciably. At 10^{-1} M a yield of 3.1 is observed in agreement with the result reported by Hayon and Allen.[17] At concentrations approaching 1 M, $G(Cl^-)$ increases to a value of about 5. An increase is expected in this region because the methyl chloride will scavenge electrons within the spurs;[5] however, the observed increase is much more than expected on the basis of results obtained with N_2O and other related systems.[18] It seems likely that at high CH_3Cl concentrations abstraction reactions produce $\cdot CH_2Cl$ radicals. Experiments similar to the present with CH_2Cl_2 show that these latter radicals do not give chloride directly or by reaction with hydrogen peroxide. However, as one possibility, they might form $CH_2(OH)Cl$ by combination with residual OH radicals. Such a compound would, of course, readily hydrolyze to form CH_2O and HCl. In order to remove OH radicals, experiments were carried out on solutions to which CH_3OH had been added. The methanol had no observed effect at CH_3Cl concentrations below 10^{-1} M but considerably lower values of $G(Cl^-)$ were observed at high CH_3Cl concentrations as is indicated in the figure. The presence of methanol should only affect secondary reactions so that the data obtained at 10^{-2} M CH_3OH (the lower curve in Figure 6) would appear to represent the true concentration dependence of electron scavenging, including reaction with the electrons within the spurs. This dependence is compared in the figure with the predictions of Schwarz.[5,19] Hayon has suggested that the parameter properly considered relative to the concentration dependence of scavenging from the spur is k[S] and in fact, to first order, this concept is implicit in Schwarz' calculations. Czapski has pointed out that depletion problems and secondary reactions within the spurs will differ from solute to solute so that this idea cannot be rigorous.[6] However such differences will affect the chemistry only in a very minor way and plots of yield as a function of k[S] should be reasonably superimposable. The data on nitrogen yields from nitrous oxide solutions given by Dainton and Logan,[18] with which Schwarz originally made his comparison, are also given in the figure and fall reasonably well along the curve when plotted at the appropriate k[S] but other data on nitrous oxide are somewhat lower, presumably because true initial yields were not measured.[6] The rate constant for reaction 2 is 15 times that for reaction 1 and accordingly in the figure the data for SF_6 have been shifted to the right relative to the CH_3Cl data by this factor.

Conclusions on the Spur Model. The general agreement of the present data with the calculations of Schwarz is most gratifying since his calculations are an *a priori* prediction of the absolute yields based on parameters previously determined for the spur model. The only important parameter which is particular to the CH_3Cl system is the rate constant for reaction 1. At low concentrations the calculated yields are $\sim$0.1 G unit higher than the observed values but would fit the observations reasonably well over the range of 10^{-2} to 10^{-1} M CH_3Cl if normalized by a factor of 0.98 as was done by Schwarz in his comparison with the data from nitrous oxide solutions. At higher concentrations the observed yields increase somewhat more sharply than predicted. The differences are, however, very minor and the data and the conclusions from the spur-diffusion model appear to be in as complete accord as one can expect at this point.

Two other facets of these results should be pointed out. First, one might expect that addition of an $\cdot$OH scavenger might release electrons to the bulk of the solution by suppression of the $e_{aq}^- + \cdot OH$ reaction within the spurs. Schwarz' calculations[19] predict that for CH_3OH up to 0.1 M this effect should be very small and the results given in Table I show that at low CH_3Cl

(17) E. Hayon and A. O. Allen, *J. Phys. Chem.*, **65**, 2181 (1961).
(18) F. S. Dainton and S. R. Logan, *Trans. Faraday Soc.*, **61**, 715 (1965).
(19) H. A. Schwarz, private communication. Dr. Schwarz kindly used the methods he previously described (ref 5) to calculate the chloride yield expected from methyl chloride solutions. This calculation was based on a rate constant for reaction of electrons with CH_3Cl of 1.1×10^9 M^{-1} sec^{-1}, trivially small abstraction rates with CH_3Cl for H and OH, and the other parameters of the spur model as previously determined. The yields predicted for 0.01 M CH_3OH solutions are given by the solid curve in Figure 6.

concentrations there is no significant dependence of the chloride yield on methanol concentration. Second, at high methyl chloride concentrations suppression of the $e_{aq}^- + \cdot OH$ reaction by the methanol should increase the yield for reaction of electrons with methyl chloride within the spur. Schwarz indicates that these increases are expected to be small for methyl chloride concentrations up to 0.1 *M*. Increases of only 0.01 and 0.08 are expected for solutions 0.5 *M* in CH_3Cl and 0.1 or 1.0 *M* in methanol.[19] The experimentally observed increases appear to be somewhat greater than this (~0.1–0.2) but the effect is of the magnitude of the uncertainty involved in the yield measurements and it can be taken that theory and experiments agree that this second effect must be small.

Although a yield of 2.75 is observed in the region of ~10^{-2} *M* CH_3Cl, it should be noted that this yield still contains a small contribution from the scavenging of electrons within the spurs. Schwarz' calculations show that an infinitely dilute methyl chloride solution should have a yield lower by 0.12 unit. This differential yield should be accurately applicable to the present study so that the yield of electrons which escape from the spur in pure water can be extrapolated from the present results to 2.63 ± 0.07. The same argument applies to the results on SF_6 solutions where the observed yield (2.76 ± 0.05) must be reduced by a similar amount to give a free electron yield of 2.64. Sehested, Corfitzen, and Fricke have extrapolated their measurements on peroxide production to a value of 2.66 and have suggested that Bielski and Allen's results should be similarly extrapolated to 2.71. The excellent agreement between the conclusions from these various experiments point out very strongly that the yield of free electrons in pure water is in the range 2.6–2.7. Most experiments with electron scavengers are, however, carried out at sufficiently high concentrations that the observed yields will be at least slightly higher.

It will be observed in Figure 6 that the increase in yield above that for very dilute solutions is approximately proportional to the square root of the solute concentration. This resembles the situation in hydrocarbons where the fraction of ions scavenged [*F*(S)] is described[20] over a wide concentration range by

$$F(S) = \frac{\sqrt{\alpha[S]}}{1 + \sqrt{\alpha[S]}} \qquad (I)$$

(α is an empirical parameter related to the rate constant for the scavenging reaction at solute concentration [S]) and leads one to attempt a similar mathematical description here. The competing processes are, of course, quite different in the two cases. In the case of hydrocarbons reaction with the scavenger competes with recombination of ionic partners which are initially separated by relatively large distances but which are constrained by their mutual coulombic force field to react with each other. In the case of aqueous solutions the competitive reactions within the spur involve, for the most part, bimolecular reactions of radicals separated at relatively small distances. Although the details are quite different, both of these circumstances involve competition between diffusion and scavenging, which mathematically gives rise to an approximate square root dependence of yield on concentration,[21] and so the experimental similarity is not too surprising. One can fit the data of Figure 6 quite well over the concentration range of 10^{-2} to 1 *M* if the scavenging from the spur is assumed to have the form of eq I. There is, of course, a considerable latitude in the assignment of the individual parameters of such an expression since the experimental measurements have been made over a fairly narrow concentration range and the limiting yields are ill defined. We have imposed the constraint that the limiting yield at high concentrations is the yield given by Schwarz for the total initial yield of electrons produced in pure water (4.78).[5] As is illustrated by the dashed curve in Figure 6, the available data obtained in the presence of 10^{-2} *M* methanol can be described by

$$G(Cl^-) = 2.55 + 2.23 \frac{\sqrt{\frac{k}{\lambda}[S]}}{1 + \sqrt{\frac{k}{\lambda}[S]}} \qquad (II)$$

with $k/\lambda = 1.3\ M^{-1}$. The low concentration limit given by eq II (2.55) is slightly less than that given above for the extrapolation *via* the calculations of Schwarz. Since the latter approach appears to be valid, eq II must break down for low solute concentrations where $k/\lambda[S] \ll 10^{-2}$ but the differences will be trivially small for all except the most detailed considerations. While eq II is properly considered solely as an empirical description of the concentration dependence of the yield it should prove to be very useful in predicting and correlating results of various electron scavenging experiments, particularly at high solute concentration.

One can at this point use arguments identical with those detailed for the ion scavenging processes in hydrocarbons[22] to transform the concentration dependence given by eq I and obtain a description of the time dependence of the electron population within the spurs. Such a treatment of eq II gives the fraction of electrons within the spur still present at time t as $e^{\lambda t}\ \mathrm{erfc}(\lambda t)^{1/2}$. Here λ is the empirical constant obtained from the observed concentration dependence in scavenged solutions but which, in fact, pertains to the electron decay in pure

(20) J. M. Warman, K.-D. Asmus, and R. H. Schuler, *J. Phys. Chem.*, **73**, 931 (1969).

(21) L. Monchick, *J. Chem. Phys.*, **24**, 381 (1955); R. M. Noyes, *Progr. React. Kinet.*, **1**, 128 (1961).

(22) S. J. Rzad, P. P. Infelta, J. M. Warman, and R. H. Schuler, *J. Chem. Phys.*, **52**, 3971 (1970).

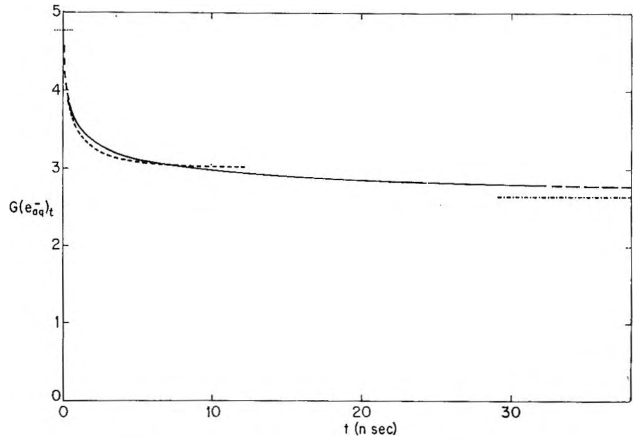

Figure 7. Time dependence for decay of the electron population in pure water which corresponds to the concentration dependence for scavenging given by the dashed curve in Figure 6 (solid curve). Total initial yield of electrons (4.78) is indicated on the left-hand axis (.....) and electrons which escape from the spurs (2.63) is indicated on the right-hand axis (-·--·-). The latter are assumed not to decay at the times involved. The decay predicted by the calculations of Schwarz (ref 6) is indicated by the dashed curve superimposed from 0 to 12 nsec.

water (*cf.* ref 22 for a discussion of this point). If we assume that the electrons which escape the spur do not decay (which should be true on the time scale of the spur reactions) then the appropriate expression for the decay of the total electron population is

$$G(e_{aq}^-)_t = 2.55 + 2.23e^{\lambda t}\,\mathrm{erfc}(\lambda t)^{1/2} \qquad \text{(III)}$$

where $G(e_{aq}^-)_t$ is the yield of electrons which exist at time t after solvation. This expression should be a reasonably good description over the time region $0.5 < \lambda t < 50$ (corresponding to the concentration region of 10^{-2} to 1 M CH_3Cl). At long times the actual dependence will drop off slightly less rapidly than given by eq III if the concentration dependence predicted by Schwarz is applicable. Because of the lack of experimental information on the concentration dependence above 1 M little can be said about the details of the time dependence at very short times. The yield is, however, still increasing at high concentrations so that there surely must be an appreciable yield of electrons of very short lifetime.

The absolute time scale for the disappearance of the electrons within the spurs in pure water can now be given because we can estimate λ as 8×10^8 sec^{-1} since for methyl chloride we know both $k/\lambda(= 1.3\ M^{-1}$ from the curve fitting) and $k(= 1.1 \times 10^9\ M^{-1}$ sec^{-1} from the direct measurement). The decay corresponding to eq III for this value of λ is given as the solid curve in Figure 7. *This curve should be regarded as a direct conclusion from the experimental observations.* It is purely phenomenological in nature and in no way involves any detailed microscopic consideration of the competing processes which occur within the spur. Schwarz[5] has approached the time dependence from this latter point of view and has predicted the dashed curve given in the figure. The similarity between the two curves is, again, most gratifying (but somewhat redundant since the concentration dependence predicted by Schwarz is so similar to the experimental one used in calculating the solid curve). Schwarz' curve is somewhat steeper at short times and shallower at long times but the differences are very small and the overall conclusions essentially identical. Thomas and coworkers have made several attempts[23,24] to observe the decay of electrons within the spurs but on the 10–100 nsec time scale found only a small component ($G \sim 0.2$)[4] which can be attributed to such a decay. In these experiments the initial spike of Figure 7 is over so quickly that, as has already been commented on by Schwarz,[5] it will be for the most part averaged out by the apparatus time constants which were several nanoseconds. With time resolution an order of magnitude better one should be able to see a decay of ~50% of the spur electrons (*cf.* Figure 7 of ref 22 for the fraction remaining at the end of a finite pulse; one must then consider the effect the detection time constants will have on averaging the available signal). Very recently Hunt and coworkers reported results from their stroboscopic experiments[25] which indicate that the decay over the time region of 30–300 psec is less than 10%. A decrease from 4.4 to 4.1 is predicted over this time interval if eq III can be extrapolated to very short times. It is also noted that Hamill has suggested[26] that in systems of this type the electrons may react before they have become solvated. If this is so then the applicable rate constant and therefore also λ will be considerably greater than the values used here and the time scale of Figure 7 will be considerably shortened. The crux of the problem is, of course, the time required for solvation. If solvation occurs in periods shorter than 10^{-11} sec then rate constants considerably greater than $10^{12}\ M^{-1}$ sec^{-1} would be required for reactions of the "dry electron" to be totally important at methyl chloride concentrations of ~0.1 M. It seems unlikely that these criteria are met in the real system so it is concluded that spur effects are, in any case, a major contributor to the observed dependence for scavenging on solute concentration.

(23) J. W. Hunt and J. K. Thomas, *Radiat. Res.*, **32**, 149 (1967).

(24) J. K. Thomas and R. V. Bensasson, *J. Chem. Phys.*, **46**, 4147 (1967).

(25) J. W. Hunt, private communication.

(26) W. H. Hamill, *J. Chem. Phys.*, **49**, 2446 (1968).

Radiolytic Degradation of the Peptide Main Chain in Dilute Aqueous Solution Containing Oxygen[1]

by Warren M. Garrison,* Mathilde Kland-English, Harvey A. Sokol, and Michael E. Jayko

Lawrence Radiation Laboratory, University of California, Berkeley, California 94720 *(Received July 17, 1970)*

In the γ radiolysis of peptides, $RCONHCHR_2$, in dilute, oxygen-saturated solution, reaction of the OH radicals at the main chain leads to formation of peptide peroxy radicals, $RCONHC(\dot{O}_2)R_2$. These react preferentially *via* $2RCONHC(\dot{O}_2)R_2 \rightarrow 2RCONHC(\dot{O})R_2 + O_2$. The alkoxy radicals are removed through the step: $O_2 + RCONHC(\dot{O})R_2 \rightarrow$ products $+ HO_2$. Experimental evidence for these oxidation modes is derived from a detailed study of reaction stoichiometry in the γ-ray-induced oxidation of aqueous *N*-acetyl-DL-alanine and poly-DL-alanine.

Introduction

Radiolytic oxidation of the peptide main chain in dilute, oxygenated solution is characterized by the formation of labile "amide-like" degradation products which yield free ammonia on mild hydrolysis.[2] Although recent work[3] has shown that the OH radical formed in the radiation-induced step[4-7]

$$H_2O \rightsquigarrow H_2O_2, H_2, OH, H, e_{aq}^-, H^+ \quad (1)$$

initiates peptide oxidation *via*

$$OH + RCONHCHR_2 \longrightarrow H_2O + RCONH\dot{C}R_2 \quad (2)$$

the nature of subsequent reactions in oxygenated solution has not been clearly formulated.[2,3] The purpose of the present work is to elucidate the mechanism of such reactions in dilute aqueous solutions of typical peptide derivatives of alanine, *viz.*, *N*-acetyl-DL-alanine and poly-DL-alanine.

Experimental Section

The *N*-acetylalanine (Cyclo Chemical Corp. NRC Grade I) was recrystallized from water. The polyalanine (Miles-Yeda Ltd.) as received contained traces of ammonia which were removed through lyophilization of a 1% polyalanine solution after the addition of sodium hydroxide to pH 9; the alkaline residue was redissolved to 1%, acidified to pH 4 with sulfuric acid, and then dialyzed to neutrality against redistilled water. Water used in preparation of solutions was from a Barnstead still and was redistilled in Pyrex first from alkaline permanganate and then from phosphoric acid. The pH adjustments of solutions to be irradiated were made with sodium hydroxide or sulfuric acid.

Solutions were irradiated under one atmosphere of oxygen in sealed Pyrex tubes. These were removed from the ^{60}Co source periodically and the contents were mixed to ensure that the solution contained excess oxygen throughout the irradiation. A 10-kc ^{60}Co γ-ray source was used to give a dose rate of 1×10^{18} eV/g-min as determined by the Fricke dosimeter [$G(Fe^{3+}) = 15.5$, $\epsilon_{305} = 2180$ at 24°].

Amide ammonia was determined by the micro-diffusion method of Conway.[8] The samples were made 2 *N* in sodium hydroxide in the outer compartment of the diffusion cell; hydrolysis and the transfer of free ammonia to the acid compartment (0.1 *N* sulfuric acid) is complete in 24 hr. Diffusates were assayed by means of Nessler reagent.

Carbonyl products were identified by filter-paper chromatography.[9] The pyruvic acid and acetaldehyde were assayed by the methods of Friedemann and Haugen[10] and Johnson and Scholes,[11] respectively.

The acetic acid was separated through lyophilization of the sample solutions after acidification with sulfuric acid. Assay was by vapor-phase chromatography[12] (Aerograph 600C). The maximal acetic acid yield from acetylalanine was obtained after the irradiated solutions were made 1 *N* in sodium hydroxide and al-

* To whom correspondence should be addressed.

(1) This work was performed under the auspices of the U. S. Atomic Energy Commission.

(2) For a recent review see W. M. Garrison, "Current Topics in Radiation Research," M. Ebert and A. Howard, Ed., Vol. IV, North-Holland Publishing Co., Amsterdam, 1968, pp 45–94.

(3) H. L. Atkins, W. Bennett-Corniea, and W. M. Garrison, *J. Phys. Chem.*, **71**, 772 (1967).

(4) N. F. Barr and A. O. Allen, *ibid.*, **63**, 928 (1959).

(5) G. Czapski and H. A. Schwarz, *ibid.*, **66**, 471 (1962).

(6) E. J. Hart and J. W. Boag, *J. Amer. Chem. Soc.*, **84**, 4090 (1962).

(7) B. H. J. Bielski and A. O. Allen, *Int. J. Radiat. Phys. Chem.*, **1**, 153 (1969), report the following 100-eV yields for the γ-ray-induced decomposition of water: $G_{OH} = 2.74$, $G_{e_{aq}^-} = 2.76$, $G_H = 0.55$, $G_{H_2} = 0.40$, $G_{H_2O_2} = 1.00$.

(8) E. J. Conway, "Microdiffusion Analysis," Crosby Lockwood and Sons, Ltd., London, 1962.

(9) W. M. Garrison, H. R. Haymond, W. Bennett-Corniea, and S. Cole, *Radiat. Res.*, **10**, 273 (1959).

(10) T. E. Friedemann and G. E. Haugen, *J. Biol. Chem.*, **147**, 415 (1943).

(11) G. R. A. Johnson and G. Scholes, *Analyst*, **79**, 217 (1954).

(12) E. M. Emery and W. E. Koerner, *Anal. Chem.*, **33**, 146 (1961).

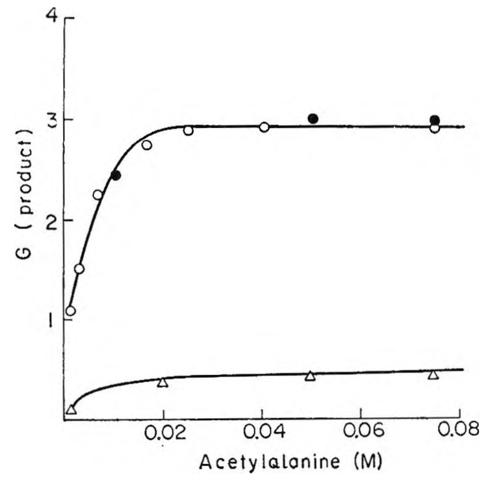

Figure 1. Effect of solute concentration in the γ radiolysis of *N*-acetylalanine in oxygenated solution: $G(NH_3)$, pH 7 (O), pH 3 (●); $G(CH_3COCOOH + CH_3CHO)$, pH 3 (△).

lowed to stand at room temperature for 15 min prior to separation and assay. Acetylalanine hydrolysis is negligible under these conditions.

Gaseous products were pumped off on the vacuum line through a Dry Ice trap. The carbon dioxide yield corresponds to that fraction removed on contact with sodium hydroxide. Analysis was confirmed by gas chromatography (Aerograph A90-P3).

Hydrogen peroxide and organic peroxide were determined after the method of Johnson and Weiss.[13]

Appropriate control and blank runs confirmed the applicability of the above analytical methods to the present systems.

Results and Discussion

The production of amide-like ammonia in the γ-ray radiolysis of *N*-acetylalanine in oxygenated solution is shown in Figure 1 as a function of peptide concentration. The ammonia yield increases abruptly with increasing solute concentration and levels off at $G(NH_3) \simeq 2.9 \simeq G_{OH}$ over the concentration range 0.02 *M* to 0.1 *M*. At *N*-acetylalanine concentrations above 0.1 *M* other reaction modes begin to contribute to the observed $G(NH_3)$ values. The chemistry of these other degradation modes in the more concentrated solutions is of quite a different nature as has been described elsewhere.[14]

Now, in dilute oxygenated solutions of *N*-acetylalanine, the reducing species H and e_{aq}^- formed in the radiation-induced step 1 are preferentially scavenged *via*

$$O_2 + e_{aq}^- \longrightarrow O_2^- \qquad (3)$$

$$O_2 + H \longrightarrow HO_2 \qquad (3a)$$

where the products of reaction 3 are related by the equilibrium,[15] $HO_2 \rightleftarrows H^+ + O_2^-$. The peptide radicals $RCONH\dot{C}R_2$ formed by OH attack *via* reaction 2 are also scavenged by oxygen, *i.e.*

$$O_2 + RCONH\dot{C}R_2 \longrightarrow RCONHC(\dot{O}_2)R_2 \qquad (4)$$

In earlier work[2] we suggested that the simplest reaction scheme for the subsequent chemistry involves

$$HO_2 + RCONHC(\dot{O}_2)R_2 \longrightarrow RCONHC(OOH)R_2 + O_2 \qquad (5)$$

$$H_2O + RCONHC(OOH)R_2 \longrightarrow RCONHC(OH)R_2 + H_2O_2 \qquad (6)$$

where the dehydropeptide derivative $RCONHC(OH)R_2$ is labile and yields ammonia and carbonyl on mild hydrolysis

$$RCONHC(OH)R_2 \longrightarrow RCONH_2 + R_2CO \qquad (7)$$

$$H_2O + RCONH_2 \longrightarrow RCOOH + NH_3 \qquad (8)$$

If degradation of the peptide main chain does occur predominantly through the scheme formulated in eq 1–8 then it is clear that the ammonia and carbonyl yields should be in the relationship, $G(NH_3) \simeq G(R_2CO) \simeq G_{OH} \simeq 2.9$. Quantitative assays of the carbonyl fraction from irradiated *N*-acetylalanine solutions show, however, that the combined yield of carbonyl products, pyruvic acid, and acetaldehyde, is quite low with $G(R_2CO) \simeq 0.4$ as shown in Figure 1.

Further study of the oxidation products derived from *N*-acetylalanine reveals that the principal nitrogen-free organic compounds produced in this system are acetic acid and carbon dioxide. Yield data are summarized in Table I. The finding that acetic acid and carbon dioxide are formed as major initial products in this system suggested to us that removal of $RCONHC(OOH)R_2$ *via* the hydrolytic reaction 6 occurs in competition with a second degradation mode which in the specific case of *N*-acetylalanine may be formulated in terms of the intramolecular rearrangement

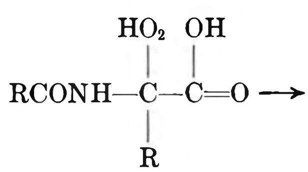

$$\longrightarrow RCONHCOR + H_2O + CO_2 \qquad (9)$$

The diacetamide configuration, RCONHCOR, is hydrolytically labile. Mild differential hydrolysis in 1 *N* sodium hydroxide at room temperature for 15 min (see

(13) G. R. A. Johnson and J. Weiss, *Chem. Ind. (London)*, 358 (1955).

(14) (a) M. A. J. Rodgers and W. M. Garrison, *J. Phys. Chem.*, **72**, 758 (1968); (b) W. M. Garrison, M. E. Jayko, M. A. J. Rodgers, H. A. Sokol, and W. Bennett-Corniea, "Advances in Chemistry Series," No. 81, American Chemical Society, Washington, D. C., 1968, p 384.

(15) G. Czapski and H. J. Bielski, *J. Phys. Chem.*, **67**, 2180 (1963).

Hydrogenation of Ethylene over Cobalt Oxide[1]

by Ken-ichi Tanaka,* Hirohisa Nihira, and Atsumu Ozaki

Tokyo Institute of Technology, O-okayama, Meguro-ku, Tokyo (*Received May 8, 1970*)

Cobalt oxide evacuated at 400–450° showed an extremely high initial catalytic activity for the hydrogenation of ethylene. However, its activity decreased as the reaction proceeded. It was found that the reduction in the activity was caused by the irreversible adsorption of hydrogen and that such hydrogen did not participate in the isotopic equilibration of H_2 and D_2 and in the hydrogenation of ethylene. In order to monitor the behavior of hydrogen and ethylene on catalysts during the hydrogenation of ethylene, the volumetric adsorption measurement during catalysis, the addition of D_2 to ethylene, the reaction of mixture of D_2 and H_2 with ethylene, and the reaction of hydrogen with mixture of C_2H_4 and C_2D_4 were carried out over three samples of Co_3O_4 catalysts. Both the hydrogenation of ethylene and the equilibration of H_2–D_2 occur on the same active sites. These sites are occupied by ethylene during the hydrogenation of ethylene. Hydrogen does not randomize before it reacts, but ethylene undergoes complete isotopic self-mixing before it reacts with hydrogen. Probable mechanisms for the hydrogenation of ethylene are discussed.

Introduction

It is known that some transition metal oxides have high catalytic activity for such reactions as the isotopic equilibration of H_2 and D_2[2a] and of C_2H_4 and C_2D_4,[2b] the isomerization of *n*-butene,[3] and the hydrogenation of ethylene,[4] and that the activity sequences of first transition metal oxides for these reactions are rather similar to that observed by Dowden, *et al.*, for the isotopic equilibration of H_2 and D_2. The first detailed studies on the hydrogenation of olefins and the exchange reaction between deuterium and hydrocarbons over oxide catalysts have been carried out by Burwell and his coworkers[5] on chromium oxide gel. Recently, the hydrogenation of olefins has been studied on TiO_2,[6] ZnO,[7,8] and also on Cr_2O_3.[7] A remarkable result obtained in these studies is that the addition of deuterium to olefins results in only d_2-alkanes if the reaction temperature is not too high. However, the reaction mechanism on oxide catalysts is still obscure, and it is desirable to know more details about kinetics and behaviors of adsorbed species during catalysis. The authors previously applied volumetric adsorption measurement during catalysis[9,10] to study the decomposition of nitrous oxide on Cr_2O_3 and Mn_2O_3, and found that the active sites responsible for the reaction constitute a small fraction of total sites.[11]

On the other hand, the isotopic mixing during the main reaction gives important information about the behavior of adsorbed species during the reaction.[2,12-14] Twigg[13] studied the hydrogenation of ethylene on nickel in this way; that is, he used unequilibrated and equilibrated isotopic mixtures of hydrogen and deuterium as reactants and found that the isotope exchange reaction between H_2 and D_2 was poisoned by the presence of ethylene. However, no difference was observed in deuterium the distribution in the product ethane for both isotope mixtures of hydrogen. Mayer and Burwell[14] applied this method to the hydrogenation of 2-butyne on palladium and arrived at the conclusion that the adsorbed hydrogen undergoes complete mixing on metals before it reacts. Kokes, *et al.*,[7] however, found that the hydrogen adsorbed on ZnO and Cr_2O_3 does not undergo rapid mixing before it reacts with ethylene. Furthermore, during dimerization of C_2H_4–C_2D_4 mixture over nickel oxide–silica catalyst, ethylene undergoes a rapid isotopic mixing prior to the dimerization.[2] Cobalt oxide is also an efficient catalyst for the isotopic mixing both in ethylene[2] and hydrogen.[1]

In this paper, in order to throw light on the behavior of hydrogen and ethylene over the oxide catalyst during the hydrogenation of ethylene, both the adsorption and the isotopic mixing during catalysis have been studied. The kinetics and the isotope effect in rate constant were also determined.

(1) This work was presented at the 25th meeting of the Catalysis Society of Japan, Oct 1969.

(2) (a) D. A. Dowden, N. Mackenzie, and B. M. W. Trapnell, *Proc. Roy. Soc. Ser. A*, **237**, 245 (1956); (b) A. Ozaki, H. Ai, and K. Kimura, 4th Int. Cong. Catalysis, Moscow, 1968.

(3) Y. Kubokawa, T. Adachi, T. Tomino, and T. Ozawa, 4th Int. Congr. Catalysis, Moscow, 1968.

(4) D. L. Harrison, D. Nicholls, and H. Steines, *J. Catal.*, **7**, 359 (1967).

(5) R. L. Burwell, *et al.*, *J. Amer. Chem. Soc.*, **82**, 6272 (1960).

(6) I. J. S. Lake and C. Kemball, *Trans. Faraday Soc.*, **63**, 2535 (1967).

(7) R. J. Kokes, *et al.*, *J. Amer. Chem. Soc.*, **90**, 6859 (1968); *J. Phys. Chem.*, **73**, 2436 (1969).

(8) A. L. Dent and R. J. Kokes, *ibid.*, **73**, 3772, 3781 (1969).

(9) K. Tamaru, *Bull. Chem. Soc. Jap.*, **31**, 666 (1958).

(10) K. Tamaru, *Advan. Catal.*, **15**, 65 (1964).

(11) K. Tanaka and A. Ozaki, *Bull. Chem. Soc. Jap.*, **40**, 420 (1967); *J. Catal.*, **8**, 307 (1967).

(12) W. M. H. Sachtler, *J. Phys. Chem.*, **64**, 1579 (1960).

(13) G. H. Twigg, *Discuss. Faraday Soc.*, **8**, 152 (1950).

(14) E. F. Meyer and R. L. Burwell, Jr., *J. Amer. Chem. Soc.*, **85**, 2877 (1963).

Experimental Section

The apparatus used in these studies was a closed circulating system connected to a gas chromatograph which permitted analysis of the circulating gases at any time. The amounts of gases adsorbed during the reaction were estimated from the material balance using gas chromatography and pressure measurement by means of a cathetometer as has been previously described for other reactions.[11] Correction was made for the analytical sample removed from the system.

Materials. *H_2.* Cylinder hydrogen was purified by passing it over a platinum/asbestos catalyst at about 300° and dried by use of a liquid nitrogen trap.

C_2H_4. Ethylene was passed through a sodium hydroxide column, condensed at liquid nitrogen temperature, and distilled from −78°.

D_2. Deuterium, obtained by the decomposition of D_2O with a magnesium ribbon, was purified by passing it through a molecular sieve column at liquid nitrogen temperature.

C_2D_4. Tetradeuterioethylene, obtained by deuteration of C_2D_2 over Girdler G-58 catalyst, was purified by a gas chromatographic column of silica gel.

The three samples of Co_3O_4 catalysts used in this study were prepared as follows.

Co_3O_4 (I). Cobalt hydroxide, obtained by precipitating reagent grade cobaltous nitrate with ammonia solution, was decomposed to Co_3O_4 by calcination at 600° for 6 hr in air. The amount and the surface area of the catalyst used were 1.0 g and 13.0 m^2 (total), respectively.

Co_3O_4 (II). The oxide, obtained by thermal decomposition of reagent grade cobaltous nitrate at about 400°, was pressed into tablets and calcined at 600–700° for 3 hr in air. The pelletted Co_3O_4 was crushed to small particles. The amount and the surface area of the catalyst used were 3.00 g and 9.4 m^2 (total), respectively.

Co_3O_4 (III). The oxide, obtained by thermal decomposition of a reagent grade cobaltous nitrate at about 400°, was boiled in distilled water and filtered repeatedly. After these treatments, the oxide was dried and calcined at 600° for 6 hr in air. X-Ray diffraction analysis showed the lines of complete Co_3O_4. The amount and the surface area of the catalyst used for the reaction were 45.6 g and 108 m^2 (total), respectively.

These three catalysts were activated by evacuation at 400–450° for 5–6 hr. This activation made the catalysts highly active even at −78° (hereafter this state of the catalyst is termed "fresh catalyst"), but its activity gradually decreased during the course of the hydrogenation of ethylene as well as between runs. On the other hand, if the fresh catalyst was exposed to hydrogen at room temperature (about 26°) for 13 hr or more, the activity decreased but no more reduction of activity was observed during the reaction as well as between runs. Accordingly, the catalysts exposed to hydrogen are denoted in this paper as "stabilized catalyst." The kinetic studies and the adsorption measurements during catalysis were carried out over the stabilized catalyst: however, the other experiments were carried out on both catalysts, fresh and stabilized ones.

The samples for mass spectrometric analyses of hydrogen, ethylene, and ethane, were separated by gas chromatography and collected in a liquid nitrogen trap. For the isotopic analyses, ionization voltages of 10 or 12 eV were used. The distribution of deuterium in ethane and in ethylene were calculated according to the results by Turkevich[15] and Amenomiya[16] with slight corrections characteristic to the mass spectrometer used. The usual correction was made for the presence of naturally occurring heavy carbon. The serial analysis of D_2 and HD during the hydrogenation of ethylene was carried out by gas chromatography with a molecular sieve 5-A column at liquid nitrogen temperature.

Results

1. The Reactivity of Hydrogen Adsorbed on a Fresh Catalyst. The catalysts evacuated at 400–450° (fresh catalysts) were markedly active for the hydrogenation of ethylene in the initial stage of the reaction; however, the activity became lower and lower during the reaction. On the other hand, if the fresh catalyst was exposed to hydrogen for 13 hr or more at room temperature prior to use, the activity was substantially decreased but stabilized throughout the run as well as between runs. This fact proves that the decrease of the activity during the reaction is at least partly caused by the adsorption of hydrogen.

Figure 1 shows a typical result of adsorption of hydrogen on a fresh catalyst [Co_3O_4 (III)] at room temperature. The major part of adsorption in this figure is irreversible, because no detectable additional adsorption was observed after a long time of evacuation at room temperature. The amount of this irreversible adsorption was about $6.4 \cdot 10^{-6}$ ml/cm^2 (STP), that is, about $1.7 \cdot 10^{14}$ molecules/cm^2. Deuterium gas was admitted at room temperature on this surface on which 6.91 ml of hydrogen had been preadsorbed, and the change in the isotopic composition of gas phase was followed by gas chromatography. As shown in Figure 2, the irreversibly adsorbed hydrogen did not exchange with deuterium at room temperature. However, when a mixture of H_2 and D_2 was introduced on the same surface, it reached isotopic equilibrium within a few minutes. Since the ordinate in Figure 2 is the gas chromatographic peak height ratio of HD to D_2, it is an arbitrary unit to indicate the extent of equilibration between D_2 and H_2 or the adsorbed hydrogen.

(15) J. Turkevich, *et al.*, *J. Amer. Chem. Soc.*, **70**, 2638 (1948).
(16) Y. Amenomiya, *et al.*, *Can. J. Chem.*, **46**, 174 (1968).

Table I: Reactions of Ethylene with Deuterium

Run	Reaction	C_2', H_2 cc (STP)	Reaction temp, °C	Reaction time, min	Conv., %	Cat.	Reactant: Hydrogen d_0	Hydrogen d_1	Hydrogen d_2	Ethylene d_0	Ethylene d_1	Ethylene d_2	Ethylene d_3	Ethylene d_4
1	$C_2H_4 + H_2$	12.6	28.5	14	50	III	100		0	100		0		0
		12.1				D_2 irr.		0			0		0	
2	$C_2H_4 + D_2$	14.5	−78	41	30	III	0		94.0	100		0		0
		20.6				fresh		6.0			0		0	
		10.7	23	2	8	II	0		96.9	100		0		0
		11.3				fresh		3.1			0		0	
		58.2	23	110	10	II	0		96.9	100		0		0
		12.4				fresh		3.1			0		0	
		11.3	23	63	50	II	0		96.9	100		0		0
		12.2				fresh		3.1			0		0	
3-1	$C_2H_4 + C_2D_4 + H_2$	7.9	20	...	20	I	100		0	69.3		0		27.7
		7.9				fresh		0			0		3.8	
		10.0	23	87	50	II	100		0	59.8		0		38.0
		11.6				fresh		0			0		2.2	
3-2	$C_2H_4 + H_2 + D_2$	14.1	29	11	23	III	48.8		49.6	100		0		0
		24.6				H_2 irr.		1.6			0		0	
		14.9	29	28	47	III	38.7		59.5	100		0		0
		23.5				H_2 irr.		1.8			0		0	
3-2	$C_2H_4 + H_2 + D_2$	7.9	20	...	20	I	43.5		55.1	100		0		0
		7.9				fresh		1.4			0		0	
		33.7	−78	300	50	III	54.6		42.6	100		0		0
		39.2				fresh		2.8			0		0	

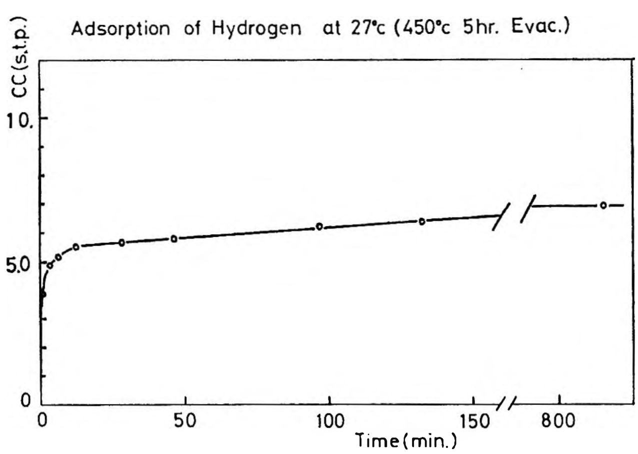

Figure 1. Time course of hydrogen adsorption on Co_3O_4 (III).

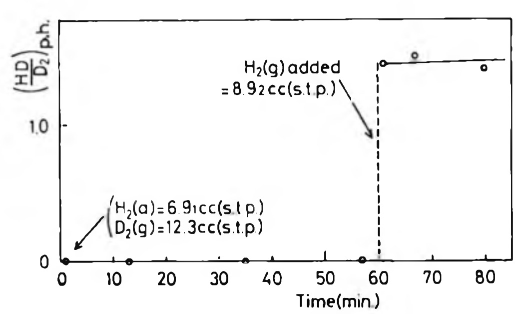

Figure 2. Exchange reaction of D_2 with the irreversibly adsorbed hydrogen and with gaseous hydrogen at room temperature on Co_3O_4 (III).

It is also important to study the contribution of irreversibly adsorbed hydrogen to the hydrogenation of ethylene. The hydrogenation of ethylene with H_2 was carried out on the catalyst (III) on which 6.9 ml of deuterium had been preadsorbed. The result analyzed by mass spectrometry is shown in Table I, run 1. This result indicates that the preadsorbed deuterium is only slightly transferred to hydrogen, ethylene, or ethane.

Another experiment was carried out to examine the contribution of hydroxyl hydrogen originally involved in the oxide. The oxide (I) was deuterated by treating it with D_2O overnight at room temperature and then evacuating it at 400°. However, the reaction between C_2H_4 and H_2 on this deuterated catalyst gave no deutero species of ethylene, ethane, or hydrogen.

2. Deuterium Distribution in the Reaction of Ethylene

Product														
Hydrogen			Ethylene					Ethane						
d_0	d_1	d_2	d_0	d_1	d_2	d_3	d_4	d_0	d_1	d_2	d_3	d_4	d_5	d_6
96.8	3.2	+	97.6	2.4	0	0	0	95.2	4.8	0	0	0	0	0
0	5.8	94.2	98.1	1.9	0	0	0	0	4.2	94.9	0.9	0	0	0
0	4.1	95.9	99.0	1.0	0	0	0	1.4	2.0	96.0	0.6	0	0	0
0	5.7	94.3	99.4	0.6	+	0	0	0	0.4	99.6	0	0	0	0
0	4.8	95.2	97.5	2.3	0.2	0	0	2.6	3.6	92.2	1.6	0	0	0
100	0	0	33.6	29.3	20.7	7.4	9.0	18.4	39.0	30.5	9.4	1.7	+	1.0
100	+	0	13.6	35.2	34.0	14.7	2.5	5.4	34.6	40.6	16.2	3.2	0	0
37.5	15.5	47.0	94.7	5.3	0	0	0	56.0	19.6	24.4	0	0	0	0
23.5	22.8	53.5	85.1	14.9	+	0	0	46.1	24.0	27.9	2.0	0	0	0
41.7	10.3	48.0	99.6	0.4	0	0	0	47.2	14.9	37.9	0	0	0	0
27.3	47.8	24.9	99.0	1.0	0	0	0	29.7	51.9	18.4	0	0	0	0

with D_2. Reactions of ethylene with deuterium were carried out on fresh catalysts (II and III) at various conditions. Deuterium distributions observed in those reactions are summarized in Table I, run 2. The main product of the reaction was ethane-d_2, with a selectivity being higher in such cases as short reaction time, low reaction temperature, and excess ethylene compared with deuterium. The isotopic exchange between ethylene and deuterium is very slow at these temperatures, as the deuterioethylene concentration is as low as 2.5% at 50% conversion of the hydrogenation.

3. Exchange Reaction during the Hydrogenation of Ethylene. Mixtures of C_2H_4 and C_2D_4 were hydrogenated on fresh catalysts (I and II) to study the behavior of ethylene over the catalyst during hydrogenation. The results are summarized in Table I run 3-1, and the deuterium distributions in ethane and ethylene at 20 and 50% of conversions are shown in Figure 3. Dotted lines in this figure are calculated distributions in ethylene assuming complete isotopic mixing between C_2H_4 and C_2D_4 used. This figure shows that the deuterium distribution in the gas-phase ethylene is not isotopically equilibrated at 20% conversion but reaches equilibrium already at 50% conversion, indicating a rapid progress of the isotopic mixing in ethylene. The deuterium distribution in ethane at 20% conversion agrees with the calculated equilibrium distribution in ethylene in spite of unequilibrated gas-phase ethylene.

In the same manner, the reaction of mixtures of H_2 and D_2 with ethylene was studied. The results are summarized in Table I, run 3-2, which shows that the extent of isotopic mixing in hydrogen is low and far from equilibrium. This fact implies that the equilibration of H_2 and D_2 is radically retarded by the presence of ethylene.

The time course of isotopic mixing in hydrogen as well as the hydrogenation of ethylene is illustrated in Figure 4, where it is clearly demonstrated that the equilibration of H_2 and D_2 is abruptly established when ethylene is removed by the hydrogenation.

4. Kinetics and Isotope Effect in the Hydrogenation of Ethylene. As described before, the stabilized catalyst showed a reproducible activity in a series of runs. Kinetic studies were carried out on the stabilized Co_3O_4 (III), *i.e.*, the catalyst stabilized by irreversible adsorption of hydrogen (6.91 ml STP). The adsorption of ethylene on this stabilized catalyst was reversible at

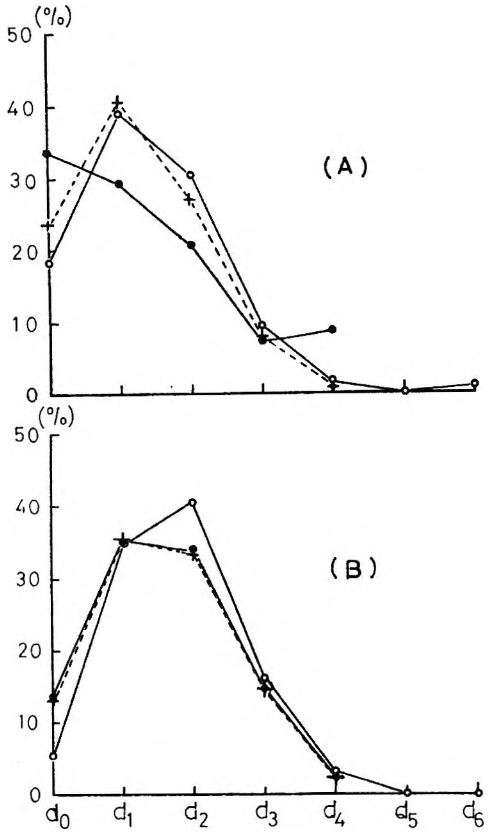

Figure 3. Deuterium distributions in ethylene and ethane obtained by the reaction of C_2H_4–C_2D_4 mixture with H_2 at room temperature (A) on Co_3O_4 (I), 20% conversion, and (B) on Co_3O_4 (II), 50% conversion: ———, observed; - - -, calculated.

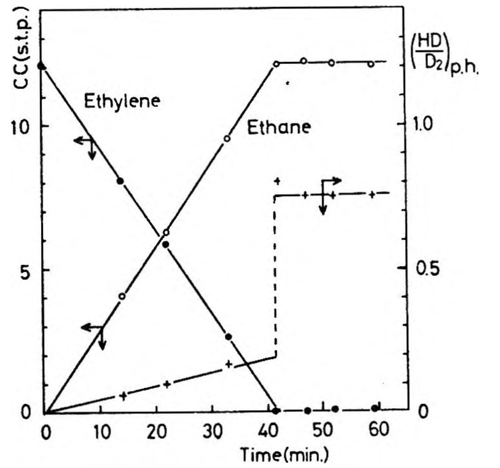

Figure 4. H_2–D_2 exchange reaction during the hydrogenation of ethylene at room temperature on Co_3O_4 (III) with excess hydrogen.

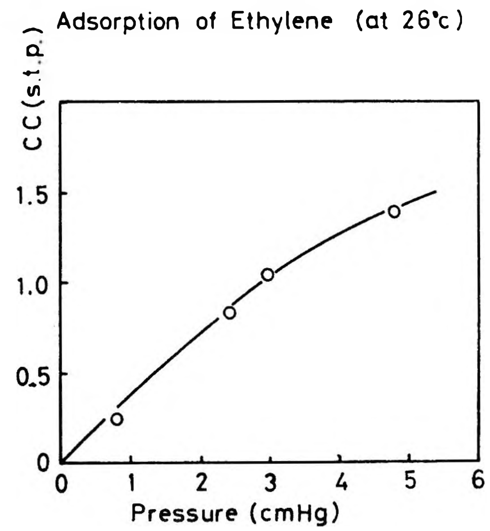

Figure 5. Adsorption of ethylene at room temperature on Co_3O_4 (III) stabilized with the irreversible adsorption of hydrogen.

26° and the adsorption depended on pressures as shown in Figure 5.

Figure 6 shows a typical time course of the hydrogenation of ethylene carried out at 26° on the stabilized catalyst. The amounts of adsorption of ethylene and hydrogen during the reaction, which were computed from the material balance, are shown in the same figure. As the reaction proceeds, the partial pressure of ethylene decreases with time, and simultaneously the adsorption of ethylene decreases. The line of C_2H_4 (a) on the figure is drawn according to the isotherm obtained in the absence of H_2 (Figure 5) and well fits the observed values during the reaction.

On the other hand, the adsorption of hydrogen during the reaction was undetectable in the pressure range studied. The range of ethylene pressure studied was 0–35 mm and that of hydrogen was 17–93 mm. In these pressure ranges, the rate of reaction was first order in hydrogen and exactly zero order in ethylene, that is, rate $= kP_{H_2}{}^1 \cdot P_{C_2H_4}{}^0$. Figure 7 shows that the above rate equation is obeyed at various temperatures. The logarithms of rate constants, obtained from the slope of lines in Figure 7, are plotted against the reciprocal of the temperature in Figure 8. The rate constants of the reaction of ethylene with deuterium obtained in a similar manner are also plotted in Figure 8. The activation energy of the reaction, $C_2H_4 + H_2$, was about 7.6 kcal/mol, and the average isotope effect obtained in the temperature range, 2–26°, was $k_H/k_D = 1.4$.

5. Poisoning by Carbon Monoxide. It was previously shown that the isotopic mixing in ethylene at 25° over Co_3O_4 activated by evacuation at high temperature is strongly poisoned by preadsorbed carbon monoxide with a fatal amount being about $2 \cdot 10^{14}$ molecules/cm^2 for a sample evacuated at 500°.[2] The effect of the preadsorbed carbon monoxide was studied on the hydrogenation of ethylene; $0.7 \cdot 10^{14}$ molecules/cm^2 of carbon monoxide adsorbed on the fresh catalyst I evacuated at 400° reduced the rate of hydrogenation to about one-tenth of the original value. The fatal amount may be estimated to be about $0.8 \cdot 10^{14}$ molecules/cm^2 for the

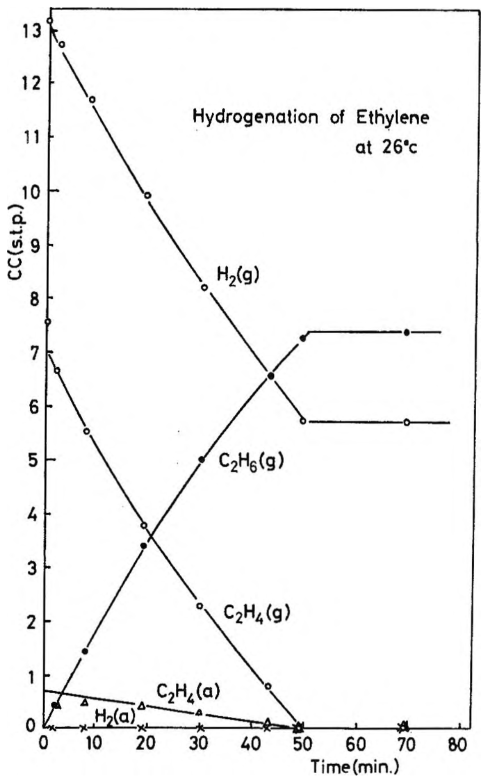

Figure 6. Adsorption of ethylene and hydrogen during the hydrogenation of ethylene on Co_3O_4 (III) at room temperature.

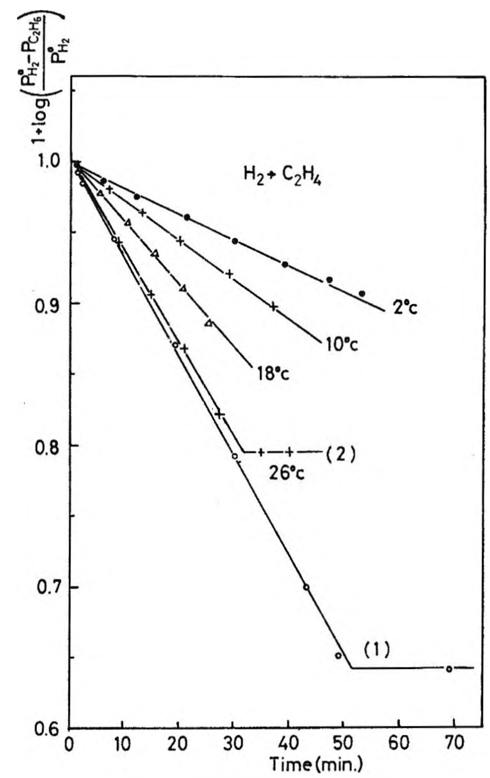

Figure 7. First-order plots of the hydrogenation of ethylene on Co_3O_4 (III).

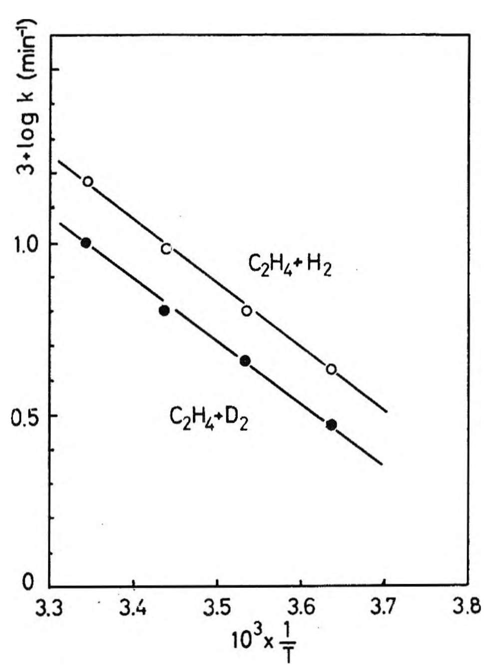

Figure 8. Arrhenius plots of the rate constants of ethylene hydrogenation and deuteration on Co_3O_4 (III).

catalyst evacuated at 400°. The difference from the above value of $2 \cdot 10^{14}$ may be caused by the difference in the evacuation temperature. Another run made with the stabilized catalyst III showed that only $1.3 \cdot 10^{12}$ molecules/cm^2 of carbon monoxide is enough to reduce the initial activity to one-tenth of the original value. This result shows that the number of active sites is drastically decreased by the irreversible adsorption of hydrogen. In this respect it is to be noted that the amount of irreversible adsorption of hydrogen, $1.7 \cdot 10^{14}$ molecules/cm^2, is nearly equal to the fatal amount of carbon monoxide. This result suggests that the irreversible adsorption of hydrogen and the adsorption of carbon monoxide occur on the same sites and that these are the active sites for the hydrogenation and the isotopic mixing.

Discussion

A number of studies have been done in the hydrogenation of ethylene on metals. It is generally accepted that the dissociation of hydrogen on metals is an indispensable process for the hydrogenation of olefin. Wise and Wood[17] have demonstrated the indispensability of hydrogen dissociation by the fact that the hydrogenation of cyclohexene readily takes place even on a gold surface if atomic hydrogen is provided. The behavior of hydrogen over metal catalysts during the hydrogenation of ethylene or alkynes was studied by Twigg[13] and Burwell.[14] Their results revealed that the hydrogen over the metal catalyst loses its molecular identity prior to the hydrogenation although the H_2–D_2 equilibration does not proceed in the presence of ethylene. On the other hand, on oxide catalysts, the addition of

(17) B. J. Wood and H. Wise, *J. Catal.*, 5, 135 (1966).

deuterium to olefins results in the corresponding d_2-compound, that is, hydrogen preserves its molecular identity in the addition reaction.[5-7]

Eischens and his coworkers[18] found in their ir spectroscopic study that hydrogen is dissociated to Zn–H and O–H on the surface at 30°. Kokes, *et al.*,[19] recently showed that rapid and reversible adsorption of hydrogen on zinc oxide is responsible for the observed O–H and Zn–H bands in the ir spectra, and they concluded that this type of adsorption participates in the hydrogenation of ethylene, but that the irreversible and slow adsorption observed on the same catalyst is out of the reaction.

In the case of Co_3O_4, it is obvious that the greater part of adsorption of hydrogen does not participate in the equilibration of H_2 and D_2 and also in the hydrogenation of ethylene as shown in Figure 2 and in Table I, run 1. If we compare the phenomenon on Co_3O_4 with that on ZnO, the greater part of adsorption observed in Figure 1 seems to correspond to the slow and irreversible adsorption on ZnO. Another type of hydrogen adsorption corresponding to the rapid and reversible one on ZnO was undetectable. A similar phenomenon was observed in the decomposition of nitrous oxide on Cr_2O_3.[11] When the oxide was evacuated at high temperatures, its initial catalytic activity for the decomposition of nitrous oxide was extremely high. However, such high activity was reduced by the irreversible adsorption of oxygen that was not involved in the reaction pathway of the decomposition reaction.

The measurement of the equilibration of H_2 and D_2 during the hydrogenation of ethylene as shown in Figure 4 demonstrates that the rate of the equilibration is strongly poisoned by the presence of ethylene and abruptly increases when ethylene is completely hydrogenated to ethane, although the apparent adsorption of ethylene during the reaction decreases according to ethylene pressure as shown in Figure 6. This shows that the observed pressure-dependent adsorption of ethylene during the reaction has no effect on the rate of equilibration, and that the active sites for the exchange reaction are covered by an undetectably small amount of pressure-independent adsorption of ethylene. It appears reasonable that the greater part of the adsorbed ethylene observed in Figure 6 is not held by the active sites, but by the other parts of the surface.

It is also noticeable that the adsorption of ethylene during the hydrogenation decreases as the reaction proceeds, but the rate of hydrogenation is practically independent of ethylene pressure as shown in Figure 6 and Figure 7. If the adsorption of ethylene shown in Figure 6 is the intermediate of the reaction, *i.e.*, the adsorption on active sites for the hydrogenation reaction, the rate of hydrogenation should depend on the amount of adsorption, which is contrary to the experimental result. If it is allowed to interpret that the zero-order kinetics in ethylene is caused by saturation of the active sites, the directly measured adsorption of ethylene in Figure 6 is not the reaction intermediate but probably physically adsorbed ethylene. Based on these results, it can be reasonably concluded that the hydrogenation of ethylene and the equilibration of D_2 and H_2 proceed on the same active sites, which make up a limited part of the surface.

The results shown in Table I, run 3 clearly show that hydrogen does not randomize before it reacts, but ethylene undergoes complete isotopic mixing before it reacts with hydrogen. The observed deuterium distribution in ethane appears to be caused by the hydrogenation of isotopically equilibrated ethylene. Since both the hydrogenation of ethylene and the isotopic equilibration of C_2D_4 and C_2H_4[2] on Co_3O_4 catalyst are poisoned by carbon monoxide, the same type of sites presumably contribute to the both reactions.

As mentioned already, the exclusive formation of dideuterioalkane from olefin and deuterium is a characteristic feature of the hydrogenation over oxide catalysts. In order to explain this simple addition of hydrogen to olefin on Cr_2O_3, Burwell, *et al.*,[5] assumed an irreversible addition of the first hydrogen to olefin. Kokes, *et al.*,[19] also adopted a similar mechanism to explain the hydrogenation of ethylene on zinc oxide, where it is supposed that ethylene is adsorbed on oxide ion, and that the ethylene adsorbed on oxide ion adjacent to imbedded zinc ion irreversibly inserts into Zn–H. In conformity with this mechanism, Dent and Kokes take into account only one type of adsorbed ethylene.

In the case of Co_3O_4, however, the ethylene adsorbed on active sites is clearly distinguishable from that on the other part of catalyst, and the latter, which is pressure-dependent adsorption, is perhaps the adsorption confined to oxide ion as Kokes, *et al.*, proposed on zinc oxide. Moreover, ethylene undergoes rapid intermolecular exchange of its hydrogen, but its hydrogen scarcely exchanges with gaseous hydrogen during hydrogenation. In order to explain this behavior of ethylene, an expected mode of ethylene on the active site is assumed as type 1 of the following

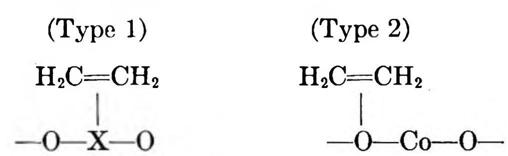

where X represents an active site, which is probably low valent cobalt, because carbon monoxide is selectively adsorbed on it. Ethylene on X, the type 1 adsorption, is pressure-independent adsorption, and that on oxide ion, the type 2 adsorption, is pressure-dependent adsorption. The number of X's on the surface is evi-

(18) R. P. Eischens, W. A. Pliskin, and M. J. D. Low, *J. Catal.*, **1**, 80 (1962).

(19) A. L. Dent and R. J. Kokes, *J. Phys. Chem.*, **73**, 3772, 3781 (1969).

dently less than that of oxide ion, as shown by the fatal amount of carbon monoxide. The rapid isotopic randomization in ethylene probably proceeds between type 1 and type 2 ethylene *via* an ethyl–cobalt intermediate.

As mentioned before, a very small amount of adsorbed ethylene effectively stops the isotopic equilibration of H_2 and D_2. It seems that the equilibration of H_2 and D_2 is blocked by the type 1 adsorption, but not by the type 2 adsorption. Kokes, *et al.*,[7] ascribed the reduction in the rate of H_2–D_2 equilibration brought about by ethylene on ZnO to the reduction of hydrogen migration on the catalyst surface.

In the present case of Co_3O_4, however, the mechanism of the reduction in the rate of equilibration seems different from that on ZnO. The blocking of the active sites by the type 1 adsorption of ethylene seems to be the real cause of the observed drastic reduction in the rate of equilibration. In this respect there is a clear difference in the kinetics of hydrogenation of ethylene over both oxides, *i.e.*

$$\text{on } Co_3O_4 \qquad r = kP_{H_2}^{1.0}P_{C_2H_4}^{0}$$

$$\text{on ZnO} \qquad r = kP_{H_2}^{0.5}\theta_{C_2H_4}^{1.0}$$

Such kinetics as observed on Co_3O_4 would be reasonable if the dissociative adsorption of hydrogen is rate-determining without retardation by ethylene. However, the drastic retardation by ethylene observed in the isotopic equilibration of hydrogen does not support this postulate.

Instead, a Rideal type attack of hydrogen on the adsorbed ethylene of type 1 as the following

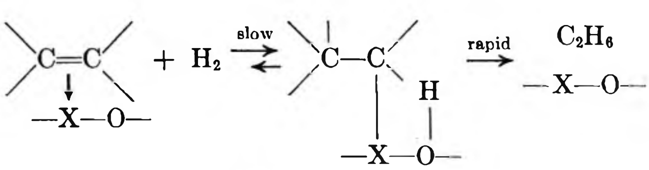

I II

seems more probable as the slow step. In this case, the rate of hydrogenation is expressed as

$$r = kP_{H_2}^{1.0}\,[\text{type 1 ethylene}] = kP_{H_2}^{1.0}P_{C_2H_4}^{0}$$

because the amount of type 1 adsorption of ethylene is independent of ethylene pressure, as indicated by the result shown in Figure 4. The neighboring oxide ion required for the hydrogen attack seems to be available with a high probability because the rather small number of active sites suggests that the cobalt atom of the active site is surrounded by the oxide ion. Although the oxide ion may be partly occupied by the type 2 adsorption of ethylene, the extent of occupation is not so high, as suggested by the observed amount of adsorption during the hydrogenation.

The essential difference between the above mechanism on Co_3O_4 and that on ZnO by Kokes, *et al.*, is found in the kinds of adsorbed species which occupy the metal atom of the active site, *i.e.*, ethylene on Co_3O_4 and hydrogen atom on ZnO. This mechanism on Co_3O_4 is consistent with the observed drastic retardation of the H_2–D_2 equilibration in the presence of ethylene and the observed preservation of molecular identity of hydrogen in the hydrogenation of ethylene. The minor formation of HD and C_2H_5D in the reaction of C_2H_4 with D_2 may be caused by the backward reaction of the step I.

From this scheme, some isotope effects in the hydrogenation of ethylene can be expected. Indeed, an average value of the isotope effect $k_H/k_D = 1.4$ was obtained on Co_3O_4 at room temperature. This value is somewhat smaller than that on ZnO, $k_H/k_D = 2$, obtained by Kokes, *et al.*, at room temperature.[19] However, it seems noticeable that a similar value of $k_H/k_D = 1.5$ was obtained by Tamaru, *et al.*, in the hydrogenation of 1,3-butadiene on ZnO at room temperature.[20] Kemball, *et al.*, reported that no isotope effect was observed in the hydrogenation of ethylene on TiO_2 at 400°.[6] This result would be natural on the basis of the present result at room temperature if the isotope effect is caused by the activation energy difference. Thus the magnitude of isotope effect in the hydrogenation of olefin seems to be similar over different oxides.

(20) S. Naito, Y. Sakurai, T. Onishi, and K. Tamaru, 25th Meeting Catalysis Society, Japan, 1969.

Raman Spectra of Pyridine and 2-Chloropyridine Adsorbed on Silica Gel

by R. O. Kagel

Chemical Physics Research Laboratory, The Dow Chemical Company, Midland, Michigan 48640 *(Received May 20, 1970)*

The Raman spectra of pyridine and 2-chloropyridine over silica gel were obtained. Pyridine forms a species hydrogen-bonded to the silica gel surface; 2-chloropyridine does not hydrogen bond to the surface probably because of steric hindrance but rather forms a condensed liquid layer.

Introduction

While the gas–solid interface has been extensively investigated by means of infrared spectroscopy, relatively few investigations have been reported on corresponding Raman studies.[1–4] Recently, Hendra and coworkers[5] observed the Raman spectra of pyridine both physisorbed and chemisorbed on several metal oxide surfaces. The metal oxides are conveniently weak Raman scatterers and the adsorption characteristics of the system can be studied over the entire spectral range (<100 to 4000 cm^{-1}), whereas the corresponding infrared study is limited in frequency range by strong infrared absorption bands due to the metal–oxygen stretching vibration. Reported here are the results of our investigations of the adsorption of pyridine and 2-chloropyridine on silica gel.

Experimental Section

Spectra were obtained on a Spex Ramalog system using as a source of excitation a Spectra Physics Model 125 He/Ne laser (60 mW at 6328 Å), and a Coherent Radiation Ar/Kr laser (~250 mW at Ar$^+$ 4880 Å). The instrument was calibrated with the He/Ne emission lines prior to recording spectra. Frequencies have been corrected accordingly. The Raman cell used in this work is patterned after a design suggested by Angell and Bulkin.[6] The cell consists of an 8-mm i.d. Pyrex tube, 12 cm long with a flat window fused on one end at 45° to the cell axis. On the other end is an O-ring seal to a stopcock for attachment to a vacuum system. The silica gel (Chromatographic grade, Silica Gel Ltd.) was put into the cell and the system evacuated to 10^{-5} Torr at 350°, followed by a high-temperature oxygen treatment (500°, 500 Torr) to remove any organic contaminates. After the system was allowed to cool to room temperature and evacuated, the adsorbates were introduced into the system at their equilibrium vapor pressure (room temperature). All the spectra were recorded with the system at room temperature.

Results and Discussion

Pyridine. A portion of the spectrum of pyridine adsorbed on silica gel, Figure 1, shows a strong band at 1010 cm^{-1} and a weaker band at 1036 cm^{-1}. (Other bands are observed at 3070, 1220, and 655 cm^{-1}.) This band system persists after prolonged evacuation (several hours) at 10^{-6} Torr but disappears with evacuation at 10^{-6} Torr and mild heating (>110°). These characteristics are typical of material associated with a surface.

A comparison of the Raman spectra of the pyridine surface species, pyridine, and those of a typical pyridinium salt ($PyH^+BF_4^-$) and a coordinated pyridine complex ($Py:ZnCl_2$) is given in Table I. Several

Table I: Comparison of Raman Spectra (cm^{-1})

Surface species	 $NH^+BF_4^-$	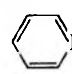 $N:ZnCl_2$	 N
3070	3030	3080	3061
1220	1208	1230	1220
	1260	1250	
1036	1032	1050	1032
1010	1011	1025	992
655	640	658	604
	660		655

similarities are noted between the band positions of the pyridine surface species, $PyH^+BF_4^-$ and $Py:ZnCl_2$. However, the overall agreement is neither sufficiently convincing to assign the structure of the pyridine surface species to a pyridinium ion or coordinated pyridine complex nor would this be in agreement with the infrared work of Parry.[7]

During the intermediate stages of removal of the surface species (by evacuation and heat) it was noted that the relative intensity ratio of the two ring modes[8]

(1) G. Karogounis and T. M. Issa, *Z. Elektrochem.*, **66**, 874 (1962).

(2) G. Karogounis and T. M. Issa, *Nature*, **195**, 1196 (1962).

(3) E. V. Pershina and Sh. Sh. Raskin, *Dokl. Akad. Nauk SSSR*, **150**, 1022 (1963).

(4) P. J. Hendra and E. J. Loader, *Nature*, **216**, 789 (1967); **217**, 637 (1970).

(5) P. J. Hendra, J. R. Horder, and E. J. Loader, *Chem. Commun.*, **1970**, 563.

(6) Private communication.

(7) E. P. Parry, *J. Catal.*, **2**, 371 (1963).

(8) J. K. Wilmhurst and H. J. Bernstein, *Can. J. Chem.*, **35**, 1183 (1957).

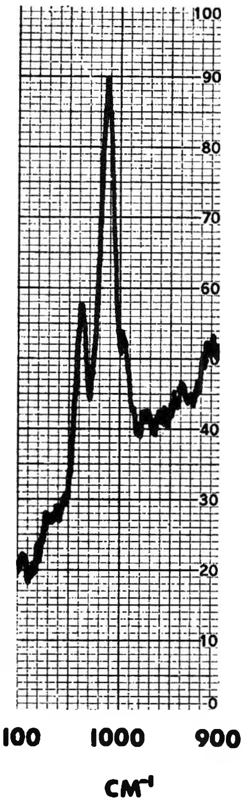

Figure 1. Raman spectrum of pyridine adsorbed on silica gel in the region 900–1100 cm^{-1} after evacuation to 10^{-6} Torr (He/Ne excitation, 6329 Å). The prominent bands appear at 1010 and 1036 cm^{-1}. (The instrument was calibrated to the He/Ne emission lines prior to scanning and a correction factor of -2 cm^{-1} was found for this region.)

at 1036 and 1010 cm^{-1} remained constant (within experimental error) at a value of ~0.45. Careful studies of pyridine intermolecularly hydrogen-bonded in solutions (10%) of $CHCl_3$, CH_2Cl_2, and H_2O show that the relative intensity ratio of these two ring modes decreases with increasing hydrogen-bond strength; liquid Py, $I(1032)/I(992) = 0.80$; Py in $CHCl_3$, $I(1035)/I(998) = 0.80$; Py in CH_2Cl_2, $I(1032)/I(992) = 0.77$; Py in H_2O, $I(1036)/I(1003) = 0.56$; surface species $I(1036)/I(1010) \cong 0.45$. The analogous quantities for $PyH^+BF_4^-$ and Py:$ZnCl_2$ are $I(1032)/I(1012) = 0.15$ and $I(1050)/I(1025) = 0.04$, respectively, which also suggests that those structures are unlikely. Both the relative band intensity ratio and band positions of pyridine in H_2O closely approximates the corresponding parameters of the pyridine surface species. We interpret these data as indicating that pyridine is hydrogen bonded to the silica gel surface (probably surface OH groups) and that the surface hydrogen bond is tighter than the intermolecular bond between liquid water and pyridine. These data are consistent with those obtained from similar Raman studies[5] and analogous infrared studies.[7]

2-Chloropyridine. The Raman spectrum of 2-chloropyridine over silica gel at its room temperature equilibrium vapor pressure is identical with that of the pure liquid. There is no evidence for the presence of any material left on the surface after evacuation at room temperature. This suggests that 2-chloropyridine only forms a liquid phase layer (presumably capillary condensation) on the surface but does not hydrogen-bond to the surface. Steric hindrance probably prevents hydrogen bond formation for this molecule.

Conclusion

The Raman effect has been demonstrated to be a useful technique for confirming and complementing analogous infrared surface studies. Work currently in progress in this laboratory indicates that this technique also can be successfully applied to systems which do not readily lend themselves to study by infrared.

In the present study, pyridine forms a species which is hydrogen-bonded to the silica gel surface: 2-chloropyridine does not hydrogen-bond to the silica gel probably because of steric hindrance but rather forms a condensed liquid layer.

Vibrational Assignments and Thermodynamic Functions for *cis*- and *trans*-1,2-Difluoro-1-chloroethylenes

by Norman C. Craig,[1] David A. Evans, Lawrence G. Piper, and Vicki L. Wheeler

Department of Chemistry, Oberlin College, Oberlin, Ohio 44074 *(Received August 14, 1970)*

Complete assignments of the vibrational fundamentals of *cis*- and *trans*-CFCl=CFH and CFCl=CFD have been obtained from infrared and Raman spectra. For *cis*-CFCl=CFH the fundamentals are: (a′) 3137, 1716, 1326, 1159, 1112, 854, 480, 361, and 224 cm^{-1}; (a″) 776, 523, and 255 cm^{-1}. For *trans*-CFCl=CFH the fundamentals are: (a′) 3120, 1708, 1290, 1196, 1150, 696, 578, 397, and 200 cm^{-1}; (a″) 776, 467, and 310 cm^{-1}. For the cis-to-trans reaction at 591°K, the equilibrium constant is 0.932 ± 0.022. From a rigid rotor, harmonic-oscillator treatment $\Delta S°_{591} = -0.12 \pm 0.26$ cal/mol °K, and $\Delta E_0°$ (electronic) = 80 ± 260 cal/mol with the cis isomer having the lower energy. Also, $\Delta H°_{591} = 10 \pm 160$ cal/mol.

This investigation of the cis and trans isomers of 1,2-difluoro-1-chloroethylene was undertaken as part of a study of nonbonded interactions in the cis–trans isomers of chlorofluoroethylenes. From thermodynamic and spectroscopic data the cis isomers of NF=NF, CFH=CFH, CFH=CClH, and CClH=CClH have been shown to have 3–0.6 kcal *less* electronic energy than the corresponding trans isomers.[2] This energy difference has been attributed to a nonbonded force acting between cis halogen atoms. CFCl=CFH was chosen as a convenient example of a trihaloethylene. In this system we expected all of the vibrational fundamentals to be accessible above 200 cm^{-1} in the infrared and side reactions to be unimportant in the iodine catalyzed cis–trans isomerization.

The present paper is concerned with obtaining a complete assignment for the vibrational fundamentals of the 1,2-difluoro-1-chloroethylenes and with extracting the electronic energy difference between the cis and trans isomers. To reinforce the vibrational assignment, *cis*- and *trans*-CFCl=CFD are included in the spectroscopic study. Apparently no previous report of the vibrational spectra of these ethylenes is in the literature. However, Nielsen, Liang, and Smith have assigned all of the fundamentals of the gem isomer, 1,1-difluoro-2-chloroethylene,[3] and we have assigned several closely related molecules.[2] No thermodynamic data appear to be available.

Experimental Section

Syntheses. CBrClFCClFH was prepared in 35% yield by reaction of CFClCFCl with hydrogen bromide on charcoal at 215°.[4] This reaction was carried out by metering the gaseous reactants, each at a rate of about 2.5 l. (NTP)/hr, into a hot tube packed with the activated charcoal (Barneby–Cheney SV2). The ethane was collected and worked up as described before, and a fraction boiling between 93 and 97° was collected.

Dehalogenation of the CBrClFCClFH with zinc dust in refluxing ethanol gave a 95% yield of *cis*- and *trans*-CFClCFH along with some CF_2CClH and CF_2CH_2. (The CF_2CClH is traceable to the CCl_2CF_2 present in the starting olefin.)

cis- and *trans*-CClFCFD were prepared by exchanging the crude olefin mixture at 80–90° with deuterium oxide saturated with calcium oxide. This exchange reaction involved two liquid phases sealed in standard-wall Pyrex tube. To prevent explosion of the tube, it was placed in a rocking bomb and pressurized to 225 psi; 2–3 days was taken for each exchange step.

Separation and purification of the cis and trans olefins were achieved by gas chromatography. Two passes at 0° through an 8-m column packed with tri-*m*-tolyl phosphate on firebrick followed by a pass at 0° through a 4-m column packed with halocarbon oil (11–21) on firebrick were used to obtain final purities above 99.5%. The trans isomer is eluted first on these columns. Samples were dried by passing them over phosphorus decoxide. Estimates of isotopic purities of the CFClCFD samples (see spectra) were obtained from the intensities of infrared bands due to undeuterated species.

Boiling points of pure *cis*-CFClCFH(−10.0°) and *trans*-CFClCFH (−13.9°) were calculated from vapor pressure measurements (lit.[5] bp 15° for mixture). Melting points were measured as −133.5° (cis) and −134.8° (trans).[4]

Spectroscopy. Infrared spectra, Figures 1–4, were recorded on a Perkin-Elmer 621 filter-grating spec-

(1) Author to whom inquiries should be addressed.

(2) See N. C. Craig, Y.-S. Lo, L. G. Piper, and J. C. Wheeler, *J. Phys. Chem.*, **74**, 1712 (1970), and other references cited therein.

(3) J. R. Nielsen, C. Y. Liang, and D. C. Smith, *J. Chem. Phys.*, **20**, 1090 (1953).

(4) N. C. Craig and D. A. Evans, *J. Amer. Chem. Soc.*, **87**, 4223 (1965).

(5) J. M. Birchall, R. N. Haszeldine, and A. R. Parkinson, *J. Chem. Soc.*, 2204 (1961).

Table I: Infrared and Raman Spectra and Assignments for *cis*-CFCl=CFH (Frequencies in cm^{-1})

Raman, liquid			Infrared, gas			Assignment		
Freq, cm^{-1}	I	pol	Freq,[a] cm^{-1}	α[b]	Band shape[c]	Freq, cm^{-1}		Symmetry species
3135	w	p	3137 (14)	0.40	A	Fund	ν_1	a′
			2871 (13)	0.062	A/B	2875	$\nu_2 + \nu_4$	A′
			2822 (13)	0.051	B	2828	$\nu_2 + \nu_5$	A′
			2362	R branch		CO_2 impurity		
			2311 (14)	0.15	A/B	2318	$2 \times \nu_4$	A′
			2264 (13)	0.060	B	2271	$\nu_4 + \nu_5$	A′
			1968		C	1971	$\nu_2 + \nu_{12}$	A″
			1938 (13)	0.004	A/B	1940	$\nu_2 + \nu_9$	A′
1714	s	p	1716 (13)	1.8	B	Fund	ν_2	a′
			1585	0.09	?	1592	$\nu_5 + \nu_7$	A′
			1547 (12)	0.35	B	1552	$2 \times \nu_{10}$	A′
						1550	$\nu_3 + \nu_9$	
			1411 (21)	0.007	C	1414	$\nu_4 + \nu_{12}$	A″
			1382 (14)	0.042	A/B	1383	$\nu_4 + \nu_9$	A′
1320	w	dp	1326 (12)	2.2	B	Fund	ν_3	a′
1149	w	dp	1159 (13)	6.1	A[d]	Fund	ν_4	a′
1102	m	p	1112 (12)	14	A/B[d]	Fund	ν_5	a′
			1048 (13)	0.95	A[d]	{1046	$2 \times \nu_{11}$	A′
						Fermi resonance with ν_6		
851	s	p	854 (13)	4.0	A[d]	Fund	ν_6	a′
781	wm	dp	776 (19)	0.71	C[d]	Fund	ν_{10}	a′
			667		C	CO_2 impurity		
524	m	dp	523 (20)	0.062	C[d]	Fund	ν_{11}	a″
						? {510	$2 \times \nu_{12}$	A′
						Fermi resonance with ν_7		
484	s	p	480 (11)	0.052	B	Fund	ν_7	a′
363	s	p	361 (13)	0.042	A[d]	Fund	ν_8	a′
258	w	dp	255	0.08	C	Fund	ν_{12}	a″
227	w	dp	224	0.19	B?	Fund	ν_9	a′

[a] Spacing between P and R branches in parentheses. [b] Absorption coefficient in cm^{-1} atm^{-1}; combination bands with intensities <0.05 omitted unless of special interest. [c] A and B band shape designations are approximate for these molecules of C_s symmetry. A/B signifies a mixed shape. [d] Multiplet structure suggestive of a chlorine isotope effect or a hot band.

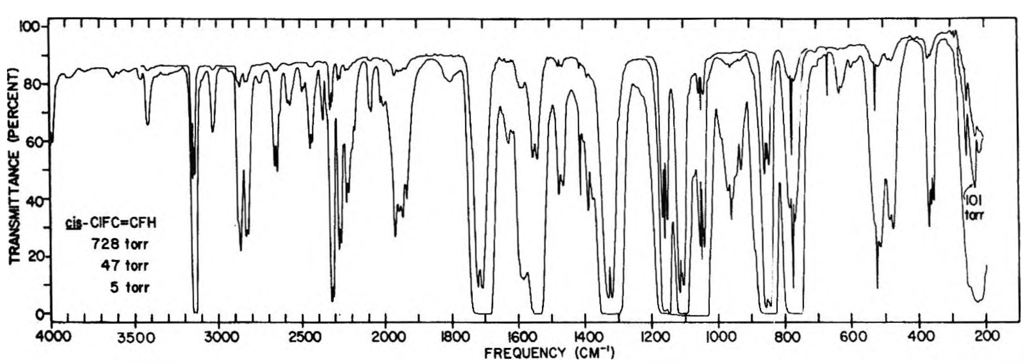

Figure 1. Gas-phase infrared spectrum of *cis*-1,2-difluoro-1-chloroethylene. (The weak features at 2350 and 667 cm^{-1} are due to impurity carbon dioxide.)

trometer that was purged with dry nitrogen. Gaseous samples were scanned at ambient temperature in 10-cm cells equipped with cesium iodide windows. Frequencies, Tables I–IV, were measured to ± 1 cm^{-1} under expanded-scale, medium–high resolution conditions. In the spectra bands due to isotopic impurities are shown with dashed lines.

Room temperature, liquid-phase Raman spectra, Tables I–IV, were recorded photographically on a Hilger E612 spectrograph with 4358-Å excitation from mercury arcs. Capillary cells (2-mm i.d.) were used for samples of about 15 mmol in size. Qualitative depolarizations were obtained by the Edsall–Wilson method. These Raman spectra were obtained by G. Y.-S. Lo at the Dow Chemical Co., Midland, Mich.

Proton nuclear magnetic resonance spectra (type

Table II: Infrared and Raman Spectra and Assignments for *cis*-CFCl=CFD (Frequencies in cm^{-1})

Raman, liquid			Infrared, gas			Assignment		
Freq, cm^{-1}	I	pol	Freq,[a] cm^{-1}	α^b	Band shape[c]	Freq, cm^{-1}		Symmetry species
			3137 (14)		A	3137	*cis*-CFClCFH impurity	
			2801 (10)	0.067	A/B	2806	$\nu_2 + \nu_4$	A′
			2433 (12)	0.082	B	2436	$2 \times \nu_3$	A′
2354?	w	p	2345 (13)	0.42	A	Fund	ν_1	a′
			2215 (12)	0.051	A/B	2220	$2 \times \nu_4$	A′
			1938	0.01	C	1943	$\nu_2 + \nu_{12}$	A″
			1914 (12)	0.035	B	1916	$\nu_2 + \nu_9$	A′
						1931	$\nu_4 + \nu_6$	A′
1698	s	p	1696	2.0	B	Fund	ν_2	a′
			1590	0.068	?	1606	$\nu_4 + \nu_{11}$	A″
						1589	$\nu_4 + \nu_7$	A′
			~1546 (14)		B	1547	*cis*-CFClCFH impurity	
			1469 (11)	0.045	A/B	1471	$\nu_5' + \nu_7$	A′
						1469	$\nu_4 + \nu_8$	
			1463		C?	1465	$\nu_3 + \nu_{12}$	A″
			1437	0.047	B	1438	$\nu_3 + \nu_9$	A′
			1326 (13)		B	1326	*cis*-CFClCFH impurity	
			1259 (14)	0.25	A[d]	1260	$2 \times \nu_{10}$	A′
						Fermi resonance with ν_3		
1204	vw		1218 (13)	5.0	B	Fund	ν_3	a′
			1159		C	1177	$\nu_9 + \nu_{12}$	A″
			1156 (12)	0.25	B	1154	$\nu_5 + \nu_9$	A′
						Fermi resonance with ν_4		
			1128 (12)	0.15	A[d]	1126	$\nu_{10} + \nu_{11}$	A′
						Fermi resonance with ν_4		
1100	m	p	1110 (13)	15	A	Fund	ν_4	a′
1045?	vw		1040 (12)	0.37	B	1041	$\nu_6 + \nu_9$	A′
						Fermi resonance with ν_4?		
			992 (13)	0.27	A	992	$2 \times \nu_{11}$	A′
						Fermi resonance with ν_5 (ν_5')		
938	w	dp	934 (13)	0.39	A[d]	Fund	ν_5	a′
			890 (13)	0.050	B[d]	877	$\nu_{10} + \nu_{12}$	A′
						838	$\nu_7 + \nu_8$	A′
						Fermi resonance with ν_6		
			853 (14)		A[d]	854	*cis*-CFClCFH impurity	
822	s	p	821 (13)	2.4	A	Fund	ν_6	a′
			776		C	776	*cis*-CFClCFH impurity	
633	sm	dp	630 (19)	0.25	C	Fund	ν_{10}	a″
502	w	dp	496 (19)	0.15	C	Fund	ν_{11}	a″
479	sm	p	~475			Fund	ν_7	a′
361	sm	p	359 (14)	0.047	A	Fund	ν_8	a′
259	vw	dp	247	0.05	C[d]	Fund	ν_{12}	a″
226	vw	dp	220	0.28	B?	Fund	ν_9	a′

[a–d] See Table I.

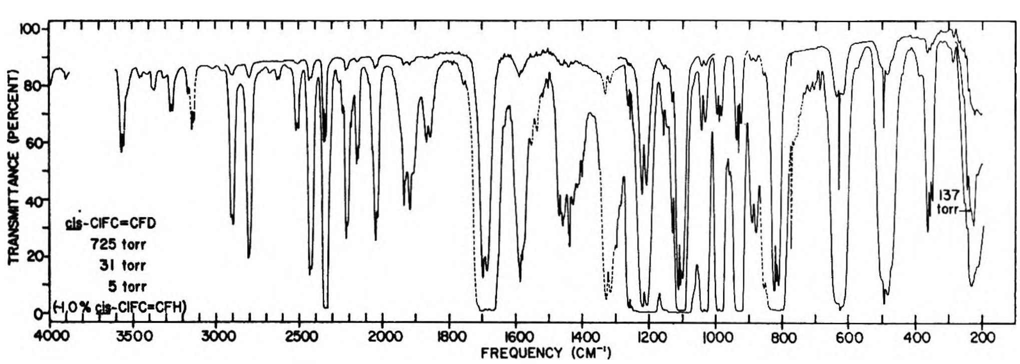

Figure 2. Gas-phase infrared spectrum of *cis*-1,2-difluoro-1-chloroethylene-2-d_1.

Table III: Infrared and Raman Spectra and Assignments for *trans*-CFCl=CFH (Frequencies in cm^{-1})

Raman, liquid			Infrared, gas			Assignment		
Freq, cm^{-1}	I	pol	Freq,[a] cm^{-1}	α[b]	Band shape[c]	Freq, cm^{-1}		Symmetry species
3121	wm	p	3120 (16)	0.39	A[d]	Fund	ν_1	a′
			2901 (14)	0.068	A/B	2904	$\nu_2 + \nu_4$	A′
			2342 (13)	0.12	?	2347	$\nu_4 + \nu_5$	A′
			1770 (12)	0.084	A/B	1774	$\nu_4 + \nu_7$	A′
						{1728	$\nu_5 + \nu_7$	A′
						Fermi resonance with ν_2 ?		
1709	s	p	1708 (11)	0.16	B	Fund	ν_2	a′
~1551	vw		1547 (13)	0.38	A[d]	1552	$2 \times \nu_{10}$	A′
						1547	$\nu_5 + \nu_8$	A′
			1387 (11)	0.11	B	1396	$\nu_4 + \nu_9$	A′
						1392	$2 \times \nu_6$	A′
1289	m	dp	1290 (14)	1.7	A	Fund	ν_3	a′
1188	vw		1196 (12)	14	A/B[d]	Fund	ν_4	a′
1151	w		1160 (14)	2.8	A[d]	{1156	$2 \times \nu_7$	A′
						Fermi resonance with ν_5		
1141	wm	p	1150	2.8	A[d]	Fund	ν_5	a′
~933	vw		935 (14)	0.19	A[d]	{934	$2 \times \nu_{11}$	A′
						Fermi resonance with ν_6		
779	m	dp	776 (23)	0.78	C[d]	Fund	ν_{10}	a″
690	s	p	696 (12)	1.9	A[d]	Fund	ν_6	a′
						{620	$2 \times \nu_{12}$	A′
			620 (13)	0.033	A/B	597	$\nu_8 + \nu_9$	A′
						Fermi resonance with ν_7		
576	m	p	578 (11)	0.13	A/B	Fund	ν_7	a′
467	m	dp	467 (24)	0.11	C	Fund	ν_{11}	a″
397	m	dp	397 (12)	0.24	B	Fund	ν_8	a′
316	m	dp	310 (23)	0.19	C	Fund	ν_{12}	a″
200	m	dp	~205 R	0.03		Fund	ν_9	a′

[a–d] See Table I.

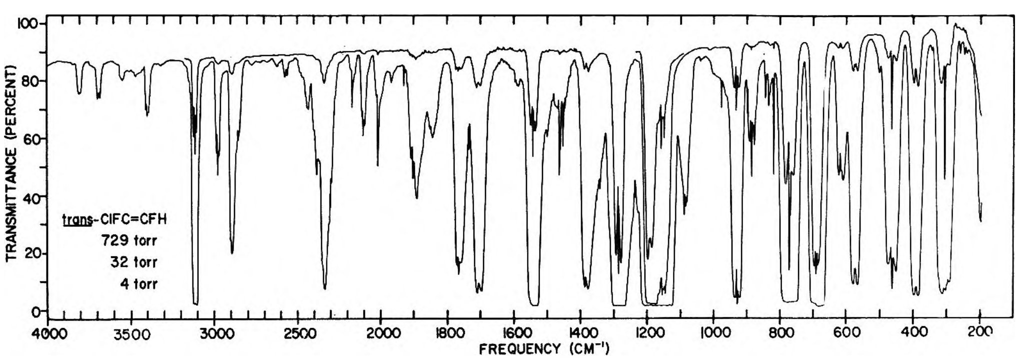

Figure 3. Gas-phase infrared spectrum of *trans*-1,2-difluoro-1-chloroethylene.

AMX) were recorded on a Varian A-60 spectrometer. Samples consisted of 20 mol % olefin in $CFCl_3$ solvent with a 1% TMS reference. For *cis*-CFClCFH: $J_{HF(gem)} = 72.9$ Hz, $J_{HF(trans)} = 12.4$ Hz, and $\delta = 6.39$ ppm; for *trans*-CFClCFH: $J_{HF(gem)} = 74.3$ Hz, $J_{HF(cis)} = 1.2$ Hz, and $\delta = 7.26$ ppm.[6]

Isomerization Equilibrium. The equilibrium constant for the cis-to-trans isomerization of CFCl=CFH in the gas phase was measured at 318 ± 1°. For the cis-to-trans reaction $K = 0.932 \pm 0.022$.[7] Iodine (about 0.5 Torr) was used as a catalyst, and analyses were performed by gas chromatography. On the 8-m tricresyl phosphate column (0°) the two isomers were not quite completely resolved. An experimentally determined correction factor of 1.008 ± 0.007 was applied to the ratio of areas measured with a planimeter. Equilibrium was approached from both the cis-rich and trans-

(6) Compare P. B. Sargeant, *J. Org. Chem.*, **35**, 678 (1970). For cis isomer: $J = 74$ and $J = 12$ Hz, $\delta = 6.05$ (neat); for trans isomer: $J = 74$ and $J = 1.2$ Hz, $\delta = 6.90$ (neat).

(7) 0.015 is the standard deviation (SD) based on 8 final measurements; 0.007 is SD in the calibration of the area ratio.

Table IV: Infrared and Raman Spectra and Assignments for *trans*-CFCl=CFD (Frequencies in cm^{-1})

Raman, liquid			Infrared, gas			Assignment		
Freq, cm^{-1}	I	pol	Freq,[a] cm^{-1}	α^b	Band shape[c]	Freq, cm^{-1}		Symmetry species
			3120 (16)		A	3120	*trans*-CFClCFH impurity	
			2882 (11)	0.092	A/B	2886	$\nu_2 + \nu_3$	A′
2348	w	p	2364 (11)[e]	0.29	A/B	2367	$\nu_3 + \nu_4$	A′
						2351	$\nu_2 + \nu_6$	A′
						2340	$2 \times \nu_4$	A′
						Fermi resonance with ν_1		
2321	m	p	2326 (15)	0.32	A	Fund	ν_1	a′
			2146 (10)	0.055	A	2151	$\nu_3 + \nu_5$	A′
			2128		C?	2129	$\nu_2 + \nu_{11}$	A″
			2118 (16)		A?	2124	$\nu_4 + \nu_5$	A″
			1766 (13)	0.079	A/B[d]	1770	$\nu_3 + \nu_7$	A′
						1743	$\nu_4 + \nu_7$	A′
						Fermi resonance with ν_2		
1683	vs	p	1689 (10)[e]	0.22	B	Fund	ν_2	a′
1655	vw		~1650			1653	$\nu_5' + \nu_7$	A′
			1326 (12)	0.10	A/B	1330	$2 \times \nu_6$	A′
1268	vw		1275 (13)	0.25	A[d]	1276	$2 \times \nu_{10}$	A′
						Fermi resonance with ν_3		
			1235 (12)	0.24	A/B	1238	$\nu_6 + \nu_7$	A′
						Fermi resonance with ν_3		
			1197 (12)	16	A/B[d]	Fund	ν_3	a′
1154	wm	p	1170 (14)	<5.7	A[d]	Fund	ν_4	a′
1137	vw		~1140			1146	$2 \times \nu_7$	A′
						1152	$\nu_5 + \nu_9$	A′
						Fermi resonance with ν_4		
			1080 (15)	0.24	A/B	1078	$\nu_{10} + \nu_{11}$	A′
						967	$\nu_7 + \nu_8$	A′
						Fermi resonance with ν_5 (ν_5')		
950	m	p	954 (9)[e]	0.51	B	Fund	ν_5	a′
			882 (15)	0.10	A	880	$2 \times \nu_{11}$	A′
						Fermi resonance with ν_6		
			776		C[d]	776	*trans*-CFClFH impurity	
659	vs	p	655 (12)	1.8	A[d]	Fund	ν_6	a′
636	s	dp	639 (~20)	0.63	C[d]	Fund	ν_{10}	a″
571	sm	p	573 (12)	0.17	A[d]	Fund	ν_7	a′
440	w	dp	440 (24)	0.13	C	Fund	ν_{11}	a″
393	m	dp?	394 (13)	0.24	A/B	Fund	ν_8	a′
295	m	dp	292 (23)	0.55	C	Fund	ν_{12}	a″
198	m	dp	<200	<0.08		Fund	ν_9	a′

[a–d] See Table I. [e] Probably Q-Q spacing.

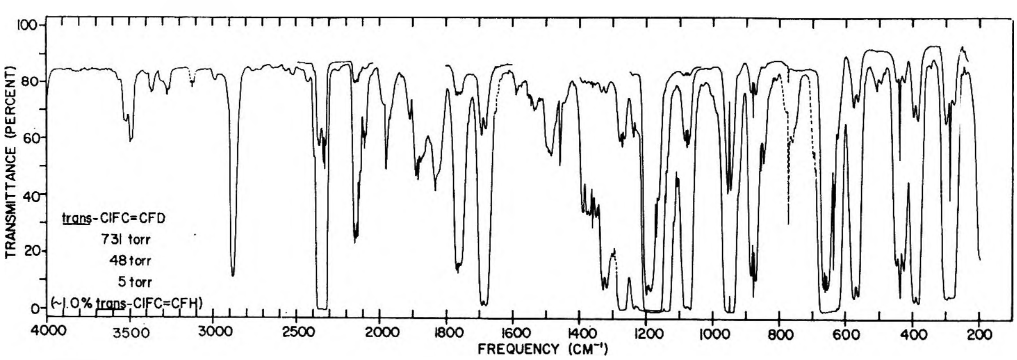

Figure 4. Gas-phase infrared spectrum of *trans*-1,2-difluoro-1-chloroethylene-2-d_1.

rich sides. During equilibrations of several days duration the pressure decreased from an initial value of about 1 atm to about 0.3 atm. This pressure decrease appeared to be due to polymerization of the haloethylene. An involatile liquid was expelled from the reaction vessel, and a higher molecular weight component (narrow bands) was observed in the infrared spectrum of the haloethylenes recovered from the isomerization mixture. In addition, hydrogen chloride was found among these reaction products.

Results and Discussion

Assignment of Configurations. Because of the low symmetry of the *cis*- and *trans*-CFCl=CFH molecules, infrared and Raman selection rules do not serve as a simple basis for assigning configurations. However, from a consideration of the relative magnitudes of nmr coupling constants, where, in general, $J_{HF(trans)} > J_{HF(cis)}$, Sargeant has recently assigned the configurations of these isomers.[6] We have confirmed these nmr assignments. Further support for this assignment of configurations comes from the larger splitting between the CF stretching frequencies of the cis isomer compared with that of the trans. Consideration of normal coordinates for CX stretching of a simplified CX=CX model and examination of the splittings between these frequencies in haloethylenes of known configurations has established the validity of the rule.[8] The considerably lower intensity of the infrared absorption band due to CC stretching of the trans species compared with that of the cis is also in accord with this assignment.

Vibrational Assignment. General. The cis and trans isomers of CFCl=CFH and of CFCl=CFD have C_s symmetry. As a consequence the nine in-plane (a′) and three out-of-plane (a″) fundamentals are infrared and Raman active with the in-plane fundamentals expected to be polarized in the Raman spectrum. In the gas-phase infrared, bands for in-plane fundamentals have shapes ranging from type A to type B, whereas the bands for the out-of-plane fundamentals are type C. From the moments of inertia (Table VI) and the expressions given by Seth-Paul and Dijkstra[9] we calculate the following PR branch separations at 320°K: *cis*-CFClCFH ($\rho^* = 2.97$, $\kappa = -0.860$), type A bands 13 cm^{-1}, type B 12 cm^{-1}, and type C 20 cm^{-1}; *trans*-CFClCFH ($\rho^* = 0.872$, $\kappa = -0.060$), type A 16 cm^{-1}, type B 12 cm^{-1}, and type C 24 cm^{-1}. Thus, for cis molecules the PR separations in bands for in-plane modes should be 12–13 cm^{-1}, and for *trans* molecules the corresponding range should be 12–16 cm^{-1}. (This difference in range of PR separations serves as yet another basis for checking the assignment of isomeric configurations.) All of the moments of inertia are large enough so that no detailed rotational structure is observable at a resolution of 0.3 cm^{-1} and above. However, isotope splitting due to ^{35}Cl–^{37}Cl species may be evident for fundamentals that are rich in chlorine motion. As Mann, Acquista, and Plyler have emphasized,[10] one can expect also to find rather intense bands for the first overtones of a″ species, particularly those due principally to CH(D) motion. This generalization is borne out in the spectra of other fluorochloroethylenes which we have studied.[2]

cis-1,2-Difluoro-1-chloroethylene. From the infrared spectrum, Figure 1, eight type A/B bands of reasonable frequency, intensity, and PR separation are available for assignment as in-plane fundamentals. The assignments at 3137, 1716, 1112, 854, 480, and 361 cm^{-1} are confirmed by polarized counterparts in the Raman spectrum (Table I). Although the 1326 and 1159-cm^{-1} bands are apparently depolarized in the Raman, no substantial doubt exists about their respective assignments as the CH deformation and one of the CF stretches. For two of the out-of-plane fundamentals, 776 and 523 cm^{-1}, clear type C bands in the infrared and depolarized bands in Raman are found. Finally, the Raman spectrum has two distinct bands in the 300–200-cm^{-1} region each of which is depolarized. Although the shapes of the corresponding infrared bands are not clearly defined, it appears that the shape of the higher frequency band is type C and that of the lower frequency one is type B. Support for this assignment comes from the repetition of the same pattern in combination bands near 1950 and 1400 cm^{-1}. The infrared spectrum of *cis*-CFClCFH in the low-frequency region is reminiscent of the spectra of *trans*-dihaloethylenes and diazenes.[2] This similarity is not surprising as *cis*-CFClCFH approximates a prolate top in shape, whereas *trans*-CFClCFH is an asymmetric top. In these near-symmetric top molecules the near degeneracy of the lowest frequency in-plane and out-of-plane fundamentals leads to large distortions in band shapes due to Coriolis coupling.

The fairly intense infrared bands at 1547 and 1048 cm^{-1} are not fundamentals but are the expected first overtones of the out-of-plane fundamentals, ν_{10} and ν_{11}. Also the distorted shape of the type C band at 523 cm^{-1} suggests an overlapped band due to the first overtone of ν_{12}. As suggested in the assignments in Table I these intense overtones may profit from Fermi resonance with neighboring fundamentals.

The 47-cm^{-1} splitting between the two CF stretching fundamentals seems anomalously small when compared with 108 cm^{-1} for *cis*-CFCl=CFD and 46 cm^{-1} for *trans*-CFCl=CFH. This small splitting is undoubtedly caused by a depression of the higher CF stretching frequency due to mixing with the CH bend. Apparently, a comparable mixing of the CF stretch and CH bend is not important in the trans isomers because the splitting decreases, from 46 to 27 cm^{-1}, upon deuteration. One might also suppose that mixing of the CD bend with the lower frequency CF stretch would raise this latter frequency and thereby decrease the splitting between the CF stretches. Thus, we consider the split-

(8) N. C. Craig, G. Y.-S. Lo, C. D. Needham, and J. Overend, *J. Amer. Chem. Soc.*, 86, 3232 (1964).

(9) W. A. Seth-Paul and G. Dijkstra, *Spectrochim. Acta*, 23A, 2861 (1967).

(10) D. E. Mann, N. Acquista, and E. K. Plyler, *J. Chem. Phys.*, 23, 2122 (1955).

ting in the deuterated species to be an upper limit and have referred to it in connection with the assignments of configuration presented above.[11]

cis-1,2-Difluoro-1-chloroethylene-2-d₁. For the most part the vibrational assignment for *cis*-CFClCFD follows directly from that of the undeuterated cis species after allowance is made for the decrease in frequency of CH-rich modes due to deuteration. The infrared spectrum of *cis*-CFClCFD is given in Figure 2, and the Raman bands are tabulated along with the detailed assignment in Table II. Assignment of the CD bending mode is not obvious in the infrared, however, as three type A/B of comparable intensity are present in the 1050–900-cm^{-1} region. Only the lower frequency of the three, the one at 934 cm^{-1}, corresponds to a Raman band of significant intensity. Like its equivalent in the *cis*-CFClCFH spectrum this band is apparently depolarized. The middle band is undoubtedly $2\nu_{11}$, strengthened in intensity by Fermi resonance with the CD bending fundamental. The higher frequency band appears to be a consequence of Fermi resonance of ν_4 with $\nu_6 + \nu_9$.

In the infrared spectrum of *cis*-CFClCFD the band structure in the 300–200-cm^{-1} region is even more obscure than that of *cis*-CFClCFH. As in the hydrogen case we have assigned the higher frequency feature to the out-of-plane fundamental, ν_{12}. Pairs of overlapped combination bands at about 1925, 1450, and 1150 cm^{-1} presumably reflect the structure of the low-frequency region.

As in the infrared spectrum of *cis*-CFClCFD first overtones of out-of-plane modes are intense. In addition to $2\nu_{11}$, which is discussed above, $2\nu_{10}$ is seen at 1259 cm^{-1}. $2\nu_{12}$ (510 cm^{-1}) would be lost under the overlapped bands due to ν_7 and ν_{11}.

trans-1,2-Difluoro-1-chloroethylene. In the infrared spectrum of *trans*-CFClCFH, Figure 3, three reasonably intense bands with type C shapes and appropriate PR separations are immediately apparent below 800 cm^{-1}. These bands at 776, 467, and 310 cm^{-1} correspond to prominent, depolarized Raman bands (Table III) and thus are confidently assigned to the three a″ fundamentals. The first overtones of each of these fundamentals appear with substantial intensity at 1547, 935, and 620 cm^{-1}, respectively, and should not be confused with a′ fundamentals.

The assignment of the a′ fundamentals is not as obvious as that for the a″ fundamentals. Five infrared bands with type A/B band shapes and with reasonable intensities, frequencies, and PR separations, 3120, 1708, 1150, 696, and 578 cm^{-1} correspond to polarized Raman bands. These frequencies are assigned to in-plane fundamentals. In the infrared the intensity of the CC stretch is rather weak, but the Raman band is appropriately strong. The position of the lower frequency, symmetric CF stretch in the infrared, is confused by the dominant intensity of the adjacent band due to the antisymmetric CF stretch and by Fermi resonance with a combination band. Although Raman bands for the other four in-plane fundamentals are apparently depolarized, for three of them well defined type A/B bands are found in the infrared at 1290, 1196, and 397 cm^{-1}. Also what appears to be an R branch of the remaining in-plane fundamental is seen just above the low-frequency limit of the spectrometer at 200 cm^{-1}.

trans-1,2-Difluoro-1-chloroethylene-2-d₁. As in the case of *trans*-CFClCFH the type-C bands for a″ fundamentals are readily apparent below 800 cm^{-1} in the infrared spectrum of *trans*-CFClCFD (Figure 4). The 639-cm^{-1} band is partly overlapped by ν_6 (a′), but the ones at 440 and 292 cm^{-1} are in the clear. These three fundamentals appear as depolarized bands in the Raman spectrum (Table IV). Once again $2\nu_{10}$ (1275 cm^{-1}) and $2\nu_{11}$ (882 cm^{-1}) are rather intense. $2\nu_{12}$ (584 cm^{-1}) would be masked by ν_7 (a′).

Seven of the a′ fundamentals have polarized Raman bands. Six of these correspond to type A/B bands at 2326, 1689, 1197, 954, 665, and 573 cm^{-1}. The infrared band at 1170 cm^{-1}, which is assigned to the symmetric CF stretch, is nearly lost in the wing of the intense 1197-cm^{-1} band. The 394-cm^{-1} band, which may be depolarized in the Raman, has a clear type B shape in the infrared. The 198-cm^{-1} Raman band, though also apparently depolarized, is certainly due to the ninth a′ fundamental. Fermi resonance with a combination band must modify the frequency of the CD stretch and possibly several other fundamentals to a lesser degree.

As in the case of the other three molecules in this series the Raman bands assigned to the CCl stretch are characteristically strong and the infrared bands show evidence of chlorine isotope splitting.

Summary. Table V summarizes the assignments of vibrational fundamentals for the two cis and two trans species. We believe that a convincing assignment has been obtained for the twelve fundamentals of each molecule. For each isomer the Rayleigh rule is satisfied as are the product rules as shown in Table VI. In addition the assignments for the cis and trans isomers are consistent with one another and with the assignment of Nielsen, Liang, and Smith for the gem isomer,[3] which is included for comparison in Table V. Group frequencies have proved to be an excellent guide to the assignments for these molecules of low symmetry and relatively few atoms.

Thermodynamic Functions. From a rigid-rotor, harmonic-oscillator treatment of *cis*- and *trans*-CFClCFH, $\Delta S°_{591} = 86.74 - 86.86 = -0.12 \pm 0.26$ cal/mol °K[12] for the reaction

(11) Although normal coordinate calculations have not been carried out for these molecules, this discussion is supported by the normal coordinates of related molecules such as CFH=CFH and CFH=CClH (ref 2).

(12) Estimates of uncertainties are based on ±2 cm^{-1} uncertainties in fundamental vibration frequencies, 0.01–0.02 Å uncertainties in bond lengths, and 1° uncertainties in bond angles.

Table V: Vibrational Fundamentals of the Difluorochloroethylenes and Deuterated Modifications of the cis-trans Isomers (Frequencies in cm^{-1})

	Approximate description	gem Isomer CF_2CClH	cis Isomer CFClCFH	cis Isomer CFClCFD[c]	trans Isomer CFClCFH	trans Isomer CFClCFD[c]
			a′			
ν_1	CH(D) str	3130	3137	2345	3120	2326[a]
ν_2	CC str	1745	1716	1696	1708[a]	1689[a]
ν_3	CH(D) bend	1333	1326[a]	934[a]	1290[a]	954[a]
ν_4	a CF str	1199	1159	1218[a]	1196	1197[a]
ν_5	s CF str	970	1112[a]	1110[a]	1150[a]	1170[a]
ν_6	CCl str	845	854	821	696[a]	665[a]
ν_7	a CF bend	579	480	479[b]	578[a]	573
ν_8	CCl bend	433	361	359	397	394
ν_9	s CF bend	201[b]	224	220	200[b]	198[b]
			a″			
ν_{10}	CH(D) wag	751	776	630	776	639
ν_{11}	CF wag	(572)[b,d]	523	496	467	440
ν_{12}	torsion	243[b]	255	247	310	292

[a] Uncorrected for probable Fermi resonance. [b] From liquid phase Raman spectrum; all others from gas phase infrared. [c] For the deuterated species numbering of ν_3, ν_4, and ν_5 has been altered for convenience in tabulation. [d] Assignment in doubt.

Table VI: Principal Moments of Inertia in amu $Å^2$;[a] Product Rule Check of Assignments

	cis Isomer I_a	cis Isomer I_b	cis Isomer I_c	trans Isomer I_a	trans Isomer I_b	trans Isomer I_c
CFClCFH	56.56	212.8	269.4	98.92	144.2	243.1
CFClCFD	59.84	213.5	273.4	101.3	147.2	248.4
		Calcd	Obsd	Calcd	Obsd	
CFClCFD / CFClCFH	a′	0.509	0.512	0.511	0.517	
	a″	0.732	0.745	0.727	0.730	

[a] Geometric parameters: r_{CC} = 1.333 Å, r_{CCl} = 1.726 Å, r_{CF} = 1.348 Å, r_{CH} = 1.079 Å, α_{CCCl} = 123.6°, α_{CCH} = 123.2°, and α_{CCF} = 121.0°. J. A. Howe, *J. Chem. Phys.*, **34**, 1247 (1961).

$$cis\text{-}CFCl{=}CFH(g) = trans\text{-}CFCl{=}CFH(g)$$

From the measured equilibrium constant, $K_{591} = 0.932 \pm 0.022$, one calculates $\Delta G°_{591} = 82.1 \pm 2.8$ cal/mol. Thus, $\Delta H°_{591} = 10 \pm 160$ cal/mol. From the statistical thermodynamic calculation $\Delta H°(\text{thermal}) = H°_{591}(\text{trans}) - H°_{591}(\text{cis}) = 9761 - 9780 = -19 \pm 32$ cal/mol,[12] and from the observed vibrational fundamentals $\Delta E_0°$ (zero point) $= 16{,}994 - 17{,}044 = -50 \pm 69$ cal/mol.[11] Thus, $\Delta E_0°$ (electronic) $= \Delta H°_{591} - \Delta H°(\text{thermal}) - \Delta E_0°(\text{zero point}) = 80 \pm 260$ cal/mol.

Of course, this value of $\Delta E_0°$(electronic) rests on the assumption that a true equilibrium constant was measured. Yet, the trihaloethylene isomerization system is not as free of side reactions as we had supposed based on experience with two dihaloethylene systems. The side reaction, presumed to be mostly polymerization, that accompanies the isomerization could prevent cis–trans equilibrium from being attained. Such a distortion seems unlikely, however, since the polymerization reactions are presumably possible with both isomers and the equilibrium constant is so near unity.[13]

The small positive value for the electronic energy of the cis isomer relative to that of the trans is reasonably consistent with the difference of 220 cal/mol between the values of 1090 cal/mol for the CFH=CFH case and 870 cal/mol for the CFH=CClH case.[2] Consequently, this trihaloethylene example supports the experimental values for the more striking dihaloethylene examples. As has been noted before, the apparent nonbonded attraction between two fluorine atoms is not much greater than that between a chlorine and a fluorine atom. It is also evident that no unexpected effect is introduced by the presence of two halogen atoms on one of the two carbon atoms.

Acknowledgments. This research was supported by the Petroleum Research Fund (2422-B). Preliminary studies were made by Eileen Crosby Gruen and Dieter Knecht. L. G. P. was supported by an NSF U. R. P. grant, and V. L. W. was supported by a grant from the American Society for Testing Materials.

(13) We do not have a satisfactory explanation for the formation of hydrogen chloride in the isomerization reaction system. This finding was not pursued.

Magnetic Susceptibility Anisotropies in Lyotropic Liquid Crystals as Studied by High-Resolution Proton Magnetic Resonance

by Torbjörn Drakenberg,* Åke Johansson, and Sture Forsén

Department of Physical Chemistry, The Lund Institute of Technology, Chemical Center, Lund 7, Sweden
(Received July 13, 1970)

Lyotropic lamellar mesomorphic phases of systems containing H_2O, *n*-octylamine (OA), and *n*-octylamine hydrochloride (OAHCl) in various proportions have been examined by means of high-resolution nmr spectroscopy. The signals from the water protons exhibit fine structure, which is very different for spinning and nonspinning samples. The experiments indicate that the fine structure arises from chemical shift differences which may be attributed to magnetic susceptibility anisotropies in the mesomorphic phase. Theoretical expressions for the line shapes have been deduced with the assumption that the magnetic field experienced by the water protons depends on the orientation of the lamellae with respect to the external magnetic field.

Introduction

Nmr investigations of anisotropic liquid crystals of the lyotropic type[1-3] have demonstrated effects interpreted as originating from an anisotropy of the magnetic susceptibility. Corkill, *et al.*,[1] have shown that the position of the resonance signal from the water protons depends on the macroscopic orientation of the mesomorphic phase, and magnetic relaxation investigations[2,3] suggest that the rapid transverse relaxation observed in anisotropic mesomorphic phases is caused by diffusion of the molecules through magnetic inhomogeneities.

Liquid crystal phases of the systems H_2O–*n*-octylamine (OA), H_2O–OA–*n*-octanoic acid, H_2O–OAHCl, and H_2O–OA–OAHCl have been shown by low-angle X-ray investigations to be of a lamellar type within certain ranges of composition.[4-6] In a randomly ordered sample all directions of these lamellae are equally probable. Deuterium wide-line spectra of these systems show powder patterns with quadrupole couplings of 1–10 KHz,[7] indicating some degree of preferential orientation of the water molecules in the layers. The fact that these powder patterns persist even after application of the magnetic field for several days implies that no spontaneous magnetic alignment of the lamellae occurs. Such powder patterns have been observed in other anisotropic liquid crystal systems.[8-11] In the systems mentioned above, however, we have also observed a fine structure of the water proton signal in high-resolution spectra (see Figure 1), which can be given a theoretical explanation based upon an anisotropy of the magnetic susceptibility. No previous reports of such line shapes are known by the authors.

Experimental Section

The measurements were carried out on Varian A-60 A and HA-100 spectrometers. The samples were weighed into 5-mm tubes which were immediately sealed off. To obtain reproducible results the phases were prepared by slowly decreasing the temperature of an isotropic solution. In some cases ultrasonic vibrations were used to homogenize the samples.

Results and Discussion

From Figures 1a and b it is obvious that there is a drastic difference in the line shape of the water signal between spinning (*ca.* 30 rps) and nonspinning samples. Measurements at 60 and 100 MHz show that the width of the pattern in Figure 1 is directly proportional to the magnetic field, indicating that the line shape arises from chemical shift differences which we attribute to magnetic susceptibility anisotropies in the lamellar phases.

Such anisotropies can have both microscopic and macroscopic origins. Firstly, a microscopic effect may be due to chemical shift anisotropies in partially oriented molecules. Another microscopic effect has been discussed by Corkill, *et al.*[1], and is based upon susceptibility phenomena in the vicinity of rod-like molecules. A macroscopic effect may arise from parallel arrangement of alternating layers with different magnetic susceptibilities. When the lamellae are oriented

* To whom correspondence should be addressed.

(1) J. M. Corkill, J. F. Goodman, and J. Wyer, *Trans. Faraday Soc.*, **65**, 9 (1969).

(2) S. A. Penkett, A. G. Flook, and D. Chapman, *Chem. Phys. Lipids*, **2**, 273 (1968).

(3) J. R. Hansen and K. D. Lawson, *Nature*, **225**, 542 (1970).

(4) S. Friberg and L. Mandell, *J. Pharm. Sci.*, **59**, 1001 (1970).

(5) S. Friberg, private communication.

(6) P. Ekwall, L. Mandell, and K. Fontell, *Mol. Cryst. Liquid Cryst.*, **8**, 157 (1969).

(7) Å. Johansson and T. Drakenberg, to be published.

(8) K. D. Lawson, and T. J. Flautt, *J. Phys. Chem.*, **72**, 2066 (1968).

(9) P. J. Black, K. D. Lawson, and T. J. Flautt, *Mol. Cryst. Liquid Cryst.*, **7**, 201 (1969).

(10) B. Ellis, A. S. C. Lawrence, M. P. McDonald, and W. E. Peel, "Liquid Crystals and Ordered Fluids," J. F. Johnson and R. S. Porter, Ed., Plenum Press, New York, N. Y., 1970.

(11) J. Charvolin and P. Rigny, *J. Phys. (Paris) Colloq.*, **30**, C4-76 (1969).

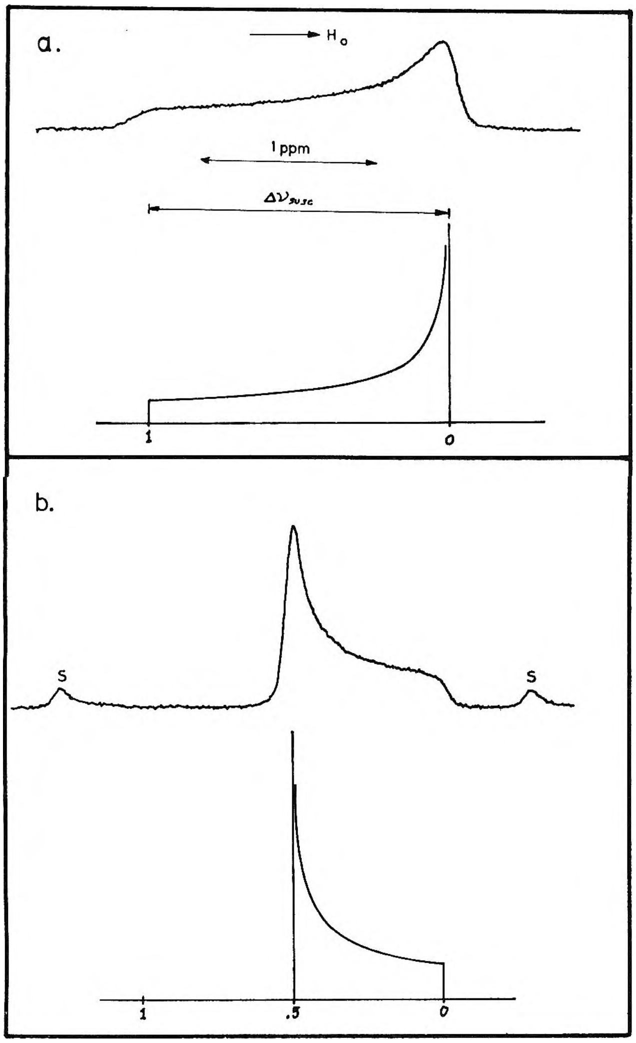

Figure 1. Experimental and theoretical line shapes of the water proton resonance in a randomly ordered lamellar mesophase (OA–OAHCl–H_2O, molar ratio 0.115:0.115:0.770): (a) nonspinning; (b) spinning (s denotes spinning side bands at twice the spinning frequency).

parallel to the external magnetic field, the magnitude of the magnetic field in the water layers is primarily determined by the magnetic susceptibility of water. When, on the other hand, lamallae are oriented perpendicular to the external magnetic field the magnitude of the magnetic field in the water layers will be determined by some kind of average between the susceptibilities of water and amphiphile. Preliminary experiments indicate that both macroscopic and microscopic effects are involved.

The following deduction of the resonance line shape of water protons is based on the assumption that the magnetic field, B, felt by the water protons depends on the angle θ, and is equal to $B_{\parallel}$ and $B_{\perp}$ at $\theta = 90$ and 0°, respectively (see Figure 2). This angular dependence will arise from any of the effects discussed above.

Let us first consider a nonspinning sample. In this case the time-independent value of B will be given by

$$B^2 = B_{\parallel}^2 \sin^2 \theta + B_{\perp}^2 \cos^2 \theta = B_{\parallel}^2 + (B_{\perp}^2 - B_{\parallel}^2) \cos^2 \theta \quad (1)$$

which leads to

$$\cos^2 \theta = (B^2 - B_{\parallel}^2)/(B_{\perp}^2 - B_{\parallel}^2) \quad (2)$$

Let $g(B)$ be the shape function for B, *i.e.*, the function corresponding to the observed line shape. Generally

$$g(B) = P(\theta)\left|\frac{d\theta}{dB}\right| \quad (3)$$

Here $P(\theta)d\theta$ denotes the probability that θ has a value between θ and $\theta + d\theta$. From Figure 3a it follows that $P(\theta)d\theta = \sin \theta d\theta$, which gives

$$g(B) = B/\sqrt{(B_{\perp}^2 - B_{\parallel}^2)(B^2 - B_{\parallel}^2)} \quad (4)$$

Let x be a normalized field variable defined as

$$x = \frac{B - B_{\parallel}}{B_{\perp} - B_{\parallel}} \quad (5)$$

and set $B_{\perp}/B_{\parallel}$ equal to a. Substitution into eq 4 then gives

$$g(x) = \frac{x(a-1)+1}{a+1}\sqrt{\frac{a+1}{x^2(a-1)+2x}} \quad (6)$$

The difference between $B_{\perp}$ and $B_{\parallel}$ is in the range of parts per million, and we can therefore make the approximation $a \simeq 1$, leading to the normalized shape function

$$g(x) = \frac{1}{2\sqrt{x}} \qquad 0 \leq x \leq 1 \quad (7)$$

This function is exhibited in Figure 1a.

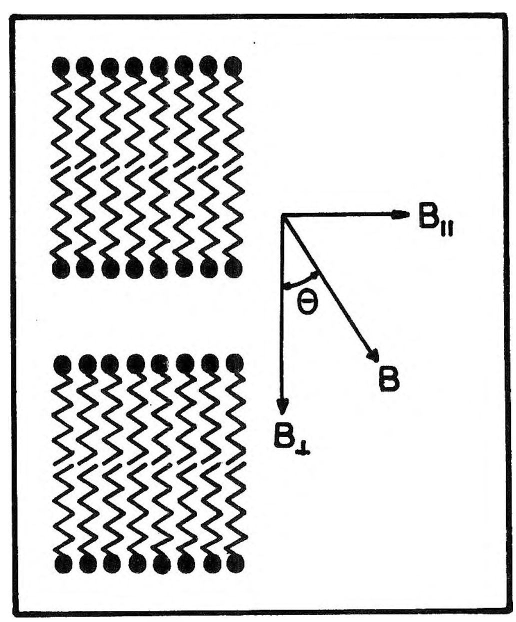

Figure 2. A schematic picture of the lamellae and the directions of $B_{\parallel}$ and $B_{\perp}$.

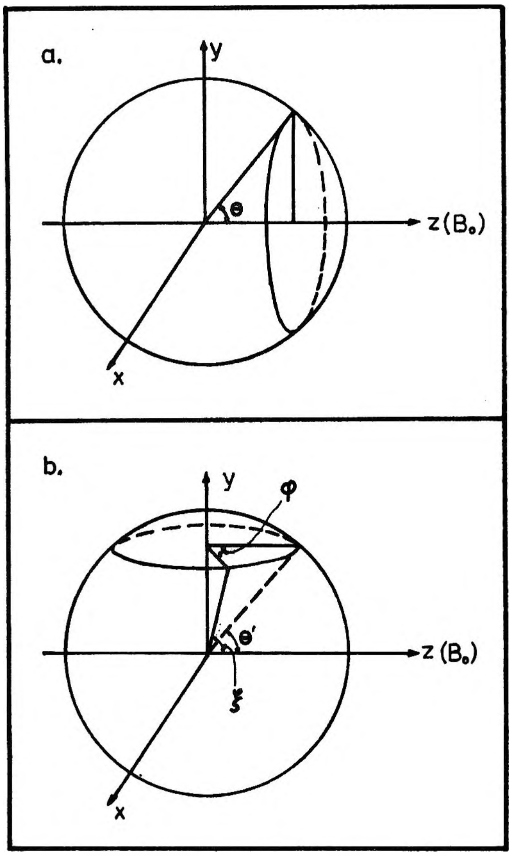

Figure 3. Coordinates used to define the optical axis directions of the lamellae: (a) nonspinning sample; (b) spinning sample.

In the case of a spinning sample B will in general be modulated with a frequency equal to twice the spinning frequency, which at low spinning rates will give rise to large side bands (Figures 1 and 4). However, in the following deduction the spinning rate about the y axis is assumed to be sufficient to average out the susceptibility variations in the xz plane (Figure 3b). The water protons will consequently feel the time average of B, denoted by $\langle B \rangle$. The instantaneous angle between the field and the direction perpendicular to the lamellar plane is denoted by ξ, and the angle of spinning measured from the yz plane is called ϕ. From Figure 3b the following expressions are easily obtained

$$\cos \xi = \cos \theta' \cos \phi \tag{8}$$

and

$$P(\theta') = \cos \theta' \qquad 0 \leq \theta' \leq 90° \tag{9}$$

The mean value of B^2 when spinning the sample is given by

$$\langle B^2 \rangle = \frac{1}{2\pi} \int_0^{2\pi} [B_{\parallel}^2 + (B_{\perp}^2 - B_{\parallel}^2) \times \cos^2 \theta' \cos^2 \phi] d\phi = B_{\parallel}^2 + {}^1/_2(B_{\perp}^2 - B_{\parallel}^2) \cos^2 \theta' \equiv B'^2 \tag{10}$$

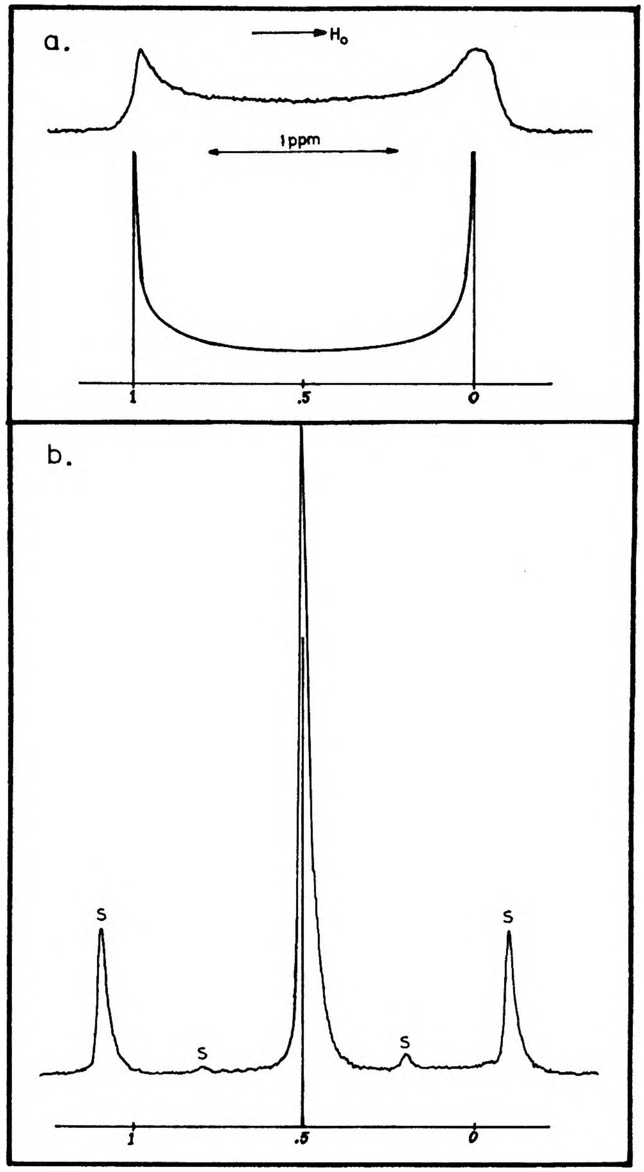

Figure 4. Experimental and theoretical line shapes of the water proton resonance in a cylindrically ordered lamellar mesophase (the same composition as in Figure 1): (a) nonspinning; (b) spinning (side bands corresponding to the spinning frequency and twice the spinning frequency are denoted by s).

or

$$\cos^2 \theta' = 2(B'^2 - B_{\parallel}^2)/(B_{\perp}^2 - B_{\parallel}^2) \tag{11}$$

As in the nonspinning case we get

$$g'(B') = P(\theta')\left|\frac{d\theta'}{dB'}\right| \tag{12}$$

Consequently, from eq 9, 11, and 12

$$g'(B') = 2B'/[(B_{\perp}^2 - B_{\parallel}^2)\sin \theta'] \tag{13}$$

Combination of eq 11 and 13 then gives

$$g'(x) = 2\left(\frac{x(a-1)+1}{\sqrt{(a+1)(\sqrt{a+1-2x^2(a-1)-4x})}}\right) \quad (14)$$

where the definition of x in eq 5 is modified, using B' instead of B. For $a = 1$

$$g'(x) = \frac{1}{\sqrt{1-2x}} \qquad 0 \leq x \leq {}^1/_2 \qquad (15)$$

A graph of $g'(x)$ is given in Figure 1b.

As can be seen from Figures 1a and b the agreement between experimental and calculated line shapes is very good for both the spinning and nonspinning cases. In both cases $x = 0$ corresponds to $\theta = 90°$, which means that the magnetic field is parallel to the lamellae. The total width of the signal, denoted by $\Delta\nu_{susc}$ in Figure 1, is equivalent to the difference in resonance frequency for the water protons corresponding to $B_{\parallel} - B_{\perp}$. Similar spectra have been observed at other lamellar phase compositions in the H_2O–OA–OAHCl system as well as in the H_2O–OA–n-octanoic acid system.

The theoretical line shapes given above are based upon the existence of a spherical distribution of lamellar directions in the sample, *i.e.*, a liquid crystalline "powder." Since some lamellar lyotropic phases tend to orient close to glass walls, a cylindrical sample geometry may in some cases give rise to nonspherical distribution of lamellar directions resulting in a modified line shape. This type of orientation has been found by Corkill, *et al.*,[1] in glass capillaries. In the case of a cylindrical arrangement of lamellae, the cylindrical axis coinciding with the spinning axis, the line shapes can easily be deduced according to the method given above. The shape functions will in this case have the forms

$$g(x) = \frac{1}{\pi}\frac{1}{\sqrt{x(1-x)}} \qquad 0 \leq x \leq 1 \qquad \text{(nonspinning)} \quad (16)$$

$$g(x) = \delta(x - {}^1/_2) \qquad \text{(spinning)} \quad (17)$$

These functions are pictured in Figures 4a and b. The latter function corresponds to a narrow resonance line centered at $x = {}^1/_2$. The experimental curves were obtained from a sample of OA–OAHCl–H_2O in a 5-mm nmr tube. The lamellar phase was allowed to form by a very slow temperature decrease of an isotropic solution.

When a line-broadening function is superimposed on the theoretical line shapes the absorption maximum in Figure 1b will be shifted toward lower x values, while the absorption maximum in Figure 4b will be unshifted. This may account for the shift observed by Corkill, *et al.*,[1] between the water proton resonance lines in randomly and cylindrically oriented samples. However, the reproduced experimental line shapes are not entirely consistent with the theoretical shape functions.

If the sample is in part spherically and in part cylindrically oriented, the observed spectrum will be a superposition of the corresponding patterns in Figures 1 and 4. The most obvious influence of a partially cylindrical orientation on the line shape will be seen in the nonspinning sample.

Acknowledgments. The authors are most grateful to Professor Peter Diehl for his comments on the manuscript and to Dr. R. E. Carter for valuable linguistic criticism.

Absolute Signs of Four-, Five-, and Six-Bond Proton–Proton Coupling Constants in Two Anhydrides

by D. J. Sardella* and G. Vogel

Department of Chemistry, Boston College, Chestnut Hill, Massachusetts 02167 *(Received June 4, 1970)*

The absolute signs of a number of four-, five-, and six-bond HH coupling constants in the spectra of two anhydrides, determined by a combination of selective spin-decoupling and spin-tickling experiments, are in excellent agreement with theoretical predictions. This, together with the generally good agreement between calculated and experimental magnitudes, leads to the conclusions that (1) σ–π interaction is the predominant mode of spin information transfer, and (2) the presence of the anhydride moiety does not produce any marked changes in most of the couplings. The absence of one five-bond coupling in anhydride **2** is problematical.

Introduction

Because of their small size, long-range proton–proton coupling constants may be of either sign. Meaningful comparisons of experimental and theoretically evaluated coupling constants, therefore, hinge upon a knowledge of the signs of the coupling constants as well as their magnitudes. In spite of this fact, the vast majority of long-range couplings tabulated in the recent literature[1a,b] are of unknown sign, pointing up the need for determinations of the signs of long-range coupling constants in systems of fixed, known stereochemistry, to allow comparison with theoretical predictions.

In connection with our interest in the mechanisms of long-range HH couplings,[2] we undertook a study of the nuclear magnetic resonance (nmr) spectra of anhydrides **1** and **2**. These systems of fixed stereochemistry display a wealth of four-, five-, and six-

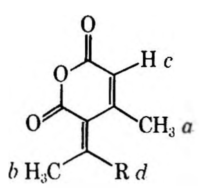

1, R = CN
2, R = H

bond HH couplings whose signs have been determined and compared with values calculated recently by Barfield[1b,3] under the assumption of a σ–π interaction mechanism. In addition, we hoped to assess the possible importance of alternate coupling pathways and to make some preliminary observations on the effect of substituents on long-range coupling constants.

Appearance of the Spectra

Anhydride **1**, in chloroform-*d* solution, exhibits a spectrum in which extensive overlapping of the methyl resonances renders interpretation and sign determination difficult. However, in benzene the spectrum is a first-order one, consisting of three well-separated resonances which indicate clearly the mutual coupling of all three proton groups. Table I summarizes the spectrum in benzene solution. The data are, however, insufficient by themselves to fix the stereochemistry about the exocyclic double bond. This matter is discussed in a later section of this paper.

Table I: The Spectrum of Anhydride **1** in Benzene Solution

Chemical shift, δ	Multiplicity	Assignment
1.77	Doublet of quartets	CH_3(a)
1.95	Presumably eight lines, six of which are visible	CH_3(b)
5.15	Multiplet	H(c)

Anhydride **2**, in chloroform-*d* solution, gives rise to a spectrum consisting of four well-separated reso-

Table II: The Spectrum of Anhydride **2** in Chloroform-*d* Solution

Chemical shift, δ	Multiplicity	Assignment
2.17	Doublet of quartets	CH_3(a)
2.47	Doublet of doublets of quartets	CH_3(b)
5.98	Multiplet	H(c)
7.23	Quartet of doublets	H(d)

* To whom correspondence should be addressed.

(1) (a) S. Sternhell, *Rev. Pure Appl. Chem.*, **14**, 15 (1964); (b) M. Barfield and B. Chakrabarti, *Chem. Rev.*, **69**, 767 (1969).

(2) (a) For our previous studies in this area, see D. J. Sardella, *Chem. Commun.*, 1613 (1968); (b) see also D. J. Sardella, *J. Mol. Spectrosc.*, **31**, 70 (1969).

(3) M. Barfield, *J. Chem. Phys.*, **42**, 4458, 4463 (1968).

nances whose assignments are summarized in Table II. The spectrum indicates the existence of five of the six possible couplings in this molecule, but leaves unspecified the configuration about the exocyclic double bond. The coupling of CH_3(b) to all other proton groups in the molecule is shown in parts a and b of Figure 1. The ring proton H(c) gives rise to a complex multiplet which, on irradiation of CH_3(a), collapses to a doublet of quartets. Finally the spectrum of CH_3(a) (Figure 2) clearly shows it to be coupled only to H(c) and CH_3(b), but not to H(d).

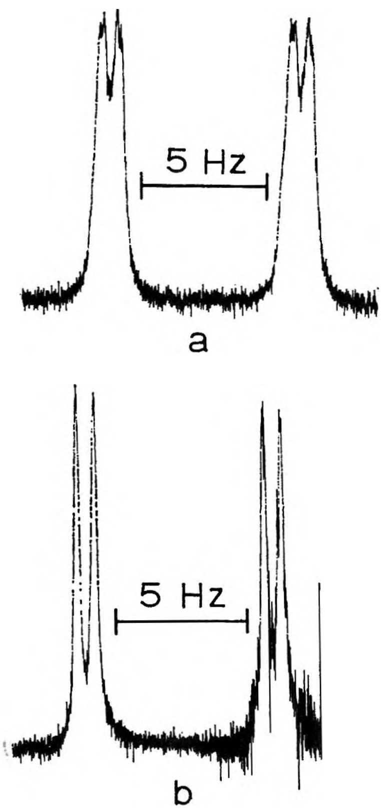

Figure 1. The spectrum of methyl group b in anhydride 2: (a) undecoupled spectrum, showing coupling of CH_3(b) to all other proton groups; (b) spectrum with CH_3(a) decoupled.

Configurations of the Anhydrides

The spectrum of anhydride **2** did not permit a choice between the two possibilities **2a** and **2b**. However,

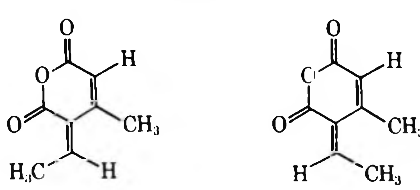

2a **2b**

we formulated the isomer as **2a** on the basis of an intramolecular nuclear Overhauser effect (NOE) experiment[4] in which irradiation of CH_3(a) produced a 12% intensity enhancement of the resonance of H(d),

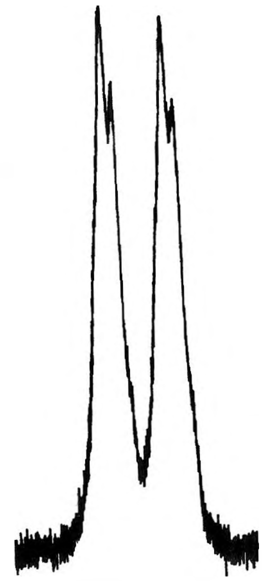

Figure 2. The spectrum of CH_3(a), showing it to be coupled to CH_3(b) and H(c), but not to H(d).

relative to irradiation at an irrelevant frequency under the same conditions.

The stereochemistry of anhydride **1** was deduced from chemical shift data in the following way. The two possible configurations are **1a** and **1b**. Assuming

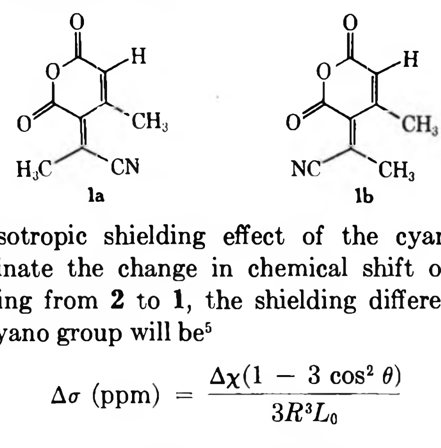

1a **1b**

the anisotropic shielding effect of the cyano group to dominate the change in chemical shift of CH_3(a) on passing from **2** to **1**, the shielding differential due to the cyano group will be[5]

$$\Delta\sigma \text{ (ppm)} = \frac{\Delta\chi(1 - 3\cos^2\theta)}{3R^3L_0} \qquad (1)$$

where $\Delta\chi$ = the diamagnetic anisotropy of the cyano group; L_0 = Avogadro's number; R = the distance (cm) between the midpoint of the CN bond and the affected proton; and θ is defined by

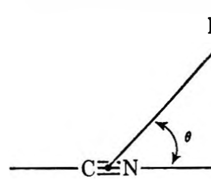

(4) F. A. L. Anet and A. J. R. Bourn, *J. Amer. Chem. Soc.*, **87**, 5250 (1965).

(5) G. S. Reddy and J. H. Goldstein, *J. Chem. Phys.*, **39**, 3509 (1963). A referee has pointed out that $\Delta\chi$ will not be independent of environment in conjugated systems, so may well differ in **1a** and **1b**. While this will undoubtedly make our calculated values of $\Delta\sigma$ *quantitatively* incorrect, the *qualitative* validity of our arguments should not change and should still suffice to define the configuration of **1**.

Inspection of Dreiding molecular models indicated the most likely conformation of CH_3(a) in **1** to be

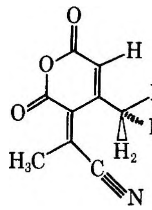

and the effect of the cyano group on the methyl proton shieldings is calculated to be $\Delta\sigma_1 = -0.196$ ppm, $\Delta\sigma_2 = \Delta\sigma_3 = -0.858$ ppm, or allowing for rotational averaging, $\overline{\Delta\sigma} = -0.64$ ppm. Taking anhydride **2** as a model compound and assuming the effects of CH and CC bond anisotropies to be comparable, we expect CH_3(a) in **1** to resonate 0.64 ppm to low field of CH_3(a) in **2**. In chloroform-*d* solution, the experimental shift difference is -0.45 ppm. By contrast, configuration **1b** would require CH_3(a) to resonate *upfield* of CH_3(a) in **2**, since $\theta \sim 180°$ for all three protons.

Signs of the Coupling Constants

The spectrum of anhydride **1** in benzene is a first-order one, enabling the relative signs of the three coupling constants to be determined by double irradiation experiments[6] like those described below for anhydride **2**. They were found to be of like sign. Since allylic couplings involving freely rotating methyl groups are invariably negative,[1] this implies $^6J_{ab}$ and $^6J_{bc}$ to be negative. The results are summarized in Table III and compared to the values calculated by Barfield[1b,3] for the corresponding couplings in hydrocarbon fragments.

Table III: Long-Range HH Couplings in Anhydride 1

Coupling	No. of bonds (n)	$^nJ_{HH}$ Experimental	$^nJ_{HH}$ Theoretical[b]
ab	6	−0.32	−0.4
ac	4	(−1.39)[a]	−1.7
bc	6	−0.77	−0.7

[a] Assumed to be negative (*cf.* ref 1b and Table IV). [b] References 1b and 3.

The absolute signs of the four long-range couplings in anhydride **2** were determined by relating them to $^3J_{bd}$ (assumed to be positive[7]) in a series of decoupling experiments summarized in Figures 3–8. The results, tabulated in Table IV and compared with Barfield's estimates of the π contributions in hydrocarbons,[1b,3] indicate generally good agreement. In addition, the fact that the allylic coupling in this anhydride has been shown to be negative strengthens the assumption that it is negative in anhydride **1**.

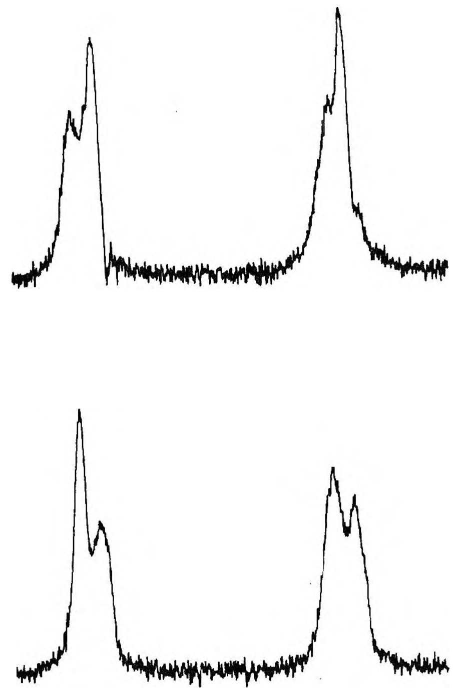

Figure 3. Double resonance spectra of CH_3(b): (a) irradiation of the high-field side of H(c) causes selective decoupling of the two high-field quartets; (b) irradiation of the low-field side of H(c) causes collapse of the low-field components.

Table IV: Long-Range HH Couplings in Anhydride 2

Coupling	No. of bonds (n)	$^nJ_{HH}$ Experimental	$^nJ_{HH}$ Theoretical[b]
ab	6	−0.20	−0.4
ac	4	−1.30	−1.7
ad	5	<0.1[a]	+0.4
bc	6	−0.66	−0.7
bd	3	(+7.60)[c]	. . .
cd	5	+0.92	+1.0

[a] Estimated from line widths. [b] References 1b and 3. [c] Assumed to be positive (*cf.* ref 7).

Discussion of Results

Inspection of Tables III and IV reveals excellent agreement between the experimentally determined signs of the long-range coupling constants in these anhydrides and the signs calculated by Barfield using his truncated matrix-sum method under the assumption of a σ–π interaction mechanism.[1b,3] In addition, there is generally good agreement between calculated and experimental magnitudes, with the exceptions of the allylic couplings in **1** and **2** and $^5J_{ad}$ in **2**. Both deviations suggest the existence of a second contribution.

(6) (a) J. D. Baldeschwieler and E. W. Randall, *Chem. Rev.*, **63**, 81 (1963); (b) R. Freeman and W. A. Anderson, *J. Chem. Phys.*, **37**, 2053 (1962).

(7) A. A. Bothner-By, *Advan. Mag. Resonance*, **1**, 195 (1965).

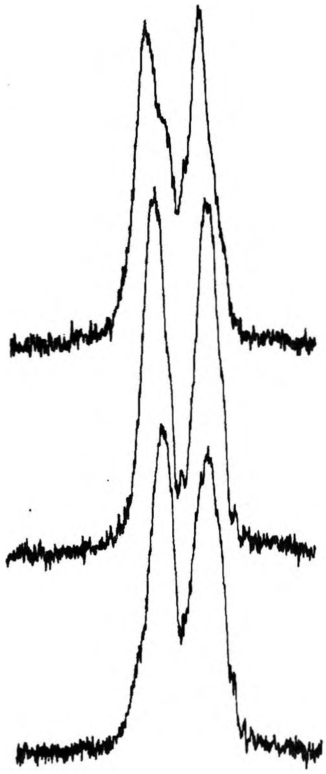

Figure 4. Double resonance spectra of CH_3(a). Center trace: normal spectrum; upper and lower traces: spin-tickling experiments in which irradiation of high- and low-field sides of H(c) caused broadening of the high- and low-field components of the quartets, respectively. These experiments and those in Figure 3 show ${}^6J_{bc}$ and ${}^4J_{ac}$ to have the same sign.

Figure 5. Center trace: single resonance spectrum of H(d); upper and lower traces: effects of irradiating low- and high-field sides of H(c), respectively, showing ${}^5J_{cd}$ to be opposite in sign from ${}^4J_{ac}$ and ${}^6J_{bc}$.

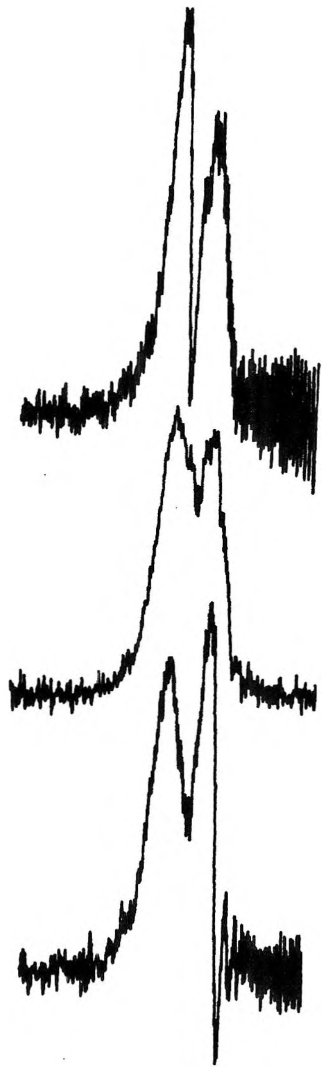

Figure 6. Observation of the low-field half of the CH_3(b) absorption. Center trace: undecoupled spectrum; upper and lower traces: selective spin decoupling experiments in which irradiation of low- (upper) and higher-field (lower) components of CH_3(a) caused collapse of the low- and high-field absorptions, respectively. Taken in conjunction with the results shown in Figure 4, this indicates ${}^6J_{ab}$ and ${}^4J_{ac}$ to be of like sign.

The deviation between calculated and experimental allylic couplings is undoubtedly due to the simultaneous occurrence of a positive σ-electron contribution. Using the empirical equation proposed by Stepanyants and Bystrov[8] to relate ${}^4J_{HH}$ to conformation, we estimate a σ contribution of +0.3 Hz for a *cis*-allylic coupling, making the theoretical estimate −1.4 Hz, in excellent agreement with experiment.

The absence of a measurable ${}^5J_{ad}$ in **2** likewise suggests at least the possibility that another coupling pathway is operating. However, this explanation seems rather unlikely in view of the fact that a recent theoretical analysis[9] led to the conclusion that the σ con-

(8) A. V. Stepanyants and V. F. Bystrov, *J. Mol. Spectrosc.*, **21**, 241 (1966).

(9) M. Barfield and M. Karplus, *J. Amer. Chem. Soc.*, **91**, 1 (1969).

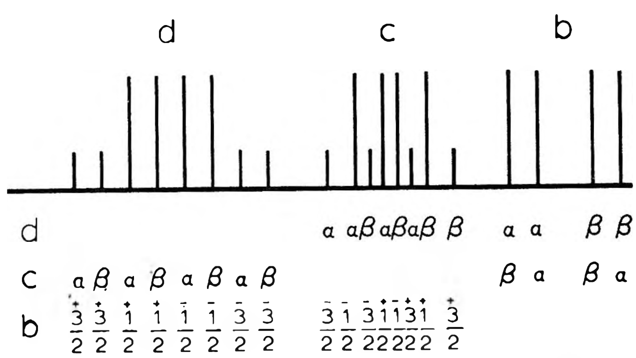

Figure 7. Spin states for the bcd subspectrum of anhydride 2, assuming $^{3}J_{bd}$ and $^{5}J_{cd}$ to be positive and $^{6}J_{bc}$ to be negative. Coupling to CH_3(a) has been neglected.

tribution to $^{5}J_{HH}$ will be positive, not negative, as our data would require.[10] Interestingly, even in the case of *cis*-1,3-pentadiene, which is alleged to exist almost solely in the *s*-trans conformation, **3**, the corresponding five-bond coupling was found[11] to be +0.21

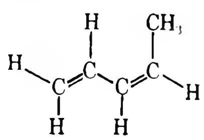

3

Hz, smaller than the predicted value of +0.4 Hz.

Table V compares our data for $^{6}J_{bc}$ and $^{5}J_{cd}$ in anhydrides **1** and **2** with the corresponding couplings in *trans*-1,3-pentadiene (**4**),[11] 5,5-dimethyl-*trans*-1,3-hexadiene (**5**),[11] *cis,trans*-1,3-hexadiene (**6**),[12] and with

Table V: Comparison of Anhydride Data with Results Reported for Butadiene Derivatives

Fragment	H_3C–butadiene–H	H–butadiene–H	Source
1	−0.77	. . .	This work
2	−0.66	+0.92	This work
4	−0.70, −0.63	+0.69, +0.65	Reference 11
	−0.74	+0.61	Reference 12
5	. . .	+0.60	Reference 11
6	−0.76	+0.76	Reference 12
$J(\pi)$	−0.7	+1.0	References 1b, 3

the estimated π contributions.[1b,3] Whereas the six-bond coupling seems relatively insensitive to substituent, the five-bond coupling exhibits a considerable variation which is consistent with the observation that, in 2-substituted butadienes, increasingly electronegative substituents increase the five-bond coupling constants.[13-15]

By contrast, the six-bond couplings in **1** and **2** behave differently. Comparison of $^{6}J_{ab}$ and $^{6}J_{bc}$ in **1** and **2** reveals an algebraic decrease in the coupling constant

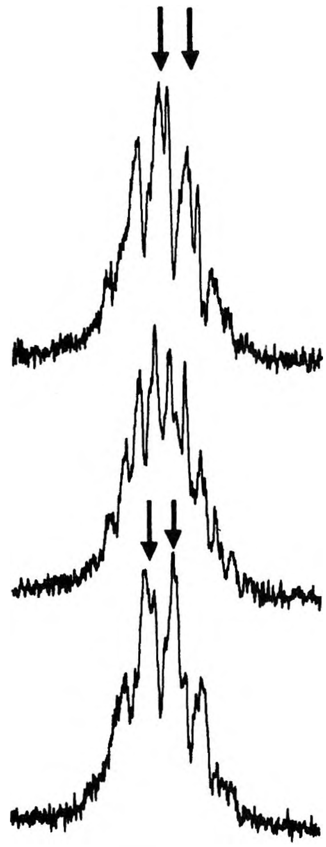

Figure 8. Part of a spin-tickling experiment which demonstrates $^{3}J_{bd}$ and $^{6}J_{cd}$ to have the same sign. Irradiation of line 3 perturbs lines 18 and 20, while irradiation of line 6 perturbs lines 17 and 19 (not shown here). Upper trace: irradiation of line 3 perturbs the higher field part of H(d) (due to perturbations of lines 12 and 15), whereas irradiation of line 6 (lower trace) perturbs the lower field portion (due to perturbation of lines 10 and 13).

as substituent electronegativity increases. If variations in the π-electron contributions are dominant, then our data imply that the effect of a given substituent on the long-range coupling constants depends not only on its electron-donating or -withdrawing power, but on its point of attachment to the butadiene moiety. This pattern of behavior is like that observed for allylic couplings in propene derivatives[1b] and four-bond couplings in other systems,[16] such as neopentane derivatives and substituted phenylacetones, suggest-

(10) Using the equations presented in ref 9 we calculate a σ contribution of +0.3 for a geometrical arrangement like that in 1c, assuming rapid rotational averaging of the methyl protons.

(11) A. L. Segre, L. Zetta, and A. DiCorato, *J. Mol. Spectrosc.*, **32**, 296 (1969).

(12) P. Albriktsen, A. V. Cunliffe, and R. K. Harris, *J. Mag. Resonance*, **2**, 150 (1970).

(13) R. T. Hobgood and J. H. Goldstein, *J. Mol. Spectrosc.*, **12**, 76 (1964).

(14) A. A. Bothner-By and D. Jung, *J. Amer. Chem. Soc.*, **90**, 2342 (1968).

(15) A. A. Bothner-By and E. Moser, *ibid.*, **90**, 2347 (1968).

(16) T. W. Proulx and D. J. Sardella, unpublished observations.

ing a connection between the nature of the substituent and the symmetries of the affected orbitals.

Experimental Section

Anhydrides **1** and **2** were prepared from α-pyrone precursors by a method to be described in detail elsewhere.[17]

Nmr spectra were recorded on a Varian Associates HA-60-IL spectrometer operating at 60 MHz in the frequency swept mode. Chemical shifts were measured directly from spectra traced on the 500-Hz scale at a sweep speed of 1.0 Hz/sec and are judged to be accurate to ±0.03 ppm. Coupling constants were read directly from spectra traced on the 50-Hz scale at sweep speeds ranging from 0.1 to 0.02 Hz/sec and are precise to ±0.03 Hz. Inaccuracies introduced by errors in chart calibration are certainly less than 2%.

Decoupling experiments were done while operating in the frequency swept mode, using either a Hewlett-Packard Model 200AB signal generator or a General Radio Model 1304B audiooscillator. Because of the small sizes of the long-range coupling constants, components of multiplets were not always well separated (*cf.* the resonance of H(c) in Figure 1c), so that it was not always possible to irradiate only one part of the multiplet. In these cases, a series of irradiations was done, beginning at the low-field side of the pattern to be irradiated and moving upfield in *ca.* 1 Hz increments until the high-field side of the multiplet was reached. Although it was not possible, under these conditions, to effect total selective spin decoupling, the patterns of skewing of affected multiplets sufficed to define the relative signs.

Acknowledgment. Partial support of this work by a National Science Foundation research grant (GP-11107) is gratefully acknowledged.

(17) G. Vogel and D. J. Sardella, to be published.

Factor Analysis of Solvent Shifts in Proton Magnetic Resonance

by Paul H. Weiner, Edmund R. Malinowski,* and Alan R. Levinstone

Department of Chemistry and Chemical Engineering, Stevens Institute of Technology, Hoboken, New Jersey 07030
(Received March 18, 1970)

Proton shifts of a series of simple substituted methanes are measured in a variety of solvents with TMS as an internal standard. A mathematical technique of factor analysis is developed and applied to the resulting data. This analysis indicates that only three factors are required to reproduce the data within experimental error. The solute shifts in three solvents (namely, acetonitrile, carbon tetrachloride, and methylene bromide) are chosen as test factors. This choice is not unique. Reasons for this choice are discussed. All solvent shifts used in the scheme can be expressed in terms of these three factors. The method is successfully extended to solutes, such as benzene and acetone, which were not included in the original analysis. It is also shown that the gas-phase shift of a solute is indeed a factor. Where the data are lacking, gas-phase shifts are predicted. Other possible factors are also considered.

Introduction

The ultimate goal in the study of solvent shifts in nmr is to account for the behavior with a minimum set of variables. Present theories unfortunately are successful only in a qualitative or semiquantitative manner. The models upon which these theories are based are questionable because of the many crude approximations involved. In the present study the goal was to develop a mathematical technique, called factor analysis,[1-7] in an attempt to decipher the number of controlling factors and to test the prevailing theories. The immediate aim was to develop a procedure for predicting the shifts of simple solutes in a large variety of solvents from a minimum of shift data.

Experimental Section

The proton spectra were recorded with a Varian A60-A spectrometer, operating at a probe temperature of

* To whom correspondence should be addressed.

(1) C. Spearman, *Amer. J. Psychol.*, **15**, 201 (1904); "The Abilities of Man: The Nature and Measurements," MacMillan, 1927; *Brit. J. Med. Psychol.*, **17**, 322 (1927); *J. Educ. Psychol.*, **28**, 629 (1937).

(2) L. S. Thurston, "Primary Mental Abilities," Chicago University Press, 1938; "Multiple Factor Analysis," Chicago University Press, 1947.

(3) E. R. Malinowski, Ph.D. Thesis, Stevens Institute of Technology, 1961; Dissertations Abstract, 23(8) Abstract 62-2027 (1963).

(4) P. T. Funke, E. R. Malinowski, D. E. Martire, and L. Z. Pollara, "Application of Factor Analysis to the Prediction of Activity Coefficients of Non-electrolytes," *Separation Sci.*, **1**, 661 (1966).

Table I: Chemical Shifts of Substituted Methane Solutes in Polar and Nonpolar Solvents, in Hz at 60 MHz, Relative to Internal TMS

	Solvents								
Solutes	CH_3CN	CH_2Cl_2	$CHCl_3$	CCl_4	CS_2	CH_2Br_2	$CHBr_3$	CH_3I	CH_2I_2
CH_4	12.1	12.1	12.7	13.8	13.3	13.8	15.2	12.9	15.1
CH_3CN	117.6	118.0	120.0	117.4	114.8	122.7	127.3	122.9[a]	128.8
CH_3Cl	181.6	181.1	180.2	178.8	176.6	182.2	184.1	180.6	185.3
CH_2Cl_2	326.9	319.8	317.4	317.1	313.9	321.2	321.8	322.5	323.5
$CHCl_3$	455.7	438.9	436.1	435.0	432.5	440.8	439.6	446.1	441.4
CH_3Br	160.4	158.8	158.7	157.2	155.8	161.3	162.9	159.6	163.7
CH_2Br_2	305.2	297.6	295.5	295.4	292.9	300.3	299.0	301.0	301.0
$CHBr_3$	425.4	412.8	410.0[a]	409.2	406.9	412.6	411.0	416.6	410.9
CH_3I	130.4[a]	129.3	129.6	128.9	128.5	132.3	133.7	131.0	135.7
CH_2I_2	238.1	233.6	232.1	232.2	232.1	234.9	234.6	235.5	235.0
CHI_3	303.3	295.8	294.5	294.7	293.1	293.9	292.5	296.0	288.2
CH_2ClBr	317.9	311.2	309.4	308.3	306.4	313.9	312.4	314.8	315.6
CH_2ClCN	256.8	248.2	246.1	244.2	242.8	252.3	253.0	255.3	257.8
$CHBrCl_2$	449.7	432.1	430.4[a]	430.0	429.0	435.4	433.0	439.6	434.9

[a] Deuterated solvent was employed.

39 ± 1°. The spectra were calibrated using a Hewlett-Packard Model 200AB wide range oscillator and a Hewlett Packard Model 523DR frequency counter. All compounds were used as obtained from commercial sources. The solutions were prepared by pipetting 1 drop of solute into approximately 1 cc of solvent, which contained a trace amount of TMS as an internal standard. It was not necessary to degas (remove O_2 from) the samples since an internal standard was used. Deuterated solvents were used when the solvent peak obscured the solute spectra. The chemical shifts obtained are shown in Table I.

Mathematical Formalism of Factor Analysis. The key steps involved in factor analysis are shown in Figure 1. First a matrix of experimental data is converted into a correlation matrix. Linear factors which reproduce the original data are obtained from the correlation matrix. These factors can be mathematically rotated into physically significant parameters, which also account for the experimental data.

Factor analysis is based upon expressing a property as a linear sum of terms, called factors. This analysis seems applicable to proton solvent shifts since almost all investigators believe that solvent shifts are a linear sum of contributions, namely, anisotropy, bulk magnetic susceptibility, van der Waals effects, reaction field, etc. In this perspective we express the proton shift S_{ik} of solute i in solvent k as a linear sum

$$S_{ik} = \sum_{j=1}^{j=r} U_{ij} V_{jk} \quad (1)$$

where U_{ij} is a solute factor and V_{jk} is a solvent factor, the sum being taken over r factors. Factor analysis is designed to tell us how many factors are involved.

In matrix form eq 1 becomes

$$[S] = [U][V] \quad (2)$$

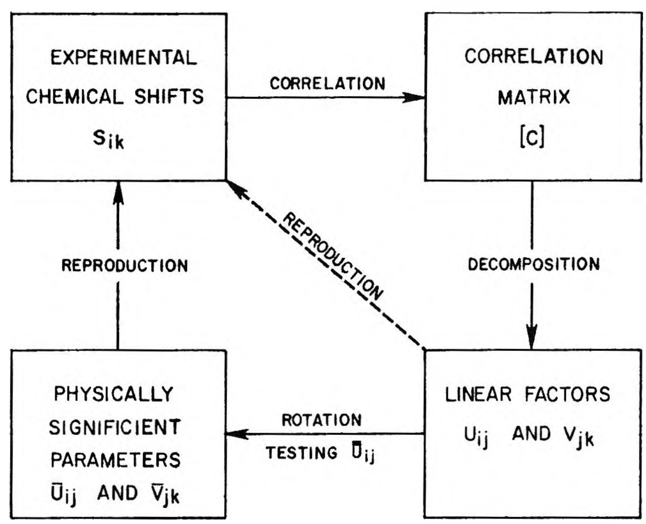

Figure 1. Key steps in factor analysis.

Both the solute–factor matrix $[U]$ and the solvent–factor matrix $[V]$ can be constructed strictly from a knowledge of the matrix of experimental values $[S]$, the shift matrix. To achieve this a square symmetric correlation matrix, $[C]$, of dimension $r \times r$, is constructed by taking the product of the shift matrix, premultiplied by its transpose

$$[C] = [S]^T[S] \quad (3)$$

Matrix $[C]$ can be diagonalized by a matrix $[B]$

$$[B]^{-1}[C][B] = [\lambda_j \delta_{jk}] \quad (4)$$

(5) R. B. Catell, "Factor Analysis," Harper and Row, New York, N. Y., 1952.

(6) K. J. Holzinger and H. H. Harman, "Factor Analysis," Univ. of Chicago Press, Chicago, Ill., 1941.

(7) D. N. Lawley and A. E. Maxwell, "Factor Analysis as a Statistical Method," Butterworths, 1963.

Here δ_{jk} is the Kronecker delta. λ_j is an eigenvalue of the set of equations

$$[C]\{B_j\} = \lambda_j\{B_j\} \quad (5)$$

where $j = 1, 2, ..., r$ and $\{B_j\}$ is the corresponding eigenvector. These eigenvectors are orthogonal and can be used as a basis set. Now

$$[B^{-1}][C][B] = [B]^{-1}[S]^T[S][B] = [B]^T[S]^T[S][B] = [U]^T[U] = [\lambda_j\delta_{jk}]$$

where

$$[U] = [S][B] \quad (6)$$

Thus the shift matrix can be expressed in terms of $[B]$ and $[S]$

$$[S] = [U][B]^T \quad (7)$$

Since eq 7 expresses the same relationship as eq 2, then

$$[B]^T = [V] \quad (8)$$

The problem, however, is to reproduce $[S]$ within experimental error using the minimum number of linearly independent eigenvectors. As a first trial we start with the eigenvector $\{B_1\}$ associated with the largest eigenvalue λ_1, and perform the following matrix multiplication

$$[S] = [U_1][B_1] \quad (9)$$

where $U_1 = \{U_{i1}\}$, a column vector, and $B_1 = \{V_{1k}\}$, a row vector. We proceed by utilizing the next largest eigenvector, and the next one, and so forth until the shift is satisfactorily reproduced. The minimum number of eigenvectors required will exactly equal the dimensionality of the factor space; *i.e.*, the number of factors involved, namely r. In other words

$$[S] = [U_1, U_2, \ldots, U_r]\begin{bmatrix} B_1 \\ B_2 \\ \cdot \\ \cdot \\ \cdot \\ B_r \end{bmatrix} \quad (10)$$

At this point the factor analysis is essentially complete. The number of factors necessary to account for the original data has been deduced. Referring to Figure 1 (see dotted line marked REPRODUCTION) the linear factors as expressed in eq 10 reproduce the experimental chemical shifts.

In their present forms the solute and solvent factors are not recognizable in terms of physical or chemical quantities. Instead they merely represent mathematic solutions to data reproduction. From the viewpoint of a chemist it is desirable to rotate the mathematical reference axes into axes which have physical significance. This procedure would provide an insight into the true fundamental factors which are operative in solvent effects. To effect such rotations we simply "guess" what these factors might be and then attempt to reproduce the data as indicated in Figure 1.

Mathematically, rotation of the axes is accomplished as

$$[\bar{U}] = [U][R] \quad (11)$$

where $[R]$ is the rotation matrix and $[\bar{U}]$ is the rotated solute–factor matrix. The inverse of the rotation matrix is used to locate the solvent–factor matrix in the new coordinate system, *i.e.*

$$[\bar{V}] = [R]^{-1}[V] \quad (12)$$

A least-squares method for obtaining the rotation matrix and for testing suspected parameters is readily deduced in the following manner. Consider a column of the rotation matrix, see eq 11. In the kth column is located the vector $(R_{1k},R_{2k},...,R_{jk})$, which when multiplied by the U_{ij} components of the ith solute gives its position, $\bar{U}_{ik}$, in the new coordinate system. The difference between the rotated solute shift $\bar{U}_{ij}$ and the actual value $\bar{\bar{U}}_{ij}$ is

$$\Delta U_{ik} = \bar{U}_{ik} - \bar{\bar{U}}_{ik} = U_{i1}R_{1k} + U_{i2}R_{2k} + \ldots + U_{ij}R_{jk} - \bar{\bar{U}}_{ik} \quad (13)$$

When this difference is minimized by standard least-squares procedures, the following equation results.

$$\{R\} = [Y]^{-1}\{X\} \quad (14)$$

where $[Y]$, $\{X\}$, and $\{R\}$ are defined as

$$\{X\} = \begin{vmatrix} \sum U_{i1}\bar{\bar{U}}_{ik} \\ \sum U_{i2}\bar{\bar{U}}_{ik} \\ \cdot \\ \cdot \\ \cdot \\ \sum U_{ij}\bar{\bar{U}}_{ik} \end{vmatrix} \quad (15)$$

$$\{R\} = \begin{vmatrix} R_{1k} \\ R_{2k} \\ \cdot \\ \cdot \\ \cdot \\ R_{jk} \end{vmatrix} \quad (16)$$

$$[Y] = \begin{vmatrix} \sum U_{i1}^2 & \sum U_{i1}U_{i2} \ldots & \sum U_{i1}U_{ij} \\ \sum U_{i1}U_{i2} & \sum U_{i2}^2 \ldots & \sum U_{i2}U_{ij} \\ \cdot & \cdot & \cdot \\ \cdot & \cdot & \cdot \\ \cdot & \cdot & \cdot \\ \sum U_{i1}U_{ij} & \sum U_{i2}U_{ij} \ldots & \sum U_{ij}^2 \end{vmatrix} \quad (17)$$

From eq 6, 15, and 17 we see that eq 14 can be rewritten as

$$\{R\} = [(1/\lambda_j)\delta_{jk}][U]^T\{\bar{\bar{U}}\} \quad (18)$$

The least-squares, vector rotator $\{R\}$, a column of $[R]$, is readily calculated from eq 18. If our suspected parameters $\{\overline{U}\}$ are true factors then $\{\overline{U}\}$ must equal $\{\overline{U}\}$ within experimental error. The elements of $\{\overline{U}\}$ are obtained from eq 11; namely

$$\{\overline{U}\} = [U]^T\{R\} \tag{19}$$

The least-squares method for rotation as developed here is completely general and is applicable even when some $\overline{U}_{ik}$ values are either unknown or purposely omitted. In this situation, of course, appropriate terms must be removed from the summations in eq 15 and 17. This procedure has a hidden advantage; it automatically yields, and thus predicts, a value of $\overline{U}_{ik}$ for those molecules whose $\overline{U}_{ik}$ values were omitted.

The final step in factor analysis is simply to regenerate the shift matrix $[S]$ using the rotated $[\overline{U}]$ and $[\overline{V}]$, *i.e.*

$$[S] = [\overline{U}][\overline{V}] \tag{20}$$

Factor Analysis of Solvent Shifts. Two criteria must be met in order to apply the technique of factor analysis to the problem of nmr solvent shifts. One is that it must be possible to separate the solvent shift into a sum of linear terms. Second, each term must be a product function of a solute and solvent factor. This places severe restrictions on the types of data which can be factor analyzed. Buckingham, Schaefer, and Schneider[8] have postulated that the solvent shift can be expressed as a linear sum of terms. The chemical shift of a solute molecule i in a solvent k is given by the following equation

$$S_{ik} = \delta_g(i) + \sigma_b(k) + \sigma_a(k) + \sigma_w(i,k) + \sigma_E(i,k) \tag{21}$$

where $\delta_g(i)$ is the gas-phase shift of solute i, $\sigma_b(k)$ is due to the bulk susceptibility of the solvent k; $\sigma_a(k)$ is the solvent shift caused by the anisotropy of the solvent k; $\sigma_w(i,k)$ is the van der Waals or dispersion interaction effect between the solute and the solvent; and $\sigma_E(i,k)$ is the reaction field interaction between the solute and solvent. The individual expressions for the various terms can be expressed as a product function of solute and solvent parameters, under special circumstances. These circumstances are discussed in a later section.

All factors need not be explicitly identified in order to use the technique of factor analysis. Factor analysis yields the minimum number of independent factors necessary to span the solvent-effect space. In many instances the exact number of factors may be somewhat indecisive due to experimental error of the data points. In such instances the cutoff is usually taken when the data are reproduced within experimental error, and the introduction of another factor does not significantly improve the fit. A group of solvents can be judiciously chosen which, separately or in conjunction, contains all of the suspected solvent effects. As an example, if hydrogen bonding effects were involved, then at least one of the solvents chosen to span the factor space must exhibit this type of interaction. The chemical shifts of solute molecules in these solvents can then be used as test factors. We could then hopefully obtain equations which would predict the shifts of the solutes in other solvents from measurements in the test solvents.

For the shift matrix, Table I was employed, purposely excluding CH_4, CH_3CN, CH_2Cl_2, CH_2ClCN, and $CHBrCl_2$ as solutes for later testing purposes. Subjecting this matrix of data to the factor analysis computer program[9] we obtained the following eigenvalues: $\lambda(1) = 9.0$; $\lambda(2) = 2.4 \times 10^{-4}$; $\lambda(3) = 5.5 \times 10^{-5}$; $\lambda(4) = 8.0 \times 10^{-6}$; $\lambda(5) = 3.0 \times 10^{-6}$; $\lambda(6) = 2.0 \times 10^{-6}$; $\lambda(7) = 8.0 \times 10^{-7}$; $\lambda(8) = 4 \times 10^{-7}$; $\lambda(9) = 9.0 \times 10^{-8}$. Each eigenvalue is a measure of the relative importance of the corresponding eigenvector. By referring to the reproduction of the shift matrix with r factors (see discussion concerning eq 9 and 10), we find that only three factors are required. With three factors the average error for data reproduction is less than ±0.5 Hz, which is well within experimental error.

At this stage, in principle, the factor analysis is complete and the original data can be reproduced with the three fundamental factors (see dotted line in Figure 1). However, it is more convenient for us to express the shifts in terms of physically significant factors. For this reason we decided to rotate the eigenvectors into three solvent vectors (acetonitrile, carbon tetrachloride, and methylene bromide). These three solvents were chosen on the expectation that they adequately span the solvent space. Acetonitrile possesses a large dipole moment and has π electrons. Methylene bromide has a large polarizability and a sizeable quadrupole moment. Carbon tetrachloride is nonpolar and contains bulky chlorine atoms.

Although there is nothing unique about this choice, one must use caution since any three solvents will not necessarily span the factor space. For example, methylene chloride, chloroform, and carbon tetrachloride jointly do not satisfactorily reproduce the data; evidently one factor is not sufficiently represented by this group.

From the rotated solvent factor matrix $[\overline{V}]$, we obtain a series of equations that predict the chemical shift of a solute in a given solvent from the measured shifts in the three chosen solvents. The resulting equations are

$$S_{i,CH_3CN} = 1.0016f_1 - 0.0038f_2 + 0.0022f_3$$

$$S_{i,CH_2Cl_2} = 0.0806f_1 + 0.7150f_2 + 0.2070f_3$$

$$S_{i,CHCl_3} = -0.0458f_1 + 0.8169f_2 + 0.2300f_3$$

$$S_{i,CCl_4} = -0.0018f_1 + 1.0041f_2 - 0.0022f_3$$

$$S_{i,CS_2} = 0.0064f_1 + 1.1281f_2 - 0.1394f_3$$

(8) A. D. Buckingham, T. Schaefer, and W. G. Schneider, *J. Chem. Phys.*, 32, 1227 (1960).

(9) A computer program and listing is available on request from the authors.

Table II: Comparison of Calculated and Experimental Chemical Shifts of Substituted Methanes[a]

	Solutes									
	CH_4		CH_3CN		CH_2ClCN		CH_2Cl_2		$CHClBr_2$	
Solvents	Exptl	Pred	Exptl	Pred	Exptl	Pred	Exptl	Pred	Exptl	Pred
CH_3CN	12.1		117.6		256.8		326.9		449.7	
CH_2Cl_2	12.1	13.7	118.0	119.4	248.2	247.5	319.8	319.5	434.5	434.0
$CHCl_3$	12.7	13.8	120.0	118.8	246.1	245.7	317.4	317.9	432.1	431.0
CCl_4	13.8		117.4		244.2		317.1		430.2	
CS_2	13.3	13.6	114.8	116.1	242.8	241.9	313.9	315.0	427.9	427.5
CH_2Br_2	13.8		122.7		252.3		321.2		435.4	
$CHBr_3$	15.2	14.3	127.3	124.6	253.0	252.3	321.8	320.9	433.0	433.3
CH_3I	12.9	12.7	122.9	119.8	255.3	254.2	322.5	322.2	439.6	440.4
CH_2I_2	15.1	13.8	128.8	128.1	257.3	258.5	323.5	321.7	434.9	434.9
Exptl range of data	3.0		14.0		15.0		13.0		21.8	
Av error		0.9		1.7		0.7		0.8		0.5

[a] These solutes were not included in the original factor analysis scheme.

Table III: Comparison of Experimental and Predicted Chemical Shifts of Various Solutes[a] Using the Solute Chemical Shifts in CH_3CN, CH_2Br_2, and CCl_4 as Solvent Factors

	Solutes													
	CH_3Cl		CH_2ClCCl_3		$CHCl_2CCl_3$		CH_3CHBr_2		$(CH_3)_2CHBr$		Acetone		Benzene	
Solvents	Exptl	Pred	Exptl	Pred	Exptl	Pred	Exptl	Pred	Exptl	Pred	Exptl	Pred	Exptl	Pred
CH_3CN	165.2		269.0		395.4		361.7		262.3		124.5		442.7	
CCl_4	163.3		255.8		363.0		347.3		252.0		125.4		435.9	
CH_2Br_2	165.8		261.8		372.7		354.0		258.7		128.8		441.2	
$CHCl_3$	163.3	164.0	257.2	256.8	366.3	364.1	350.6	348.6	257.3	253.3	129.7	126.4	441.1	437.3
CS_2	161.9	162.1	254.1	253.8	362.1	360.0	345.1	344.8	248.8	249.8	122.4	124.3	433.4	433.0
CH_3I	165.7	164.7	263.0	264.6	377.2	384.2	354.4	356.4	256.7	259.7	126.1	125.9	439.1	438.9
Exptl range of data	3.8		14.9		33.3		16.5		13.5		7.3		9.3	
Av error of predictions		0.6		0.8		4.0		1.6		2.7		1.3		1.4

[a] These solutes were not included in the original factor analysis scheme.

$$S_{i,CH_2Br_2} = -0.0010f_1 + 0.0090f_2 + 0.9922f_3$$

$$S_{i,CHBr_3} = -0.2562f_1 - 0.0527f_2 + 1.3118f_3$$

$$S_{i,CH_3I} = 0.5613f_1 - 0.2237f_2 + 0.6527f_3$$

$$S_{i,CH_2I_2} = -0.1092f_1 - 1.1972f_2 + 2.2946f_3$$

where

$$f_1 = S_{i,CH_3CN},\ f_2 = S_{i,CCl_4},\ \text{and}\ f_3 = S_{i,CH_2Br_2}$$

The equations above for acetonitrile, carbon tetrachloride, and methylene bromide, the test factors, each exhibit three finite coefficients. This is due to experimental error and computer roundoff.

The accuracy of these equations can be tested on the solutes which were purposely left out of the factor analysis scheme. The results are presented in Table II. For the simple substituted methanes, the agreement, although slightly beyond experimental error, is reasonably satisfactory.

As a test of the generality of these equations we have calculated the chemical shifts of some nonmethane solutes. These data are presented in Table III. The agreement, especially for such solutes as benzene and acetone, is quite surprising.

A Search for the Three Fundamental Factors. As described in the previous section, factor analysis shows that three factors span the solvent-effect space. These factors were rotated into three solvent vectors (acetonitrile, carbon tetrachloride, and methylene bromide). Evidently the three fundamental factors are sufficiently contained within these three solvents but have not been identified by this procedure. In principle we should be able to rotate the factors resulting from factor analysis into the true fundamental factors.

According to Buckingham–Schaefer–Schneider,[8] see eq 21, the gas-phase shift of the solute should be a fundamental factor, since these shifts represent those of the unperturbed solute molecules. In this case the solute factor $U_{ij} = \delta_i$ (gas) and the solvent factor $V_{jk} = 1$. Rotation into the gas-phase shifts was indeed successful as shown in Table IV. The agreement between the experimental values and those resulting from factor anal-

Table IV: Test of Gas-Phase Chemical Shifts as a Solute Factor Using Three Factors in the Rotation Matrix[a]

Solute	δ_g (predicted)[b]	δ_g (exptl)[c]	Difference
CH_3Cl	168.2	...	...
$CHCl_3$	427.1	427.3	−0.2
CH_3Br	147.1	146.9	0.2
CH_2Br_2	285.5	285.0	0.5
$CHBr_3$	406.8	406.9	−0.1
CH_3I	118.5	119.0	−0.5
CH_2I_2	227.6	...	...
CHI_3	301.5	...	...
CH_2ClBr	297.7	...	...

[a] In hertz at 60 MHz, relative to gaseous TMS. [b] These values correspond to $\bar{U}_i$. [c] The values correspond to $\bar{\bar{U}}_i$.

ysis is well within experimental error. One bonus gained by identifying the gas-phase shift as a solute factor is that gas-phase shifts are automatically predicted for the molecules where data are not available. The predicted values are also shown in Table IV.

The reaction field term, as developed by Buckingham, Schaefer, and Schneider,[8] under appropriate conditions, has the form

$$\sigma_R = -\chi \times 10^{-12} \frac{2}{3} \frac{(\epsilon_v - 1)(n_u^2 - 1)}{2\epsilon_v + n_u^2} \frac{\mu_u}{\alpha_u} \cos(\theta_u) \quad (22)$$

where subscripts u and v again refer to solute and solvent; μ is the permanent dipole moment; α is the polarizability; θ is the angle between μ and the CH bond of the solute proton in question; n is the index of refraction; χ is a constant for the CH bond; ϵ is the dielectric constant. Equation 22 can be factored into a solute and solvent term if an average value of n_u^2 is substituted into this relation; namely, $n_u^2 \approx 2.5$. Thus

$$\sigma_R \cong -\chi \times 10^{-12}\left[\frac{\mu_u}{\alpha_u}\cos(\theta_u)\right]_{\text{solute}} \times \left[\frac{\epsilon_v - 1}{2\epsilon_v + 2.5}\right]_{\text{solvent}} \quad (23)$$

In this form the solute factor ($\mu_u/\alpha_u \cos\theta$) can be tested by the procedure described previously. Surprisingly, rotation into this suspected fundamental factor was unsuccessful. There are several possible reasons for this failure. The total reaction field effect may be so small that it is obliterated by experimental error. Furthermore, quadrupolar effects may not be negligible, as is commonly assumed.

The van der Waals factor, σ_w, can be expressed as a product function for nonpolar solutes in nonpolar solvents.[10–12] However, for polar solutes in polar solvents, theoretical formulas have not been developed. Consequently, no formula exists for testing by factor analysis.

The anisotropy shift is a product function in which the solute factor $U_{ij} = 1$ and the solvent fact $V_{jk} = \sigma_a$ (solvent). Since the present study involves internal standards this effect cannot be one of the three fundamental factors.

Acknowledgment. The computations were carried out at the Computer Center (supported in part by a grant from the National Science Foundation) of Stevens Institute of Technology, for which we record our appreciation. Also, the authors gratefully acknowledge the support of the U. S. Army Research Office (Durham), Contract No. DA-31-124-ARO(D)-90.

(10) A. A. Bothner-By, *J. Mol. Spectrosc.*, **5**, 52 (1960).
(11) H. J. Bernstein, private communication.
(12) E. R. Malinowski and P. H. Weiner, *J. Amer. Chem. Soc.*, **92**, 4193 (1970).

Vibronic Contributions to Optical Rotation

by R. T. Klingbiel and Henry Eyring*

Institute for the Study of Rate Processes, The University of Utah, Salt Lake City, Utah 84112 (*Received June 15, 1970*)

The rotatory strength arising from vibronic interactions is calculated for the n–π^* transition in four (2,2,1)-bicycloheptanones. The valence force field vibrational normal modes and CNDO–molecular orbitals are used. Only two modes are found to borrow intensity appreciably: the 1945-cm^{-1} C=O stretch and the 1810-cm^{-1} C—C=O out-of-plane bend. Both modes contribute nearly equally but with opposite sign. Progressions in these two modes may explain the reversal of sign observed in the CD of isofenchone and epi-isofenchone.

I. Introduction

An optically active, isotropic medium rotates plane polarized light ϕ radians per unit path length[1]

$$\phi = 4\pi N/hc \sum_a \rho_a \sum_b \omega^2 R_{ba}/(\omega_{ba}^2 - \omega^2) \quad (1)$$

$$R_{ba} = Im(a|\vec{\mu}|b)(b|\vec{m}|a) \quad (2)$$

where N is the number of molecules, ρ_a is the probability of a molecule being in state a, ω is the incident frequency of the radiation, b labels a state other than state a such that the difference in energy between states a and b is $h\omega_{ba}/2\pi$. R_{ba} is the rotatory strength of a transition between states b and a. It is seen that the transition must have associated with it a nonorthogonal electric dipole moment, $\vec{\mu}$, and magnetic dipole moment, $\vec{m}$. The rotatory strength is directly measurable from the circular dichroism spectrum, $\theta_{ba}(\lambda)$

$$R_{ba} = (3hc/8\pi^3N)\int d\lambda\theta_{ba}(\lambda)/\lambda \quad (3)$$

If the summation of states in (2) is extended to include vibronic states then, within the limitations of the Born–Oppenheimer[2,3] approximation, the rotatory strength may be written[4] as

$$R_{KN} = \sum_{k,n} R_{Kk,Nn} \quad (2')$$

$$R_{Kk,Nn} = Im(Nn|\vec{\mu}|Kk)(Kk|\vec{m}|Nn) \quad (4)$$

$$(Nn|\vec{\mu}|Kk) = (N^0|\vec{\mu}|K^0)(n|k) + \sum\nolimits_r \vec{C}_r(n|Q_r|k) \quad (5)$$

$$(Kk|\vec{m}|Nn) = (K^0|\vec{m}|N^0)(k|n) + \sum\nolimits_r \vec{B}_r(k|Q_r|n) \quad (6)$$

$$\vec{C}_r = \sum\nolimits_s \lambda_{SKr}(N^0|\vec{\mu}|S^0) + \lambda_{SNr}(S^0|\vec{\mu}|K^0) \quad (7)$$

$$\vec{B}_r = \sum\nolimits_s \gamma_{SKr}(N^0|\vec{m}|S^0) + \lambda_{SNr}(S^0|\vec{m}|K^0) \quad (8)$$

The vibronically coupled components of the electric and magnetic transition dipoles, $\vec{C}_r$ and $\vec{B}_r$, are sums of zeroth-order "borrowed" transition moments. The perturbation coefficients λ_{SKr} and λ_{SNr} are calculated from first-order perturbation theory in terms of the zeroth-order wave functions. The vibronic perturbation to the electronic portion of the Hamiltonian is due to the rth vibrational normal mode, Q_r

$$\lambda_{SKr} = (S^0|H_r'|K^0)/(E_k^0 - E_s^0) \quad (9)$$

$$H'_r = \partial H/\partial Q_r \quad (10)$$

II. Calculation

In calculating the various terms in eq 5 through 10, the following approximations are applied: (1) the zeroth-order electronic wave functions are calculated by means of a CNDO scheme for the simplest molecule containing the chromophore of interest; (2) the vibrational wave functions are the solutions to the simple harmonic oscillator in the internal coordinate representation; transitions only from the ground state are considered; (3) the method of Pople and Sidman is employed to calculate H'_r; (4) a valence force field is used to calculate the vibrational normal modes. Each of these approximations will now be discussed briefly.

(*1*) *CNDO Molecular Orbitals.* The method of the complete neglect of differential overlap is well described in the literature by its originators.[5–8] We adapted the computer program obtained from the quantum chemistry program exchange[9] to our needs. The resulting coefficients for formaldehyde are given in Table I. The transition moments for a one electron operator, $\hat{O}$, were calculated from determinantal wave functions differing at most in one molecular wave function, θ_j.

$$(S^0|\hat{O}|K^0) = \pm(\theta_i|\hat{O}|\theta_1) = \sum\nolimits_\mu\sum\nolimits_\nu C_{i\mu}C_{i\nu}\int \phi_\mu\hat{O}\phi_\nu d\tau \quad (11)$$

where the $C_{k\nu}$ are the appropriate coefficients in Table I and the ϕ_μ are the Slater atomic orbitals

* To whom correspondence should be addressed.

(1) H. Eyring, J. Walter, and G. E. Kimball, "Quantum Chemistry," Wiley, New York, N. Y., 1944.

(2) M. Born and J. R. Oppenheimer, *Ann. Phys. (Leipzig)*, **84**, 457 (1927).

(3) H. C. Longuet-Higgins, *Advan. Spectrosc.*, **2**, 429 (1961).

(4) O. E. Weigang, *J. Chem. Phys.*, **43**, 3609 (1965).

(5) J. A. Pople, D. P. Santry, and G. A. Segal, *ibid.*, **43**, S129 (1965).

(6) J. A. Pople and G. A. Segal, *ibid.*, **43**, S136 (1965).

(7) J. A. Pople and G. A. Segal, *ibid.*, **44**, 3289 (1965).

(8) J. A. Pople, D. L. Beveridge, and P. A. Dobosh, *J. Amer. Chem. Soc.*, **90**, 4201 (1968).

(9) Quantum chemistry program exchange, Indiana University, Bloomington, Ind.

Table I: CNDO Calculated LCAO-MO for Formaldehyde

ϕ/θ	1 (σ_1)	2 (σ_2)	3 (σ_3)	4 (n_1)	5 (π)	6 (n_2)	7 (π^*)	8 (σ_1^*)	9 (σ_2^*)	10 (σ_3^*)
2s (O)	0.7810	0.4180		−0.2875				0.0630		−0.3586
$2p_x$ (O)			0.6030			0.7741			−0.1928	
$2p_y$ (O)	−0.1659	0.2759		−0.7601				−0.1555		0.5425
$2p_z$ (O)					0.7639		−0.6453			
2s (C)	0.4827	−0.5592		0.0160				−0.6135		0.2786
$2p_x$ (C)			0.6151			−0.2975			0.7301	
$2p_y$ (C)	0.2970	0.3480		0.5046				0.2432		0.6906
$2p_z$ (C)					0.6453		0.7639			
1s (H)	0.1438	−0.3970	0.3590	−0.2057		−0.3952		0.5178	−0.4636	0.1062
1s (H)	0.1438	−0.3970	−0.3590	−0.2057		0.3952		0.5178	0.4636	0.1062
Sym	A_1	A_1	B_1	A_1	B_2	B_1	B_2	A_1	B_1	A_1

$$\phi(2S) = (Z'^5/96\pi)^{1/2} r \exp(-Z'r/2) \quad (12)$$

$$\phi(2P_\alpha) = (Z'^5/32\pi)^{1/2} r \exp(-Z'r/2) \cos\theta_\alpha \quad (13)$$

and $Z' = 3.9, 5.2$ for carbon and oxygen, respectively; $\cos\theta_\alpha$ is the direction cosine to the α axis. The angular momentum operator, $\vec{L}$, and radial vector, $\vec{r}$, are both defined with respect to the molecular origin. Hence for the ith electron localized on the σth nuclei

$$\vec{r}_i = \vec{r}_{\sigma i} + \vec{r}_\sigma \quad (14)$$

$$\vec{L}_i = (\vec{r}_{\sigma i} + \vec{r}_\sigma) \times \vec{p}_i = \vec{L}_\sigma + \vec{r}_\sigma + \vec{p}_{\sigma i} \quad (15)$$

therefore, eq 11, 14, and 15 become

$$(S^0|\vec{m}|K^0) = \sum_\sigma\sum_\mu\sum_\nu \times C_{s\mu}C_{k\nu}(\int\phi_\mu L_\sigma\phi_\nu \mathrm{d}\tau + \vec{r}_\sigma x\int\phi_\mu P\phi_\nu \mathrm{d}\tau)\mu_B \quad (16)$$

$$((S^0|\vec{\mu}|K^0) = \sum_\sigma\sum_\mu\sum_\nu \times C_{s\mu}C_{k\nu}(\int\phi_\mu\vec{r}_{\sigma i}\phi_\nu \mathrm{d}\tau + \int\phi_\mu\vec{r}_\sigma\phi_\nu\, \mathrm{d}\tau)e \quad (17)$$

The integral $\int\phi_\mu\vec{r}_\sigma\phi_\nu \mathrm{d}t$ is the transition density and should be significant only for π–π^* transitions, in which case it is equal to unity. A few calculated transition moments and their observed values are given in Tables II and III.

Table II: Calculated Transition Properties

Transition	Sym	Polar-ization	Energy, eV	Electric moment, D	Magnetic moment, μ_B
$n_2 \rightarrow \pi^*$	A_2	R_y	18.7	0	0.7936
$n_2 \rightarrow \sigma_1^*$	B_1	T_x,R_z	29.2	0.3755	0.6282
$\pi \rightarrow \pi^*$	A_1	T_y	35.0	0.335	0

Table III: Transition Properties of Formaldehyde

Transition	Energy, eV	mμ	Oscillator strength
$n_2 \rightarrow \pi^*$	3.50	230–353	2.4×10^{-3}
$n_2 \rightarrow \sigma^*$	7.09	165–175	0.04
$\pi \rightarrow \pi^*$	8.0	156	0.1–0.5
Rydberg	10–13		Strong

(2) Vibrational Wave Functions. We assume, for simplicity, the vibrational potential energy to be represented by the same harmonic function except for a displacement of the excited state to a larger equilibrium value of the internal coordinate, Q^0. Physically, this assumes the molecule retains its symmetry and force constants in the excited state, but increases its energy and internuclear distances. The assumption of conserved symmetry is consistent with the Franck–Condon principle which states that the nuclei are essentially stationary during the brief interval required for the electronic transition. After the transition, the nuclei and electrons relax into a new equilibrium configuration of minimum energy; this relaxation does not affect the transition probability or polarization, however. The remaining assumptions greatly simplify[10–14] the mathematical evaluation of the vibrational overlap and transition integrals $(n|k)$ and $(n|Q_r|k)$, respectively. The displacement of the excited state is expressed by

$$Q_k^0 - Q_N^0 = \lambda/\sqrt{\beta} \quad (18)$$

where β is the mean square deviation of the normal mode in question. Writing

$$|n) = (\sqrt{\beta_N/\pi}/2^n n!)H_n(\sqrt{\beta_N}Q_N)\exp(-\beta_N Q_N{}^2/2) \quad (19)$$

and similarly for $|k)$, then[15] with $\beta_N = \beta_k = \beta$

$$(n|k) = \exp(-\lambda^2/4)(-\lambda/\sqrt{2})^{n-k} \times (k!/n!)^{1/2} L_n^{n-k}(\lambda^2/2) \qquad n \geqslant k \quad (20)$$

$$(n|k) = \exp(-\lambda^2/4)(\lambda/\sqrt{2})^{k-n} \times (n!/k!)^{1/2} L_n^{k-n}(\lambda^2/2) \qquad k \geqslant n \quad (21)$$

$$L_n^\alpha(x) = (x^{-\alpha}/n!)e^x(d^n/dx^n)(x^{n+\alpha}e^{-x}) \quad (22)$$

(10) M. Gouterman, *et al.*, *J. Chem. Phys.*, **35**, 1059 (1961).
(11) M. Gouterman, *et al.*, *ibid.*, **41**, 2280 (1964).
(12) M. Gouterman, *et al.*, *ibid.*, **42**, 351 (1965).
(13) M. Gouterman, *et al.*, *ibid.*, **46**, 1019, 2257 (1967).
(14) M. Gouterman, *et al.*, *ibid.*, **50**, 4137 (1969).
(15) S. Koide, *Z. Naturforsch*, **15a**, 123 (1960). See comments in ref 10 for sign correction and normalization convention.

We shall ignore "hot bands" and, therefore, set $n = 0$,

$$(0|k) = \exp(-\lambda^2/4)(\lambda^{2k}/Z^k k!)^{1/2} \quad (23)$$

Consequently

$$(0|Q|k) = \sum_m (0|m)(m|Q|k)$$

where $|m)$ are a complete set of vibrational states in the excited state. Using (23) and

$$(m|Q|k) = \delta_{m,k\pm1}(n_>/2\beta)^{1/2} \quad (24)$$

where $n_>$ = the greater of m or k

$$(0|Q|k) = \exp(-\lambda^2/4)\{(\lambda^{2(k-1)}/2^{k-1}(k-1)!)^{1/2} \times (k/2\beta)^{1/2} + (\lambda^{2(k+1)}/2^{k+1}(k+1)!)^{1/2}(k+1/2\beta)^{1/2}\} \quad (25)$$

The displacement parameter λ may be estimated from the value of k for which (25) is maximum. Let $\xi = (\lambda^2/2^k k!)^{1/2}$, then ξ will be maximum for the value of k which also maximizes log ξ. Using Sterling's approximation

$$\mathrm{d} \log \xi/\mathrm{d}\xi = 0 = \log(\lambda^2/2k)$$

therefore

$$k_{\max} \equiv \Delta = \lambda^2/2$$

Equations 23 and 25 are conveniently expressed in terms of this new parameter, Δ

$$(0|k) = \exp(-\Delta^2)\{\Delta^k/k!\}^{1/2} \quad (23')$$

$$(0|Q_r|k) = \exp(-\Delta^2)\{(\Delta^{k-1}/(k-1)!)^{1/2} \times (k/2\beta)^{1/2} + (\Delta^{k+1}/(k+1)!)^{1/2}(k+1/2\beta)^{1/2}\} \quad (25')$$

$$1/\beta = (0|Q_r{}^2|0) = h/4\pi\omega_r \quad (26)$$

(3) *The Vibronic Perturbation.* Pople, Murrel, and Sidman[16,17] have represented the vibronic perturbation, (10), as

$$H'_r = \sum_i \sum_\sigma Z_\sigma e^2 \frac{\partial \vec{r}_\sigma}{\partial Q_r} \cdot \frac{\vec{r}_{i\sigma}}{r|_{i\sigma}|^3} \quad (10')$$

which may be visualized as a dipole-dipole interaction between the electric dipole moment of the ith electron on the σth nuclei with the "vibrational dipole" from the displacement of the σth nuclei (with charge Z_σ) from its equilibrium position due to the rth normal mode. The vibrational dipole moment may be determined from a normal mode calculation. Therefore

$$\lambda_{SKr} = \left(\sum\sum Z_\sigma e^2 \frac{(S^0|\vec{\mu}|K^0)}{|r_{i\sigma}|^3} \cdot \frac{\partial \vec{r}_\sigma}{\partial Q_r}\right) \Big/ (E_k{}^0 - E_s{}^0) \quad (9')$$

where $(S^0|\vec{\mu}|K^0)$ is given by (17).

(4) *Normal Mode Calculation.* The calculation of vibrational normal modes in terms of a set of four types of internal coordinates (bond stretch, angle bend, torsional twist, and out-of-plane bend) has been carefully documented.[18] If B represents a transformation matrix between cartesian coordinates, $\vec{X}$, and internal coordinates, $\vec{S}$, then the theory of small vibrations leads to an expression for the kinetic energy, T, of a vibrating system

$$2T = \dot{\vec{S}}^\dagger G^{-1}\dot{\vec{S}} \quad (27)$$

where

$$G = BM^{-1}B^\dagger \quad (28)$$

and

$$\vec{S} = B\vec{x} \quad (29)$$

M is a diagonal matrix whose elements $M_{\sigma\sigma}$ are the mass of the σth particle. The potential energy, V, is given by the diagonal matrix F, whose elements F_{jj} are the force constants for the small displacement of the jth internal coordinate.

$$2V = \vec{S}^\dagger F\vec{S} \quad (30)$$

The vibrational normal modes, $\vec{Q}_r$, are expressible in terms of the interval coordinate by the matrix L^{-1}

$$\vec{Q}_r = L^{-1}\vec{S} \quad (31)$$

where L^{-1} is obtained from the eigenvalue equation

$$FG(L^{-1})^\dagger = (L^{-1})^\dagger\lambda \quad (32)$$

It is not difficult to show that the normal modes are connected to the Cartesian coordinates by matrix A, where

$$\vec{x} = A\vec{Q}_r = \left(\frac{\partial \vec{X}}{\partial \vec{Q}_r}\right)\vec{Q}_r \quad (33)$$

and

$$\vec{A} = M^{-1}B^\dagger(L^{-1})^\dagger \quad (34)$$

The elements of A are the required[19] partial differential coefficients appearing in eq 9′. The internal coordinates are illustrated in Figure 1 and the corresponding force constants in Table IV.

III. Bicyclo[2.2.1]heptanones

The total number of terms contributing to equation 2′ is greatly limited by group theoretical restrictions. For the n–π^* carbonyl transition considered, $|N^0) = n_2(B_1)$ and $|K)^0 = \pi^*(B_2)$. Consequently, under the C_{2v} group $n_2 \times \pi^* \equiv A_2$ which transforms as R_y, *i.e.*, the n_2–π^* transition is pure magnetic dipole allowed so that we may set $(N^0|\vec{\mu}|K^0) = 0$ to zeroth order. Furthermore for $(N^0|\vec{m}|N^0)\cdot\vec{C}_r \neq 0$, $\vec{C}_r$ must transform as T_y, that is, as A_1. From Table I the only term contributing to $\vec{C}_r$, therefore, is

(16) J. N. Murrel and J. A. Pople, *Proc. Roy. Soc. Ser. A*, 69, 245, (1956).

(17) J. A. Pople and J. W. Sidman, *J. Chem. Phys.*, 27, 1270 (1957).

(18) E. B. Wilson, J. C. Decius, and P. C. Cross, "Molecular Vibrations," McGraw-Hill, New York, N. Y., 1955.

(19) Correct normalization is essential so that $AMA = I$ (35) in order that the magnitude of $\partial\vec{x}/\partial Q_r$ be correct. This is a physical requirement of the solution to (32); normally, only *relative* magnitudes are required and (35) is not enforced.

$$\vec{C}_r = \lambda_{\pi^*\sigma_2^*r}(n_2|\vec{\mu}|\sigma_2^*) + \lambda_{\pi n_2 r}(\pi|\vec{\mu}|\pi^*) \quad (36)$$

$$\lambda_{\pi^*\sigma_2 r} \propto (\sigma_2^*|\vec{\mu}|\pi^*) \approx 0 \quad (37)$$

$$\lambda_{\pi\sigma_2 r} \propto (n_2|\vec{\mu}|\pi) \approx 0 \quad (38)$$

where both λ coefficients are found to be zero from the CNDO coefficients in Table I and eq 17. Similar considerations restrict the only nonvanishing terms involving $\vec{C}_r \cdot \vec{B}_r$. These are given in Table V, and (2′) has been simplified to the sum of three terms, each a sum over all normal modes.

Table IV: Force Constants

Internal coordinate	Units	Force constant	Value[a]
Bond stretch	mdyne/Å	K_r	4.699
		K_d	4.554
		K_s	4.588
		K_R	4.387
		$K_{R'}$	4.337
		$K_{R''}$	4.534
		K_{co}	12.1[b]
		K_{cc}	7.0[c]
Angle bend	mdyne Å/(rad)²	H_α	0.540
		H_β	0.645
		H_δ	0.550
		H_γ	0.656
		H_ζ	0.657
		H_ω	1.130
		H_ϕ	1.084
		H_λ	1.086
		H_c	3.6[b]
		H_d	0.72[b]
Torsional bend	mdyne Å/(rad)²	T_r	0.024[e]
		T_π	0.720[d]
Out-of-plane-bend	mdyne Å/(rad)²	F_{co}	0.550[d]

[a] From R. G. Snyder and J. H. Schachtschneider, *Spectrochim. Acta*, **21**, 169 (1965), unless otherwise stated. [b] G. Herzberg, "Infrared and Raman Spectra of Polyatomic Molecules," D. Van Nostrand Co., Inc., New York, N. Y., 1955, p 193. [c] Average of C—C and C=C of ethylene (see *b*). [d] Assumed same as ethylene (see *b*). [e] From torsional frequency of ethane (280 cm⁻¹).

Table V: Configurations Contributing to $\vec{C}_r \cdot \vec{B}_r$

Polarization	$\vec{C}_r$	(Calcd) × 10¹⁸	$\vec{B}_r$	(Calcd) × 10²⁰
X	$n_2 \rightarrow \sigma_1^*$	0.375	$n_1 \rightarrow \pi^*$	0.870
X	$n_2 \rightarrow \sigma_2^*$	3.35	$n_1 \rightarrow \pi^*$	0.870
Z	$n_1 \rightarrow \pi^*$	0.248	$n_2 \rightarrow \sigma_1^*$	0.628
Z	$n_1 \rightarrow \pi^*$	0.248	$n_2 \rightarrow \sigma_2^*$	0.0

The vibrational analysis of the bicyclo[2.2.1]heptanones are all quite similar and the complete vibrational analysis is given only for (+)-camphor in Table VI. Only two of the vibrational normal modes in the 3–16-μ region dominate the $\vec{C}_r \cdot \vec{B}_r$ term. They are the C=O stretch, ν_{17}, and the planar C—C=O bend, ν_{18}. All other normal modes are at least one and, more generally, two to three orders of magnitude smaller. Beyond 16 μ additional modes begin to contribute; however, their large contribution arises from their large root mean square displacement as expressed by eq 26, and it is questionable whether these large displacements are physically existent or for that matter even consistent with the approximation of small vibrations. We therefore have ignored any contributions from these low-frequency terms (below 600 cm⁻¹).

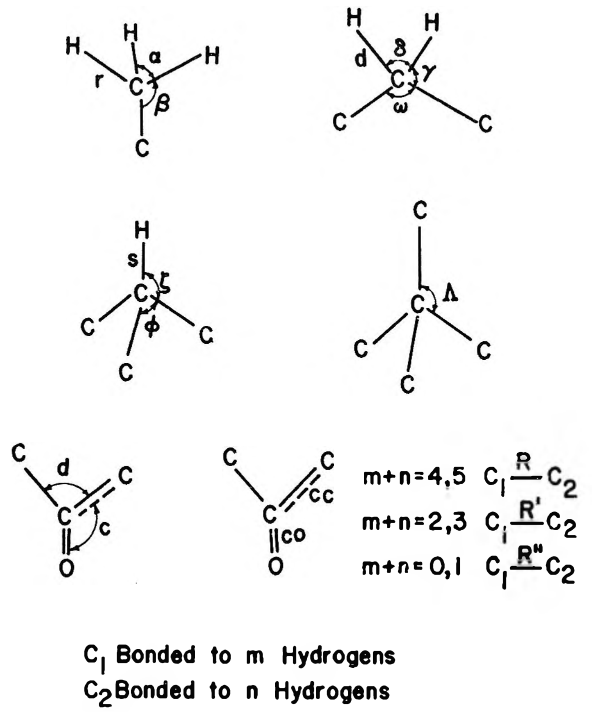

Figure 1. Internal coordinates.

We are particularly interested in the unusually large solvent effects exhibited by the bicyclo[2.2.1]heptanones. Figure 2 reproduce the results of Rassat[20] on the effect of going from pure ethanol to pure cyclohexane upon the CD spectra of isofenchone (I) and epiisofenchone (II).

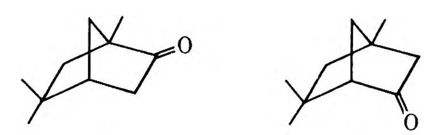

I II

It has been suggested[20-23] that the changes observed in

(20) A. Rassat, "Optical Rotatory Dispersion and Circular Dichroism in Organic Chemistry," G. Snatzke, Ed., Sadtler Research Laboratories, Inc., Philadelphia, Pa., 1967.

(21) (a) A. Moscowitz, K. M. Wellman, and C. Djerassi, *Proc. Nat. Acad. Sci.*, **50**, 799 (1963); (b) K. M. Wellman, P. H. A. Laur, W. S. Briggs, A. Moscowitz, and C. Djerassi, *J. Amer. Chem. Soc.*, **87**, 66 (1965).

(22) H. Gervais and A. Rassat, *Bull. Soc. Chim. Fr.*, 743 (1961).

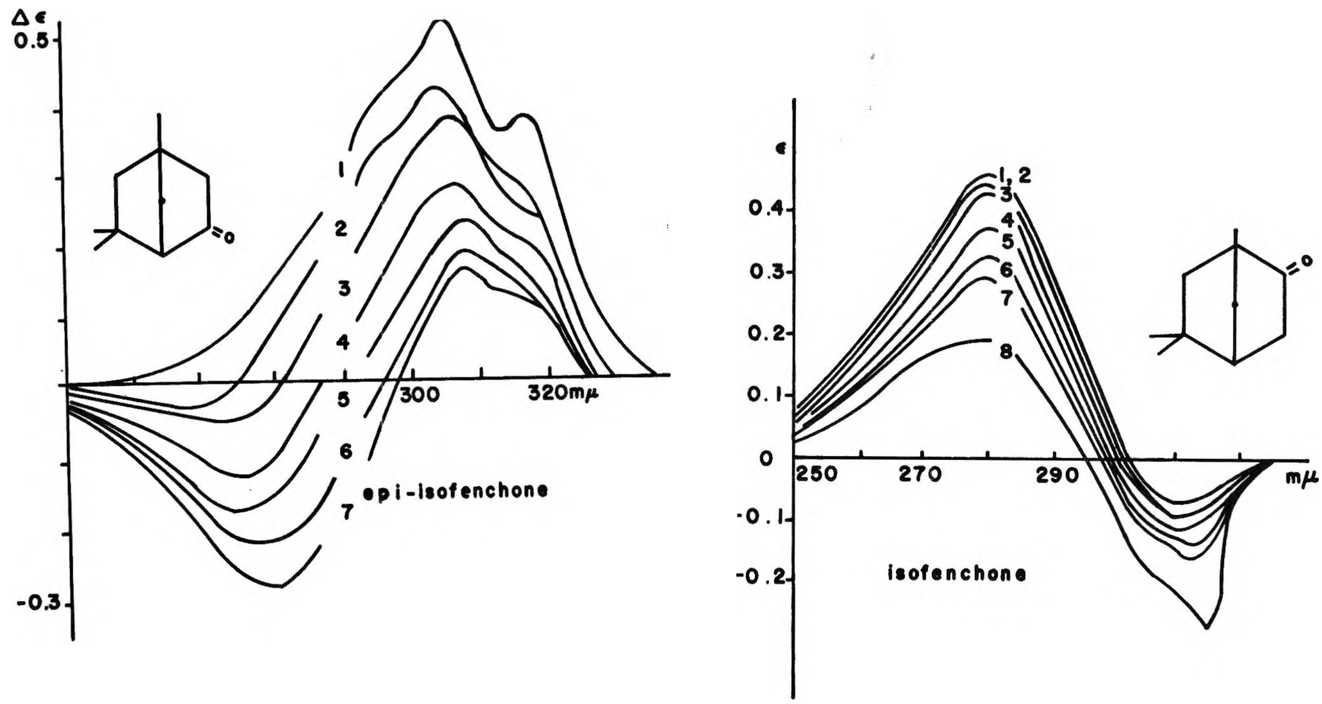

Figure 2. (a) CD curves of epiisofenchone in a mixed solvent study (cyclohexane–ethanol). Curves 1 and 7 represent pure cyclohexane and ethanol, respectively. (b) CD curves in a mixed solvent study (cyclohexane–ethanol). Curves 1 and 8 represent pure ethanol and cyclohexane, respectively.

the CD spectra upon changing the polarity of the solvent is caused by an equilibrium between the solvated and nonsolvated form of the molecule.

The circular dichroism associated with either the solvated or free species could have the same or opposite sign depending on the chirality of their respective solvent cages. The solvent cage can interact with the chromophore by means of the local field arising from the solvent cage's dissymmetric polarizability or by means of a redistribution of energy among the solutes vibrational modes. The latter mechanism may be equally important when vibronic progressions are capable of contributing to the total rotatory strength. Each harmonic of the progression is capable of contributing some fraction of the borrowed rotatory strength R_{KN}.

In the case of the bicyclo[2.2.1]heptanones, the maximum of the vibrational progression ν_{17} may be assumed to occur near the 0–4 transition. This follows from the spectroscopic evidence that the C=O bond increases in length from 1.21 Å, in the ground state, to nearly 1.32 Å in the lowest excited singlet state ($^1A_2n - \pi^*$). Substituting this change into eq 18 where

$$(Q_k^0 - Q_N^0) \simeq \mu(0.11 \text{ Å})$$

and μ is the reduced mass of the C=O system, one arrives at a $\Delta = 4.35$. Furthermore the ν_{17} frequency in the $^1A_2$ state of formaldehyde is 1182 cm^{-1} (1198 cm^{-1} for acetone), which leads one to expect a maximum in the ν_{17} progression nearly 4800 cm^{-1} above the 0–0 transition at 345 mμ. This would place the maximum near 275 mμ. The observed change in the carbonyl

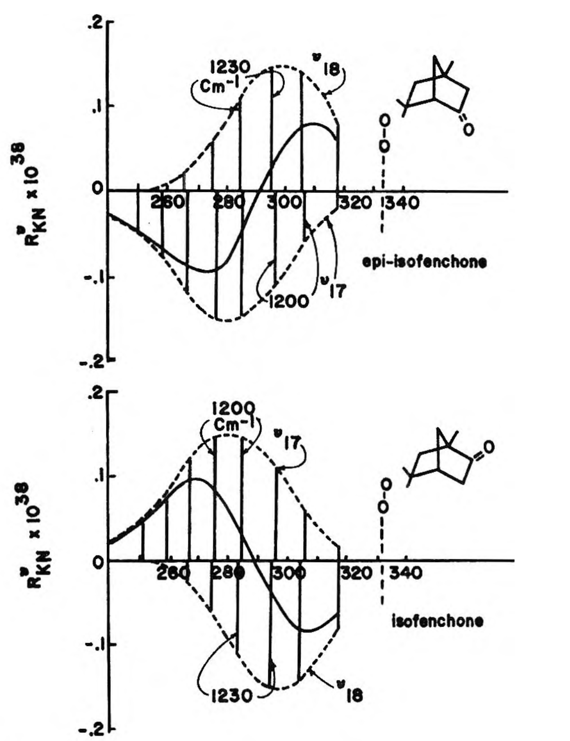

Figure 3.

bond length is not unusual for excited states since the equilibrium position is highly sensitive to the electronic charge distribution. Bond angles are less likely to change, however, as it would require a rehybridization

(23) C. Coulombeau and A. Rassat, *Bull. Soc. Chim. Fr.*, 2673 (1964).

Table VI: Vibrational Normal Modes of Camphor

No.	Cm⁻¹	μ	Assignment[a]
1	2975	3.36	(a,a) gm C-H st (99%)
2	2974	3.36	(−a,−a) gm C-H st (99%)
3	2973	3.36	(a,−a) gm C-H st (99%)
4	2972	3.36	(a,−a) gm C-H st (22%); a bhm C-H st (76%)
5	2972	3.37	(−a,a) gm C-H st (78%); a bhm C-H st (22%)
6	2972	3.37	(−a,a) gm C-H st (99%)
7	2927	3.42	(a,−a) me C-H st (94%)
8	2923	3.42	a me C-H st (96%) (sbme)
9	2920	3.42	(a,a) me C-H st (90%)
10	2905	3.44	bhh C-H st (97%)
11	2860	3.50	s me C-H st (99%) (sbme)
12	2858	3.50	(s,s) me C-H st (99%)
13	2857	3.50	(s,−s) me C-H st (98%)
14	2857	3.50	s bhm C-H st (99%)
15	2856	3.50	(s,−s) gm C-H st (97%)
16	2856	3.50	(s,s) gm C-H st (99%)
17	1945	5.14	cy st (70%); C-cy st (15%); C-cy-C b, C-C-O b (15%)
18	1810	5.52	C-cy st (25%); C-C-O b (55%)
19	1601	6.25	gm C-C st (34%); (a,a) gm C-H b (40%)
20	1571	6.37	gm C-C st (10%); (a,a) gm C-H b (62%)
21	1557	6.42	C-C-H b diffuse
22	1522	6.57	me b (21%); C-C st (12%) diffuse
23	1511	6.62	me scis b (45%)
24	1506	6.64	me scis b (21%)
25	1481	6.75	diffuse
26	1473	6.79	diffuse
27	1465	6.83	C-C-H bend diffuse
28	1462	6.83	a bhm C-H b (80%)
29	1457	6.87	a bhm C-H b (70%)
30	1443	6.93	a bhm C-H b (35%); pb C-C st (15%)
31	1437	6.96	(a,a) gm C-H b (99%)
32	1436	6.97	(a,a) gm C-H b (99%)
33	1420	7.04	me scis (30%)
34	1415	7.07	gm C-H b (90%)
35	1393	7.18	diffuse
36	1359	7.36	C-C-H b diffuse, bhh (25%)
37	1296	7.72	C-C-H b diffuse
38	1232	8.12	C-C-H b diffuse, bhh (31%)
39	1211	8.26	me twist (25%)
40	1193	8.38	me wag (25%); bhm C-C st (12%)
41	1154	8.67	me wag (34%); bhm C-C st (8%)
42	1151	8.69	me twist (65%)
43	1134	8.84	me twist (46%)
44	1095	9.13	C-C-H bend diffuse
45	1042	9.60	gm C-C-H bend (92%)
46	1017	9.83	diffuse
47	1005	9.95	C-C st (32%); bhh C-H b (12%)
48	969	10.32	diffuse
49	946	10.58	bhm C-H b (32%); me H-C-H b (40%)
50	926	10.79	bhm C-H b (40%)
51	919	10.88	me, me C-C st (33%)
52	908	11.01	gm C-H bend (98%)
53	901	11.10	diffuse
54	872	11.4	C-C st (16%); sb CH_2 b (40%); pb CH_3 b (27%)
55	818	12.2	C-C st (42%); sb CH_2 b (29%); pb CH_3 b (7%)
56	768	13.0	C-C st (13%); pb C-CH_2 st (12%); sb CH_3 b (56%)
57	727	13.7	C-C st (27%); sb CH_2 b (26%); sb cy b (16%)
58	707	14.1	C-C st (45%); sb CH_2 b (17%); sb cy b (7%)
59	613	16.3	C-C st (20%)
60	602	16.6	pb C-CH_3 st (19%); bh CH_3 b (12%); p cy b (29%)
61	562	17.8	cy b (17%); cy p (13%)
62	530	18.9	bh C-CH_3 st (23%); bh CH_3 b (17%)
63	452	22.1	pb C-CH_3 st (12%); pb C-CH_3 b (40%)

Table VI (*Continued*)

No.	Cm⁻¹	μ	Assignment[a]
64	410	24.4	pb C-CH_3 st (5%); pb C-CH_3 b (26%)
65	403	24.8	bhh b (15%); pb C-CH_3 b (36%)
66	314	31.9	bh CH_3 b (58%)
67	308	32.5	bh b (57%); pb b (20%)
68	258	38.8	bh b (18%); pb b (66%)
69	250	40.0	bh b (59%); pb b (35%)
70	208	48.0	bh b (60%)
71	162	61.8	bh b (59%); pb b (24%)
72	120	83.4	pb C-CH_3 t (98%)
73	114	87.7	pb C-CH_3 t (83%); bh C-CH_3 t (13%)
74	113	88.5	pb C-CH_3 t (13%); bh C-CH_3 t (87%)
75	82	120	C-C t (46%); bh C-CH_3 b (32%)

[a] a = asymmetric, s = symmetric, st = stretch, b = bend, t = torsion, p = out-of-plane bend, pb = primary bridge, sb = secondary bridge, bh = bridge head, bhm = bridge heat methyl, bhh = bridge head hydrogen, gm = geminal methyl, me = methylene, cy = carbonyl, sbme = secondary bridge containing me, sbcy = secondary bridge containing cy, scis = scissor bend, diffuse = no single distortion predominant.

of their atomic orbitals. As a result, the displacement of the harmonic potential in the excited state is less for angle-bend coordinates than for bond stretch. We therefore expect the ν_{17} progression to have its maximum transition probability at frequencies further removed from the 0–0 transition than those of ν_{18} (C–C=O angle bend) progression. The vibrational progression of ν_{18} is taken to occur near the 0–2 transition.

The change in relative intensity of the two vibronic contributions must depend on the solvene environment. As Rassat correctly noted, the fact that the vibronic maxima do not shift in frequency in different solvents indicates an equilibrium between different species. We would only add that the constancy in ν of the vibronic maxima means that the valence force constants are not changing with solvation. The ordinate of Figure 3 represents the rotatory strength of each harmonic as it appears at the frequency plotted on the abscissa. In reality the CD spectra would be approximated by a sum of Gaussian bands centered at the 0–n frequencies having an area equal to R_{KN} (ν).

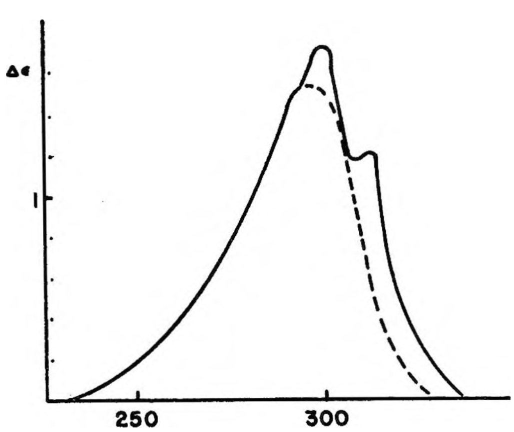

Figure 4. CD curves of camphor in cyclohexane (—) and methanol (----).

Figures 4 and 5 show the CD spectra[20] of (+)-camphor (III) and (+)-fenchone (IV).

III IV

It can be seen that only one band appears in these compounds. It was conceivable that the normal modes would result in the disappearance of one progression for these particular configurations. However, Table VII shows that this is not the case; instead a single band must be due either to a reduced probability of exciting one progression or to an overlap of both progressions.

Table VII: Comparison of Calculated and Observed Rotatory Strengths

Compd	Calcd[a] × 10^{39}	Obsd[b] × 10^{40}
Isofenchone	7.80 (ν_{17})	2.02
	−5.85 (ν_{18})	
Epiisofenchone	−7.70 (ν_{17})	
	6.45 (ν_{18})	
Camphor	−8.24 (ν_{17})	15.1
	6.17 (ν_{18})	
Fenchone	8.20 (ν_{17})	4.55
	−6.12 (ν_{18})	

[a] Sum of contributions from first nine harmonics. [b] Cyclohexane.

IV. Discussion

We have successfully shown that chromophores possessing local symmetry within the framework of a dissymmetric molecule, acquire rotatory strength by means of the dissymmetric normal modes interacting

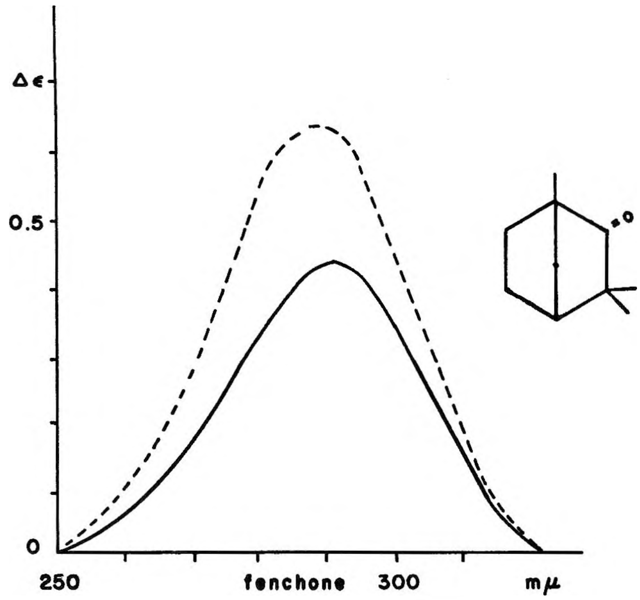

Figure 5. CD curves of fenchone in cyclohexane (——) and ethanol (----).

with the chromophore's electronic states. Furthermore, the particular cases studied demonstrate that carbonyl chromophores are most strongly affected by those normal modes involving C=O stretch and C–C=O in-plane bend. Progressions involving these two modes should contribute to the rotatory strength with opposite sign. That the major vibronic contributions should arise from so few normal modes could not have been expected prior to a complete calculation.

These results are basic to the consideration of two further questions. (1) What portion of the observed rotatory strength of an electronic transition can be attributed to the vibronic interactions arising from dissymmetric molecular vibrations? (2) Can the net effect of different vibronic progressions possibly account for the change in sign observed in many circular dichroism spectra in the region of a single electronic transition?

To examine the first question we must compare the calculated rotatory strengths with the experimental values obtained by using

$$R_k = 0.696 \times 10^{-42} \int \frac{[\theta_k(\lambda)]\,d\lambda}{\lambda} \quad (39)$$

where $[\theta_k(\lambda)]$ is the molecular ellipticity

$$[\theta_k(\lambda)] = \theta(\lambda)M/10cl$$

M = molecular weight, C = concentration in g/ml, l = path length in cm, and θ is the observed ellipticity in degrees at the wavelength λ. We can see from Table VII that the calculated values are generally one order of magnitude too large. We may gain some insight as to the source of this error by considering the individual contributions from the several terms making up the rotatory strength as expressed by eq 4, which shows that the rotatory strength is approximately proportional: (a) to the fourth power of a transition dipole moment; (b) inversely to the square of the transition energy; (c) to the square of the mean displacement of the nuclei; (d) to eZ/r_i^3.

The first two contributions depend on the molecular orbital calculations used; Table II compares the calculated dipole moments with those calculated from the integrated absorption spectra. In using the oscillator strength to calculate the electric dipole moments we have used

$$D_k^2 = 91.8 \times 10^{-40} \int d\nu \epsilon_k(\nu)/\nu$$

$$f_k = 4.32 \times 10^{-19} \int \epsilon_k(\nu) d\nu$$

$$D_k^2 \approx 2.12 \times 10^{-30} f_k/\nu_k$$

where $\epsilon_K(\nu)$ is the molar extinction coefficient for the Kth electronic band at frequency ν, and f_k is the oscillator strength. The energies for formaldehyde were too large by approximately a factor of 4.

The third contribution depends on the accuracy of the normal mode calculation. The calculated root mean square deviations are about 0.1 Å for ν_{17} and ν_{18}. The final contribution depends on our dipole–dipole approximation. The effective shielding of the neighboring groups has been ignored to that the charge Z_σ will be less than unity, in reality, and the radial dependence will most certainly decrease more rapidly than $1/r^3$. It is to be expected, therefore, that our greatest error will lie within this final term.

In considering the second question we must recognize that the conservation of rotatory strength and the constancy of the vibronic maxima upon change of solvent polarity together indicate an equilibrium between solvated and nonsolvated species. A comparison of the calculated and observed shapes of the circular dichroism spectra of isofenchone and epiisofenchone suggest that in a more polar solvent the C=O stretching mode (ν_{17}) predominates over the out-of-plane bending mode (ν_{18}), whereas in a less polar solvent ν_{18} predominates. Although a change in sign of the CD within a single electronic transition is not observed for (+)-camphor or (+)-fenchone the same general trend applies. That is to say, if the more polar solvent enhances vibronic progressions of ν_{17}, then the calculated signs given in Table VII predict the total rotatory strength to decrease for (+)-camphor and increase for (+)-fenchone when going from a less polar to a more polar solvent. Figures 4 and 5 show this to be the case. However, for these compounds even in the nonpolar solvent cyclohexane neither vibronic progression is capable of dominating the total rotatory strength so as to make it negative. Perhaps this is an example where the solvent cage polarizability perturbs the chromophore more than do the vibronic interactions.

In conclusion, it has been demonstrated in what manner vibronic progressions can contribute to a molecule's rotatory strength. Certain progressions will predominate depending on the solvent environment. To determine whether a solvent cage contributes more strongly to the rotatory strength *via* a redistribution of these vibronic progressions or *via* a dissymmetric local field would require a detailed knowledge of solvent–solute interactions and solvent cage structure. Lacking such detailed knowledge, certain trends in the circular dichroism spectra of four bicyclo[2.2.1]heptanones are shown to be consistent with the calculated sign of the two dominant vibronic progressions present in the carbonyl chromophore.

Acknowledgment. This work was partially supported by National Institutes of Health Grant, GM12862-05 and American Chemical Society Petroleum Research Fund Grant 753-C. We wish to thank Allen K. MacKnight and Gary J. Clark for their assistance with many aspects of the normal mode calculation and, in particular, for their aid with computer programming techniques.

Extended Hückel Calculations on Polypeptide Chains. II.

The ϕ–ψ Energy Surface for a Tetrapeptide of Glycine

by Angelo R. Rossi, Carl W. David,

Department of Chemistry, The University of Connecticut, Storrs, Connecticut 06268

and Robert Schor*

Department of Physics and Institute of Materials Science, The University of Connecticut, Storrs, Connecticut 06268
(Received June 23, 1970)

The ground- and excited-state potential energy surfaces for a tetrapeptide of glycine have been calculated using the extended Hückel method. The results are compared to both the extended Hückel calculations on the dipeptide and the semiempirical force calculations on a polypeptide of glycine. The present ϕ–ψ map, although similar to the Hoffmann–Imamura map, does show significant differences in the details of the sterically allowed regions. The map predicts a minimum in the α helix region in agreement with experiment and with the results of Scott and Scheraga obtained by semiclassical force calculations.

Introduction

Theoretical studies of the regular conformations of isolated helices (in a vacuum) of polypeptide chains with no intermolecular interactions have been carried out by many workers[1–3] using semiempirical potential functions for barriers to rotation around single bonds, nonbonded interactions, dipole–dipole interactions between amide groups, and hydrogen bonding potential energy functions.

More recently, semiempirical quantum mechanical techniques have been used to study glycyl and alanyl residues,[4] polypeptide chains,[5] and model peptide molecules.[6] In this paper we shall present by use of extended Hückel theory (EHT) a detailed study of the stereochemistry of a polypeptide chain long enough to include 4 peptide units or 3 residues, *i.e.*, slightly more than one pitch of the helix.

The objective of the present work is to compare the results of the extended Hückel theory with those of the semiclassical force calculations on polyglycine. In addition, a study of the increased chain length using molecular orbital techniques is obtained.

Method

The EHT[7] provides an approximate solution to the LCAO molecular Hartree–Fock equations in which all valence electrons are explicitly treated, all overlap inte-

* To whom correspondence should be addressed.

(1) D. A. Brant and P. J. Flory, *J. Amer. Chem. Soc.*, **87**, 663, 2791 (1965).

(2) G. N. Ramachandran, C. M. Venkatachalm, and S. Krimm, *Biophys. J.*, **6**, 849 (1966).

(3) R. A. Scott and H. A. Scheraga, *J. Chem. Phys.*, **45**, 2091 (1966).

(4) R. Hoffmann and A. Imamura, *Bipolymers*, **7**, 207 (1969).

(5) A. Rossi, C. W. David, and R. Schor, *Theoret. Chim. Acta*, **14**, 429 (1969).

(6) J. F. Yan, F. A. Momany, R. Hoffmann, and H. A. Scheraga, *J. Phys. Chem.*, **74**, 420 (1970).

(7) R. Hoffmann, *J. Chem. Phys.*, **39**, 1397 (1963); **40**, 2474, 2480, 2745 (1964).

grals are calculated, but electron repulsion is not explicitly included. The off-diagonal matrix elements in the Wolfsberg–Helmholtz approximation[8] are given by

$$H_{ij} = 0.5K(H_{ii} + H_{jj})S_{ij}$$

where S_{ij} are the overlap matrix elements, H_{ii} are valence state ionization potentials, and K is assigned the usual value of 1.75. The input to the computer program are atomic coordinates,[9] Slater exponents,[6] and the values of s and p coulomb integrals.[4] The output consists of one-electron energy levels, the total one-electron orbital energy, partial charges localized on each atom, and a Mulliken population analysis.[10] The EHT parameters for this calculation are given in Table I.

Table I: Parameters of the Extended Hückel Calculation[14]

Coulomb Integrals

Electron	Value (eV)
H (1s)	−13.6
C^α (2s)	−21.4
C^α (2p)	−11.4
C′ (2s)	−21.4
C′ (2p)	−11.4
N (2s)	−26.0
N (2p)	−13.4
O (2s)	−32.3
O (2p)	−14.8

Slater Exponents

Atom	Value
H	1.300
C^α	1.625
C′	1.625
N	1.950
O	2.275

The method for determining the coordinates of the atoms in the helical conformations of the polypeptide chain as shown in Figure 1 is due to Némethy and Scheraga.[11] The peptide unit is considered to have a rigid planar structure with fixed bond angles and bond lengths. The coordinates of the atoms in a peptide unit for the bond angles and distances taken from Leach, Némethy, and Scheraga[9] are given in Table II. The standard convention[12] for the rotation angles ϕ and ψ which define the conformations of a polypeptide chain was used.

The calculations were performed on an IBM 360/65 computer. (The execution time for a tetrapeptide of glycine was approximately 1 minute for each point on the potential energy surface.) The largest grid width was taken to be 30°, but a width as small as 5° was used for studying certain energy contours which varied more rapidly with ϕ and ψ.

Table II: Coordinates for the Atoms in a Peptide Unit[9]

Atom	X (Å)	Y (Å)	Z (Å)
C′	1.42	1.58	0.00
O	1.61	1.80	0.00
N	2.37	−0.34	0.00
H (amide)	2.18	−1.32	0.00
C^α	3.80	0.000	0.00
$H^{\alpha a}$	0.36	0.54	0.89
$H^{\alpha a}$	0.36	0.54	−0.89

[a] The C–H distance was taken to be 1.09 Å, which reflects electron diffraction data on aliphatic hydrocarbons (R. A. Bonham, L. S. Bartell, and A. D. Kohl, *J. Amer. Chem. Soc.*, **81**, 4765 (1959)).

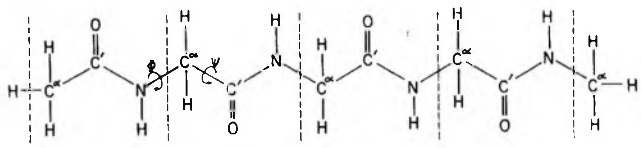

Figure 1. Diagrammatic representation of a tetrapeptide of glycine including the rotation angles ϕ(N–C^α) and ψ(C^α–C′) about the single bonds.

Results

A. Conformational Analysis. As it is not possible using EHT or other molecular orbital techniques to decompose the total energy into physically identifiable components such as nonbonded interactions, hydrogen-bonding potential energy functions, dipole–dipole interactions, and barriers to rotation around single bonds, the following discussion refers to the total orbital energy.

The ground- and first excited-state potential energy surfaces for four peptide units (three residues) are displayed in Figures 2 and 3, respectively. The most stable conformation has been assigned zero energy. Since R = H, the map is centrosymmetric about the point $(\phi,\psi) = (\pi,\pi)$. The results of the present calculations are comparable in the regions of high steric repulsions to those of Hoffmann and Imamura.[4] The most significant differences are the appearance of a local minimum in the α helical region and the bending of the contours to resemble more closely the results of the classical calculations. The similarities are attributed to the dominant role of the hard-sphere contacts while the differences are clearly due to the increased chain length. Although preliminary calculations on the pentapeptide

(8) M. Wolfsberg and L. Helmholtz, *J. Chem. Phys.*, **20**, 837 (1952).

(9) S. J. Leach, G. Némethy, and H. A. Scheraga, *Biopolymers*, **4**, 369 (1966).

(10) R. S. Mulliken, *J. Chem. Phys.*, **23**, 1833, 1841, 2338, 2343 (1955).

(11) G. N. Némethy and H. A. Scheraga, *Biopolymers*, **4**, 369 (1966).

(12) J. T. Edsall, P. J. Flory, J. C. Kendrew, A. M. Liquori, G. Némethy, G. N. Ramachandran, and H. A. Scheraga, *Biopolymers*, **4**, 121 (1966); *J. Biol. Chem.*, 241 (1966); *J. Mol. Biol.*, 15 (1966).

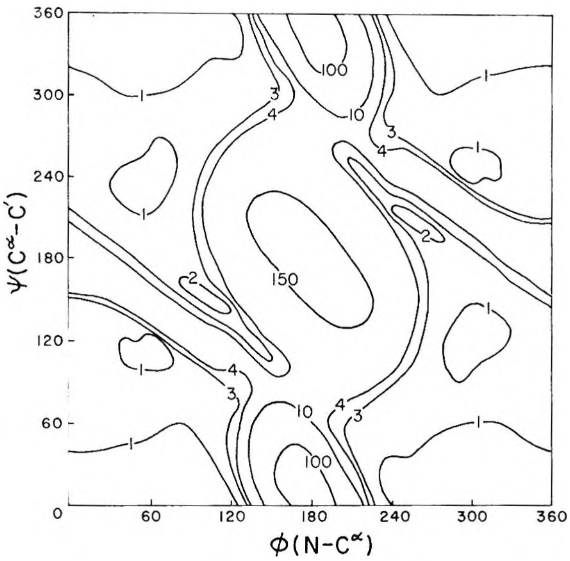

Figure 2. Ground-state potential energy surface for a tetrapeptide of glycine calculated by extended Hückel theory. The contours of constant energy are relative to the most stable conformation chosen as zero energy and are in units of kcal/mol of residue.

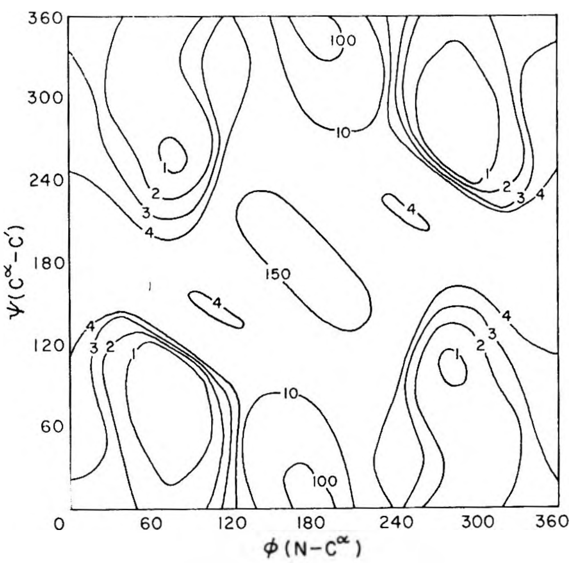

Figure 3. Excited-state potential energy surface for a tetrapeptide of glycine calculated by extended Hückel theory. The contours of constant energy are relative to the most stable conformation which is chosen as zero energy and are in units of kcal/mol of residue.

and the hexapeptide do not appear to give any significant differences, a more thorough investigation of the effect of increases in the chain length should perhaps be considered.

The general resemblance of the ground-state potential energy surface shown in Figure 2 compared to previous classical calculations is noteworthy. The large regions of high steric repulsion are in about the same locations. A minimum for the 2-kcal contour is found in the region $\phi = 85$–$120°$, $\psi = 140$–$165°$ which falls within the range given by the classical calculation. The experimental values for the standard positions of the right- and left-handed α helices are $\phi = 132°$, $\psi = 123°$, and $\phi = 228°$, $\psi = 237°$, respectively, with as much as $\pm 10°$ variance[13] so that the present 2-kcal contours come close to these points. Slightly deeper but comparable minima are predicted in the extended chain region. This is consistent with the fact that the presence of glycyl residues particularly in a regular sequence reduces the stability of the α helix.[14] In our previous work,[5] we predicted a somewhat deeper minima at the α helical conformation due to the use of the Cusach approximation and a different method of chain termination. The most noteable difficulties are that deep minima are predicted at conformations which are not observed experimentally. Since the difference of the calculated energy between the local minima and the absolute minima are small, they may be due to the approximations involved in the EHT method and/or to the neglect of intermolecular forces. It may be possible to resolve these difficulties by performing more detailed calculations.

The singly excited-state potential energy surface shown in Figure 3 must be considered provisional. The shape of the contours is similar to our ground-state map for both the regions of high steric repulsions and the allowed regions. The results are also similar to the excited-state map for glycyl residues of Hoffmann and Imamura.[4] A local minimum in the α helical region is again predicted. The other contours become more localized to give sharper peaks. In agreement with the dipeptide calculation, the first electronic transition (∼5 eV) of these residues corresponds to an excitation of an electron identifiable as a combination of lone pairs on all the carbonyl groups (considerably delocalized to nearby atoms) to a π^* orbital on all the amide groups and can therefore be considered as an n–π^* transition.

B. Charges and Population Analysis. The partial charges, which are sensibly independent of the rotation angles ϕ and ψ, are given in Table III for the extended chain and the α helical conformations. The charges, although taken from the first and fourth peptide units, are representative of the atoms in the entire chain. The present results for the charge distribution around the peptide bond are comparable to those obtained by using EHT for *N*-methyl acetamide.[6] There is an exaggerated charge separation for the atoms in the C′—O bond of the peptide unit which is not unexpected on the basis of EHT calculations. In going from the extended to the α helical conformation, the carbonyl oxygen on the first peptide unit slightly decreases its negative charge with a corresponding increase of the charge on

(13) J. A. Schellman and C. Schellman in "The Proteins," Vol. 2, H. Neurath, Ed., Academic Press, New York, N. Y., 1964, p 1.

(14) G. N. Ramachandran and V. Sasisekharan in "Advances in Protein Chemistry," Vol. 23, G. B. Anfinsen, Jr., M. L. Anson, J. T. Edsall, and F. M. Richards, Ed., Academic Press, New York, N. Y., 1968, p 283.

Table III: Gross Charges on the Atoms in a Planar Peptide Unit for Various Helical Conformations of the Tetrapeptide of Glycine

Conformation	Atomic charges						
	N[a]	H[a]	O[b]	C′[b]	C[b]	Hα[b]	Hα[b]
Fully extended chain	−0.32	+0.24	−1.23	+1.08	+0.19	+0.03	+0.03
Antiparallel-chain pleated sheet	−0.31	+0.23	−1.23	+1.07	+0.19	+0.03	+0.02
Parallel-chain pleated sheet	−0.31	+0.23	−1.23	+1.07	+0.19	+0.03	+0.02
Right-handed α helix	−0.36	+0.25	−1.20	+1.08	+0.19	+0.03	+0.02

[a] Atomic charge taken from fourth peptide unit. [b] Atomic charge taken from first peptide unit.

Table IV: Overlap Populations for the Bonds in a Planar Peptide Unit as a Function of the Rotation Angles (ϕ, ψ) for a Tetrapeptide of Glycine [Values for the Hydrogen Bond Interaction (>N—H...O = O<) Are Also Given]

Conformation	Rotation angles		N...O distance, Å	∠H-N...O, degrees	Overlap populations					
	ϕ	ψ			C^{α}—C′[a]	C′—N[a]	N—C^{α}[a]	N—H[b]	H...O[c]	O=C′[a]
Fully extended chain	0.0	0.0	12.32	90	0.794	1.030	0.667	0.732	0.000	0.808
Antiparallel-chain pleated sheet	38.0	325.0	11.68	85	0.790	1.035	0.664	0.732	0.000	0.805
Parallel-chain pleated sheet	61.0	293.0	10.47	73	0.784	1.037	0.660	0.732	0.000	0.803
Right-hand α helix	132.0	123.0	2.83	0	0.785	1.033	0.663	0.720	0.015	0.807
Neighboring helix	122.0	128.0	2.56	10	0.785	1.033	0.663	0.705	0.034	0.808

[a] Overlap population taken from first peptide unit. [b] Overlap population taken from fourth peptide unit. [c] Overlap population between the oxygen on the first peptide and the amino hydrogen on the fourth peptide unit.

the nitrogen atom of the fourth peptide unit. The charge on the amide hydrogen, however, remains more nearly constant for these conformations. These slight changes in the charge distributions of the nitrogen and oxygen atoms may reflect a weak interaction in the process of forming the intramolecular hydrogen bond.

The overlap populations for the bonds in a planar peptide unit are given in Table IV. These values are substantially independent of the conformation and of the particular peptide unit which is being considered. There is considerably more electron density between the C′–N bond than between either the C^{α}–C′ or N–C^{α} single bonds which is expected for planar peptide linkages with double bond character. The overlap population between the carbonyl oxygen of the first and the amino hydrogen of the fourth peptide unit has a small positive value for the α helical conformation and is zero for the extended forms. The overlap population for the N–H bond decreases about the same amount while the C′–O overlap population remains sensibly constant. This small increase in the overlap population for the O...H interaction at the α helix is the same order of magnitude calculated for similar hydrogen bonded systems[15,16] and perhaps indicates a weak association in the formation of the hydrogen bond. As the O...N distance in the α helix is decreased, the O...H overlap population increases significantly.

It should perhaps be emphasized that as is usual in Hoffmann and other molecular orbital techniques we have not included the hydrogen bond explicitly in the calculation. As noted previously, all the Coulomb integrals were taken as valence state ionization potentials (Table I) and essentially no further empirical elements are introduced into the calculation. We make no claims as to the detailed nature of the hydrogen bond. It seems reasonable, however, to attempt to correlate the strength of the hydrogen bond with the Mulliken overlap population between the carbonyl oxygen of the first peptide unit and the amino nitrogen of the fourth peptide unit.

It is gratifying to note that the essential features of the present calculations appear to be reproduced in our more elaborate CNDO/2 calculations which are in progress.

Conclusion

The overall agreement of our predicted ground-state potential energy surface to that obtained from the semiclassical force calculation as well as the fact that both calculations predict a minimum near the α helix conformation gives some basis for confidence in the approximate validity of the present calculational technique as applied to problems in protein stereochemistry.

Acknowledgments. The authors wish to thank Professor Roald Hoffmann for a fruitful discussion and for giving us a more efficient and faster executing version of

(15) W. Adam, A. Grimison, R. Hoffman, and C. Z. de Ortiz, *J. Amer. Chem. Soc.*, **90**, 1509 (1968).
(16) K. Morokuma and J. R. Winick, *J. Chem. Phys.*, **52**, 1301 (1970).

his program. This work is being supported by Grant No. GB-6852 of the National Science Foundation. The computational part of this work was carried out at the Computer Center of the University of Connecticut which is supported in part by Grant No. GP-1819 of the National Science Foundation.

Structure of Electrical Double Layer between Mercury and Dimethyl Sulfoxide in the Presence of Chloride Ions

by Sang Hyung Kim, Terrell N. Andersen, and Henry Eyring

Department of Chemistry, University of Utah, Salt Lake City, Utah 84112 *(Received August 25, 1970)*

The adsorption of the chloride ion on a mercury electrode from solutions of lithium chloride in dimethyl sulfoxide (DMSO) has been studied by measuring the interfacial tension of the electrode as a function of potential and concentration at 25°. The adsorption could be described by a virial isotherm in which the free energy of adsorption varied linearly with electrode charge, and in which the second virial coefficient (ion–ion repulsion term) is large. Specific adsorption of chloride ions is stronger from DMSO than from water. The inner layer capacity is analyzed into its components and the relative distances from the surface to the inner and outer Helmholtz planes (x_1 and x_2, respectively) are deduced. $(x_2 - x_1)/x_2$ is larger for adsorption of Cl^- ions from DMSO than from water.

Introduction

Despite the electrochemical interest in nonaqueous solvents[1,2] quantitative double layer data are still sparse for electrodes in these solutions. The dielectric properties of dimethyl sulfoxide (DMSO) and its use in high energy batteries has stimulated some work[2,3] relating to the structure of the Hg–solution interphase, although analyses of specific adsorption have not been reported.

Kolthoff and Reddy[4] obtained an electrocapillary curve of 0.1 M $NaClO_4$ in DMSO using a dropping Hg electrode. Burrus[5] made polarographic measurements in DMSO and obtained the electrocapillary maximum (ecm) for Hg in 0.1 M and 1 M $KClO_4$. Payne[6] measured electrocapillary curves and double layer capacities for a number of inorganic salts in DMSO and in mixtures of DMSO with water. He did not attempt to analyze his data and hence to obtain the adsorption of ions because of the lack of thermodynamic data.

Activity coefficients in DMSO have recently been reported.[7–15] With the aid of these data an attempt is made to obtain and quantitatively analyze double layer data in DMSO. In the present paper electrocapillary curves for Hg in DMSO containing LiCl were obtained. The specific adsorption of Cl^- ions is calculated, and the adsorption isotherm and potential distribution across the inner double layer are discussed.

Experimental Section

The interfacial tension was measured by means of a Lippmann type capillary which utilized a fine, tapered capillary. Details of the setup may be found elsewhere.[16]

The procedure for measuring the surface tension was

(1) R. Payne, *Advan. Electrochem. Electrochem. Eng.*, **7**, 1 (1970).
(2) J. N. Butler, *ibid.*, **7**, 77 (1970).
(3) J. N. Butler, *J. Electroanal. Chem.*, **14**, 89 (1967).
(4) I. M. Kolthoff and T. B. Reddy, *J. Electrochem. Soc.*, **108**, 980 (1961).
(5) R. T. Burrus, Ph.D. Thesis, University of Tennessee, 1962; University Microfilm No. 63-4101.
(6) R. Payne, *J. Amer. Chem. Soc.*, **89**, 489 (1967).
(7) T. Skerlak and V. Milicevic, *Glas. Drus. Hem. Technol. SR Bosen Hercegovine*, **11**, 49 (1962); *Chem. Abstr.*, **61**, 3749f (1964).
(8) J. S. Dunnett and R. P. H. Gasser, *Trans. Faraday Soc.*, **61**, 922 (1965).
(9) M. D. Archer and R. P. H. Gasser, *ibid.*, **62**, 3451 (1966).
(10) W. H. Smyrl, Ph.D. Thesis, University of California, Berkeley, 1966.
(11) W. H. Smyrl and C. W. Tobias, *J. Electrochem. Soc.*, **113**, 754 (1966).
(12) G. Holleck, D. R. Cogley, and J. N. Butler, *ibid.*, **116**, 952 (1969).
(13) J. M. Crawford and R. P. H. Gasser, *Trans. Faraday Soc.*, **63**, 2758 (1967).
(14) M. Salomon, *J. Electrochem. Soc.*, **116**, 1392 (1969).
(15) M. Salomon, *ibid.*, **117**, 325 (1970).
(16) S. H. Kim, Ph.D. Thesis, University of Utah, 1971.

similar to that of Smolders.[17] The mercury head was slowly raised until the first drop of mercury was expelled from the capillary, and the mercury height was measured at this point. Before each measurement mercury was expelled from the tip of the capillary by shaking the flexible tubing between the capillary and reservoir. The buoyancy correction was calculated for each experiment from the depth of the electrolyte and capillary in the cell, and from density data.[13] Measurements were made with a cathetometer to a precision of 0.005 cm.

A schematic representation of the cell, showing the various compartments and liquid junctions between the capillary test electrode and 1 M aqueous calomel reference electrode, is shown below.

Hg | Hg_2Cl_2 | 1 M aq KCl || 0.1 M LiCl in DMSO ¦ x M LiCl in DMSO ¦ x M LiCl in DMSO | Hg in capillary

The water–DMSO junction was made with an aqueous saturated KCl–agar salt bridge and was kept constant in each experiment by employing solutions of the same concentration. The liquid junction between the 0.1 M LiCl in DMSO and the x M LiCl in DMSO was made through a fritted glass.

Potential measurements were made with a Leeds and Northrup Type K-3 potentiometer to a precision of ±0.05 mV. The capillary electrode was polarized with a storage battery in series with Helipots using an aqueous calomel counter electrode (different from the reference electrode) which was in a side compartment separated from the main compartment by a frit.

Analytical reagent grade (Mallinckrodt) DMSO was used without further purification. Baker analyzed reagent grade LiCl was oven-dried at 180–200° for approximately 6 hr and then stored in a dessicator until it was put into solution. Virgin mercury was used in the electrometer. All glassware was cleaned with Chromerge solution, rinsed, and soaked in water doubly distilled from an alkaline permanganate solution and oven-dried. Prior to each measurement the solution was flushed with high purity nitrogen which was deoxygenated by the procedure of Meites,[18] then dehydrated in an anhydrous calcium chloride column, and presaturated by bubbling it through DMSO. Nitrogen bubbling was stopped during the measurements. The streaming mercury electrode[19,20] was used to measure the point of zero charge (pzc) and to check the reproducibility of the liquid junction potential. This potential was reproducible to within ±1 mV. All measurements were carried out at 25 ± 0.5°.

The radius of the capillary was determined by taking the interfacial tension of Hg|aqueous 0.05 M Na_2SO_4 at the ecm (−0.467 V *vs.* nce) to be 426.2 ± 0.2 dynes/cm which was found from sessile drop measurements made by Smolders.[21] The radius of the capillary tip determined in this way was 1.33×10^{-3} cm.

Results

Electrocapillary curves for LiCl in DMSO at eight concentrations between 0.0033 and 1.045 M were obtained between ∼−0.3 and −1.2 V (*vs.* aqueous nce). At more positive potentials the measurements were not reproducible and it was evident from polarization studies that faradaic processes occurred. From the work of others[22] the accessible potential range for a comparable system was found to be −0.246 to −2.206 V (nce). The measured potentials (E_m) were converted to the potential scale of a reference electrode reversible to the chloride ion (*i.e.*, to the E^- scale) according to the equation

$$E^- = E_m + E_{lj} + \frac{RT}{F}\ln a_\pm \quad (1)$$

Here E_{lj} is the liquid junction potential between DMSO containing 0.1 M LiCl and x M LiCl and the mean ionic activities were taken from the data of Holleck, *et al.*[12] Calculation of the E_{lj} was made using the Henderson equation with a transference number for Li^+ in DMSO of 0.323. This value was calculated from the mobility data of Dunnett and Gasser.[8] The electrocapillary curves on the E^- scale are shown in Figure 1. The potentials and

Table I: The Potentials and Interfacial Tensions at the Electrocapillary Maximum[a]

	Sme,	Electrocapillary curves			
C, mol/l.	$-E_m$, mV	$-E_m$, mV	$-E_c$, mV	$-E^-$, mV	γ_z, dyn/cm
0.0033	371	406	379	531	370.2
0.0119	406	416	400	522	368.8
0.0758	431	431	429	510	367.0
0.1000	436	432	432	508	366.9
0.3276	462	459	468	518	365.2
0.5332	475	469	482	522	363.6
0.8742	486	480	496	525	362.9
1.045	489	482	500	525	362.4

[a] $E_c = E_m + E_{lj}$, E (ecm) and γ_z are obtained from the polynomial curve fitting (see text).

(17) C. A. Smolders, *Recl. Trav. Chim. Pays-Bas*, **80**, 699 (1961).

(18) L. Meites and T. Meites, *Anal. Chem.*, **20**, 984 (1948).

(19) D. C. Grahame, E. M. Coffin, and J. I. Cummings, Technical Report No. 2 to the Office of Naval Research, Aug 11, 1950.

(20) D. C. Grahame, E. M. Coffin, J. I. Cummings, and M. A. Poth, *J. Amer. Chem. Soc.*, **74**, 1207 (1952).

(21) C. A. Smolders, *Recl. Trav. Chim. Pays-Bas*, **80**, 635 (1961).

(22) J. L. Jones and H. A. Hritsche, Jr., *J. Electroanal. Chem.*, **12**, 334 (1966).

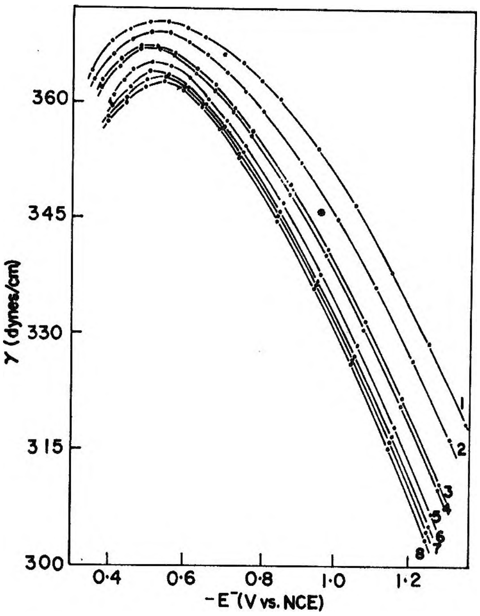

Figure 1. Electrocapillary curves for LiCl solutions in DMSO at 25°: (1), 0.0033 *M;* (2), 0.0119 *M;* (3), 0.0758 *M;* (4), 0.1000 *M;* (5), 0.3276 *M;* (6), 0.5332 *M;* (7), 0.8742 *M;* (8), 1.045 *M*.

interfacial tensions at the ecm obtained from the electrocapillary curves and from the streaming mercury electrode (sme) are given in Table I.

The electrocapillary curves (γ *vs.* E^-) were fitted to an *nth* degree polynomial in E^- (for $3 \leq n \leq 8$) using a least-square curve-fitting method (University of Utah, UNIVAC 1108, Program Library No. 0032). The best fit was chosen for the polynomial having the least standard error of $|\gamma_{\text{expt}} - \gamma_{\text{calcd}}|$. The calculated interfacial tensions were in agreement with the measured values within the experimental error of ± 0.3 dyne/cm except at a few potentials.

The surface charge density on the electrode (q) at a given E^- was calculated by analytical differentiation of the polynomial, and then the potential, E^-, for integral values of q was obtained by interpolation of the q *vs.* E^- graphs. The polynomial for γ *vs.* E^- also gives the γ for integral values of q. In this way Parsons' function,[23] $\xi^- \equiv \gamma + qE^-$, for integral values of q was obtained. The calculated values of ξ^- were plotted against $2RT/F \ln a_\pm$ at various constant values of q. The slope of these curves gives the surface excess of Li^+ ($F\Gamma_+$) according to Parsons' analysis[24] and the adsorption equation

$$-d\xi^- = E^- \, dq + \Gamma_+ \, d\mu \qquad (2)$$

This differentiation was analytically performed by fitting the curves to a polynomial ($2 \leq n \leq 4$). The best fit obtained was for a parabola, and the resultant computed surface excesses of Li^+ are shown in Figure 2. Using $F\Gamma_+$ and q, the surface excess of Cl^- ($-F\Gamma_-$) was calculated from the equation

$$q = -(F\Gamma_+ - F\Gamma_-) \qquad (3)$$

and is plotted in Figure 2. The results show that chloride ions are so strongly adsorbed that at all values of q and at all concentrations the surface excess of lithium ions is positive. From the similarity of the surface excess curves (Figure 2) to those for aqueous alkali halide solutions[25] it seems reasonable to assume that the lithium ions are present entirely in the diffuse layer; *i.e.*, the lithium ions are not specifically adsorbed so that $F\Gamma_+ = q_+^{2-s}$. Payne[6] also came to the same conclusion from the electrocapillary curves and the double layer capacity measurements of different alkali metal compounds (0.1 M KPF_6, $LiClO_4$, NH_4Cl, KBr, and KI) in DMSO. With this assumption the potential of the outer Helmholtz plane (ϕ_2) was calculated from $F\Gamma_+$, and the charge due to the chloride ions in the diffuse layer (q_-^{2-s}) was calculated from ϕ_2 according to diffuse layer theory[26] assuming that ϵ in the

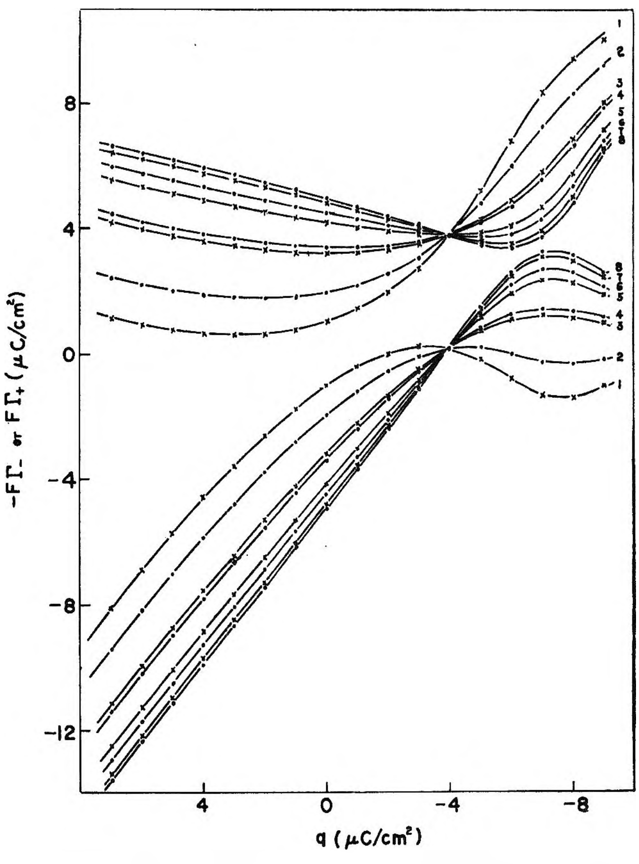

Figure 2. Surface excesses of Li^+ cations ($F\Gamma_+$) (upper curves) and Cl^- anions ($-F\Gamma_-$) (lower curves) as a function of the electrode charge (q) at the same corresponding concentrations as given in Figure 1.

(23) R. Parsons, *Trans. Faraday Soc.*, **51**, 1518 (1955).

(24) R. Parsons, *Can. J. Chem.*, **37**, 308 (1959).

(25) M. A. V. Devanathan and B. V. K. S. R. A. Tilak, *Chem. Rev.*, **65**, 635 (1965).

(26) D. C. Grahame and B. Soderberg, *J. Chem. Phys.*, **22**, 449 (1954).

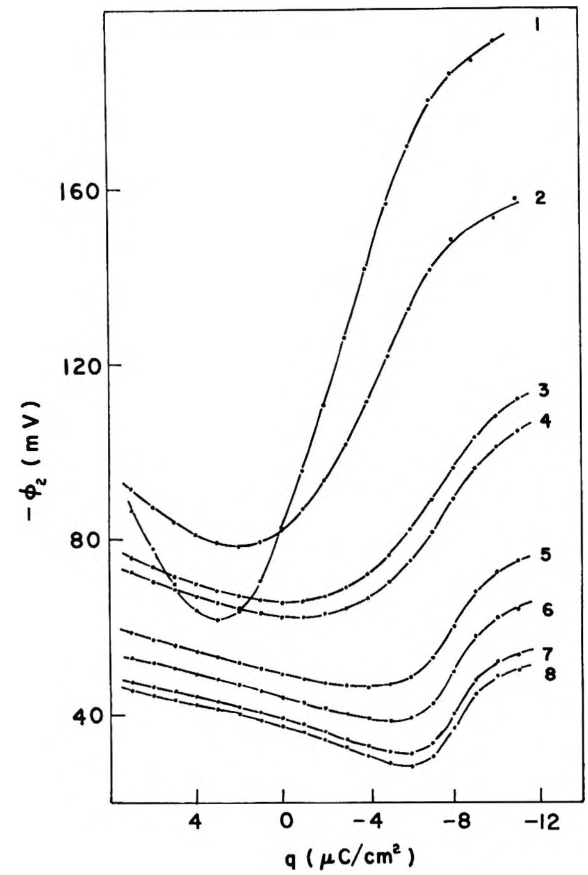

Figure 3. Potential of the outer Helmholtz plane (ϕ_2) as a function of the charge (q) at various concentrations of LiCl. Concentrations same as in Figure 1.

diffuse layer is equal to the bulk dielectric constant of DMSO which is 46.6.[27] The plot of ϕ_2 *vs.* q is shown in Figure 3. It is noted that a minimum appears and that ϕ_2 is always negative over the entire range of charge, indicating that specific adsorption of anions occurs at all charges. In the absence of specifically adsorbed ions, ϕ_2 changes its sign at the pzc.[28] The difference between $-F\Gamma_-$ and q_-^{2-s} gives the amount of specifically adsorbed anions (q_-^1).

The above method of calculating q_-^1 can have inherent inaccuracies from the graphical differentiation used to get $F\Gamma_+$.[29,30] Therefore, the technique developed by Parsons[31,32] was used in which the surface pressure due to specifically adsorbed anions (Φ) is obtained and compared with the theoretical surface pressure equation calculated by substituting an isotherm into the Gibbs adsorption equation and integrating. The surface pressure of the specifically adsorbed anions at constant q is given in terms of Parsons' function by

$$\Phi = \frac{1}{2}\left(\xi_0{}^+ - \xi^+ - \int_{-\infty}^{\mu} \frac{q_-^{2-s}}{F}\,\mathrm{d}\mu\right) \tag{4}$$

$\xi^+ = \gamma + qE^+$ where E^+ is the potential of the capillary electrode with respect to a reference electrode reversible to the cation; $\xi_0{}^+$ is the value of ξ^+ for a solution from which there is no specific adsorption. The term in the integral in eq 4 subtracts the contribution of the anions in the diffuse layer from the surface pressure. Equation 4 is derived and discussed by Parsons,[23,33] and the factor of one-half is introduced by the arguments of Payne.[29] As discussed by Parry and Parsons[32] the absolute surface pressure due to the diffuse layer (the last term in eq 4) cannot be obtained at positive values of q because the term q_-^{2-s} is positive everywhere (anions are repelled from the diffuse layer). Rather only the variation of this contribution between the limits of concentration studied can be evaluated. This contribution (which we shall denote by the letter I) is evaluated from the integral

$$I = -\int_{\mu_0}^{\mu} \frac{q_-^{2-s}}{F}\,\mathrm{d}\mu \tag{5}$$

where μ_0 is the chemical potential of the lowest concentration studied. Using q_-^{2-s} values obtained from the thermodynamically calculated values of Γ_+, I was determined by analytical integration of the parabolic curves of q_-^{2-s} *vs.* $2RT/F \ln a_\pm$. Thus the effective surface pressure which was obtained is given by

$$\Phi \simeq -{}^1/_2(\xi^+ + I) \tag{6}$$

The specific adsorption, q_-^1, was obtained by taking the slope of the $-{}^1/_2(\xi^+ + I)$ *vs.* $\log a_\pm$ curves analogous to eq 2. This is equivalent to the slope $\mathrm{d}\Phi/\mathrm{d}\log a_\pm$ since $\xi_0{}^+$ is a function of charge but not concentration and since the difference between I and

$$\int_{-\infty}^{\mu} q_-^{2-s}/F\,\mathrm{d}\mu$$

is independent of concentration for a given charge. q_-^1 obtained in this way is plotted in Figure 4 as a function of q at various LiCl concentrations. These values of q_-^1 are in agreement with the values calculated from the difference of $-F\Gamma_-$ and q_-^{2-s} except at the extreme concentrations where the deviations are as much as 1 $\mu C/cm^2$. Also the logarithmic isotherms at constant q (q_-^1 *vs.* $\log a_\pm$) are shown in Figure 5. Unlike the adsorption of Cl^- in H_2O,[34] the present system follows the logarithmic isotherm as does I^- in H_2O and in formamide.[1]

(27) P. G. Sears, G. R. Lester, and L. R. Dawson, *J. Phys. Chem.*, **60**, 1433 (1956).

(28) P. Delahay, "Double Layer and Electrode Kinetics," Wiley, New York, N. Y., 1965, p 42, Figures 3–6.

(29) R. Payne, *J. Chem. Phys.*, **42**, 3371 (1965).

(30) J. Lawrence and R. Parsons, *Trans. Faraday Soc.*, **64**, 751 (1968).

(31) R. Parsons, *Proc. Roy. Soc., Ser. A*, **261**, 79 (1961).

(32) J. M. Parry and R. Parsons, *Trans. Faraday Soc.*, **59**, 241 (1963).

(33) R. Parsons, "Soviet Electrochemistry," Vol. 1, A. N. Frumkin, Ed., Consultants Bureau New York, N. Y., 1961, p 18.

(34) D. C. Grahame and R. Parsons, *J. Amer. Chem. Soc.*, **83**, 1291 (1961).

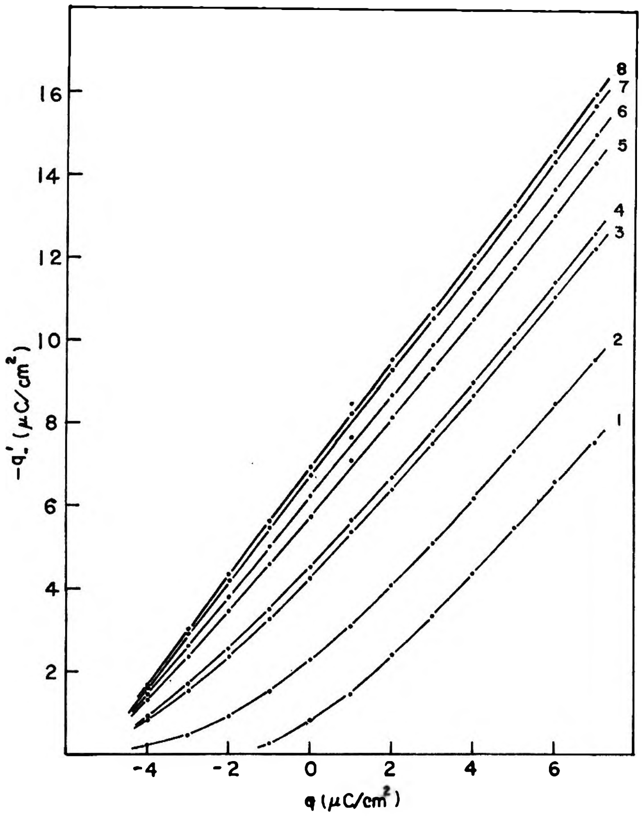

Figure 4. Amounts of specifically adsorbed anions (q_-^1) as a function of electrode charge (q) at the same corresponding concentrations as given in Figure 1.

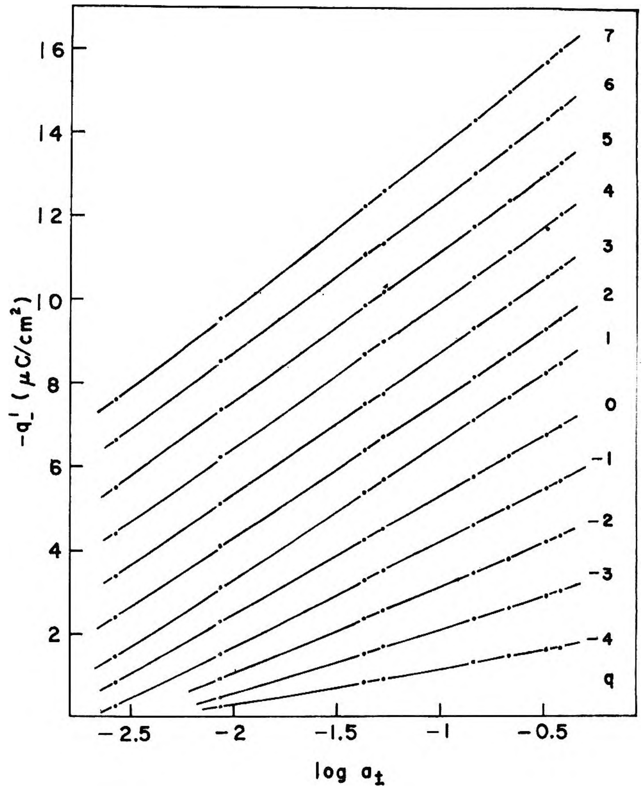

Figure 5. Amount of specifically adsorbed anions (q_-^1) as a function of log $a_\pm$. The electrode charge (q) in μC/cm^2 is indicated by each line.

The curves of $-{}^1/_2(\xi^+ + I)$ *vs.* log $a_\pm$ at constant q have the same shapes as the surface pressure *vs.* log $a_\pm$ curves but their positions on the surface pressure axis and hence their absolute value at any value of $a_\pm$ is undetermined. The individual curves for different values of q could be superimposed on a common curve by moving the curves parallel to the X and Y axes by amounts f(q) and F(q), respectively, which are functions only of q (*cf.* Figure 6). This same observation was previously made for thiourea[31] and sodium benzene-*m*-disulfonate[32] in water, I^- in formamide,[29] and ClO_4^- in sulfolane.[30] The superposition of these $-{}^1/_2(\xi^+ + I)$ *vs.* log $a_\pm$ curves on the surface pressure curve for $q = -4$ μC/cm^2 was performed and the functions F(q) and f(q) were obtained. Also a composite surface pressure curve for the specifically adsorbed anions was determined from all the experimental points. The deviations of the experimental points from the common curve were less than ± 0.4 dyn/cm.

The shift on the abscissa of the surface pressure curves is equal to the variation of the standard free energy of adsorption with charge[31]

$$\frac{\mathrm{d}f(q)}{\mathrm{d}q} = \frac{\mathrm{d}\left(-\dfrac{\Delta G}{kT}\right)}{\mathrm{d}q} = \frac{\mathrm{d}\ln\beta}{\mathrm{d}q} \tag{7}$$

This is plotted in Figure 7 which shows that the standard free energy of adsorption is a linear function of q, as found previously for the other cases of single ion adsorption.[29,30,32,35] This indicates that ΔG depends only on the electrode–particle interaction analogous to that between a layer of charge and an adjacent charged metal plate.

The composite surface pressure curve, obtained as described above, was replotted as log Φ *vs.* log $a_\pm$ + f(q) and compared with various surface pressure equations.[31,36] We find that the two-dimensional virial equation and the Frumkin isotherm fit the experimental data equally well. The equations of state and isotherms for these isotherms are

virial

$$\Phi = kT(\Gamma + B\Gamma^2) \tag{8a}$$

$$\ln a_\pm - \frac{\Delta G}{kT} = \ln\Gamma + 2B\Gamma \tag{8b}$$

Frumkin

$$\Phi = kT\,\Gamma_s\left[\ln\left(\frac{\Gamma_s}{\Gamma_s - \Gamma}\right) + A\,\frac{\Gamma^2}{2\Gamma_s^2}\right] \tag{9a}$$

$$\ln\left(\frac{a_\pm}{\Gamma_s} - \frac{\Delta G}{kT}\right) = \ln\left(\frac{\Gamma}{\Gamma_s - \Gamma}\right) + A\,\frac{\Gamma}{\Gamma_s} \tag{9b}$$

where Γ is the surface concentration of the specifically adsorbed anions in units of ions/cm^2 ($\Gamma = -q_-^1/e_0$); Γ_s is

(35) R. Parsons, *Trans. Faraday Soc.*, **55**, 999 (1959).

(36) R. Parsons, *J. Electroanal. Chem.*, **7**, 136 (1964).

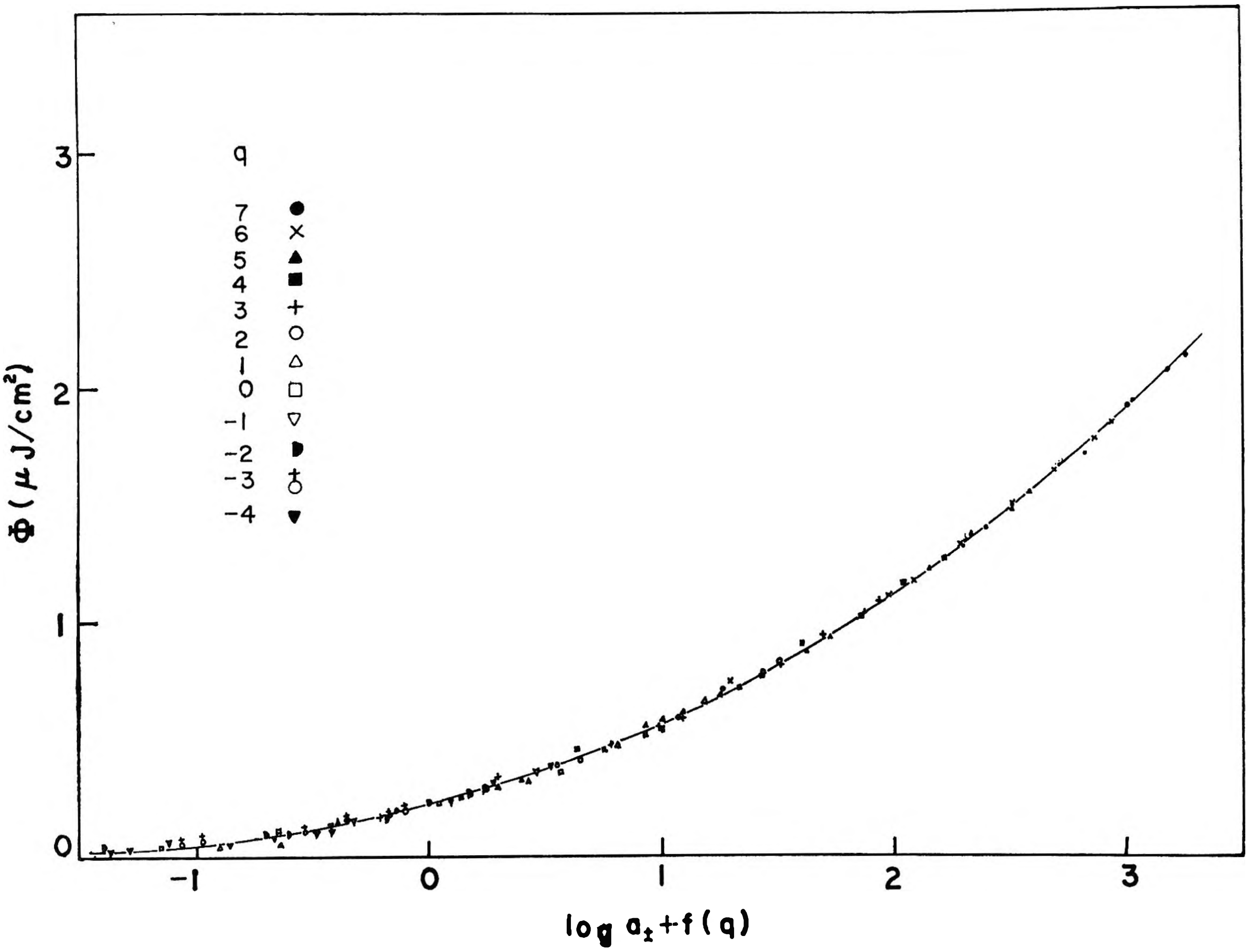

Figure 6. Composite surface pressure curve of specifically adsorbed anions as a function of the mean ionic activity ($a_\pm$). q is in units of μC/cm^2.

the saturation value of Γ; B is a two-dimensional second virial coefficient; A is an adsorbed ion-ion interaction constant of which the sign is positive or negative corresponding to the repulsive or attractive force, respectively; ΔG is the standard free energy of adsorption at zero coverage defined with the standard state of 1 molality in the bulk solution and 1 ion/cm^2 in the adsorbed state. In the right-hand sides of the above isotherms we have neglected $-2B$ in eq 8b, and $1/\Gamma_s$ and $-A/\Gamma_s$ in eq 9b because of the negligibly small quantities.

In the Frumkin isotherm the constants A and Γ_s always appear together and cannot be independently obtained. Because the experimental data correspond only to low surface coverages and due to the large repulsion constant, the Frumkin isotherm takes the form of the virial isotherm.[29] Therefore, we have fitted the present data to the virial isotherm, obtaining the constants $B = 400$ Å^2/ion and $\log \beta = 15.64 + 0.335q$ which corresponds to $\Delta G = -21.4$ kcal/mol at the pzc. The solid line drawn in Figure 6 was calculated from these constants. With these constants $q_-{}^1$ was also calculated as a function of $\log a_\pm$ at constant charge and compared with the values obtained from the differentiation of the individual surface pressure curves (these latter values are used for further calculation). The agreement was within ± 0.3 μC/cm^2, except at the extreme concentrations and negative charges, where the deviation was up to 1.3 μC/cm^2. The limit of this deviation was due to the scatter of points on the composite surface pressure curve. This scatter may have been due to experimental precision, but one cannot rule out the possibility that the isotherm constant B may vary with charge.

As pointed out by Parsons,[36] the surface pressure might be insensitive in assigning isotherms. The virial isotherm was therefore tested by plotting $\log -q_-{}^1/a_\pm$ *vs.* $-q_-{}^1$ at constant q using the values of $q_-{}^1$ obtained from the individual surface pressure *vs.* $\log a_\pm$ curves. The straight lines obtained should yield a slope of $2B/2.303e_0$ and an intercept of $\log \beta e_0$. The plots are shown in Figure 8. From the intercepts $\log \beta$ is found to be given by $\log \beta = 15.90 + 0.294q$ which corresponds to $\Delta G = -21.7$ kcal/mol at the pzc. Again the linearity of the variation of the standard free energy of

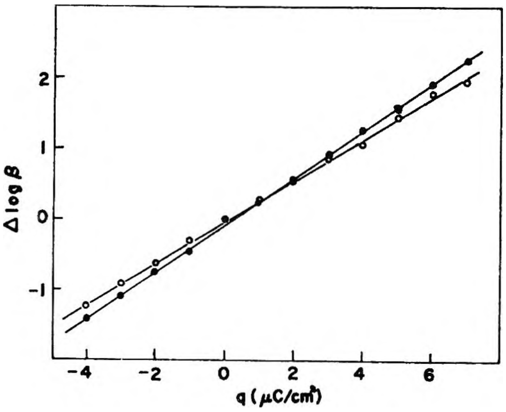

Figure 7. Variation of the standard free energy of adsorption (log β) of chloride ions due to the electrode charge (q): -●-●-, calculated from the plots of Figure 6; -O-O-, calculated from the plots of Figure 8.

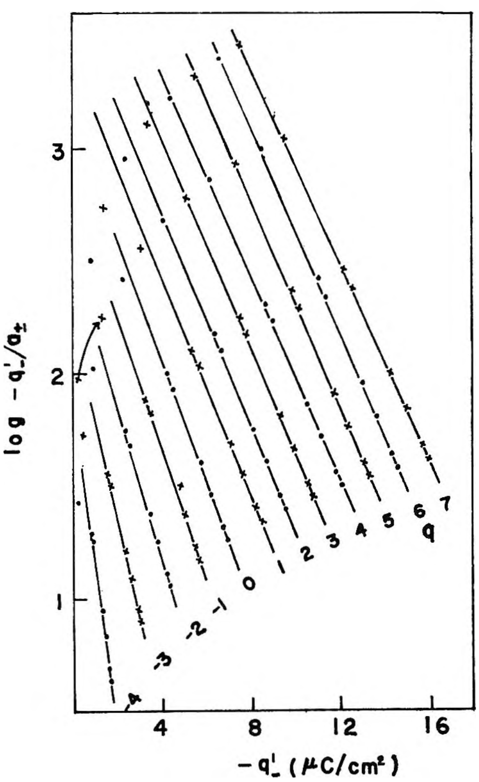

Figure 8. Test of the virial isotherm for adsorption of chloride ions. The electrode charge (q) in $\mu C/cm^2$ is indicated by each line.

adsorption with charge is confirmed (see Figure 7). The two methods of fitting the isotherm are thus seen to give comparable free energies of adsorption and variation of this free energy with q.

From the slopes of Figure 8 the second virial coefficient (B) is obtained and plotted as a function of q in Figure 9. B increases from 403 to 1411 Å²/ion as q decreases from 6 to -4 $\mu C/cm^2$. Such an increase in B with a decrease in q has been found in the systems

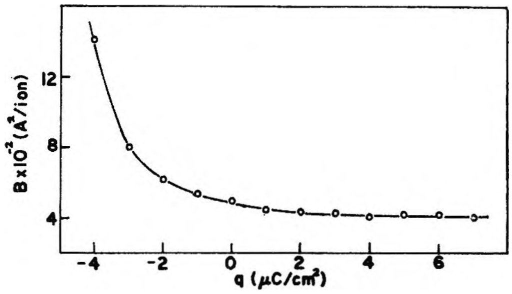

Figure 9. Variation of the two-dimensional second virial coefficient (B) for adsorption of chloride ions due to the electrode charge (q).

Br^- [37] and I^- [35] in water, KI + KF in methanol,[38] and ClO_4^- [30] in sulfolane.

Esin and Markov plots[39,40] were prepared in Figure 10 and were linear with the Esin and Markov coefficient being 1.2, irrespective of q, in the range of strong specific adsorption of anions. This coefficient is given from the analog of eq 2 as

$$\left(\frac{\partial E^+}{\partial \frac{2RT}{F}\ln a_\pm}\right)_q \simeq \left(\frac{\partial q_-^1}{\partial q}\right)_\mu \qquad (10)$$

Since the plots of q_-^1 against q at constant concentration in Figure 4 are linear, the linearity of the Esin and Markov plots is confirmed. The slopes of these plots of Figure 4 are from 1.1 to 1.3 which agrees well with 1.2 from Figure 10. This shows the consistency of the experimental data. The linear relationship of eq 10 is typical of specific adsorption of ions in H_2O,[39,41,42] in formamide,[1,29] and in CH_3OH-H_2O mixtures.[43]

Discussion

Comparison of Adsorption in Other Systems. The adsorption of DMSO on Hg is stronger than that of water as shown by comparing the interfacial tension between the Hg and the pure solvents[1,6] (γ_{Hg-H_2O} = 427 dyn/cm and $\gamma_{Hg-DMSO}$ = 370.6 dyn/cm). Also Payne observed no desorption peaks of DMSO from the capacity measurements of DMSO–water mixtures[6] similar to those found for most ordinary organic molecules in water; this also indicates that DMSO is strongly adsorbed. However, the experimental adsorption data of the Cl^- on Hg from both solvents show that the adsorp-

(37) J. Lawrence, R. Parsons, and R. Payne, *J. Electroanal. Chem.*, **16**, 193 (1968).

(38) J. D. Garnish and R. Parsons, *Trans. Faraday Soc.*, **63**, 1754 (1967).

(39) R. Parsons, *Proc. Intern. Congr. Surface Activity, 2nd, London*, **3**, 38 (1957).

(40) See ref 28, pp 53–59.

(41) S. Minc and J. Andrzejczak, *J. Electroanal. Chem.*, **17**, 101 (1968).

(42) H. Wroblowa and K. Müller, *J. Phys. Chem.*, **73**, 3528 (1969).

(43) S. Minc, J. Jastrzebska, and J. Andrzejczak, *Electrochim. Acta*, **14**, 821 (1969).

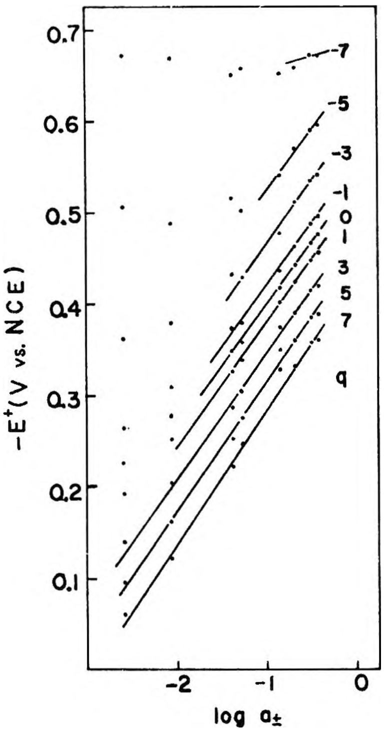

Figure 10. Esin and Markov plots for LiCl in DMSO. The electrode charge in $\mu C/cm^2$ is indicated by each line.

tion from DMSO is stronger than that from H_2O (*e.g.*, at the pzc $q_-^{1} = -4.5\ \mu C/cm^2$ and -2.7[44] or 1[45] $\mu C/cm^2$ for 0.1 *M* LiCl in DMSO and H_2O at 25°, respectively). On the other hand, the anions in aprotic solvents like DMSO are less solvated.[14,46,47] Also the free energy of transfer of LiCl from H_2O to DMSO is reported to be 4.865 kcal/mol at 25°.[14] Comparison of the solvation numbers given by Salomon[15] for LiCl in DMSO and H_2O indicates that LiCl and hence Cl^- is less solvated in DMSO. From these results it is likely that the solvation energy, and not the adsorption of solvent molecules, governs the relative specific adsorption of ions from these two solvents.

The standard free energy of adsorption of Cl^- (ΔG) at the pzc obtained by the virial isotherm is -21.7 kcal/mol at 25°. This value is comparable to the standard free energy of adsorption of CNS^- in H_2O at 20° (-21.6 kcal/mol)[41] and I^- in formamide at 25° (-21.5 kcal/mol)[29] obtained from the Frumkin isotherm (the standard states are the same). Therefore, the specific adsorption of Cl^- from DMSO may be nearly as strong as those of CNS^- from H_2O and of I^- from formamide.

From the direct plot of the virial isotherm we obtained large positive second virial coefficients varying with the charge on the electrode. The positive value of B indicates that the interaction between adsorbed ions is primarily repulsive. The second virial coefficient of a two-dimensional imperfect gas is given in terms of the interaction energy $U(r)$ between pairs of ions separated by a distance r, by

$$B = \pi \int_0^\infty (1 - \exp[-U(r)/RT])r\, dr \qquad (11)$$

If $U(r)$ is the electrostatic interaction between an adsorbed ion and an adsorbed ion–image pair (the ion–ion distance is r), $U(r)$ is given by

$$U(r) = \infty \text{ if } 2r_c \geqslant r \geqslant 0$$

and

$$U(r) = \frac{e_0^2}{4\pi\epsilon_0\epsilon r}\left[1 - \left(1 + 4\frac{x_1^2}{r^2}\right)^{-1/2}\right] \qquad (12)$$

if $2r_c \leqslant r \leqslant \infty$ where r_c is the crystallographic radius of the chloride ion, and ϵ_0 and ϵ are the dielectric constants of free space and of the medium, respectively. Introducing eq 12 into eq 11 and integrating, we obtain finally

$$B = 20.36 + 971.6\frac{x_1^2}{\epsilon} \text{ in Å}^2\text{/ion} \qquad (13)$$

Here we used $r_c = 1.81$ Å[48] and 20.36 Å^2/ion is the coarea term. Using $x_1 = 1.81$ Å and B shown in Figure 9, we obtain ϵ to be 8.1 to 2.3 as q goes from positive to negative values. On the other hand, if we assume $\epsilon = 7$, x_1 corresponds to 1.7 − 2 Å except in the case of $q = -4\ \mu C/cm^2$. These values are close to r_c of Cl^-. In spite of the simplest model, it seems clear that B increases as q decreases. This semiquantitative calculation was suggested by Parsons.[49,50] However, such an electrostatic interpretation cannot completely explain the origin of the repulsive forces expressed by B since B differs with the identity of the ion and the composition of the solution.[1] We have assumed that the adsorbed ions are a mobile monolayer lying between the solvent molecules and the homogeneous mercury surface. Perhaps this simple model fails in that it neglects the role of the solvent molecules. However, the adsorption of Cl^- from DMSO appears to be simpler than the other system studied previously. Without knowing the actual double layer parameters (x_1, x_2, and ϵ, etc.), only a semiquantitative interpretation is possible. Independent measurements of the double layer parameters are desirable.

The potential of zero charge of Hg in DMSO solutions exhibiting little ionic specific adsorption (~ -0.3 V *vs.* aqueous nce,[6] -0.255 V *vs.* aqueous nce obtained from

(44) H. Wroblowa, Z. Kovac, and J. O'M. Bockris, *Trans. Faraday Soc.*, **61**, 1523 (1965).

(45) R. G. Barradas and E. W. Hermann, *J. Phys. Chem.*, **73**, 3619 (1969).

(46) A. J. Parker, *Quart. Rev.* (*London*), **16**, 163 (1962).

(47) A. J. Parker, *Chem. Rev.*, **69**, 1 (1969).

(48) R. C. Weast, Ed., "Handbook of Chemistry and Physics," 50th ed, The Chemical Rubber Publishing Co., Cleveland, Ohio, 1969.

(49) W. Anderson and R. Parsons, *Proc. Intern. Congr. Surface Activity, 2nd, London*, **3**, 45 (1957).

(50) R. Parsons, *Advan. Electrochem. Electrochem. Eng.*, **1**, 1 (1961).

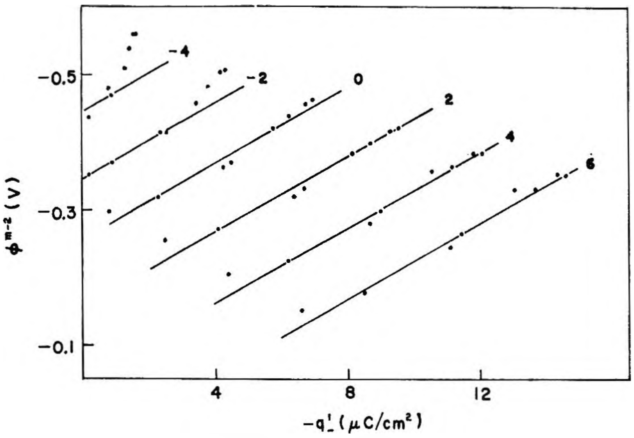

Figure 11. Potential difference across the inner layer (ϕ^{m-2}) as a function of amount of specifically adsorbed anions (q_-^1). The electrode charge (q) in μC/cm² is indicated by each line.

the extrapolation to $q_-^1 = 0$ in Figure 11) is more positive than those in aqueous solutions (−0.48 V *vs.* nce[51]). If the DMSO–H_2O junction potential is small, this difference may be attributed to the relative orientation of the two types of solvent molecules at the Hg surface. Hence DMSO dipoles may be oriented with their positive dipole end pointed preferentially toward the metal (as suggested also by Payne[6]), while water molecules appear to have little preferential orientation at the pzc.[52,53]

Distance Ratio of Inner and Outer Helmholtz Plane. The potential difference across the inner layer (ϕ^{m-2}) was calculated by subtracting ϕ_2 from the potential measured on a fixed scale, $E_c = E^- - RT/F \ln a_{\pm}$, and at constant values of q.[53a] ϕ^{m-2} is shown as a function of q_-^1 in Figure 11. These plots are linear and parallel except at the lowest concentrations. At the most negative values of q the experimental points appear to be best fitted by a line of greater slope. This may be due to errors in the calculation of q_-^1 and ϕ_2, or to interference due to the specific adsorption of cations. However, the variation is of doubtful significance in the present treatment and we have made the plots linear and parallel so that the distance ratio of the metal surface to the inner and outer Helmholtz plane could be calculated. This linear and parallel approximation is also supported by the fact that the standard free energy of adsorption (ΔG) is a linear function of charge q (as found from the surface pressure data and the test of the virial isotherm) and ΔG is related to Figure 11 by the approximation[30,32,35]

$$\left(\frac{\partial \phi^{m-2}}{\partial q_-^1}\right)_q \simeq \frac{RT}{F}\frac{\mathrm{d}\ln \beta}{\mathrm{d}q} \qquad (14)$$

Departures from linearity similar to those in Figure 11 were also found in the case of adsorption of ClO_4^- in sulfolane[30] and Tl^+ in water.[54] From Figure 11 we can write the changes in ϕ^{m-2} in terms of charges due to q_-^1 and q; *i.e.*

$$\mathrm{d}\phi^{m-2} = \left(\frac{\partial \phi^{m-2}}{\partial q_-^1}\right)_q \mathrm{d}q_-^1 + \left(\frac{\partial \phi^{m-2}}{\partial q}\right)_{q_-^1} \mathrm{d}q \qquad (15)$$

The coefficients of $\mathrm{d}q_-^1$ and $\mathrm{d}q$ appear to be independent of q_-^1 and q, and we may think of them as the reciprocals of the integral capacities of the inner region; *i.e.*

$$1/(\partial \phi^{m-2}/\mathrm{d}q_-^1)_q = {}_{q_-^1}K^i$$

and

$$1/(\partial \phi^{m-2}/\partial q)_{q_-^1} = {}_qK^i$$

These integral capacities were obtained from Figure 11 and are ${}_{q_-^1}K^i \sim$ 35 to 36 μF/cm² and ${}_qK^i \sim$ 10 to 22 μF/cm². If the dielectric constants in ${}_qK^i$ and ${}_{q_-^1}K^i$ are equal we may calculate the distance ratio $(x_2 - x_1)/x_2$ as

$$\frac{x_2 - x_1}{x_2} = \frac{{}_qK^i}{{}_{q_-^1}K^i} \qquad (16)$$

where x_1 and x_2 are the distances from the electrode surface to the inner and outer Helmholtz planes, respectively. Equation 16 comes from considering the potential drop ϕ^{m-2} as being comprised of the drop across two condensers in series, the metal to iHp and the iHp to oHp. Over the range of q values studied, this ratio is between 0.5 and 0.6 (increasing slightly with decreasing q as in the case of Br^- in H_2O;[37] see Figure 13). The corresponding value of Cl^- in H_2O[34] was found to be between 0.2 and 0.1, changing in the opposite way with charge. If x_2 is assumed to be the sum of the thickness of a DMSO monomolecular layer (∼4.8 Å)[6,55] and the crystal radius of Li^+ (∼0.68 Å),[48] the resulting value of x_1 is 2.8 to 2.2 Å which is greater than the crystal radius of Cl^- (∼1.81 Å). Also if x_1 is assumed to be 1.8 Å, x_2 is 3.6 to 4.5 Å; such an arrangement would indicate that Li^+ ions sit inside the DMSO monomolecular layer. Here we should mention that the dielectric constant in the metal −iHp may be less the $\epsilon_{iHP-oHP}$ which would also lead to small x_2 values. From the values of ${}_{q_-^1}K^i$, $x_1 = 1.8$ Å, and $x_2 = 3.6$ to 4.5 Å, the dielectric constant (ϵ) can be obtained as 7.4 to 11.4. These values seem to be comparable with those obtained from eq 13. However, this kind of consideration is qualitative since a simple electrostatic model has been considered.

Determination of ϕ_1. For the analysis of the potential

(51) D. C. Grahame, *Chem. Rev.*, **41**, 441 (1947).

(52) N. F. Mott and R. J. Watts-Tobin, *Electrochim. Acta*, **4**, 79 (1961).

(53) J. O'M. Bockris, M. A. V. Devanathan, and K. Müller, *Proc. Roy. Soc., Ser. A*, **274**, 55 (1963).

(53a) NOTE ADDED IN PROOF. ϕ^{m-2} as used here differs by a fixed constant from the absolute value of the inner potential across the inner double layer. However in this work only *differences* in this potential are used, so neglecting this unknown constant does not influence the result.

(54) P. Delahay and G. G. Susbielles, *J. Phys. Chem.*, **70**, 647 (1966).

(55) R. Thomas, C. R. Shoemaker, and K. Eriks, *Acta Crystallogr.*, **21**, 12 (1966).

dependence of charge transfer rates, it is of interest to calculate the potential at an anion site in the inner Helmholtz plane (ϕ_1). For this purpose Grahame[56] developed two methods: the first one combined an assumed isotherm with an assumed potential distribution across the inner double layer; the second method takes into account the discreteness of charge in the inner Helmholtz plane. We have used the first method to calculate ϕ_1. Grahame[56] used a Henry's law isotherm in the form

$$q_{-}^{1} = ka_{\pm} \exp(\Phi' + \phi_1)F/RT \qquad (17)$$

where Φ' is the so-called Stern adsorption potential related to the chemical or geometrical influences impelling the ions to the interface and k is a constant. Here the electrostatic interactions between the adsorbed ions and between the ions and the double layer are considered in ϕ_1. Also Grahame considered that the field is constant in the inner layer, such that the potential difference between the inner and outer Helmholtz plane $\phi_1 - \phi_2$ is assumed equal to a fraction $\gamma/(\beta + \gamma)$ of the potential difference between the metal and the outer Helmholtz plane (ϕ^{m-2}). By using the isotherm (eq 17) and this linear potential drop approximation Grahame could obtain the ratio $\gamma/(\beta + \gamma)$ and Φ' which varied with charge. Parry and Parsons[32] modified Grahame's approach by keeping the idea of the constant field approximation and by considering a Langmuir isotherm such that the noncoulombic interactions between the adsorbed ions were accounted for. The potential ϕ_1 in eq 17 is the potential at an anion site or at a vacant anion site (the so-called micropotential) and is different from the average potential at the inner Helmholtz plane. The difference arises from the discreteness of charge effect in the inner Helmholtz plane. For very low coverages by the adsorbed anions, the constant field approximation is valid and the $\gamma/(\beta + \gamma)$ calculated from an isotherm like eq 17 becomes the same as $(x_2 - x_1)/x_2$ obtained from the integral capacity ratio. At the more negative charges on the electrode this situation was found for the systems Cl^-,[34] I^-,[56] and benzene-*m*-disulfonate[32] in H_2O. At high surface coverage the constant field approximation, however, breaks down[52] and the electrode resembles more a model with "smeared out" charges. Thus, the potential drop due to the adsorbed ions becomes relatively more important. Hence $\gamma/(\beta + \gamma)$ becomes larger than $(x_2 - x_1)/x_2$ and approaches the limit of unity. Parry and Parsons[32] therefore considered ϕ_1 to be the sum of two contributions, one due to the charge on the metal, ${}_q\phi^{m-2}$, and the other due to the specifically adsorbed ions, ${}_{q_{-}1}\phi^{m-2}$. Then

$$\phi_1 - \phi_2 = \frac{x_2 - x_1}{x_2}\,{}_q\phi^{m-2} + \frac{\gamma}{\beta + \gamma}\,{}_{q_{-}1}\phi^{m-2} \qquad (18)$$

Payne[29] used the above equation with the Langmuir isotherm and found the charge-independent Φ'. Also he tried to relate this isotherm based on ϕ_1 to the Frumkin isotherm obtained by the surface pressure method.

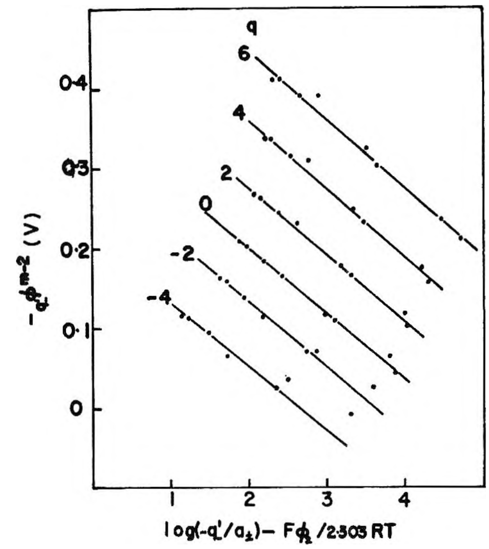

Figure 12. Plot of eq 19 for the various values of the electrode charge (q). q in $\mu C/cm^2$ is indicated by each line.

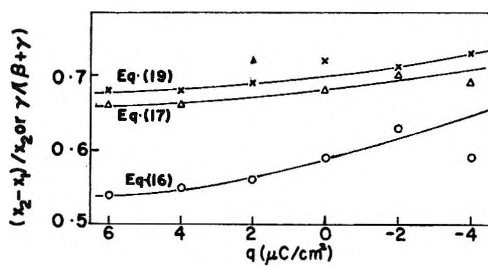

Figure 13. Variation of the distance ratio $(x_2 - x_1)/x_2$ or $\gamma/(\beta + \gamma)$ due to the electrode charge (q) obtained by different methods.

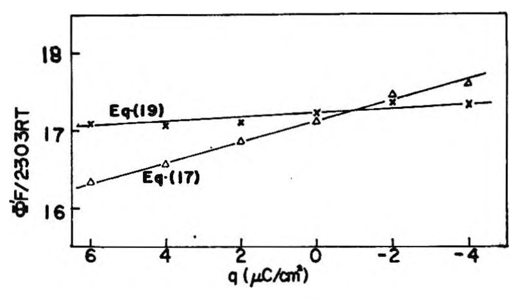

Figure 14. Variation of the Stern adsorption potential in the dimensionless form ($\Phi'F/2.303RT$) due to the electrode charge (q) obtained by different methods.

Since ϕ_1 may include metal–ion and ion–ion interactions, eq 17 could have the form of the virial isotherm. In order to incorporate ϕ_1 into the virial isotherm obtained in the previous section we combined eq 17 and 18, obtaining the equation

(56) D. C. Grahame, *J. Amer. Chem. Soc.*, **80**, 4201 (1958).

$$_{q^1}\phi^{m-2} = \frac{2.303RT}{F}\frac{\beta + \gamma}{\gamma}\log\frac{-q_-^{1}}{a_\pm} - \frac{F\phi_2}{2.303RT} - \frac{\beta + \gamma}{\gamma}\Phi' + \frac{2.303RT}{F}\ln e_0 + \frac{x_2 - x_1}{x_2}{}_q\phi^{m-2} \quad (19)$$

Here we used $k = -e_0$ in eq 17. At the various electrode charges, $_{q_-^1}\phi^{m-2}$ was calculated by subtracting the extrapolated value of ϕ^{m-2} to $q_-^1 = 0$ ($\phi_{q_-^1=0}^{m-2}$) from ϕ^{m-2}; likewise $_q\phi^{m-2}$ was obtained by subtracting the extrapolated value of ϕ^{m-2} (to $q_-^1 = 0$) at $q = 0$ from $\phi_{q_-^1=0}^{m-2}$. By plotting $_{q_-^1}\phi^{m-2}$ *vs.* $\log -q_-^1/a_\pm - F\phi_2/2.303RT$ for the different q's, $\gamma/(\beta + \gamma)$ and $\Phi'F/2.303RT$ as a function of q can be obtained from the slopes and intercepts. $(x_2 - x_1)/x_2$ obtained from the integral capacity ratio was used to calculate $\Phi'F/2.303RT$. The plots of eq 19 are shown in Figure 12. Figures 13 and 14 show the variations of $(x_2 - x_1)/x_2$ on $\gamma/(\beta + \gamma)$ and $\Phi'F/2.303RT$ with q, respectively, together with those values obtained by Grahame's method (eq 17 with $k = -e_0$). The tendency for $\gamma/(\beta - \gamma)$ to approach $(x_2 - x_1)/x_2$ is observed as the electrode becomes negatively charged, and at low coverages the validity of the constant field approximation is confirmed. At high coverages it appears as if the smeared-out charge model would be applicable in this particular system. The constant chemical term of the standard free energy of adsorption ($\Phi'F/2.303RT$) is independent of charge within 0.8%, which shows that the separation of the electrochemical free energy of adsorption into chemical and electrical parts is satisfactory in the present system.

Comparing eq 8b and 19 we may assume that log β at the pzc is equal to $\Phi'F/2.303RT$, and that (d log $\beta/\mathrm{d}q\cdot q$) and $2\beta q_-^1/e_0$ are probably related to $_q\phi^{m-2}\cdot(x_2 - x_1)/x_2$ and $_{q_-^1}\phi^{m-2}\ \gamma/(\beta + \gamma)$, respectively; also ϕ_2 contributes to both q- and q_-^1-dependent terms. ΔG ($q = 0$) $= -21.7$ kcal/mol is compared with the mean value of $\Phi' = 23.4$ kcal/mol. The small discrepancies are not understood at this time.

Acknowledgments. The authors gratefully acknowledge the financial support of this work from the U. S. Army Research Office (Durham) under Grant No. DA ARO-D-31-1240 G 1110 and from the American Chemical Society Petroleum Fund Grant No. 753-C.

Electrolytic Formation of Paramagnetic Intermediate in the Titanium(IV)–Hydrogen Peroxide System

by Helen B. Brooks and F. Sicilio*

Department of Chemistry, Texas A & M University, College Station, Texas 77843 *(Received August 4, 1970)*

Electrolysis of Ti^{IV}–H_2O_2 solutions in an esr–flow system has been employed to study the lower field paramagnetic intermediate, S_1, previously observed in the Ti^{III}–H_2O_2 reaction system. In the electrolytic system S_1 is formed at the anode, so that a direct oxidation of Ti^{IV}–H_2O_2 complex is implied. This result supports the formulation of S_1 as $TiOO\cdot^{3+}$. The electrolytic system is not affected by methanol; so presumably no $\cdot OH$ radicals are produced in this system. S_1 does react with allyl alcohol. Hence, the system is effective in observing whether reactions between substrate and S_1 occur, without the interference of $\cdot OH$ reactions that complicate the Ti^{III}–H_2O_2–substrate reaction system.

Introduction

In the Ti^{III}–H_2O_2 reaction system, two paramagnetic intermediates are observed by electron spin resonance.[1–4] Several investigators[2–4] agree that the lower field intermediate, S_1 ($g = 2.0132$), is a complex of Ti^{IV} and $HOO\cdot$. One formulation for S_1 is $TiOO\cdot^{3+}$.[3,4] However, investigators are not in agreement on the identity of the higher field intermediate, S_2 ($g = 2.0118$).

In the present study Ti^{IV}–H_2O_2 solutions were electrolyzed and the intermediates, S_1 and S_2, were observed by esr spectroscopy. Some of the reactions of S_1 could thus be studied indirectly.

Experimental Section

Reagents. Solutions of Ti^{IV} were prepared from

* To whom correspondence should be addressed.

(1) F. Sicilio, R. E. Florin, and L. A. Wall, *J. Phys. Chem.*, **70**, 47 (1966).
(2) K. Takakura and B. Rånby, *ibid.*, **72**, 164 (1968).
(3) H. Fischer, *Ber. Bunsenges., Phys. Chem.*, **71**, 685 (1967).
(4) W. A. Armstrong, *Can. J. Chem.*, **47**, 3737 (1969).

W. H. Curtin & Co. 20% $TiCl_3$ reagent. The $TiCl_3$ was oxidized by adding excess hydrogen peroxide prepared from Baker Analyzed Reagent (30% solution). The supporting electrolyte was 0.5 or 0.2 M H_2SO_4. Solutions of higher pH were not studied because precipitation occurs. Potassium nitrosodisulfonate, $NO(SO_3K)_2$, Frémy's salt, was prepared according to Moser.[5]

Apparatus. Esr spectra were recorded on a Varian 4502-15 spectrometer. The solution was pumped into a 10-l. reservoir and a nitrogen pressure of 2 atm was applied. The solution was then forced through a Varian V-4556 electrolytic flat cell adapted for continuous flow with connections of Tygon tubing. One electrode was the platinum grid electrode standard with the cell, the other a straight platinum wire. A Heathkit transistorized power supply (Model EUW-17) was connected to electrolyze the solution. The flow rate was regulated by a needle valve in the exit line and measured by timing the collection of known quantities of effluent solution.

Results

During electrolysis of the Ti^{IV}–H_2O_2 solution two resonances were observed. The g values were determined to be 2.0132 and 2.0118 by comparison with Frémy's salt. These resonances correspond, respectively, to the S_1 and S_2 intermediates observed during the reaction of Ti^{III} and H_2O_2. The S_1 species was predominant in all of the electrolysis experiments. S_2 was barely observed in only three experiments (the concentration of S_2 was always less than 1% the concentration of S_1). No quantitative studies of the S_2 radical were thus possible. On the other hand, quantitative studies of S_1 were performed under a variety of conditions.

Effect of Polarity. In several experiments the electrodes were separated by 3 cm, and the polarity of the electrodes was changed. When the direction of flow of the solution was from anode to cathode, the S_1 concentration was approximately 10^{-7} M. But, when the direction of flow of the solution was from cathode to anode, S_1 was not observed even when the sensitivity of the esr spectrometer was increased by a factor of 10.

In the system with the direction of flow from anode to cathode, the concentration of S_1 was found to be approximately the same around both electrodes and in the intervening gap. This type of experiment is subject to large experimental errors due to variations in width of the flat cell, due to displacement of solution by the electrode, and due to the necessity of retuning the esr spectrometer at each position. Hence, these results are only qualitative.

On the other hand, the measurements at one position can be compared quantitatively. Near the cathode the concentration of S_1 increased slowly with time after constant voltage was applied to the cell. The increase in $[S_1]$ was greater with the electrode of larger area. For example, when the electrode of larger area was the cathode, the concentration of S_1 increased by 50% in the time interval 1–3 min after applying the voltage. The slow buildup and the area effect both indicate that adsorption of S_1 on the cathode occurs without immediate reduction of S_1. Evidently, there is an intervening step in the reduction of S_1.

Effects of Alcohols. Intensities of the S_1 signal as a function of alcohol concentration are listed in Table I. Solutions within each set of data were run contiguously. The cell position and the instrument settings were not changed within one set of data so the relative intensities may be compared quantitatively.

Table I: Effects of Added Alcohol[a]

	Area of S_1 (arbitrary units)[b]					
[Methanol]	Set I[c]			Set II[d]		
	A[e]	B	C	A	B	C
0.0	60	58	45	130	160	160
0.1	83	59	41	150	200	220
0.3	80	58	36			
1.0	82	55	35	150	160	160

[Allyl alcohol]	Set III[c]			Set IV[c]			Set V[c]		
	A	B	C	A	B	C	A	B	C
0.0				50	40	25	220	200	160
0.1			80	92	92	70	350	400	300
0.3	66		66				160	180	160
0.7	40		50		32	16			
1.0							60		63

[a] $[Ti^{IV}]_0$ = 0.05 M; $[H_2O_2]_0$ = 0.30 M. Electrode gap $\simeq$ 7 mm. Line width was 1.9 G. Applied potential was 25 V. [b] Precision is within ±20%. [c] Electrolyte, 0.5 M H_2SO_4. [d] Electrolyte, 0.25 M H_2SO_4. [e] A, B, and C denote flow rates of the solution, 7, 3, and 1.6 ml/sec, respectively.

In the Ti^{III}–H_2O_2 reaction, other workers[4,6,7] have found that methanol competes favorably for the ·OH radical product of this reaction. Therefore, methanol was added to the electrolysis system, and S_1 concentrations were observed. The S_1 concentration did not change significantly up to 1.0 M methanol indicating that ·OH is not involved in either the formation of S_1 or the decay of S_1. Thus, the reduction of Ti^{IV} to Ti^{III} with subsequent reaction of Ti^{III} and H_2O_2 is not a significant pathway to S_1 in the Ti^{IV}–H_2O_2 electrolysis system.

In contrast to methanol, allyl alcohol has a definite effect on the S_1 concentration. The concentration of S_1 increases with a small addition of allyl alcohol, 0.1 M, and decreases with larger additions of alcohol. No organic radicals are observed, but the lifetimes of the

(5) W. Moser and R. A. Howie, *J. Chem. Soc. A*, 3039 (1968).
(6) R. O. C. Norman and P. R. West, *ibid.*, *B* 389 (196).
(7) R. E. James and F. Sicilio, *J. Phys. Chem.*, **74**, 2294 (1970).

organic radicals are shorter than the lifetime of S_1.[7] The organic radicals may be present in such a small steady-state concentration that they are not observed.

Discussion

The principal Ti^{IV} species present in the Ti^{IV}–H_2O_2 solution is thought to be TiO_2^{2+}.[8] As seen from the polarity effects, the formation of S_1 occurs at the anode. The simplest mechanism for formation of S_1 is reaction 1.

$$\underset{}{TiO_2^{2+}} \longrightarrow \underset{S_1}{TiOO\cdot^{3+}} + e^- \quad (1)$$

S_1 is the same species supported by Fischer[3] and Armstrong[4] for the Ti^{III}–H_2O_2 system. This reaction is probably not the only oxidation occurring in the system, since the experiments were all performed with a large voltage, 7–25 V, in order to form S_1 in observable quantities.

The cathode reaction is more complex as indicated by the slow adsorption of S_1 on the cathode. Hence, no direct reduction of S_1 is proposed. Instead, a plausible two-step process is proposed where reaction 2 is slower than reaction 3

$$\underset{S_1}{TiOO\cdot^{3+}} + H_2O_2 \longrightarrow O{=}Ti{-}O\cdot^{+} + O_2 + 2H^+ \quad (2)$$

$$O{=}Ti{-}O\cdot^{+} + e^- \longrightarrow O{=}Ti{=}O \quad (3)$$

$$2H^+ + O{=}Ti{=}O + H_2O_2 \longrightarrow TiO_2^{2+} + 2H_2O \quad (3a)$$

Reaction 3a is written since precipitation does not occur in this system; reactions 3 and 3a may be concerted reactions. Other mechanisms which must be considered require that electrolytes in the solution are reduced (reactions 4 and 5)

$$2H^+ + SO_4^{2-} + e^- \longrightarrow \cdot SO_3^{1-} + H_2O \quad (4)$$

$$2H^+ + SO_4^{2-} + 2e^- \longrightarrow SO_3^{2-} + H_2O \quad (5)$$

and the products subsequently react with S_1. Because of the necessarily high voltage one cannot discriminate between mechanisms. The principal reactions should be the ones favored kinetically.

The reactions of S_1 with substrate eliminate some possible reactions and suggest others. Since the concentration of S_1 is independent of the presence of methanol, reactions involving $\cdot OH$ and direct abstraction reactions involving S_1 are eliminated. The change in S_1 concentration with allyl alcohol as a substrate suggests that addition reactions involving S_1 do occur. For small concentrations of allyl alcohol (0.1 M), the increase in S_1 can be explained by the competition between allyl alcohol and S_1 for other radicals formed at the anode. For example, H_2O_2 may also be oxidized as in reaction 6.

$$H_2O_2 \longrightarrow HOO\cdot + e^- + H^+ \quad (6)$$

If reaction 7 competes favorably with reaction 8

$$\cdot OOH + CH_2{=}CHCH_2OH \longrightarrow \text{products} \quad (7)$$

$$\cdot OOH + \underset{S_1}{TiOO\cdot^{3+}} \longrightarrow TiO_2^{2+} + O_2 + H^+ \quad (8)$$

the result will be an increase in the observed concentration of S_1. As the concentration of allyl alcohol is further increased, the alcohol reacts directly with S_1 as in reaction 9

$$TiOO\cdot^{3+} + CH_2{=}CHCH_2OH \longrightarrow \text{products} + Ti^{IV} \quad (9)$$

In the absence of allyl alcohol the decay of S_1 can be described by reaction 10

$$2S_1 \longrightarrow TiO_2^{2+} + O_2 + Ti^{IV} \quad (10)$$

In the presence of allyl alcohol, reaction 9 complements reaction 10 in reducing the concentration of S_1.

In conclusion, two main points have been established. First, the main pathway to S_1 in the electrolysis system is through oxidation of the Ti^{IV}–H_2O_2 complex. This oxidation supports the formulation of S_1 as a complex of Ti^{IV} and $\cdot OOH$, such as $TiOO\cdot^{3+}$. Second, this system is effective in determining if reaction occurs between S_1 and various substrates, without, the interference of $\cdot OH$ reactions that are present in the Ti^{III}–H_2O_2–substrate systems.

Acknowledgment. This research was supported by the Robert A. Welch Foundation Grant A-177.

(8) J. A. Connor and E. A. V. Ebsworth, *Advan. Inorg. Chem. Radiochem.*, 6, 280 (1964).

Transport Processes in Hydrogen-Bonding Solvents. V. Conductance of Tetraalkylammonium Salts in 2-Propanol

by Sister Mary A. Matesich,[1]

Department of Chemistry, Ohio Dominican College, Columbus, Ohio 43219

John A. Nadas,[2] and D. Fennell Evans[3]

Department of Chemistry, Case Western Reserve University, Cleveland, Ohio 44106 *(Received July 20, 1970)*

Precise conductance measurements are reported for Me_4NCl, Bu_4NCl, Me_4NBr, Et_4NBr, Pr_4NBr, Bu_4NBr, Et_4NI, Pr_4NI, Bu_4NI, i-Am_3BuNI, $Hept_4NI$, and Bu_4NClO_4 in 2-propanol at 25°. The data were analyzed with the Fuoss–Onsager equation and with a modified equation proposed by Justice. The association constants were found to increase with increasing anion size and to be larger by a factor of 2–3 than would be predicted from the behavior in the normal alcohols. The association constants are discussed in terms of a multiple-step association process and in terms of a diminished dielectric constant in the vicinity of the ion pairs.

Introduction

Electrolytes in the primary alcohols[4,5] and amides[6] appear to exhibit many of the properties previously observed only in water[7,8] and attributed to the unique structure of that solvent. In the alcohols, ionic association was found to increase with anionic size, a result contrary to the prediction of electrostatic theory. This was interpreted in terms of a multiple-step association process involving hydrogen bonded solvation of anions in the homologous series methanol through 1-pentanol. In water and formamide, an analysis of the concentration dependence of conductance shows that the results are consistent with a small amount of ionic association similar to that observed in the normal alcohols and suggests a rather general pattern of behavior in hydrogen-bonding solvents. In order to study this further we have investigated electrolytes in 2-propanol, an alcohol which is expected to show somewhat different hydrogen-bonding behavior.

Experimental Section

Conductivity grade 2-propanol was prepared by drying the Fisher reagent grade alcohol over calcium oxide for several days and then distilling from a fresh batch of calcium oxide. The distillation was carried out in a 1.3-m Stedman column under nitrogen, and only the middle fraction was retained. The solvent density was measured in a single-neck pycnometer and found to be 0.78097. The viscosity of 0.02079 P was determined using two Cannon–Ubbelohde viscometers. Dannhauser and Bahe's value of 19.41 was used for the dielectric constant.[9]

The tetraalkylammonium salts were purified by recrystallization. The solvents used in the recrystallizations and the temperature at which the salts were dried have been given elsewhere.[4,10]

The electrical equipment, conductance cells, and techniques were similar to those reported previously. Briefly, the measurements were carried out in Kraus-type conductance cells and increments of salt were added to the cell in small Pyrex cups with the aid of the Hawes–Kay cup-dropping device,[11] except for Me_4NCl and Bu_4NCl. Because of the extreme hygroscopic nature of these salts and the difficulties in weighing (with sufficient accuracy) the small amounts required, a Kimax weight buret with a Teflon stopcock was used instead of the cup-dropping device. The cell was initially filled with solvent to a level above that of the tubes which connect the electrode compartment to the erlenmeyer flask. A concentrated stock solution was added to the conductance cell from the weight buret in small increments. The manipulations were held to a minimum and were accomplished rapidly to minimize contamination by atmospheric moisture.

Results

The measured equivalent conductance and corresponding electrolyte concentration in moles per liter are given in Table I. Also given is A, the density increment used to calculate the volume concentrations.

(1) Supported by The Research Participation for College Teachers Program of the National Science Foundation.

(2) Supported by the Undergraduate Research Participation Program of the National Science Foundation.

(3) To whom all correspondence should be addressed.

(4) D. F. Evans and P. Gardam, *J. Phys. Chem.*, **72**, 3281 (1968).

(5) D. F. Evans and P. Gardam, *ibid.*, **73**, 158 (1969).

(6) J. Thomas and D. F. Evans, *ibid.*, **74**, 3812 (1970).

(7) T. L. Broadwater and D. F. Evans, *ibid.*, **73**, 3985 (1967).

(8) R. L. Kay and D. F. Evans, *ibid.*, **70**, 2325 (1966).

(9) W. Dannhauser and L. W. Bahe, *J. Chem. Phys.*, **40**, 3058 (1964).

(10) D. F. Evans, C. Zawoyski, and R. L. Kay, *J. Phys. Chem.*, **69**, 3878, 4208 (1965).

(11) J. L. Hawes and R. L. Kay, *ibid.*, **69**, 2420 (1965).

Table I: Equivalent Conductances in 2-Propanol at 25°

10^4C	Λ
Me_4NCl $A = 0.02$	
2.293	17.623
3.421	16.258
4.067	15.667
6.573	13.939
8.773	12.896
11.429	11.959
13.766	11.312
16.691	10.656
18.054	10.397
Et_4NBr $A = 0.06$	
1.730	21.881
3.488	19.778
6.086	17.800
8.811	16.399
10.427	15.743
12.461	15.063
14.496	14.484
17.163	13.843
Pr_4NBr $A = 0.10$	
1.657	19.821
3.462	18.039
5.746	16.552
8.081	15.464
10.734	14.522
13.745	13.690
17.277	12.920
21.006	12.269
Bu_4NCl $A = 0.01$	
0.9667	18.833
2.299	17.488
3.727	16.496
5.352	15.634
7.190	14.872
8.763	14.335
10.539	13.816
11.753	13.515
Bu_4NClO_4 $A = 0.21$	
1.609	19.929
3.480	17.216
5.726	15.282
8.078	13.923
10.834	12.776
13.189	12.036
17.021	11.092
22.292	10.137
i-Am_3BuNI $A = 0.12$	
0.9616	19.272
2.144	17.236
3.385	15.835
4.813	14.673
6.413	13.692
8.583	12.690
11.099	11.812
14.069	11.018
Me_4NBr $A = 0.08$	
2.066	18.709
4.172	16.279
6.342	14.714
8.810	13.476
11.574	12.467
14.347	11.692
17.260	11.041
21.260	10.322
Et_4NI $A = 0.10$	
3.593	20.523
6.592	18.171
18.153	14.048
22.848	13.142
27.646	12.432
Pr_4NI $A = 0.11$	
1.674	20.551
3.705	18.257
6.139	16.549
7.976	15.608
10.699	14.522
14.579	13.401
17.259	12.795
21.504	12.015
Bu_4NBr $A = 0.09$	
1.765	18.247
3.720	16.478
6.548	14.864
9.660	13.670
12.797	12.784
16.938	11.895
21.595	11.139
27.265	10.428
Bu_4NI $A = 0.10$	
1.348	19.500
2.937	17.432
4.830	15.852
6.825	14.683
8.839	13.787
11.177	12.967
13.763	12.246
17.038	11.519
$Hept_4NI$ $A = 0.13$	
0.8398	17.976
2.110	15.952
3.578	14.498
5.057	13.476
6.831	12.544
8.954	11.707
10.763	11.137
12.988	10.604

These increments were obtained by density measurements on the most concentrated solutions used in the conductance measurements and were assumed to follow the relationship $d = d_0 + A\tilde{m}$, where $\tilde{m}$ is the concentration in moles per kilogram of solution.

Conductance data were analyzed both by the Fuoss–Onsager equation[12] and by the modified equations proposed by Justice.[13]

Table II gives the three parameters Λ_0, K_A, and $\mathring{a}$,

Table II: Conductance Parameters in 2-Propanol at 25°, Calculated from Eq 1

Salt	Λ_0	$\mathring{a}$	K_A	$\sigma\Lambda$
Me_4NCl	23.65 ± 0.06	8.8 ± 0.7	1880 ± 30	0.02
Bu_4NCl	20.69 ± 0.02	8.9 ± 0.5	670 ± 10	0.008
Me_4NBr	24.49 ± 0.03	6.9 ± 0.3	1790 ± 15	0.01
Et_4NBr	26.15 ± 0.01	7.9 ± 0.2	1110 ± 5	0.005
Pr_4NBr	23.09 ± 0.02	6.5 ± 0.2	850 ± 10	0.009
Bu_4NBr	21.52 ± 0.02	6.2 ± 0.2	890 ± 10	0.01
Et_4NI	27.62 ± 0.06	7.3 ± 0.4	1200 ± 20	0.01
Pr_4NI	24.47 ± 0.02	6.1 ± 0.2	1100 ± 10	0.01
Bu_4NI	23.08 ± 0.02	6.6 ± 0.3	1300 ± 10	0.008
i-Am_3BuNI	22.53 ± 0.01	8.0 ± 0.3	1690 ± 10	0.007
$Hept_4NI$	20.67 ± 0.05	15 ± 2	1670 ± 40	0.02
Bu_4NClO_4	25.38 ± 0.02	5.2 ± 0.2	1950 ± 10	0.009

along with their standard deviations, calculated using the least-squares fit program of Kay[14] for the Fuoss–Onsager equation.

$$\Lambda = \Lambda_0 - S(C\gamma)^{1/2} - EC\gamma \ln (C\gamma) + (J - B\Lambda_0)C\gamma - K_A f^2 C\gamma\Lambda \quad (1)$$

The viscosity correction term B was set equal to zero since the value of B does not affect Λ_0 or K_A, but only the value of $\mathring{a}$. As in most other solvents,[10] $\mathring{a}$ does not correlate with crystallographic radii and seems more characteristic of the solvent than of the salt. It is thus difficult to interpret as an ion-size parameter.

Some indication of the precision of the measurements can be obtained from the iodide–bromide difference of 1.47 ± 0.06 in Λ_0 for the Et_4N^+, Pr_4N^+, and Bu_4N^+ salts. The corresponding bromide–chloride difference is 0.85 ± 0.01 for the Me_4N^+ and Bu_4N^+ salts.

The lack of transference numbers precludes the calculation of single-ion limiting conductances from data of Table II. If, however, the Walden product for i-Am_3BuN^+ and $Hept_4N^+$ ions in isopropyl alcohol and ethanol are employed,[4] the estimated limiting ionic conductances given in Table III can be computed. The

(12) R. M. Fuoss and F. Accascina, "Electrolyte Conductance," Interscience Publishers, New York, N. Y., 1959.
(13) R. Bury, M. C. Justice, and J. C. Justice, *C. R. Acad. Sci. Paris*, **268**, 670 (1969).
(14) R. L. Kay, *J. Amer. Chem. Soc.*, **82**, 2099 (1960).

Table III: Estimated Limiting Ionic Conductances at 25°

Ion	λ_0	Ion	λ_0
Me_4N^+	13.10	$Hept_4N^+$	7.78
Et_4N^+	14.68	Cl^-	10.55
Pr_4N^+	11.53	Br^-	11.45
Bu_4N^+	10.14	I^-	12.94
i-Am_3BuN^+	9.55	ClO_4^-	15.24

dependence of ionic mobility on size in 2-propanol is similar to that in other alcohols.[5]

Justice[15] has recently suggested that Bjerrum's critical distance[16] q for 1–1 electrolytes

$$q = \frac{e^2}{2\epsilon kT} \tag{2}$$

which represents that distance between a pair of ions at which the Coulombic attraction is balanced by the average thermal energy, should be used in the Fuoss–Onsager equation in place of the ion-size parameter. It was argued that ions closer together than $r = q$ are paired and do not contribute to the conductance. If one in addition includes terms in $(C\gamma)^{3/2}$ in the modified form of the Fuoss–Hsia equation given by Fernandez-Prini[17] and sets $E = E_1\Lambda_0 - 2E_2$,[18] eq 3 results

$$\Lambda = \gamma(\Lambda_0 - S(C\gamma)^{1/2} + EC\gamma \log C\gamma + J_{(r)}C\gamma + J_{3/2(r)}(C\gamma)^{3/2}) \tag{3}$$

where γ is defined by

$$K_A = \frac{1 - \gamma}{\gamma^2 C f_\pm^2} \tag{4}$$

and the activity coefficients of the free ions are calculated according to the expression[12]

$$\ln f_\pm = -\frac{\beta''(C\gamma)^{1/2}}{1 + \kappa r \gamma^{1/2}} \tag{5}$$

In applying these equations to isopropyl alcohol solutions the Bjerrum value $r = q = 14.4$ Å was used to calculate $J(r)$ and $f_\pm$. The adjustable parameters were Λ_0, K_A, and $J_{3/2}(r)$. The results are given in Table IV.

Although it is questionable whether this treatment is consistent with the hydrodynamic boundary conditions,[19] it contains a well defined distance parameter and gives values of K_A whose dependence upon dielectric constant is in accord with the prediction of theory.[15] As is evident from a comparison of Λ_0 values in Tables II and IV, this parameter is not changed significantly in the Justice treatment. The value of r calculated from the adjusted $J_{3/2}$ terms can be compared to q. Exact agreement would not be expected because the $J_{3/2}$ term is forced to carry uncertainties due to the neglect of higher order concentration terms in the conductance equation and any other approximations. However, the close agreement observed tends to confirm the validity of the Justice treatment.

Discussion

In Figure 1 the association of electrolytes in 2-propanol is compared to that observed in the normal alcohols in a plot of log K_A *vs.* $1/\epsilon$. In every case, the association constants for electrolytes in 2-propanol are larger by a factor of 2–3 than would be predicted from the behavior in the normal alcohols. For comparison, typical association constants in 1-propanol (ϵ 20.4) are $K_A(Bu_4NCl) = 150$, $K_A(Bu_4NBr) = 270$, $K_A(Bu_4NI) = 415$, and $K_A(Bu_4NClO_4) = 770$. As has already been pointed out, association constants in the normal alcohols are unusual in two regards; (1) with few exceptions they increase with increasing anionic size, a behavior that is contrary to the predictions of Coulombic theory, and (2) they are much larger than predicted on the basis of simple Coulombic theory. In 2-propanol the same inverted dependence of K_A upon size is observed, but the disparity between the calculated and observed association constant is even larger. It is these factors that we wish to discuss in some detail.

There is no universal agreement as to what constitutes an ion pair. According to one view, two ions may be regarded as paired if they are in actual contact, that is, if their separation is equal to the sum of their radii. Fuoss[20] has calculated that the concentration of such ion pairs in a dilute solution in a dielectric continuum can be calculated by

$$K_A = \frac{4\pi \mathring{N} a_K^3}{3000} \exp\left(\frac{e^2}{a_K \epsilon kT}\right) \tag{6}$$

where the equilibrium constant is for reaction

$$C^+ + A^- \underset{k_r}{\overset{k_f}{\rightleftharpoons}} C^+A^- \tag{7}$$

Eigen[21] also obtained the result given in eq 6 from a consideration of diffusion-controlled rates of formation and dissociation of ion pairs since

$$K_A = \frac{k_f}{k_r} \tag{8}$$

Thus eq 6 applies to any process in which ion pair formation and dissociation are controlled only by coulombic and thermal forces.

Alternatively, two ions may be regarded as paired if

(15) J. C. Justice, R. Bury, and C. Treiner, *J. Chim. Phys.*, **65**, 1708 (1968); J. C. Justice, *ibid.*, **66**, 1193 (1969).

(16) N. Bjerrum, *Kgl. Dan. Vidensk. Selsk.*, **7**, 9 (1926).

(17) R. M. Fuoss and K. L. Hsia, *Proc. Natl. Acad. Sci. U. S.*, **57**, 1550 (1967); **58**, 1818 (1967); R. Fernandez-Prini, *Trans. Faraday Soc.*, **65**, 3311 (1969).

(18) M. S. Chen, Ph.D. Thesis, Yale University, 1969.

(19) R. M. Fuoss, private communication.

(20) R. M. Fuoss, *J. Amer. Chem. Soc.*, **80**, 5059 (1958).

(21) M. Eigen, *Z. Phys. Chem.* (*Frankfurt am Main*), 176 (1954).

Table IV: Conductance Parameters in 2-Propanol at 25°, Calculated from Eq 3

Salt	Λ_0	K_A	$R_{J3/2}$	$\sigma\Lambda$
Me_4NCl	23.72 ± 0.05	1960 ± 20	12 ± 1	0.009
Bu_4NCl	20.70 ± 0.01	734 ± 6	10.7 ± 0.8	0.006
Me_4NBr	24.55 ± 0.02	1887 ± 6	14.6 ± 0.2	0.004
Et_4NBr	26.20 ± 0.01	1183 ± 4	13.6 ± 0.2	0.003
Pr_4NBr	23.145 ± 0.007	951 ± 2	13.2 ± 0.2	0.003
Bu_4NBr	21.590 ± 0.008	999 ± 3	13.2 ± 0.1	0.003
Et_4NI	27.73 ± 0.07	1300 ± 18	13.4 ± 0.6	0.009
Pr_4NI	24.52 ± 0.02	1195 ± 8	14.1 ± 0.5	0.009
Bu_4NI	23.121 ± 0.009	1394 ± 4	13.7 ± 0.2	0.003
i-Am_3BuNI	22.56 ± 0.01	1772 ± 5	12.4 ± 0.5	0.004
$Hept_4NI$	20.67 ± 0.03	1670 ± 20	3 ± 5	0.012[a]
Bu_4NClO_4	25.44 ± 0.01	2072 ± 5	15.6 ± 0.2	0.003

[a] Highest concentration too small.

Table V: Predicted and Observed Association Constants for Tetraalkylammonium Salts at 25° for Estimated Interionic Distances

Solvent	ϵ	K_A, eq 8			K_A, eq 9			Range of K_A, obsd
		5 Å	8 Å	10 Å	5 Å	8 Å	10 Å	
MeOH	32.62	10	11	14	16	3	...[e]	14–36[a]
EtOH	24.33	32	23	25	63	27	11	90–199[b]
1-PrOH	20.45	76	40	39	142	66	40	262–903[b]
2-PrOH	19.41	102	48	45	180	86	54	734–2127[c]
1-BuOH	17.45	194	71	63	300	136	93	811–2473[d]

[a] Data of ref 10. [b] Data of ref 4. [c] This work, Table IV. [d] Data of ref 5. [e] Equation 9 cannot be used because 10 Å is greater than q.

the distance between their centers is less than the Bjerrum q (eq 2). To calculate K_A in this case, one must integrate from the distance of closest approach, which may be approximated as the sum of the crystallographic radii, to q. Assuming that the solvent is a continuous dielectric, Bjerrum[16] derived

$$K_A = \frac{4\pi \mathring{N}}{1000}\left(\frac{e^2}{\epsilon kT}\right)^3 \int_2^b e^t t^{-4}\,dt \qquad (9)$$

where

$$b = \frac{e^2}{r\epsilon kT} \qquad (10)$$

The upper limit corresponds to $r = q$. The lower limit corresponds to $r = a$, the distance of closest approach.

The Bjerrum equation has been criticized on the grounds that the discrete, molecular nature of the solvent makes the integration of eq 7, based on a continuous distribution of ions as a function of r, physically unrealistic. This criticism is well founded. However, eq 6 is also unrealistic in solvents of intermediate dielectric constant or for multivalent electrolytes where ions farther apart than actual contact still do not contribute to the conductance, and thus are effectively associated.

The sum of the crystallographic radii of the smallest ions studied here, Me_4N^+ and Cl^-, is 5.28 Å. Thus a values below 5 Å seem unrealistic, and a values as large as 10 Å would be reasonable for the larger ions or for tightly solvated ions. In Table V K_A values calculated from eq 6 and 9 for five alcohols are compared to the range of K_A values actually observed for tetraalkylammonium salts. In all cases both equations underestimate K_A. In order to calculate association constants of the magnitude of those observed within the continuum framework of eq 6 and 9, unrealistically small ionic contact distances of 2.5 to 3.0 Å would be needed.

If ionic mobilities determine the rate of formation of ion pairs, k_f of eq 8, then the unusually high values for K_A must reflect small values for k_r. In other words, it is "harder" for ions to diffuse apart than the Coulomb potential predicts. Continuum models thus fail. We propose two explanations based on a consideration of the behavior of solvent molecules in the vicinity of the ion pair.

One explanation is that two or more different kinds of ion pairs exist.[4] The ion pairs initially formed may either diffuse apart or react to form the second kind. For tetraalkylammonium ions the simplest scheme is

$$R_4N^+ + A^-(ROH)_n \underset{}{\overset{K_1}{\rightleftharpoons}} R_4N^+(ROH)_nA^- \overset{K_2}{\rightleftharpoons} R_4N^+A^-(ROH)_{n-1} + ROH \qquad (11)$$

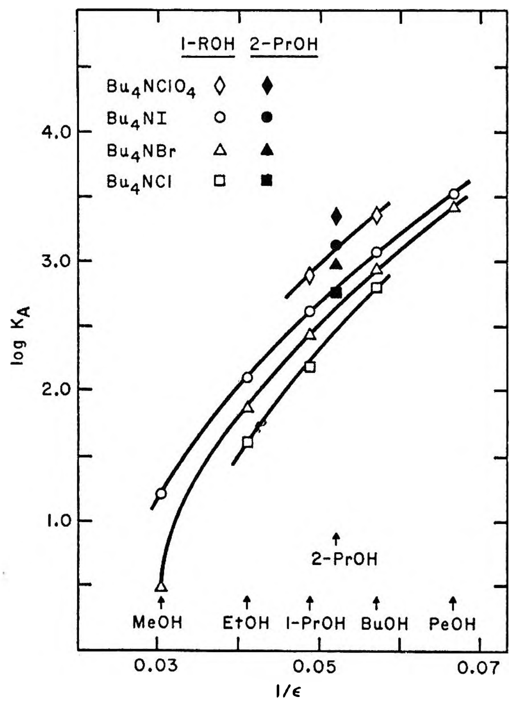

Figure 1. Comparison of association constants for the tetrabutylammonium salts in 2-propanol and the normal alcohols.

With the assumption that essentially every anion in solution is solvated by n solvent molecules it can be shown that the apparent association constant is given by

$$K_A = K_\Sigma = \frac{\sum C_{(\text{ion pairs})}}{(C_{R_4N^+})(C_{A^-(ROH)_n})} = K_1\{1 + K_2/[\text{ROH}]\} \quad (12)$$

The Fuoss–Eigen equation (6) can be used to estimate K_1. For the dielectric constants of the alcohols eq 6 is not a sensitive function of a between 8 and 12 Å which is a reasonable range for solvent-separated ion pairs. Average values of K_1, for a values between 8 and 12 Å, of 25, 40, 46, and 65 for ethanol, 1-propanol, 2-propanol, and 1-butanol, respectively, have been used to calculate K_2 according to eq 12 from the Fuoss–Onsager K_A values (Table II). The K_2 values given in Table VI differ from those reported[4] previously because they have been corrected for the solvent concentration.

Also included in Table VI are relative acidities of the alcohols. The primary alcohols are 8 to 12 times more acidic than 2-propanol, and consequently would be expected to hydrogen-bond more effectively with anions. The diminished hydrogen-bonding ability of 2-propanol would result in less stabilization for the solvent-separated ion pairs in this solvent than in the primary alcohols. Consequently, K_2 values for 2-propanol would be larger than for the primary alcohols. Since the case of desolvation of anions is inversely related to their radii and directly related to the magnitude of K_2, K_2 should

Table VI: Estimated Values of K_2 for Tetrabutylammonium Salts from Eq 12

Salt	EtOH	1-PrOH	2-PrOH	1-BuOH
Bu_4NCl	9.5	36	180	94
Bu_4NBr	34	75	240	130
Bu_4NI	67	120	350	190
Bu_4NClO_4	...	240	540	360
Acidity, K_e[a]	0.95	0.5	0.076	0.6

[a] K_e = $[A^-]/[HA][2\text{-PrO}^-]$ for alcohols HA by indicator titration: J. Hine and M. Hine, *J. Amer. Chem. Soc.*, **74**, 5266 (1952).

be in the order $ClO_4^- > I^- > Br^- > Cl^-$, as observed. Thus the multiple-step association process qualitatively accounts for the association behavior in the alcohols and for the large values of K_A in 2-propanol.

The Justice–Bjerrum treatment, however, suggests another explanation for the high association constants observed in the alcohols.

It has been recognized for some time that alcohols have anomalously high dielectric constants for their dipole moments.[22] 2-Propanol and all of the normal alcohols, methanol through pentanol, have dipole moments[23] (as determined in the gas phase) and dielectric constants[4,5] which fall within the ranges 1.63 to 1.69 and 15.0 and 32.6 D, respectively. In contrast, esters such as methyl acetate, ethyl acetate, and ethyl formate and halogenated hydrocarbons such as iodomethane and dichloromethane have dipole moments[24] ranging from 1.7 to 1.9 and 1.4 to 1.6 D, respectively, but dielectric constants of 6 to 7 which are considerably lower than those observed for the alcohols. The magnitude of ϵ in alcohols has been attributed to structures arising from hydrogen bonding as reflected in the high values for the Kirkwood g factor.[9] However, within the Bjerrum distance q extensive hydrogen bonding between alcohol molecules is unlikely because of the orientation of alcohol dipoles by the ions. Therefore the effective dielectric constant within the Bjerrum sphere $r = q$ may be appreciably smaller than the bulk dielectric constant.

A naive approach for estimating this effect is to set the dielectric constant within q equal to some constant value smaller than the bulk dielectric constant and to continue to use the bulk dielectric constant for $r > q$. This step function for the dielectric constant creates

(22) W. M. Latimer and W. H. Rodebush, *J. Amer. Chem. Soc.*, **42**, 1419 (1920); L. Pauling, "The Nature of the Chemical Bond," Cornell University Press, Ithaca, N. Y., 1939.

(23) A. A. Maryott and F. Buckly, National Bureau of Standards Circular No. 537, U. S. Government Printing Office, Washington, D. C., 1953.

(24) A. A. Maryott and E. R. Smith, National Bureau of Standards Circular No. 514, U. S. Government Printing Office, Washington, D. C., 1951.

problems in the electrostatic analysis of ionic interactions. However, a diminution of dielectric constant in the immediate vicinity of an ion seems physically reasonable for hydrogen-bonding solvents and a qualitative estimate of its effect on the association constant is provided with the naive model.

Equation 9, which applies within q, has been used with an effective dielectric constant of 10 to estimate values of K_A as a function of a. The calculated values agree with the range of K_A observed as given in Table IV when the reasonable a values between 8 and 14 Å are employed.

The same pattern is observed with the other alcohols. A reasonable value of ϵ_{eff} can be found to reproduce the observed range of association constant. However, this explanation does not account for the dependence of K_A upon the nature of the anion, whereas in the first explanation this can be attributed to a specific solvent–ion interaction.

Two explanations based on the behavior of solvent molecules in the immediate vicinity of the ion pairs have thus been offered for the high association of tetraalkylammonium salts in alcohols, which cannot be explained by continuum models. Relaxation measurements and studies involving solvents with different hydrogen-bonding characteristics are in progress. These should help elucidate the relative importance of multistep association processes and diminished dielectric constant on ionic association.

Acknowledgment. We wish to thank Professor J. C. Justice for computing the results given in Table IV and for many helpful discussions. This work was supported by Contract No. 14-01-001-1281 with the Office of Saline Water, U. S. Department of the Interior.

Ionic Interactions in Solution. II. Infrared Studies

by R. P. Taylor[1] and I. D. Kuntz, Jr.*

Frick Chemical Laboratory, Princeton University, Princeton, New Jersey 08540 *(Received June 15, 1970)*

Hydrogen bonding between phenol and a number of anions is studied by infrared spectroscopy. Small anions have multiple solvation equilibria, and stepwise association constants are determined by measuring solvation numbers (phenolation numbers) as a function of anion and phenol concentration. Concomitant nmr studies indicate that low concentrations of phenol markedly influence ion association equilibria in low dielectric solvents. In these solvents the evidence suggests that solvation of anions by phenol changes contact to solvent-separated ion aggregates. The phenol–anion association constants appear to be independent of the type and degree of ion association.

Introduction

A number of workers have shown that strong hydrogen bonds exist between alcohols and halide anions in solution.[2a,b] Equilibrium constants for the formation of 1:1 alcohol–halide anion complexes have been measured in CCl_4 solution.[2b] We have shown that this hydrogen bonding interaction can strongly influence ion association for halide salts in low dielectric solvents.[3]

In the present work we measure anion solvation numbers by investigating the effects of a variety of salts on the OH stretching frequency of phenol. We determine the effect of phenol on the ion association equilibrium by correlating these results with concomitant nmr studies.

Experimental Section

Infrared spectra were recorded on a Beckman IR-12 spectrophotometer operating in the double beam absorption mode. Barnes liquid cells with potassium bromide windows and 0.5-mm Teflon spacers were used. Measured absorbances were usually between 0.20 and 0.80 absorbance unit and were in general reproducible to ±0.01 absorbance unit. We estimate the ambient temperature for the ir experiment as about 40°. Nmr spectra were recorded on a Varian A-60-A spectrometer, and chemical shifts (relative to internal TMS, 1% v/v), accurate to ±1 Hz, were measured by the usual methods. Ambient probe temperature was 40°.

Methylene chloride was distilled from P_2O_5 onto

* To whom correspondence should be addressed.

(1) NSF Predoctoral Fellow, 1969–1970.

(2) (a) A. Allerhand and P. von R. Schleyer, *J. Amer. Chem. Soc.*, **85**, 1223 (1963); (b) R. D. Green, J. S. Martin, W. B. McG. Cassie, and J. B. Hyne, *Can. J. Chem.*, **47**, 1639 (1969).

(3) R. P. Taylor and I. D. Kuntz, Jr., *J. Amer. Chem. Soc.*, **92**, 4813 (1970).

molecular sieves. Control experiments indicated that the traces of water (~0.1% by volume) which this solvent absorbs on exposure to air had no effect on the experimental results. Carbon tetrachloride (spectroscopic grade) was dried over P_2O_5 and filtered before use. Nitromethane (spectroscopic grade) was used without further purification. Phenol was distilled under vacuum into a separatory funnel with a Teflon stopcock and stored in a desiccator.[4] Solutions of known phenol concentration were prepared gravimetrically by heating the separatory funnel and allowing the phenol to drip out into preweighed 50-ml volumetric flasks which were reweighed and filled to mark with solvent.[4] Such stock solutions were then used to prepare solutions of the salts. The salts were purchased or prepared by standard techniques, recrystallized, and dried for a few hours at 80° under reduced pressure before they were used.

Experimental Procedure. Mathematical Preliminaries. If we assume the existence of a number of mononuclear complexes between phenol molecules and a given anion, then the following equations hold.[5]

$$\mathrm{PhOH} + \mathrm{X^-} \underset{}{\overset{K_1}{\rightleftarrows}} (\mathrm{PhOH}\ldots\mathrm{X^-})$$

$$\mathrm{PhOH} + (\mathrm{PhOH}\ldots\mathrm{X^-}) \overset{K_2}{\rightleftarrows} ((\mathrm{PhOH})_2\ldots\mathrm{X^-}) \quad (1)$$

The K_n's are the appropriate stepwise association constants. We define the anion's solvation number $\bar{n}$ (in this case phenolation number) as

$$\bar{n} = \frac{\varphi_T - \varphi_F}{X_T^-} \quad (2)$$

where φ_T is the total concentration of phenol in solution, φ_F is the concentration of free phenol, and X_T^- is the formal anion concentration. The equations can be rearranged to give (for the case of $n = 3$)

$$\bar{n} = \frac{\varphi_F[K_1 + 2K_1K_2\varphi_F + 3K_1K_2K_3\varphi_F^2]}{1 + K_1\varphi_F + K_1K_2\varphi_F^2 + K_1K_2K_3\varphi_F^3} \quad (3)$$

The observed solvation number $\bar{n}$ should depend upon the stepwise association constants and the concentration of free phenol. φ_F is the only independent variable, as seen in eq 3. Plots of $\bar{n}$ *vs.* φ_F must superimpose for all values of X_T^- and φ_T for each system studied.

Results and Discussion

Ir. The absorbance of the free OH peak of phenol (at 3585 cm^{-1}) in methylene chloride follows Beer's law behavior up to moderate phenol concentrations (~0.1 *M*). When a variety of salts are added to such solutions, the free phenol OH peak intensity decreases and a broad intense hydrogen bonded peak develops at lower frequency. φ_F is measured directly from the ir experiment from the height of the free peak, and X_T^- and φ_T are known as they are simply the formal concentrations

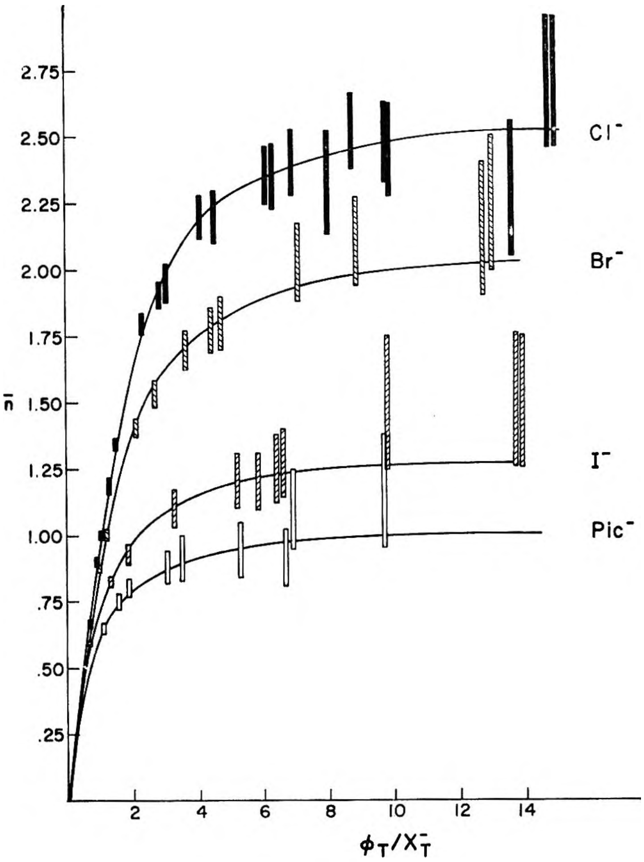

Figure 1. Average value plots, $\bar{n}$ *vs.* phenol concentration/salt concentration (φ_T/X_T^-), for the interaction of phenol with the anions of a number of methyltriphenylphosphonium salts. The salt concentrations are varied, the concentration of phenol is held fixed [0.118 *M* ± 0.001 *M*]: ■, Cl^-; ▨, I^-; ▧, Br^-; □, Pic^- (Picrate; 2,4,6-trinitrophenolate). The lines drawn through the experimental points were calculated based on the following parameters which were obtained from analysis of the data points for the methyltriphenylphosphonium salts [Other phenol concentrations were used, see Figure 2]: Cl^-, $K_1 = 400$; $K_2 = 26$; $K_3 = 26$; Br^-, $K_1 = 112$; $K_2 = 19$, $K_3 = 7$; I^-, $K_1 = 29$; $K_2 = 8$; $K_3 = 0$; Pic^-, $K_1 = 18$; $K_2 = 5$; $K_3 = 0$.

of anion and phenol. Thus, $\bar{n}$ can be determined by eq 2.

Plots of $\bar{n}$ *vs.* φ_T/X_T^- (Figure 1) for the interaction of halide and picrate anions with phenol in methylene chloride clearly indicate that there exist multiple solvation equilibria. As predicted in eq 3, $\bar{n}$ depends upon φ_f (see Figure 2). Stepwise association constants were calculated by fitting the data to eq 4 (see Table I).

$$\varphi_F = \varphi_T - \frac{[X_T^-][K_1\varphi_F + 2K_1K_2\varphi_F^2 + 3K_1K_2K_3\varphi_F^3]}{1 + K_1\varphi_F + K_1K_2\varphi_F^2 + K_1K_2K_3\varphi_F^3} \quad (4)$$

The uncertainty in $\bar{n}$ clearly depends upon X_T^- and φ_T

(4) L. Joris, Ph.D. Thesis, Princeton University, 1967.

(5) F. J. C. Rossotti and H. Rossotti, "The Determination of Stability Constants," McGraw-Hill Book Co., Inc., New York, N. Y., 1961.

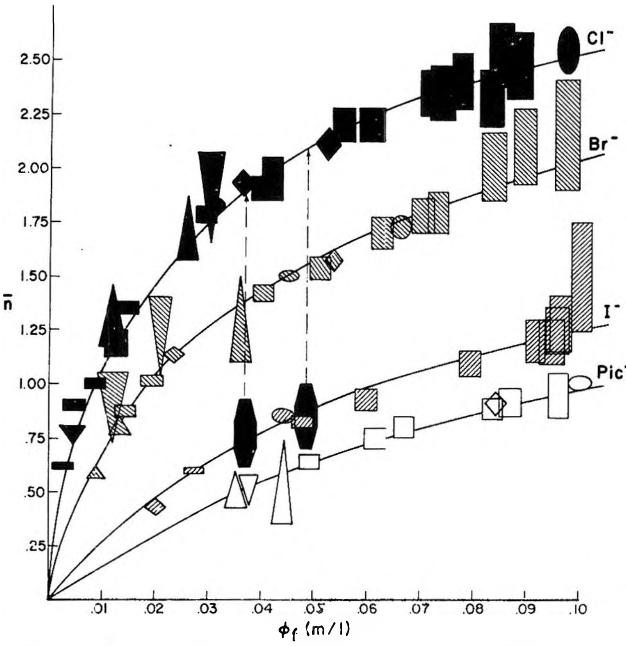

Figure 2. $\bar{n}$ *vs.* concentration of free phenol (φ_f) for the phenol–anion interactions. The lines drawn through the experimental points were calculated based on the K_n values of Figure 1. Some of the data points of Figure 1 were omitted for clarity. Cl^- points: ▮, taken from Figure 1; ⬮, cation is $CH_3P^+Ph_3$ and phenol concentration = 0.1849 *M*; ◆, cation is $CH_3As^+Ph_3$ and phenol concentration = 0.0513 *M*; ▲, cation is $(C_2H_5)_4N^+$ and phenol concentration = 0.0873 *M*; ▼, cation is $CH_3P^+Ph_3$ and phenol concentration = 0.0513 *M*; ⬣, cation is $(C_2H_5)_3N^+H$ and phenol concentration = 0.0873 *M*; Br^- points: ▧, taken from Figure 1; ◍, cation is $CH_3P^+Ph_3$ and phenol concentration = 0.1849 *M*; ◈, cation is $(n\text{-}C_4H_9)_4N^+$ and phenol concentration = 0.118 *M*; ▲, cation is $CH_3P^+Ph_3$ and phenol concentration = 0.0513 *M*; ▼, cation is $(C_2H_5)_4N^+$ and phenol concentration = 0.0873 *M*. I^- points: ▨, taken from Figure 1; ◍, cation is $CH_3P^+Ph_3$ and phenol concentration = 0.1849 *M*; ◇, cation is $CH_3P^+Ph_3$ and phenol concentration = 0.0513 *M*. Pic^- points: ▯, taken from Figure 1) ◯, cation is $CH_3As^+Ph_3$ and phenol concentration = 0.1849 *M*; ◇, cation is $CH_3P^+Ph_3$ and phenol concentration = 0.1849 *M*; △, cation is $CH_3P^+Ph_3$ and phenol concentration = 0.0513 *M*; ▽, cation is $CH_3As^+Ph_3$ and phenol concentration = 0.0513 *M*.

but the experimental uncertainty in φ_F is constant, and eq 4 was used to give equal weight to all data.[6] Excellent fits were obtained; the average deviation between calculated and observed values of φ_F was less than 0.002 *M*. We have also measured such multiple solvation equilibria in other solvents (Table I).

For a variety of quaternary onium salts, differences in cation effects are small (Figure 2). Triethylammonium hydrochloride is clearly a special case as it falls far below the line for the other chloride salts (Figure 2). We believe that in this case hydrogen bonding between the cation and anion substantially reduces the phenol–chloride interaction. A second possibility is that phenol acts as a base toward the cation.[7] Further ir studies could resolve this question.

The relative magnitudes of the K_1's show the expected dependence on anion charge density.[8] The fact that

Table I

Anion[a]		Solvent: methylene chloride K_1 (l./mol)	K_2 (l./mol)	K_3 (l./mol)
Cl^-		400 ± 120	25 ± 10	25 ± 10
Br^-		100 ± 30	20 ± 8	7 ± 3
I^-		30 ± 9	10 ± 4	0
Pic^-[b]		20 ± 6	5 ± 2	0
Anion	**Solvent**			
Br^-[c]	Carbon tetrachloride	1300 ± 600	150 ± 50	30 ± 10
Br^-[a]	Methylene chloride	100 ± 30	20 ± 8	7 ± 3
Br^-[d]	Nitromethane	30 ± 10	3 ± 2	0

[a] Methyltriphenylphosphonium salt was used. [b] Pic^-: Picrate anion (2,4,6-trinitrophenolate). [c] Tetrabutylammonium salt was used. Lower phenol concentrations were used (φ_F was always less than 0.02 *M*) to minimize effects of phenol dimerization. [d] Tetrabutylammonium salt was used.

the association constants for formation of the 2:1 and 3:1 complexes are substantially smaller than for the 1:1 complexes suggests that there must be considerable distortion of the electron density of the anions on formation of the 1:1 hydrogen bonded complex.

We emphasize that the K_n's are not absolute, but relative. Other equilibria may be important. Nitromethane and methylene chloride are certainly not inert; they may interact with the anions and can act as weak bases toward phenol. For example, we determined the equilibrium constant for formation of the hydrogen bond between phenol and nitromethane in carbon tetrachloride to be about 2 l./mol. In addition, the cations may compete with the phenol to achieve close proximity to the anions; that is, the observed K_n's may be influenced by the effects of ion association. However, we believe this latter effect is unimportant (see below).

Nmr. The α-methyl nmr frequencies of the methyltriphenylphosphonium salts dissolved in methylene chloride are nearly insensitive to salt concentration (Figure 3). However, in the presence of low concentrations of phenol the chemical shifts show marked salt concentration dependence (Figure 3). In addition, for fixed salt concentrations, addition of small amounts of phenol significantly alters the cation chemical shifts (Table II). These effects are more pronounced at lower temperature (Table II).

We offer the following interpretation of these nmr results. There should be extensive ion association in a low dielectric solvent such as methylene chloride.[9,10]

(6) W. F. Wentworth, *J. Chem. Educ.*, **42**, 96 (1965).
(7) H. B. Flora and W. R. Gilkerson, *J. Amer. Chem. Soc.*, **92**, 3273 (1970).
(8) R. D. Green and J. S. Martin, *ibid.*, **90**, 3659 (1968).
(9) J. T. Denison and J. B. Ramsey, *ibid.*, **77**, 2615 (1955).
(10) R. M. Fuoss, *ibid.*, **80**, 5059 (1958).

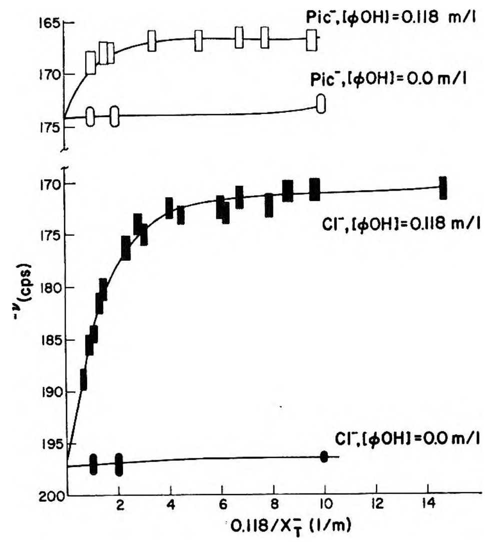

Figure 3. Chemical shifts of some methyltriphenylphosphonium salts as a function of salt concentration in methylene chloride. Results in the presence and absence of 0.118 M phenol are shown. The reciprocal of salt concentration × 0.118 is plotted on the abscissa to facilitate comparison with the results in Figure 1.

Table II: Effect of Phenol on the α-Methyl Proton Magnetic Resonance Frequencies of Some Methyltriphenylphosphonium Salts in Methylene Chloride[a]

Salt	[PhOH] = 0.0 M $-\nu$	[PhOH] = 0.25 M $-\nu$	[PhOH] = 0.25 M $\Delta\nu$
	T = 40°		
$CH_3P^+Ph_3Cl^-$	196.8	167.4	29.4
$CH_3P^+Ph_3I^-$	185.6	170.9	14.6
$CH_3P^+Ph_3Pic^-$	173.8	162.9	10.9
	T = −44°		
$CH_3P^+Ph_3Cl^-$	193.1	157.6	35.5
$CH_3P^+Ph_3I^-$	185.0	162.4	22.6
$CH_3P^+Ph_3Pic^-$	177.2	156.6	20.6

[a] Salt concentrations are 0.05 M.

We assume that ion association significantly affects the cation chemical shifts only when contact species are formed.[3] There is also evidence that, for the anions under consideration, ion association (involving contact species) causes the cation chemical shifts to be displaced downfield.[3] If we accept the above, then we conclude from the nmr and ir results that phenol coordinates to the anions through hydrogen bonding and thus considerably reduces the concentration of contact species. The temperature dependence of this effect is consistent with the negative enthalpy which characterizes hydrogen bond formation.[11]

The fact that relatively low concentrations of phenol can significantly affect the cation chemical shifts suggests that the hydrogen bonding interaction between phenol and the anions must be at least competitive with the electrostatic effects which favor formation of contact species in methylene chloride.[9,10] More importantly, we shall show below that the observed trend of the K_n's in different solvents indicates that the phenol–anion equilibria are in fact independent of the degree of ion association.

Intuitively we would expect the effects of ion association would be greatest in carbon tetrachloride (dielectric constant = 2.2), reduced somewhat in methylene chloride (dielectric constant = 8), and almost negligible in nitromethane (dielectric constant = 34.2).[12] Continuum theory[9,10] would predict that the ion association equilibrium constants in carbon tetrachloride and nitromethane would differ by more than 15 orders of magnitude. If we assume that anions paired with cations have a weaker hydrogen bonding interaction with phenol than do "free" anions, then the K_n's should be smallest in carbon tetrachloride and largest in nitromethane.

In fact, we observe just the *opposite* trend in the K_n's (Table I). Part of the decrease in the K_n's is due to hydrogen bonding between phenol and the two higher dielectric solvents. In nitromethane (~15 M) the concentration of free phenol (that is, phenol not hydrogen bonded to nitromethane) would be $\sim 1/(1 + KS) \sim 1/31$ as large as the concentration of free phenol in carbon tetrachloride (K = 2 l./mol, and S = nitromethane concentration).[13] The K_n values are in agreement with this prediction (Table I).

It is clear that the K_n's do not decrease in lower dielectric solvents as expected from the effects of ion association. The trend we observe can be explained by interaction of phenol with the various solvents. We conclude that the association of halide anions with quaternary onium cations does not affect the strength of the phenol–anion hydrogen bonds.

It should be recalled that our nmr results indicate that the concentration of contact species *is* significantly reduced when phenol–anion hydrogen bonds are formed. Whether phenol acts by forming free solvated ions or solvent-separated ion pairs[14] is open to question, but there is strong evidence that solvent-separated ion pairs are the predominant species for salts in low dielectric

(11) G. C. Pimentel and A. L. McClellan, "The Hydrogen Bond," Freeman and Co., San Francisco, Calif., 1960.

(12) Dielectric constants at 40°, estimated from the data in A. A. Maryott and F. A. Smith, "Table of Dielectric Constants of Pure Liquids," National Bureau of Standards Circular No. 514, U. S. Government Printing Office, Washington, D. C., issued August, 1951.

(13) I. D. Kuntz, F. P. Gasparro, M. D. Johnson, and R. P. Taylor, *J. Amer. Chem. Soc.*, **90**, 4778 (1968).

(14) Associated species of higher stoichiometry probably exist in CCl_4 and CH_2Cl_2, but the same arguments apply.

solvents which contain low concentrations of "coordinating solvent."[15,16] The discussion that follows, however, is unaltered if free ions are formed instead of solvent-separated species.

If we assume that the addition of phenol leads to the formation of solvent-separated ion pairs in carbon tetrachloride (dielectric constant = 2.2) and methylene chloride (dielectric constant = 8.0), then our results indicate that the *difference* in free energy between contact and solvent-separated species is the same in both solvents. This effect may be explained in either of two ways.[17] (a) The short-range properties of ions in solution are independent of the dielectric constant of the medium. (b) Alternatively, the free energies of the two species vary from solvent to solvent, but they do so in parallel. While our experiments do not allow us to distinguish between these two possibilities, we note that the results *are* in opposition to continuum theories,[9,10] which would predict that the difference in free energies between contact and solvent-separated species should *increase* as the dielectric constant of the solvent is lowered. We conclude that the magnitude of the contact interionic interactions in solution must be considerably less than would be expected on the basis of continuum theory, and, as previously mentioned, must be no stronger than specific short-range effects such as hydrogen bonding or ion–dipole interactions.

We can imagine certain instances in which these contact interactions would be considerably stronger. Direct hydrogen bonding between cation and anion would be one case; the formation of a covalent bond between cation and anion would be a second example.[18] Lastly, small cations (*e.g.*, Li^+) or multiply charged species might show cation effects on the hydrogen bonding ability of anions.

Our results can be readily generalized to include other protic systems. Multiple solvation equilibria should be possible for anions of high charge density in most alcohols and water. Whereas the total amount of ion association will (to first approximation) depend upon the solvent's dielectric constant,[9,10] it is likely that the nature of the associated species will be strongly influenced by the relative strength of the solvent–anion hydrogen bond.

Evans and Gardam[19] reached a similar conclusion in their investigation of the conductance of the tetraalkylammonium salts in the straight-chain alcohols. Their results are most consistent with a two-state association model which allows for the existence of both contact and solvent-separated ion pairs.

(15) E. D. Hughes, C. K. Ingold, S. Patai, and Y. Packer, *J. Chem. Soc.*, 1206 (1957).

(16) See, for example, the work of Smid and coworkers on systems involving ion–dipole interactions: L. L. Chan and J. Smid, *J. Amer. Chem. Soc.*, **90**, 4654 (1968), and earlier papers.

(17) We thank Professor Spiro for some helpful suggestions regarding this discussion.

(18) Some heavy metal halides exhibit this behavior. See G. E. Coates, "Organo-Metallic Compounds," Wiley, New York, N. Y., 1956, p 151.

(19) D. F. Evans and P. Gardam, *J. Phys. Chem.*, **73**, 158 (1969).

Gravitational Stability in Isothermal Diffusion Experiments of Four-Component Liquid Systems[1]

by Hyoungman Kim

Institute for Enzyme Research, University of Wisconsin, Madison, Wisconsin 53706 *(Received July 7, 1970)*

The conditions for gravitational stability in free diffusion and the diaphragm cell method of studying diffusion in four-component systems are obtained. For each boundary condition, three criteria should be satisfied in order to definitely avoid convective mixing during the diffusion experiments.

Introduction

In any diffusion experiment, it is imperative to have gravitational stability everywhere in the column of diffusing liquid during the entire duration of the experiment, for otherwise, convective mixing will render meaningless the diffusion coefficients obtained from the experiment. In the study of diffusion of a two-component system, initial stability at the time of boundary formation will ensure that there is density stability

(1) This investigation was supported in part by Public Health Service Research Grant AM-05177 from the National Institute of Arthritis and Metabolic Diseases.

everywhere in the diffusion cell during the entire diffusion process. In the diffusion of multicomponent systems, however, this is generally not the case, especially when the cross-term diffusion coefficients are large. Therefore it is desirable to derive criteria for gravitational stability in diffusion experiments of multicomponent systems. For the case of free diffusion of ternary systems, Wendt[2] obtained these criteria and Reinfelds and Gosting[3] subsequently simplified them. Here the procedure of Wendt is adopted in order to derive the conditions of gravitational stability for studies of diffusion in four-component systems by free diffusion and diaphragm cell methods.[4,5]

The general condition for density stability of any fluid system at time t may be expressed as[2]

$$(\partial d/\partial x)_t \geqslant 0 \quad (1)$$

where x is the position coordinate in the direction of increasing gravitational field. Here d is the density of the fluid which is generally a function of x and t. In the isothermal diffusion of a multicomponent system the density of the solution is determined solely by the concentrations of the solutes and may be expressed by a linear function of individual solute concentrations if these solute concentrations, C_i, are not far from the mean solute concentrations, $\bar{C}_i = [(C_i)_A + (C_i)_B]/2$, of the solutes in the upper and lower solutions A and B placed initially in the diffusion cell. For the four-component systems the expression assumes the form

$$d = d(\bar{C}_1,\bar{C}_2,\bar{C}_3) + \sum_{i=1}^{3} H_i(C_i - \bar{C}_i) \quad (2)$$

where $d(\bar{C}_1,\bar{C}_2,\bar{C}_3)$ is the density of a solution in which each solute is at its mean concentration, $\bar{C}_i$, for the experiment and H_i are the density derivatives, $(\partial d/\partial C_i)_{C_{j \neq i},T,P}$, where T is the temperature and P is the pressure (j = 1, 2, 3). Differentiation of eq 2 with respect to x and introduction of the resulting equation into relation 1 gives the desired density stability condition in terms of the solute concentration gradients

$$\sum_{i=1}^{3} H_i(\partial C_i/\partial x)_t \geqslant 0 \quad (3)$$

It may be seen that the values of one or two terms, $H_i(\partial C_i/\partial x)_t$, can be negative without inducing convective mixing as long as the sum of the three terms in relation 3 is either equal to or greater than zero at all levels in the diffusion cell.

Free Diffusion. The expression for the solute concentration distribution in four-component free diffusion is[4]

$$C_i = \bar{C}_i + \sum_{j=1}^{3} \Psi_{ij}\Phi(\sqrt{\sigma_j}y) \quad (i = 1, 2, 3) \quad (4)$$

where

$$y = x/2\sqrt{t} \quad (5)$$

$$\Phi(q) = \frac{2}{\sqrt{\pi}}\int_0^q e^{-q^2}\,dq \quad (6)$$

$$\Psi_{1j} = \frac{(\sigma_l - \sigma_k)}{2g_1(\sigma)}\left\{\Delta C_1\left[\frac{D_{11}}{|D_{ij}|} + E_1\sigma_j - \sigma_j(\sigma_k + \sigma_l)\right] + \Delta C_2\left[\frac{D_{12}}{|D_{ij}|} + E_2\sigma_j\right] + \Delta C_3\left[\frac{D_{13}}{|D_{ij}|} + E_3\sigma_j\right]\right\} \quad (7a)$$

$$\Psi_{2j} = \frac{(\sigma_l - \sigma_k)}{2g_1(\sigma)}\left\{\Delta C_1\left[\frac{D_{21}}{|D_{ij}|} + F_1\sigma_j\right] + \Delta C_2\left[\frac{D_{22}}{|D_{ij}|} + F_2\sigma_j - \sigma_j(\sigma_k + \sigma_l)\right] + \Delta C_3\left[\frac{D_{23}}{|D_{ij}|} + F_3\sigma_j\right]\right\} \quad (7b)$$

$$\Psi_{3j} = \frac{(\sigma_l - \sigma_k)}{2g_1(\sigma)}\left\{\Delta C_1\left[\frac{D_{31}}{|D_{ij}|} + G_1\sigma_j\right] + \Delta C_2\left[\frac{D_{32}}{|D_{ij}|} + G_2\sigma_j\right] + \Delta C_3\left[\frac{D_{33}}{|D_{ij}|} + G_3\sigma_j - \sigma_j(\sigma_k + \sigma_l)\right]\right\} \quad (7c)$$

and

$$g_1(\sigma) = \sigma_1^2(\sigma_3 - \sigma_2) + \sigma_2^2(\sigma_1 - \sigma_3) + \sigma_3^2(\sigma_2 - \sigma_1) \quad (8)$$

where the indices j, k, l are cyclic.

In the above equations D_{ij} are the diffusion coefficients,[6] each ΔC_i is the initial concentration difference of solute i between the lower and the upper solutions, and

$$E_1 = (D_{22}D_{33} - D_{23}D_{32})/|D_{ij}| \quad (9a)$$

$$E_2 = (D_{13}D_{32} - D_{12}D_{33})/|D_{ij}| \quad (9b)$$

$$E_3 = (D_{12}D_{23} - D_{13}D_{22})/|D_{ij}| \quad (9c)$$

$$F_1 = (D_{23}D_{31} - D_{21}D_{33})/|D_{ij}| \quad (9d)$$

$$F_2 = (D_{11}D_{33} - D_{13}D_{31})/|D_{ij}| \quad (9e)$$

$$F_3 = (D_{13}D_{21} - D_{11}D_{23})/|D_{ij}| \quad (9f)$$

$$G_1 = (D_{21}D_{32} - D_{22}D_{31})/|D_{ij}| \quad (9g)$$

$$G_2 = (D_{12}D_{31} - D_{11}D_{32})/|D_{ij}| \quad (9h)$$

$$G_3 = (D_{11}D_{22} - D_{12}D_{21})/|D_{ij}| \quad (9i)$$

(2) R. P. Wendt, *J. Phys. Chem.*, **66**, 1740 (1962).

(3) G. Reinfelds and L. J. Gosting, *ibid.*, **68**, 2464 (1964).

(4) H. Kim, *ibid.*, **70**, 562 (1966).

(5) H. Kim, *ibid.*, **73**, 1716 (1969).

(6) All the diffusion coefficients here are referred to a volume fixed frame of reference unless specified otherwise. Rigorously these have to be represented as $(D_{ij})_v$, but, in order to simplify the equations, the subscript v is omitted.

where

$$|D_{ij}| = \begin{vmatrix} D_{11} & D_{12} & D_{13} \\ D_{21} & D_{22} & D_{23} \\ D_{31} & D_{32} & D_{33} \end{vmatrix} \quad (10)$$

Here x is measured downward from the position of the initial boundary formation. The σ_i are obtained from the condition

$$\begin{vmatrix} E_1 - \sigma & E_2 & E_3 \\ F_1 & F_2 - \sigma & F_3 \\ G_1 & G_2 & G_3 - \sigma \end{vmatrix} = 0$$

and are related to the diffusion coefficients as follows.[4]

$$\sigma_1 + \sigma_2 + \sigma_3 = (D_{11}D_{22} + D_{11}D_{33} + D_{22}D_{33} - D_{12}D_{21} - D_{13}D_{31} - D_{23}D_{32})/|D_{ij}| \quad (11a)$$

$$\sigma_1\sigma_2 + \sigma_1\sigma_3 + \sigma_2\sigma_3 = (D_{11} + D_{22} + D_{33})/|D_{ij}| \quad (11b)$$

and

$$\sigma_1\sigma_2\sigma_3 = 1/|D_{ij}| \quad (11c)$$

In order for eq 4 to be physically meaningful, all σ_i are positive and unequal;[7] hence we have

$$\sigma_1 > \sigma_2 > \sigma_3 > 0 \quad (12)$$

Here the sequence among the three σ_i is rather arbitrary because all the functions of σ_i are symmetrical with regard to these parameters. From this condition eq 11 are all positive definite.

Equation 4 is now differentiated with respect to x and introduced into relation 3 to obtain

$$\sum_{j=1}^{3} [H_1\Psi_{1j} + H_2\Psi_{2j} + H_3\Psi_{3j}]\sqrt{\frac{\sigma_j}{\pi t}}e^{-\sigma_j y^2} \geq 0 \quad (13)$$

In this relation each term is the product of an exponential function (of σ_j, t, and x) and a linear function of $H_i\Psi_{ij}$ multiplied by $\sqrt{\sigma_j/\pi t}$. For $y = 0$ (hence $x = 0$) the values of all $\exp(-\sigma_j y^2)$ are unity and at this point relation 13 becomes

$$\sum_{j=1}^{3} [H_1\Psi_{1j} + H_2\Psi_{2j} + H_3\Psi_{3j}]\sqrt{\sigma_j} \geq 0 \quad (14)$$

As the absolute value of y increases the value of each $\exp(-\sigma_j y^2)$ decreases exponentially, and $\exp(-\sigma_1 y^2) < \exp(-\sigma_2 y^2) < \exp(-\sigma_3 y^2) < 1$. Compared with $\exp(-\sigma_3 y^2)$ the value of the first two exponentials are negligible near both ends of the boundary, and the differences are larger the bigger the value of $y = x/2\sqrt{t}$. Hence for very large values of $|y|$ the first and second terms in relation 13 (j = 1 and 2) may be set equal to zero regardless of the values within the brackets and from this it is clear that the following condition has to be met.[8]

$$H_1\Psi_{13} + H_2\Psi_{23} + H_3\Psi_{33} \geq 0 \quad (15)$$

Both relations 14 and 15 are necessary conditions for density stability. If relation 14 is not met convective mixing *will* occur in the region of the original sharp boundary position and if relation 15 is not satisfied convective mixing *will* occur near both ends of the diffusion boundary.[9]

Even if conditions 14 and 15 are satisfied, this is not sufficient to ensure gravitational stability and the region of intermediate y values must be considered. We consider the regions of y where $\exp(-\sigma_1 y^2)$ is negligible compared to $\exp(-\sigma_2 y^2)$ and $\exp(-\sigma_3 y^2)$. If the value of $(H_1\Psi_{12} + H_2\Psi_{22} + H_3\Psi_{32})\sqrt{\sigma_2}$ in relation 13 is negative and its absolute value is much larger than that of $(H_1\Psi_{13} + H_2\Psi_{23} + H_3\Psi_{33})\sqrt{\sigma_3}$, but relation 14 is still satisfied [when $(H_1\Psi_{11} + H_2\Psi_{21} + H_3\Psi_{31})$ has a very large positive value], then even if $\exp(-\sigma_3 y^2)$ is much larger than the corresponding exponential for σ_2, cases may arise when relation 13 cannot be satisfied. On the other hand, if the condition

$$[H_1\Psi_{12} + H_2\Psi_{22} + H_3\Psi_{32}]\sqrt{\sigma_2} + [H_1\Psi_{13} + H_2\Psi_{23} + H_3\Psi_{33}]\sqrt{\sigma_3} \geq 0 \quad (16)$$

is satisfied, the last term in relation 13 will always overwhelm the second term since the exponential function of σ_3 is always greater than that of σ_2. If the three conditions 14, 15, and 16 are all satisfied, condition 13 is also satisfied for all values of y. The violation of condition 16, however, will not necessarily bring about convective mixing; this will depend on the relative values of $\exp[-\sigma_2 y^2]$ and $\exp[-\sigma_3 y^2]$. Therefore relation 16 becomes the sufficient condition.

By introducing eq 7 these relations may now be rearranged in terms of $H_i\Delta C_i$. From relation 14

$$[{}^1/_2 g_1(\sigma)]\sum_{i=1}^{3} H_i\Delta C_i[X_i(H)g_2(\sigma) + Y_i(H)g_3(\sigma) - g_4(\sigma)] \geq 0 \quad (17)$$

(7) If a σ_i is negative, $\Phi(\sqrt{\sigma_i}y)$ is no longer the probability integral and as $y \to \infty$, the concentration of solutes becomes infinite. Therefore none of the σ_i can be negative. If any σ_i is zero, from eq 11e $|D_{ij}|$ becomes infinite, which would create the impossible condition that one or more D_{ij} be infinite. Finally if any two of the three σ_i are identical $g_1(\sigma)$ becomes zero and the solute concentrations become infinite for all values of y. From these considerations it is clear that relation 12 should hold.

(8) Relation 15 can also be obtained by dividing relation 13 by $\sqrt{\sigma_1/\pi t}\exp(-\sigma_1 y^2)$ to give

$$[H_1\Psi_{11} + H_2\Psi_{21} + H_3\Psi_{31}] + [H_1\Psi_{12} + H_2\Psi_{22} + H_3\Psi_{32}]\sqrt{\sigma_2/\sigma_1}e^{(\sigma_1-\sigma_2)y^2} + [H_1\Psi_{13} + H_2\Psi_{23} + H_3\Psi_{33}]\sqrt{\sigma_3/\sigma_1}e^{(\sigma_1-\sigma_3)y^2} > 0 \quad (1')$$

From relation 12 it is apparent that when $|y|$ is very large

$$\exp[(\sigma_1 - \sigma_3)y^2] \gg \exp[(\sigma_1 - \sigma_2)y^2] \gg 1$$

and in order to satisfy condition 1′ condition 15 has to be met.

(9) A similar situation arises in the free diffusion of ternary systems. If relation 20 in ref 2 is not met convective mixing will occur at both ends of the boundary while violation of relation 21 of ref 2 will induce convective mixing in the vicinity of the original sharp boundary position. Relation 20 together with relation 21 makes the sufficient condition. This differs somewhat from the position taken by Wendt.

here

$$X_i(H) = (H_1D_{1i} + H_2D_{2i} + H_3D_{3i})/(H_i|D_{ij}|) \quad (18)$$

$$Y_i(H) = (H_1E_i + H_2F_i + H_3G_i)/H_i \quad (19)$$

$$g_2(\sigma) = (\sigma_3 - \sigma_2)\sqrt{\sigma_1} + (\sigma_1 - \sigma_3)\sqrt{\sigma_2} + (\sigma_2 - \sigma_1)\sqrt{\sigma_3} \quad (20)$$

$$g_3(\sigma) = (\sigma_3 - \sigma_2)\sigma_1\sqrt{\sigma_1} + (\sigma_1 - \sigma_3)\sigma_2\sqrt{\sigma_2} + (\sigma_2 - \sigma_1)\sigma_3\sqrt{\sigma_3} \quad (21)$$

and

$$g_4(\sigma) = (\sigma_3^2 - \sigma_2^2)\sigma_1\sqrt{\sigma_1} + (\sigma_1^2 - \sigma_3^2)\sigma_2\sqrt{\sigma_2} + (\sigma_2^2 - \sigma_1^2)\sigma_3\sqrt{\sigma_3} \quad (22)$$

From the inequality condition 12, it may be seen that the value of $g_1(\sigma)$ is negative definite[10,11] and relation 17 may be multiplied by $2g_1(\sigma)$ to obtain

$$\sum_{i=1}^{3} H_i\Delta C_i[X_i(H)g_2(\sigma) + Y_i(H)g_3(\sigma) - g_4(\sigma)] \leqslant 0 \quad (23)$$

Likewise relation 16 is transformed into

$$\sum_{i=1}^{3} H_i\Delta C_i\{X_i(H)[(\sigma_3 - \sigma_1)\sqrt{\sigma_2} + (\sigma_1 - \sigma_2)\sqrt{\sigma_3}] + Y_i(H)[(\sigma_3 - \sigma_1)\sigma_2\sqrt{\sigma_2} + (\sigma_1 - \sigma_2)\sigma_3\sqrt{\sigma_3}] - [(\sigma_3^2 - \sigma_1^2)\sigma_2\sqrt{\sigma_2} + (\sigma_1^2 - \sigma_2^2)\sigma_3\sqrt{\sigma_3}]\} \geqslant 0 \quad (24)$$

Introducing eq 7 into relation 15 and dividing the resulting equation by $(\sigma_2 - \sigma_1)/2g_1(\sigma)$, remembering this quantity is positive, we get

$$\sum_{i=1}^{3} H_i\Delta C_i[X_i(H) + Y_i(H)\sigma_3 - \sigma_3(\sigma_1 + \sigma_2)] \geqslant 0 \quad (25)$$

Thus we have three conditions (independent of time and position) which if satisfied ensure gravitational stability in free diffusion of four-component systems. Of these, relations 23 and 25 are necessary conditions and satisfaction of all three inequalities is sufficient to ensure gravitational stability. For a given system at given mean solute concentrations, the value of the diffusion coefficients and the density derivatives, H_i, are fixed so the left-hand sides of relations 23–25 are sums of the three $H_i\Delta C_i$, multiplied by appropriate numerical values. Therefore, for a given composition of a given four-component system, the ΔC_i are the only adjustable parameters to be used in satisfying conditions 23–25.

When all the cross-term diffusion coefficients in a four-component system are negligible we have the following relations

$$\sigma_1 + \sigma_2 + \sigma_3 = 1/D_{11} + 1/D_{22} + 1/D_{33} \quad (26a)$$

$$\sigma_1\sigma_2 + \sigma_1\sigma_3 + \sigma_2\sigma_3 = 1/D_{11}D_{22} + 1/D_{11}D_{33} + 1/D_{22}D_{33} \quad (26b)$$

$$\sigma_1\sigma_2\sigma_3 = 1/D_{11}D_{22}D_{33} \quad (26c)$$

$$X_1(H) = 1/D_{22}D_{33} \quad (27a)$$

$$X_2(H) = 1/D_{11}D_{33} \quad (27b)$$

$$X_3(H) = 1/D_{11}D_{22} \quad (27c)$$

$$Y_i(H) = 1/D_{ii} \qquad (i = 1, 2, 3) \quad (28)$$

Using these relations the gravitational stability condition 23 can be transformed into

$$\sum_{i=1}^{3} \frac{H_i\Delta C_i}{\sqrt{D_{ii}}} \geqslant 0 \quad (29)$$

Relation 24 may be likewise transformed into

$$\frac{H_2\Delta C_2}{\sqrt{D_{22}}} + \frac{H_3\Delta C_3}{\sqrt{D_{23}}} \geqslant 0 \quad (30)$$

and from relation 25 one obtains

$$H_3\Delta C_3 \geqslant 0 \quad (31)$$

In free diffusion experiments with ternary systems, the values of ΔC_i are usually made to range from zero to certain positive values so that the concentration difference fractions, α_i, of the solutes on the basis of refractive index[3,4] will range from zero to unity. Relations 29 through 31 indicate that this range of ΔC_i will guarantee gravitational stability for experiments with four-component systems when the cross-term diffusion coefficients are negligible. For ternary systems studied thus far where the cross-term diffusion coefficients were relatively small, the ΔC_i ranges used also satisfied the condition for the gravitational stability.[2,3] For cases where the cross-term diffusion coefficients are very large,[12]

(10) The equations 8, 20, 21, and 22 can be transformed into

$$g_1(\sigma) = (\sigma_1 - \sigma_2)(\sigma_1 - \sigma_3)(\sigma_3 - \sigma_2)$$

$$g_2(\sigma) = (\sqrt{\sigma_1} - \sqrt{\sigma_2})(\sqrt{\sigma_1} - \sqrt{\sigma_3})(\sqrt{\sigma_2} - \sqrt{\sigma_3})$$

$$g_3(\sigma) = -g_2(\sigma)[\sqrt{\sigma_1\sigma_2} + \sqrt{\sigma_1\sigma_3} + \sqrt{\sigma_2\sigma_3}]$$

$$g_4(\sigma) = g_2(\sigma)[\sigma_1\sigma_2 + \sigma_1\sigma_3 + \sigma_2\sigma_3 + \sigma_1\sqrt{\sigma_2\sigma_3} + \sigma_2\sqrt{\sigma_1\sigma_3} + \sigma_3\sqrt{\sigma_1\sigma_2}]$$

From the inequality condition 12, it is immediately clear that

$$g_1(\sigma) < 0$$

$$g_2(\sigma) > 0$$

$$g_3(\sigma) < 0$$

and

$$g_4(\sigma) > 0$$

(11) These transformations were kindly made by Professor L. J. Gosting.

(12) Although there may be some upper limits as to the size of the cross-term diffusion coefficients relative to the main diffusion coefficients, no theoretical limitation exists so far. The relation $D_{11}D_{22} - D_{12}D_{21} > 0$ for ternary systems is not necessarily a limiting condition because, if one of the cross-term diffusion coefficients is negative, this relationship will hold regardless the size of the cross-term diffusion coefficients. Even if the signs of the cross-term diffusion coefficients are the same, one coefficient can be enormously large if the other one is very small. The same situation also arises in four-component systems.

this may not be generally the case as shown by one of the following numerical evaluations of the coefficients for $H_i\Delta C_i$ in relations 23–25. We assign illustrative values for the main diffusion coefficients as

$$D_{11} = 10^{-6}; \quad D_{22} = 2.5 \times 10^{-6}; \quad D_{33} = 5 \times 10^{-6}$$

If we first assume that all the cross-term diffusion coefficients are zero except for $(H_1/H_3)D_{13} = 2.5 \times 10^{-6}$, then relation 23 becomes

$$H_1\Delta C_1 + 0.63H_2\Delta C_2 + 0.10H_3\Delta C_3 \geqslant 0$$

Also relation 24 becomes

$$0.87H_2\Delta C_2 + H_3\Delta C_3 \geqslant 0$$

and relation 25 reduces to

$$H_3\Delta C_3 \geqslant 0$$

Thus even for this case where $(H_1/H_3)D_{13}$ is very large, but with the other cross-term diffusion coefficients equal to zero, one will have gravitational stability as long as $H_i\Delta C_i \geqslant 0$.

Next, when D_{11}, D_{22}, and D_{33} have the values assigned above and $(H_1/H_2)D_{12} = 5 \times 10^{-7}$, $(H_1/H_3)D_{13} = -10^{-6}$, $(H_2/H_1)D_{21} = 10^{-7}$, $(H_2/H_3)D_{23} = -2 \times 10^{-6}$, $(H_3/H_1)D_{31} = 10^{-7}$, and $(H_3/H_2)D_{32} = 10^{-7}$, relation 23 becomes

$$H_1\Delta C_1 + 0.53H_2\Delta C_2 + 0.71H_3\Delta C_3 \geqslant 0$$

From relation 24

$$H_1\Delta C_1 + 8.90H_2\Delta C_2 + 6.85H_3\Delta C_3 \geqslant 0$$

and from relation 25

$$-H_1\Delta C_1 - 1.8H_2\Delta C_2 - 36.8H_3\Delta C_3 \geqslant 0$$

Here the only way to satisfy all three conditions is to make $H_3\Delta C_3$ slightly negative. Thus it is clear that when the cross-term diffusion coefficients are comparable in size to those of main diffusion coefficients, the current practice of preparing the solutions for diffusion experiments may give rise to the density instability. It is therefore recommended that whenever one suspects that one or more of the cross-term diffusion coefficients for the system to be studied are large, the approximate values of the diffusion coefficients (and predetermined H_i values) be introduced into relations 23–25 in order to determine the safe range of ΔC_is. The estimate of the diffusion coefficients of nonelectrolytes is very difficult, but for electrolyte systems methods are available for obtaining the approximate values of the diffusion coefficients.[13–15]

For the general case of a system with $n + 1$ components, the expressions for the solute concentration distributions are similar to the equations for systems with three or four components.[4,16,17] For this general case each Ψ_{ij} is a linear function of the n concentration differences and σ_i are roots of a polynomial of nth degree. When the expressions for the concentration distribution are differentiated and introduced into eq 3 one will obtain a condition corresponding to relation 13. This condition will have n terms and each term is a product of $\sqrt{\sigma_i/\pi t}\exp(-\sigma_i y^2)$ and a linear function of $n - H_i\Psi_{ij}$s. The argument used for the four-component system may be also used here to obtain n conditions for the gravitational stability and if the following inequality can be assumed

$$\sigma_1 > \sigma_2 > \ldots > \sigma_{n-1} > \sigma_n > 0 \qquad (32)$$

then the n conditions have the following general form

$$\sum_{i=m}^{n}\sum_{j=1}^{n} H_j\Psi_{ji}\sqrt{\sigma_i} \geqslant 0 \qquad (33)$$

where $m = 1, 2, \ldots, n$. Here the necessary conditions are the relation 33 for $i = 1$ and $i = n$ and the rest of the conditions become the sufficient conditions.

Diaphragm Cell Method. With this method the diaphragm itself gives an inherent density stability and the problem of convective flow is far less serious than in free diffusion. However, Stokes[18] showed that for accurate diffusion, it is important to place the denser solution in the lower compartment.[19]

When the steady state is reached in the diaphragm, it is generally assumed that each solute concentration gradient within the diaphragm is constant, and for this case relation 3 assumes the form

$$\sum_{i=1}^{3} H_i\Delta C_i(t) \geqslant 0 \qquad (34)$$

The solute concentration differences between the two compartments of a diaphragm cell during the diffusion, $\Delta C_i(t)$, may be expressed as[4]

$$\Delta C_i(t) = 2\sum_{j=1}^{3}\Psi_{ij}\Phi(t/\sigma_j) \qquad (i = 1, 2, 3) \quad (35)$$

where

$$\Phi(t/\sigma_j) = e^{-(k/\sigma_j)t} \qquad (36)$$

Here k is the diaphragm cell constant. Equation 35 is now substituted into relation 34 and the resulting relation is divided by $e^{-(k/\sigma_3)t}$ to obtain

(13) L. J. Gosting in "Advances in Protein Chemistry," Vol. XI, Edsall, *et al.*, Ed., Academic Press, New York, N. Y., 1956; also I. J. O'Donnell and L. J. Gosting in "Structure of Electrolytic Solutions," W. J. Hamer, Ed., Wiley, New York, N. Y., 1959, p 160.

(14) R. P. Wendt, *J. Phys. Chem.*, **69**, 1227 (1965).

(15) D. G. Miller, *ibid.*, **70**, 2639 (1966); **71**, 616, 3588 (1967).

(16) H. L. Toor, *A.I.Ch.E. J.*, **10**, 448, 460 (1964).

(17) W. E. Stewart and R. Prober, *Ind. Eng. Chem., Fundam.*, **3**, 224 (1964).

(18) R. H. Stokes, *J. Amer. Chem. Soc.*, **72**, 763 (1950).

(19) Here we are considering only the vertical position of the cell in which the diaphragm is horizontal.

$$[H_1\Psi_{11} + H_2\Psi_{21} + H_3\Psi_{31}] \times \exp[kt(1/\sigma_3 - 1/\sigma_1)] + [H_1\Psi_{12} + H_2\Psi_{22} + H_3\Psi_{32}] \times \exp[kt(1/\sigma_3 - 1/\sigma_2)] + [H_1\Psi_{13} + H_2\Psi_{23} + H_3\Psi_{33}] \geqslant 0 \quad (37)$$

and from the relation 12

$$\exp[kt(1/\sigma_3 - 1/\sigma_1)] \geqslant \exp[kt(1/\sigma_3 - 1/\sigma_2)] \geqslant 1 \quad (38)$$

When $t = 0$, relation 34 simply becomes

$$\sum_{i=1}^{3} H_i\Delta C_i \geqslant 0 \quad (39)$$

For the other extreme case when t is very large, the first term in relation 37 will overwhelm the other terms (relation 38) and the condition

$$H_1\Psi_{11} + H_2\Psi_{21} + H_3\Psi_{31} \geqslant 0 \quad (40)$$

has to be satisfied. Upon introduction of eq 7 this condition is transformed into

$$\sum_{i=1}^{3} H_i\Delta C_i[X_i(H) + Y_i(H)\sigma_1 - \sigma_1(\sigma_2 + \sigma_3)] \geqslant 0 \quad (41)$$

For the intermediate values of t we assume that the last term in relation 37 is negligible compared to the other two terms. If the value of $[H_1\Psi_{12} + H_2\Psi_{22} + H_3\Psi_{32}]$ is negative and much larger than that of $[H_1\Psi_{11} + H_2\Psi_{21} + H_3\Psi_{31}]$, whatever the gain made by the exponential function of the first term in relation 37 with the increase in the value of t may not be sufficient to overcome the second term. On the other hand, if we have the condition

$$[H_1\Psi_{11} + H_2\Psi_{21} + H_3\Psi_{31}] + [H_1\Psi_{12} + H_2\Psi_{22} + H_3\Psi_{32}] \geqslant 0 \quad (42)$$

relation 37 is satisfied for all values of t as long as both conditions 39 and 41 are met. Relation 42 is now expressed in terms of $H_i\Delta C_i$ by substituting eq 7 and rearranging the resultant expression to obtain

$$\sum_{i=1}^{3} H_i\Delta C_i\{X_i(H)(\sigma_1 - \sigma_2) + Y_i(H)\sigma_3(\sigma_1 - \sigma_2) - [\sigma_1(\sigma_3^2 - \sigma_2^2) + \sigma_2(\sigma_1^2 - \sigma_3^2)]\} \leqslant 0 \quad (43)$$

Thus relation 39 becomes a necessary condition because the violation of this condition will bring initial convective mixing. The relation 43 is the sufficient condition and the violation of this condition may or may not bring density instability. This will mainly depend on the sign and size of the second term of relation 42. If one is considering the whole range of t, then condition 41 is a necessary condition. However, within the ordinary experimental range of t this condition may become another sufficient condition.[20]

The numerical evaluation of the coefficients for $H_i\Delta C_i$ in relations 41 and 43, using the values of $D_{11} = 10^{-6}$, $D_{22} = 2.5 \times 10^{-6}$, $D_{33} = 5 \times 10^{-6}$ and $(H_1/H_3)D_{13} = 5 \times 10^{-7}$, gives

$$H_1\Delta C_1 - 0.63H_3\Delta C_3 \geqslant 0$$

and

$$H_1\Delta C_1 + H_2\Delta C_2 - 0.13H_3\Delta C_3 \geqslant 0$$

respectively. Here all the rest of the cross-term diffusion coefficients are assumed to be negligible. For this case it is not enough to make all the $H_i\Delta C_i$ positive for the initial condition in order to avoid the convective mixing. It should be noticed that with the same set of diffusion coefficients, $H_i\Delta C_i$ can be all positive in free diffusion.

For the ternary systems the condition for the density stability is represented as

$$H_1\Delta C_1(t) + H_2\Delta C_2(t) \geqslant 0 \quad (44)$$

The equation for a solute concentration difference in the diaphragm cell for a three-component system is[21-23]

$$\Delta C_i(t) = 2[K_i^+e^{-(k/\sigma_+)t} + K_i^-e^{-(k/\sigma_-)t}] \quad (45)$$

where

$$K_1^+ = \frac{(\sigma_+ - E)\Delta C_1 - F\Delta C_2}{2(\sigma_+ - \sigma_-)} \quad (46a)$$

$$K_2^+ = \frac{(\sigma_+ - H)\Delta C_2 - G\Delta C_1}{2(\sigma_+ - \sigma_-)} \quad (46b)$$

$$K_1^- = \frac{F\Delta C_2 - (\sigma_- - E)\Delta C_1}{2(\sigma_+ - \sigma_-)} \quad (46c)$$

$$K_2^- = \frac{G\Delta C_1 - (\sigma_- - H)\Delta C_2}{2(\sigma_+ - \sigma_-)} \quad (46d)$$

In the above equations σ_+, σ_-, E, F, G, and H are constants which are related to the diffusion coefficients by the equations

(20) When all the cross-term diffusion coefficients are zero, relations 41 and 43 can be converted into

$$H_1\Delta C_1 \geqslant 0 \quad (2')$$

and

$$H_1\Delta C_1 + H_2\Delta C_2 \geqslant 0 \quad (3')$$

respectively. These conditions result from the fact that if the faster component, rather than the slower one, diffuses from the upper compartment to the lower compartment of the cell, a net accumulation in the upper compartment may result producing the density instability. Again the positive values of $H_i\Delta C_i$ for all components will ensure the gravitational stability.

(21) E. R. Gilliland, R. F. Baddour, and D. J. Goldstein, *Can. J. Chem. Eng.*, **35**, 10 (1957).

(22) F. J. Kelly, Ph.D. Thesis, University of New England, Armidale, New South Wales, Australia, 1961.

(23) J. K. Burchard and H. L. Toor, *J. Phys. Chem.*, **66**, 2015 (1962).

$$\sigma_+ = {}^1/_2\{D_{11} + D_{22} + \sqrt{(D_{22} - D_{11})^2 + 4D_{12}D_{21}}\}/|D_{ij}|' \quad (47a)$$

$$\sigma_- = {}^1/_2\{D_{11} + D_{22} - \sqrt{(D_{22} - D_{11})^2 + 4D_{12}D_{21}}\}/|D_{ij}|' \quad (47b)$$

$$E = D_{11}/|D_{ij}|' \quad (48a)$$

$$F = D_{12}/|D_{ij}|' \quad (48b)$$

$$G = D_{21}/|D_{ij}|' \quad (48c)$$

$$H = D_{22}/|D_{ij}|' \quad (48d)$$

and

$$|D_{ij}|' = D_{11}D_{12} - D_{12}D_{21} \quad (49)$$

Introduction of eq 45 into relation 44 and division of the resulting expression by $e^{-(k/\sigma_-)}$ gives

$$[H_1K_1{}^+ + H_2K_2{}^+]\exp[kt(1/\sigma_- - 1/\sigma_+)] + [H_1K_1{}^- + H_2K_2{}^-] \geqslant 0 \quad (50)$$

If we assume $\sigma_+ > \sigma_-$, we have the relation

$$\exp[kt(1/\sigma_- - 1/\sigma_+)] \geqslant 1 \quad (51)$$

And from the argument used previously for the four-component systems, gravitational stability will be ensured when the following conditions are satisfied.

$$H_1K_1{}^+ + H_2K_2{}^+ \geqslant 0 \quad (52)$$

$$H_1K_1{}^+ + H_2K_2{}^+ + H_1K_1{}^- + H_2K_2{}^- \geqslant 0 \quad (53)$$

Equations 46 are now introduced into relation 52 to obtain

$$H_1\Delta C_1[D_{22} - D_{11} - 2(H_2/H_1)D_{21} + U] + H_2\Delta C_2[D_{11} - D_{22} - 2(H_1/H_2)D_{12} + U] \geqslant 0 \quad (54)$$

where

$$U = [(D_{22} - D_{11})^2 + 4D_{12}D_{21}]^{1/2} \quad (55)$$

and from relation 53

$$H_1\Delta C_1 + H_2\Delta C_2 \geqslant 0 \quad (56)$$

For the general case of $n + 1$ component systems, the same argument employed so far gives n conditions for the gravitational stability which have the general form

$$\sum_{i=1}^{m}\sum_{j=1}^{n} H_j\Psi_{ji} \geqslant 0 \quad (57)$$

$$m = 1, 2, 3, \ldots, n - 1, n$$

Discussion

The paradox of these conditions for gravitational stability is that this stability can be checked only *after* values of the diffusion coefficients are experimentally obtained; ideally it would be desirable to find, *before* performing the experiments, the range of ΔC_i which will not give rise to the convective mixing. One obvious question will be whether it is possible to have a small density instability that leads to false D_{ij} values which still satisfy the criteria given. There seems to be no simple answer to this. However, the extent of convective mixing will be greatly influenced by different values of ΔC_i and this can be expected to give far greater variations in D_{ij} than result from the usual experimental errors. Therefore if approximate values of D_{ij} are not available in advance, so prior estimation of safe ranges of ΔC_i is not possible, it is advisable to obtain values of the D_{ij} for wide ranges of ΔC_i; if each value of a given D_{ij} agrees within the expected experimental error, then by using the criteria given in the text one may confirm density stability in the experiments.

Acknowledgment. The author wishes to thank Professor Louis J. Gosting for his assistance and encouragement during the course of this work and for his criticism of the manuscript.

Appendix

By using the method similar to the one employed by Kirkaldy[24] it will be shown here that eq 11c is positive definite. The phenomenological equation for isothermal diffusion of a four-component system is

$$(J_i)_0 = (L_{i1})_0X_1 + (L_{i2})_0X_2 + (L_{i3})_0X_3 \times \quad (i = 1, 2, 3) \quad (58)$$

where $(J_i)_0$ is the solvent fixed flow of component i, $(L_{ij})_0$ is a solvent-fixed phenomenological coefficient, and X_i is the thermodynamic force. The entropy production, σ, for this case can be represented as[25]

$$T\sigma = (J_1)_0X_1 + (J_2)_0X_2 + (J_3)_0X_3 \quad (59)$$

where T is the absolute temperature. Upon substitution of eq 58 into eq 59 one obtains a quadratic form

$$T\sigma = \sum_{i=1}^{3}\sum_{j=1}^{3}(L_{ij})_0X_iX_j \quad (60)$$

From the second law of thermodynamics $T\sigma > 0$, and therefore

$$\sum_{i=1}^{3}\sum_{j=1}^{3}(L_{ij})_0X_iX_j \geqslant 0 \quad (61)$$

This relation has the following sets of necessary and sufficient conditions[26]

$$(L_{11})_0 \geqslant 0 \quad (62a)$$

$$(L_{22})_0 \geqslant 0 \quad (62b)$$

$$(L_{33})_0 \geqslant 0 \quad (62c)$$

(24) J. S. Kirkaldy, *Can. J. Phys.*, 36, 899 (1958).

(25) See, for example, S. R. DeGroot, "Thermodynamics of Irreversible Processes," Interscience, New York, N. Y., 1952.

(26) See, for example, G. Hadley, "Linear Algebra," Addison-Wesley, Reading, Mass., 1961, p 260.

$$(L_{11})_0(L_{22})_0 - (L_{12})_0(L_{21})_0 \geqslant 0 \quad (63a)$$

$$(L_{11})_0(L_{33})_0 - (L_{13})_0(L_{31})_0 \geqslant 0 \quad (63b)$$

$$(L_{22})_0(L_{33})_0 - (L_{23})_0(L_{32})_0 \geqslant 0 \quad (63c)$$

and

$$(L_{11})_0(L_{22})_0(L_{33})_0 + (L_{12})_0(L_{23})_0(L_{31})_0 + (L_{13})_0(L_{21})_0(L_{32})_0 - (L_{11})_0(L_{23})_0(L_{32})_0 - (L_{12})_0(L_{21})_0(L_{33})_0 - (L_{13})_0(L_{22})_0(L_{31})_0 \geqslant 0 \quad (64)$$

The relation between the solvent-fixed phenomenological coefficients, $(L_{ij})_0$, and the solvent fixed diffusion coefficients, $(D_{ij})_0$, are given by the expression[27]

$$(D_{ik})_0 = \sum_{j=1}^{3} (L_{ij})_0\mu_{jk} \quad (65)$$

where

$$\mu_{jk} = (\partial\mu_j/\partial C_k) \quad (66)$$

The μ_j are the chemical potentials. Using eq 65 we obtain the relationship

$$|D_{ij}|_0 = |L_{ij}|_0 \times |\mu_{ij}| \quad (67)$$

where

$$|D_{ij}|_0 = (D_{11})_0(D_{22})_0(D_{33})_0 + (D_{12})_0(D_{23})_0(D_{31})_0 + (D_{13})_0(D_{21})_0(D_{32})_0 + (D_{11})_0(D_{23})_0(D_{32})_0 - (D_{12})_0(D_{21})_0(D_{33})_0 - (D_{13})_0(D_{22})_0(D_{31})_0 \quad (68)$$

$$|L_{ij}|_0 = (L_{11})_0(L_{22})_0(L_{33})_0 + (L_{12})_0(L_{23})_0(L_{31})_0 + (L_{13})_0(L_{21})_0(L_{32})_0 - (L_{11})_0(L_{23})_0(L_{32})_0 - (L_{12})_0(L_{21})_0(L_{33})_0 - (L_{13})_0(L_{22})_0(L_{31})_0 \quad (69)$$

and

$$|\mu_{ij}| = \mu_{11}\mu_{22}\mu_{33} + \mu_{12}\mu_{23}\mu_{31} + \mu_{13}\mu_{21}\mu_{32} - \mu_{11}\mu_{23}\mu_{32} - \mu_{12}\mu_{21}\mu_{33} - \mu_{13}\mu_{22}\mu_{31} \quad (70)$$

According to Prigogine and Defay[28]

$$|\mu_{ij}| \geqslant 0 \quad (71)$$

and from relations 64 and 67 it is apparent that

$$|D_{ij}|_0 \geqslant 0 \quad (72)$$

The relationship between the solvent-fixed and volume-fixed diffusion coefficients are given by[27]

$$(D_{ik})_0 = (D_{ik})_v + (C_i/C_0\bar{v}_0) \sum_{j=1}^{3} \bar{v}_j(D_{jk})_v \begin{pmatrix} i = 1, \ldots, q \\ k = 1, \ldots, q \end{pmatrix} \quad (73)$$

where $\bar{v}_i$ is the partial specific volume of component i and here the component zero represents the solvent. Introduction of eq 73 into relation 72 brings

$$|D_{ij}|_v[1 + (C_1\bar{v}_1/C_0\bar{v}_0) + (C_2\bar{v}_2/C_0\bar{v}_0) + (C_3\bar{v}_3/C_0\bar{v}_0)] \geqslant 0 \quad (74)$$

where $|D_{ij}|_v$ represents eq 68 when $(D_{ij})_v$ are replaced by $(D_{ij})_v$. It should be remembered that the diffusion coefficients discussed in the main text are all $(D_{ij})_v$ although the subscript $\bar{v}$ is omitted for the sake of simplicity. If all three partial specific volumes are positive

$$|D_{ij}|_v \geqslant 0 \quad (75)$$

If, however, one or more partial specific volumes are negative relation 75 holds only when

$$[1 + (C_1\bar{v}_1/C_0\bar{v}_0) + (C_2\bar{v}_2/C_0\bar{v}_0) + (C_3\bar{v}_3/C_0\bar{v}_0)] \geqslant 0 \quad (76)$$

(27) J. G. Kirkwood, R. L. Baldwin, P. J. Dunlop, L. J. Gosting, and G. Kegeles, *J. Chem. Phys.*, **33**, 1505 (1960).

(28) I. Prigogine and R. Defay, "Chemical Thermodynamics," Longmans Green and Co., London, 1954, p 224.

The 200-nm Band of NCO^-

by J. Leopold, D. Shapira, and A. Treinin*

Department of Physical Chemistry, Hebrew University, Jerusalem, Israel *(Received May 19, 1970)*

Environmental effects on the 200-nm absorption band of NCO^- were investigated. The nature of solvent and temperature effects leads to assignment of this band to a charge-transfer-to-solvent type of transition. The oscillator strength $f = 0.023$ is not in discord with this assignment. There is no indication for gain of intensity caused by solvent perturbation.

The absorption band of NCO^- in aqueous solution near 200 nm has recently been assigned[1] to the orbitally forbidden $^1\Sigma^- \leftarrow {}^1\Sigma^+$ transition. However, this band is quite intense and therefore it was assumed to have gained intensity from a solvent perturbation. As far as we know there is no convincing evidence for such a striking hyperchromic effect induced by solvation. In the case of NO_3^- a similar effect was proposed to account for the large discrepancy between calculated and observed intensity of the 300-nm band (which is weak even in solution).[2] Indeed, its oscillator strength was found to depend on the polarity of the solvent, decreasing by a factor of ~ 2 on replacing water by CH_3CN. However, the intensity could be only slightly reduced below this value by further lowering the polarity of the solvent, the main effect being due to H bonding.[3]

No attempt was made to examine environmental effects on the spectrum of NCO^- in order to check the validity of the alleged hyperchromic effect. Moreover, environmental effects provide a convenient tool for establishing the nature of transitions by comparison with some known reference spectra. The results of such an investigation are presented here.

Experimental Section

Materials. KNCO (Fluka) was purified by the method described elsewhere.[1] Its decomposition leads to spurious absorption near 250 nm, which could be removed only after several recrystallizations and finally drying the material at room temperature under vacuum. *Tetramethylammonium cyanate* was prepared by adding freshly prepared $Pb(NCO)_2$ to an equivalent amount of $N(CH_3)_4I$ in methanol, shaking overnight, filtering, and evaporating the filtrate to dryness under vacuum. The material was rinsed several times with acetone to remove $Pb(NCO)_2$ and then dried thoroughly. Its purity was checked by measuring the spectrum in water; it was identical with that of KNCO. $N(CH_3)_4NCO$ was used to introduce NCO^- into organic solvents. The organic solvents were of spectroscopic grade. D_2O (99.7%, Fluka, Puriss) was used without further purification. Water was triply distilled and all other materials were of Analar grade.

Absorption Spectra. The spectra were measured with a 450 Perkin-Elmer spectrophotometer. The temperature of solution in the cell compartment was kept constant within 0.5° in the range 5–60°. For comparison the spectra of NCO^- and I^- were measured under the same conditions.

Results

All solutions were found to obey Beer's law in the range 10^{-2} to $10^{-3}M$. Figure 1 shows the spectrum of 10^{-2} *M* NCO^- in various media. In water at 20° $\lambda_{max} = 194$ nm, $\epsilon_{max} = 1.1 \times 10^3 M^{-1} cm^{-1}$, and oscillator strength $f = 2.3 \times 10^{-2}$. (λ_{max} was determined by the method of midpoints.[4] f was calculated using the approximation:[5] $f = 4.32 \times 10^{-9} \times 1.06, \epsilon_{max}\ \Delta\nu_{1/2}$. The value of f is close to that previously recorded[1] but ϵ_{max} is higher). There are pronounced environmental effects on the transition energy but not on the intensity of the band. Moreover, the shifts are typical for charge-transfer-to-solvent (CTTS) spectra:[6] $h\nu_{max}$ increases in the order $CH_3CN < H_2O < D_2O <$ alcohol; the CTTS origin of the band is clearly demonstrated in Figure 2, which records transition energy against $h\nu_{max}$ of I^- in the same solvent, *i.e.*, the CTTS value of the solvent.[7] The two plots shown correspond to $h\nu(NCO^-)$ at ϵ_{max} and $\epsilon_{max}/2$. The former is less reliable because the absorption near the peak appears to include some contribution from an overlapping band (Figure 2). Still except for mixed solvents the points appear to lie on straight lines. The deviations displayed by mixed solvents can be explained by assuming that in the same mixture the solvation layers of NCO^- and I^- have different compositions, that of NCO^- being richer in water. (NCO^- is smaller than I^-; see later.)

* To whom correspondence should be addressed.

(1) J. W. Rabalais, J. R. McDonald, and S. P. McGlynn, *J. Chem. Phys.*, **51**, 5103 (1969).

(2) S. J. Strickler and M. Kasha, "Molecular Orbitals in Chemistry, Physics and Biology," Academic Press, New York, N. Y., 1964, p 241.

(3) E. Rotlevi and A. Treinin, *J. Phys. Chem.*, **69**, 2645 (1965).

(4) G. Scheibe, *Ber.*, **58**, 586 (1925).

(5) C. Sandorfy, "Electronic Spectra and Quantum Chemistry," Prentice-Hall, Englewood Cliffs, N. J., 1964.

(6) M. J. Blandamer and M. F. Fox, *Chem. Rev.*, **70**, 59 (1970).

(7) I. Burak and A. Treinin, *Trans. Faraday Soc.*, **59**, 1490 (1963).

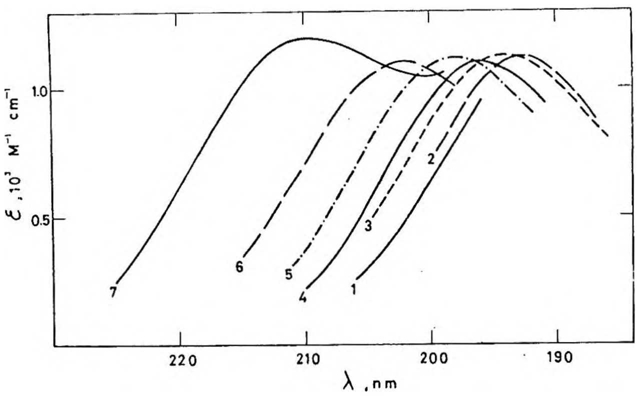

Figure 1. The spectrum of NCO^- in methanol (1), D_2O (2), H_2O (3), CH_3CN + 25% H_2O (4), CH_3CN + 10% H_2O (5), CH_3CN + 3% H_2O (6), and pure CH_3CN (7).

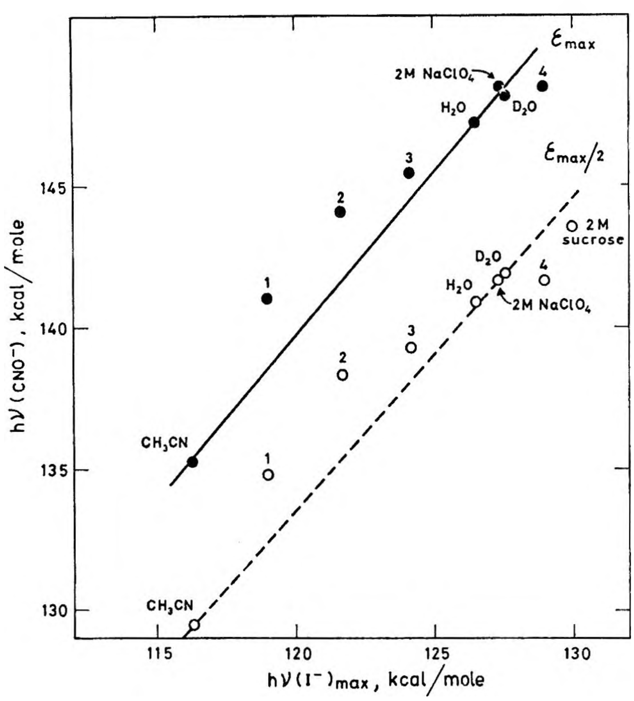

Figure 2. The relation between the transition energy of NCO^- at ϵ_{max} and $\epsilon_{max}/2$ and $h\nu_{max}$ of I^- in the same solvent. Solvent mixtures: CH_3CN with 3% (1), 10% (2), and 25% water (3); 10 *M* CH_3OH in water (4).

The band has relatively high temperature sensitivity (Figure 3). In water and CH_3CN $d(h\nu_{max})/dT = -12$ and -20 cm^{-1}/deg, respectively. These values are close to that displayed[6] by I^-. The band in CH_3CN undergoes the regular change of shape with change of temperature,[6] but its oscillator strength remains constant.

Discussion

Our results indicate that the 200-nm band of NCO^- does not gain its intensity from solvent perturbation. Still it may borrow intensity from an allowed transition by coupling with vibrations of proper symmetry.

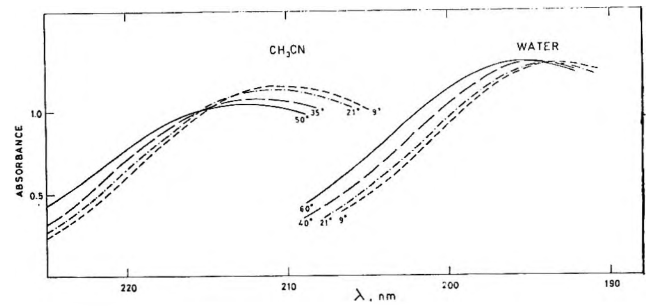

Figure 3. The effect of temperature on the spectrum of 1.14×10^{-2} *M* and 9.5×10^{-3} *M* $N(CH_3)_4NCO$ in water and CH_3CN, respectively (1-mm path length).

However, there is no need for this assumption because the band appears to originate from an orbitally allowed CTTS transition. The oscillator strength of such transitions decreases with the radius of the ion;[8] OH^- (r = 1.4 Å), Cl^- (r = 1.81 Å), and I^-(r = 2.16 Å) display CTTS bands with f = 0.04, 0.09, and 0.47, respectively.[8] The thermochemical radius of NCO^- is 1.59 Å,[9] from which $f \sim 0.06$ could be estimated. This rough interpolation involving ions of different complexity is used only to show that the observed oscillator strength of NCO^- is not unreasonable for a CTTS transition.

Using the theoretical expression[10] for $h\nu_{max}$ of a CTTS band in aqueous solution and putting r_{NCO^-} = 1.59 Å, we obtain $E_{NCO^-} \sim 73$ kcal, where E is the vertical ionization potential of the ion (the electron affinity pertaining to equilibrium configuration should be somewhat lower). Independently, r_{NCO^-} and E_{NCO^-} could be estimated from the parameters of the lines in Figure 2, as described elsewhere.[7] The values thus derived are $r_{NCO^-} \sim 1.8$ Å and $E_{NCO^-} \sim 76$ kcal. In view of the limited number of pure solvents employed in drawing the lines, the agreement is satisfactory and supports our assignment.

The CTTS bands of halide and pseudohalide ions have $h\nu_{max}$ increasing in the order;[11] $NCTe^- < NCSe^- < I^- < NCS^- < Br^- < N_3^- \sim NCO^- < Cl^-$. Except the change in putting NCO^- before Cl^-, the same sequence has been established for other electron-transfer processes involving these ions, both chemical and electrochemical.[11] This is emphasized here because in their recent works McGlynn, *et al.*, found no indication for CTTS transitions in the spectra of NCO^-, NCS^-, and N_3^-.[1,12,13] The environmental effects previously re-

(8) J. Jortner and A. Treinin, *Trans. Faraday Soc.*, **58**, 1503 (1962).
(9) G. A. Krestov, *J. Struct. Chem.* (USSR), **3**, 391 (1962).
(10) G. Stein and A. Treinin, *Trans. Faraday Soc.*, **55**, 1086 (1959).
(11) E. Gusarsky and A. Treinin, *J. Phys. Chem.*, **69**, 3176 (1965).
(12) J. R. McDonald, V. M. Scherr, and S. P. McGlynn, *J. Chem. Phys.*, **51**, 1723 (1969).
(13) J. R. McDonald, J. W. Rabalais, and S. P. McGlynn, *ibid.*, **52**, 1332 (1970).

ported[11,14,15] were either misinterpreted (as in the case of NCS^-[12]) or overlooked. The bands of NCS^- and N_3^- at ~220 nm and ~190 nm, respectively, were also assigned to orbitally forbidden transitions.[12,13] In these cases too the intensities of the bands appear to be hardly affected by polarity of solvents and the band shifts are those expected from CTTS transitions.[11,14,15] McGlynn, *et al.*, based much of their discussions on band correlations between spectra of the anion X^- and that of HX or other covalent compounds of X. However, it is difficult to ascertain which band (or bands) of, *e.g.*, HX correlates with a particular band of X^-, in particular since there is no simple correlate to a CTTS transition in a covalent molecule. Thus I^- and HI (and several other covalent iodides) have close absorption bands,[16] but they cannot be simply correlated. In the correlations proposed by McGlynn, *et al.*, bands of covalent cyanates are much weaker than the alleged forbidden transition of NCO^- at 200 nm; this is rather difficult to explain since perturbations caused by protonation should be larger than those induced by solvation.

The nature of CTTS transitions is still unclear, but the similarity between corresponding spectra of halides and pseudohalides indicates that the latter are not sub-Rydberg transitions. The relation of CTTS spectra to Rydberg transitions seems to be an important problem in spectroscopy of anions.[17] They probably involve considerable charge expansion into the polarized solvent, this being responsible for the characteristic environmental effects.

Acknowledgment. We are indebted to Mr. A. Gordin for his technical assistance.

(14) D. Shapira and A. Treinin, *J. Phys. Chem.*, **70**, 305 (1966).
(15) I. Burak and A. Treinin, *J. Chem. Phys.*, 39, 189 (1963).
(16) H. H. Jaffé and M. Orchin, "Theory and Applications of Ultraviolet Spectroscopy," Wiley, New York, N. Y., 1962, p 504.
(17) C. K. Jørgensen, "Halogen Chemistry," Vol. 1, Academic Press, New York, N. Y., 1967, p 280.

NOTES

The Thermodynamics of Mixed Chloride–Nitrate Systems[1a,b] from Glass Electrode Measurements

by J. Padova

Soreq Nuclear Research Center, Yavne, Israel *(Received April 6, 1970)*

Over the past decade it has become apparent that the glass electrode can be made to respond selectively to ions other than H^+[2a,b] and it has been widely used in the determination of the activity of aqueous solutions of sodium and potassium salts.[3–10] In this paper, measurements of potassium chloride activity coefficients in aqueous mixtures with potassium nitrate are reported and compared with earlier data[11] obtained from gravimetric isopiestic measurements.

Measurements were carried out at constant ionic strength (0.2–2.5 *m*) in order to test Harned's rule[12]

$$\log \gamma_i = \log \gamma_i(0) - \alpha_{ij} I_j \qquad (1)$$

where γ_i is the mean activity coefficient of electrolyte i in a mixture of electrolytes i + j at a constant molal ionic strength I defined by $I = {}^1/_2 \Sigma m_i Z_i^2$, m being the molal concentration and Z_i the charge on the ion, $\gamma_i(0)$ is the mean activity coefficient of electrolyte i in the pure solution at the same ionic strength, I_j is the ionic strength of component j. The constant α_{ij} is the

(1) (a) Presented in part at the 156th National Meeting of the American Chemical Society, Atlantic City, Sept 8–13, 1968. (b) Research sponsored by the U. S. Atomic Energy Commission under contract with the Union Carbide Corp.

(2) (a) G. Eisenman, "Glass Electrodes for Hydrogen and Other Cations," Marcel Dekker, New York, N. Y., 1967; (b) G. Eisenman, "Advances in Analytical Chemistry and Instrumentation," Vol. 4, C. N. Reilly, Ed., Wiley-Interscience, New York, N. Y., 1965, p 215.
(3) M. M. Shultz and A. E. Parfenov, *Vestn. Lennigrad Univ. Ser. Fiz. Khim.*, 13, 118 (1958).
(4) (a) R. D. Lanier, *J. Phys. Chem.*, **69**, 2697 (1965); (b) R. D. Lanier, *ibid.*, **69**, 3992 (1965).
(5) E. W. Moore and J. W. Ross, *J. Appl. Physiol.*, **20**, 1332 (1965).
(6) J. M. T. M. Gieskes, *Z. Physik. Chem.*, (*Frankfurt am Main*), **50**, 78 (1966).
(7) M. H. Lietzke and R. W. Stoughton, *J. Tennessee Acad. Sci.*, **42**, 26 (1967).
(8) M. H. Lietzke, R. Shea, and R. W. Stoughton, *ibid.*, **43** (1968).
(9) P. B. Hoestetler, A. H. Truesdell, and C. L. Christ, *Science*, **155**, 1537 (1967).
(10) P. Schindler and E. Wälti, *Helv. Chim. Acta*, **51**, 539 (1968).
(11) S. Amdur, J. Padova, and A. Schwartz, *Israel J. Chem.*, **5**, 23 (1967).
(12) H. S. Harned and B. B. Owen, "The Physical Chemistry of Electrolyte Solutions," ACS Monograph Series, 3rd ed, Reinhold, New York, N. Y., 1958, p 600.

slope of the linear variation of the mean activity coefficient of γ_i as a function of the ionic strength I_j of component j, or

$$\alpha_{ij} = \left(\frac{\partial \log \gamma_i}{\partial I_j}\right)_{I=0} \quad (2)$$

Experimental Section

The apparatus has already been described elsewhere.[4,13] The measuring circuit consists of a vibrating reed electrometer in conjunction with a Leeds and Northrup K-3 potentiometer and a Brown recorder.

The emf cell, K-sensitive glass electrode || KCl + KNO_3 solution AgCl(s); Ag(s), was immersed in a constant temperature bath at 25° controlled to within ±0.01° and the whole setup placed inside an aluminum shield to minimize interference during the emf determination.

The cationic glass electrode (Beckamn 39137) is described in the Beckman literature.[14] The silver–silver chloride electrode was prepared from optical silver chloride crystals[15] by electrolytically depositing silver at the point of contact between the crystal and a silver wire pressed to it. It has been shown[15] that these electrodes maintain stability for long periods of time even when frequently moved from one solution to another. The solutions were prepared by weight from recrystallized reagent grade salts and distilled water which had been run through a deionizing column. They were saturated with silver chloride by passing through a packed column of freshly precipitated and dried silver chloride crystals and mixed at constant ionic strength before a determination was made. Because of the low solubility of silver chloride, variations in its contributions to the potential should not be important.[4a]

Potential readings were made for a series of mixed solutions containing potassium chloride and potassium nitrate at a constant ionic strength I. In order to eliminate any error due to unexpected drift in the measured values a potential reading of a pure potassium chloride solution at the same ionic strength I was taken before and after each determination.

On the other hand, since the "standard potential" of a glass electrode has no readily interpretable meaning and changes with time, daily values of $\Delta E_M = E_{sat} - E_M$ were determined. E_{sat} is the potential reading for a saturated solution of potassium chloride which serves as a reference point and E_M is the potential reading of an aqueous solution of potassium chloride at an ionic strength M. The potentials were read within half an hour, on the average, when the drift of the cell potential, as indicated by the Brown recorder became less than 0.01 mV.

Results and Discussion

The mean activity coefficient γ_1 of potassium chloride in a mixed aqueous solution of potassium nitrate may be calculated from the measured potentials of the mixed

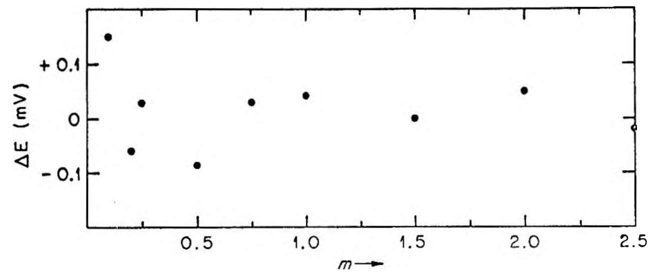

Figure 1. The deviation function ΔE at various molalities.

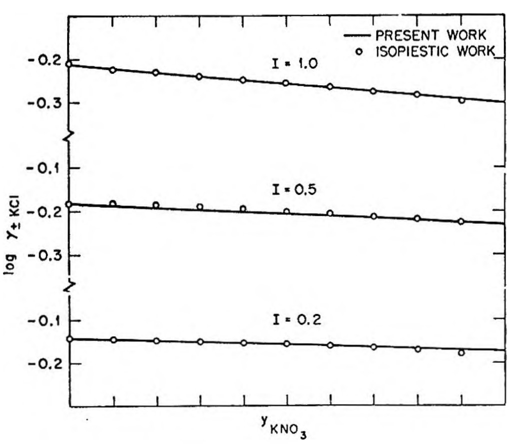

Figure 2. The activity coefficient of KCl at constant ionic strengths I.

solution E and E_M of a pure KCl solution at the same ionic strength M by the Nernst equation

$$E - E_M = 0.05915 \log \frac{m_K m_{Cl} \gamma_1^2}{a^2_{\pm M}} \quad (3)$$

where $a_{\pm M}$ is the mean activity of KCl, m_K and m_{Cl} are the potassium and chloride ion concentrations, respectively, in g-ions/kg of water in the mixed solution.

Since the potentials of all of the solutions could not be determined on the same day a definitive test of the cell performance was obtained by the calculation of a deviation function ΔE

$$\Delta E = 0.1183 \log \frac{a_{+M}}{a_{+M}} - \delta_N{}^M \quad (4)$$

where $a_{\pm M}$ and $a_{\pm N}$ are the mean activity coefficients of potassium chloride in aqueous solutions at an ionic strength of M and N, respectively, as given by Robinson and Stokes[16a] and

$$\delta_N{}^M = \Delta E_M - \Delta E_N \quad (5)$$

(13) K. A. Kraus, R. W. Holmberg, and C. J. Borkowski, *Anal. Chem.*, **22**, 341 (1950).

(14) Beckman Instructions 1155-A, Beckman Instruments, Inc., Fullerton, Calif. 12TW392, 81154.

(15) J. Greyson, *J. Electrochem. Soc.*, **106**, 745 (1962).

(16) (a) R. A. Robinson and R. H. Stokes, "Electrolyte Solutions," 2nd ed, Butterworths, London, 1959; (b) K. A. Kraus, R. J. Raridon, and W. H. Baldwin, *J. Amer. Chem. Soc.*, **86**, 2571 (1964).

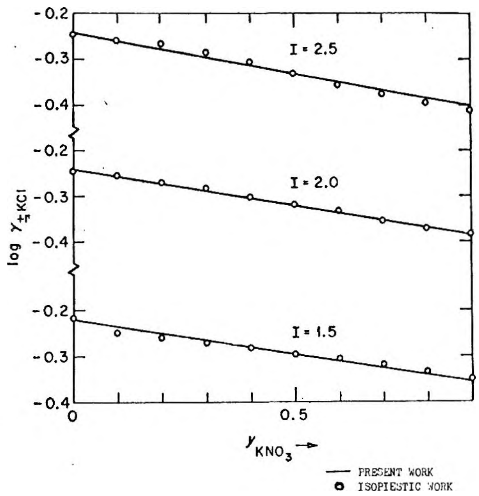

Figure 3. The activity coefficient of KCl at constant ionic strengths I.

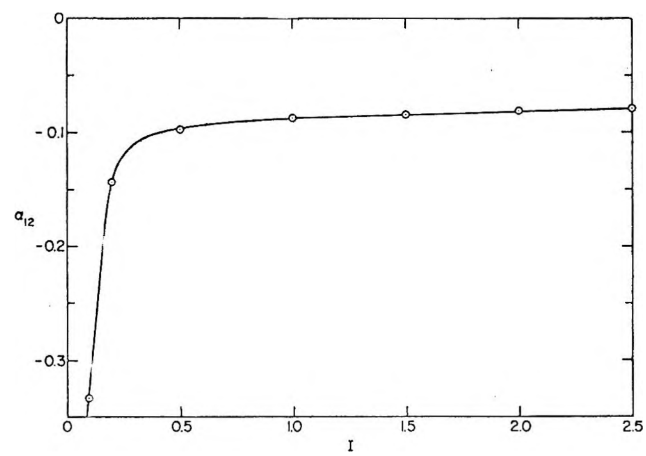

Figure 4. Harned's constant α_{12} at various total molalities.

The values of ΔE referred to an ionic strength of $I = 3.0$ are given in Figure 1. It may be seen that all the present data except for one point at a low KCl concentration are well within ± 0.1 mV of the reference line. This confirms previous evidence[4b-10] that results obtained using the alkali sensitive glass electrode system agree with the literature at least as well as the literature values agree with one another.

The mean activity coefficient of a KCl saturated solution was calculated from these results and found to be 0.590 in good agreement with Robinson and Stokes' extrapolated value[16a] and Kraus'[16b] value of 0.588.

The mean activity coefficients of potassium chloride in aqueous solutions of potassium nitrate were obtained from the emf measurements by eq 3 and are plotted in Figures 2 and 3 together with values computed from the isopiestic data[11] by the McKay–Perring transform.[17] Both sets of data seem to be in good agreement. It may be seen that in all cases Harned's rule[12] is obeyed within experimental error. The values of α_{12} seem to be independent of I for I values between 1.5–2.5 as shown

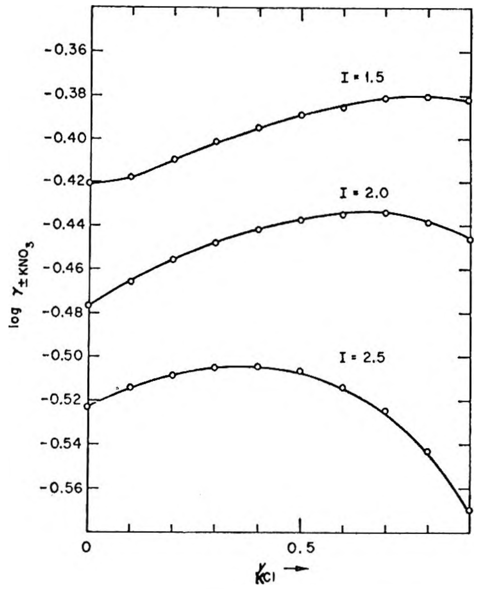

Figure 5. The activity coefficients of KNO_3 in mixed solution.

in Figure 4 and then seem to increase with decreasing I, in agreement with evidence both from experiment[18] and from Friedman's ionic solution theory[19] that the Harned rule coefficients may tend toward infinite values at zero ionic strength.

On the other hand, to describe fully the concentration behavior of the mean activity coefficient of potassium nitrate in the mixed solution requires a quadratic term the coefficient of which is denoted by subscript 21.[20] Since Harned's rule applies to potassium chloride in the mixture, it is possible to calculate subscript 21 for potassium nitrate in the same mixture as was deduced by Robinson and Stokes[20] and McKay.[21]

This concurs with the results for KNO_3[22] obtained independently by the gravimetric isopiestic methods which show that two parameters are needed to represent the variations of the activity coefficient at constant ionic strength (Figure 5).

Two other similar systems have been studied. The sodium chloride sodium nitrate system has been investigated using both the cationic glass electrode[4b] and the gravimetric isopiestic methods[23] to measure the activity of the sodium chloride in the mixture. The lithium chloride–lithium nitrate system has only been investigated by the gravimetric isopiestic method.[24] A con-

(17) H. A. C. McKay and J. K. Perring, *Trans. Faraday Soc.*, **49**, 163 (1953).

(18) J. N. Butler and R. Huston, *J. Phys. Chem.*, **71**, 4479 (1967).

(19) H. L. Friedman, "Ionic Solution Theory Based on Cluster Expansion Methods," Monographs in Statistical Physics and Thermodynamics, Vol. 3, Interscience, New York, N. Y., 1962.

(20) Reference 16a, pp 442–443.

(21) H. A. C. McKay, *Trans. Faraday Soc.*, **51**, 902 (1955).

(22) S. Amdur, J. Padova, and A. Schwartz, *J. Chem. Eng. Data*, **15**, 417 (1970).

(23) A. N. Kirgintsev and A. V. Lukyanov, *Russ. J. Phys. Chem.*, **38**, 867 (1964).

venient way of comparing the results for the three system makes use of the excess free energy function. Robinson and Bower[25] have shown the excess free energy of mixing at constant ionic strength, for two 1:1 electrolytes which follow Harned's rule, is given by eq 6.

$$\frac{\Delta G^E}{2.303AT} = -m_1m_2\{(\alpha_{12} + \alpha_{21}) + 2[m_1\beta_{12} + m_2\beta_{21} - {}^2/_3(\beta_{12} - \beta_{21})(m_1 - m_2)]\} \quad (6)$$

For the LiCl–$LiNO_3$[24] system over the ionic strength range $I = 2$–10 it may be shown that

$$\frac{\Delta G^E}{2.303RT} = -0.0027(m_1m_2)(m - 10) \quad (7)$$

and for the KCl–KNO_3 system where I ranges from 1 to 2.5 that

$$\frac{\Delta G^E}{2.303RT} = -0.020(m_1m_2)(1 + 2m - m_2) \quad (8)$$

For the NaCl–$NaNO_3$ system[4b] over the ionic range $1 \leqslant I \leqslant 6$ it would seem that the sum $\alpha_{12} + \alpha_{21}$ is dependent on the total molality[23] with behavior similar to that in the KCl–KNO_3 system. It is therefore apparent that there is slightly different behavior in the LiCl–$LiNO_3$, NaCl–$NaNO_3$, and KCl–KNO_3 systems. The same results could be obtained through Friedman's theory.[19]

It would seem that the larger deviation from ideality may be due to the difference in the symmetry of the nitrate and chloride ions since such mixtures[26,27] have shown much larger heat effects than mixtures of halides with a common cation or of alkali metals with a common anion.

Acknowledgment. The author wishes to thank Dr. K. A. Kraus and Dr. Y. Wu for the use of their laboratory and equipment.

(24) R. A. Robinson and C. K. Lim, *Trans. Faraday Soc.*, **49**, 1144 (1953).

(25) R. A. Robinson and V. E. Bower, *J. Res. Nat. Bur. Stand. Sect. A*, **69**, 439 (1965).

(26) Y. C. Wu, M. B. Smith, and T. F. Young, *J. Phys. Chem.*, **69**, 1868, 1873 (1965).

(27) R. M. Wood and R. W. Smith, *ibid.*, **69**, 2975 (1965).

Absolute Partial Molar Ionic Volumes

by Edward J. King

Department of Chemistry, Barnard College, New York, New York 10027 *(Received June 10, 1970)*

For investigation of ion–solvent interactions it is important to know the contribution of each ion to the standard partial molar volume of a salt. The determination of absolute partial molar ionic volumes has recently been reviewed by Panckhurst[1] and Millero.[2] Most determinations are based on assumptions about ionic radii in solution and the electrostatic and intrinsic contributions to the partial molar ionic volumes. In view of the variety of assumptions which have been made, it is not surprising that estimates[2] of the partial molar volume of the hydrogen ion in aqueous solution at 25° range from 0 to -7.6 ml mol^{-1}. These values need to be compared with the results of other methods that are independent of such assumptions. Zana and Yeager,[3] for example, obtained -5.4 ml mol^{-1} from vibration potential measurements. Their method of calculation has been criticized[1] and defended.[2] Conway, Verrall, and Desnoyers[4] plotted the partial molar volumes of tetraalkylammonium halides against the molar masses of the cations; the partial molar volume of the halide ion was taken to be the intercept at zero molar mass. Panckhurst[1] has criticized the use of molar mass of the cation as the independent variable, citing other possible choices. A modification of the method of Conway, Verrall, and Desnoyers is now proposed that avoids ambiguity.

The new method is based on the concepts of van der Waals volume and packing density introduced for solutes in solution in an earlier paper.[5] It is assumed that ions in solution have the same internal dimensions and intermolecular contact distances as those in crystals,[6] but differ in having lower coordination numbers. The van der Waals volume V_w of an ion is its intrinsic volume minus the volume change that results when it forms hydrogen bonds with solvent molecules.[7] The geometrical model[7] used for calculating V_w is shown in Figure 1. Atoms are treated as overlapping spheres with volumes determined by covalent bond lengths,[8] hydrogen bond lengths,[9] and van der Waals radii.[7] Some of these lengths are given in Figure 1. The C–N covalent bond length is uncertain: several X-ray diffraction studies of crystalline alkylammonium salts give values around

(1) M. H. Panckhurst, *Rev. Pure Appl. Chem.*, **19**, 45 (1969).

(2) F. Millero in "Structure and Transport Processes in Water and Aqueous Solutions," R. A. Horne, Ed., Interscience, New York, N. Y., in press. Millero has recalculated the results of earlier workers so that all estimates are based on the most reliable partial molar volume data.

(3) R. Zana and E. Yeager, *J. Phys. Chem.*, **71**, 521 (1967).

(4) B. E. Conway, R. E. Verrall, and J. E. Desnoyers, *Trans. Faraday Soc.*, **62**, 2738 (1966).

(5) E. J. King, *J. Phys. Chem.*, **73**, 1220 (1969).

(6) R. H. Stokes, *J. Amer. Chem. Soc.*, **86**, 979 (1964); S. W. Benson and C. J. Copeland, *J. Phys. Chem.*, **67**, 1194 (1963).

(7) A. Bondi, *ibid.*, **68**, 441 (1964).

(8) G. D. Stucky, *Acta Crystallogr.*, **B24**, 330 (1968); J. Lindgren and I. Olovsson, *ibid.*, **B24**, 549, 554 (1968); J. D. McCullough, *ibid.*, **17**, 1067 (1964); M. Bonamico, G. A. Jeffrey, and R. K. McMullan, *J. Chem. Phys.*, **37**, 2219 (1962); T. Migchelsen and A. Vos, *Acta Crystallogr.*, **23**, 796 (1967); P. F. Zanazzi, *ibid.*, **B24**, 499 (1968); R. K. McMullan, M. Bonamico, and G. A. Jeffrey, *J. Chem. Phys.*, **39**, 3295 (1963).

(9) G. S. Pimentel and A. L. McClellan, "The Hydrogen Bond," Freeman, San Francisco, Calif., 1960, Chapter 9.

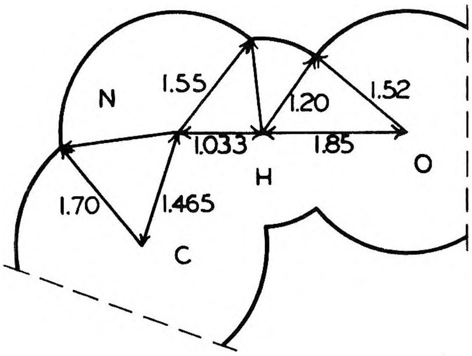

Figure 1. Geometrical model for calculation of van der Waals volumes. Portions of an alkylammonium ion and a water molecule are shown. Bond lengths and radii are given in Angström units.

1.465 Å while others give values near 1.52 Å.[8] Bondi's table of group contributions[7] to V_w makes it easy to compute the van der Waals volumes of long chain ions.

The packing density of a solute in solution is defined as the ratio of its van der Waals volume to its partial molar volume[5]

$$d = V_w/V^{\ominus} \quad (1)$$

It has been observed[5] that for a given class of molecular solutes the packing densities approach a uniform value as the size of the molecules increases. That such plateau densities also exist for ions is evident from the data of Table I. All alkylammonium bromides whose cations have van der Waals volumes greater than about 50 ml mol^{-1} have a packing density of 0.654 within an average deviation of only 0.3%. Similar constancy is observed for the more limited number of chlorides and iodides for which accurate partial molar volumes are known.[2] (In all three series the tetraethylammonium halides are significantly out of line. The reason for this deviation is unknown.) Since the bromide ion is common to the series in Table I, constancy of packing densities of the salts implies that all the larger cations have the same packing density d_+.

Table I: Properties of Some Alkylammonium Bromides in Aqueous Solution at 25°

Substance	$V^{\ominus}$ (salt) ml mol^{-1}	V_w (cation) ml mol^{-1}	d (salt)	References
NH_4Br	42.57	11.9	0.720	*a*
$MeNH_3Br$	60.82	22.8	0.682	*a*
$EtNH_3Br$	77.65	33.0	0.666	*a*
n-$PrNH_3Br$	94.15	43.2	0.658	*a*
n-$BuNH_3Br$	110.20	53.4	0.655	*a*
Me_4NBr	114.2	55.3	0.648	*b–e*
n-$PeNH_3Br$	126.15	63.7	0.653	*a*
n-$HxNH_3Br$	142.04	73.9	0.652	*a*
n-$HpNH_3Br$	157.94	84.1	0.651	*a*
n-$OcNH_3Br$	173.86	94.4	0.650	*a*
Et_4NBr	173.8	96.2	0.659	*b–d*
n-Pr_4NBr	239.6	137.1	0.650	*b,d*
n-Bu_4NBr	301.0	178.0	0.654	*b,f*
n-Pe_4NBr	363.9	219.0	0.653	*d*

[a] E. Desnoyers and M. Arel, *Can. J. Chem.*, **45**, 359 (1967). [b] F. Franks and A. T. Smith, *Trans. Faraday Soc.*, **63**, 2586 (1967). [c] H. E. Wirth, *J. Phys. Chem.*, **71**, 2922 (1967). [d] B. E. Conway, R. E. Verrall, and J. E. Desnoyers, *Trans. Faraday Soc.*, **62**, 2738 (1966). [e] L. G. Hepler, J. M. Stokes, and R. H. Stokes, *ibid.*, **61**, 20 (1965). [f] L. A. Dunn, *ibid.*, **64**, 1898 (1968).

The absolute partial molar volume of the hydrogen ion can be obtained in the following way. If we subtract the well established[2] standard partial molar volumes of the hydrohalic acids from those of the alkylammonium halides, the effect of the anion cancels

$$V^{\ominus}(\text{RAmmX}) - V^{\ominus}(\text{HX}) = V^{\ominus}(\text{RAmm}^+) - V^{\ominus}(\text{H}^+) \quad (2)$$

Then we use the definition of packing density to eliminate the partial molar volume of the alkylammonium ion

$$V^{\ominus}(\text{RAmmX}) - V^{\ominus}(\text{HX}) = \frac{1}{d_+}V_w(\text{RAmm}^+) - V^{\ominus}(\text{H}^+) \quad (3)$$

Since d_+ is constant for large cations, the left-hand side should be a linear function of the van der Waals volume with intercept equal to $-V^{\ominus}(\text{H}^+)$.

For the determination of $V^{\ominus}(\text{H}^+)$ we have 22 salts, containing 13 different cations, with accurately known values of the partial molar volume. These include the ten bromides of Table I beginning with *n*-butylammonium bromide, six chlorides,[10] and six iodides.[10] If the C–N covalent bond length is taken to be 1.465 Å, we obtain $d_+ = 0.655 \pm 0.003$ and $V^{\ominus}(\text{H}^+) = -4.9 \pm 0.7$ ml mol^{-1} where the uncertainties are standard deviations obtained from a least-squares analysis. This value for the absolute partial molar volume of the hydrogen ion is in good agreement with the result, -5.4 ml mol^{-1} reported by Zana and Yeager.[3]

The purpose of this note is not to promulgate one more value for the absolute partial molar volume of the hydrogen ion but to propose a method of determining absolute partial molar volumes that has a sound empirical basis and is capable of further improvement. The method is not restricted to spherical ions. It invokes no semitheoretical expression for electrical or intrinsic contributions to the partial molar volume. It does provide a way of taking into account hydrogen bonding between solute and solvent. This makes it possible to use data for primary, secondary, and tertiary ammonium ions as well as those for quaternary ions. The extrapolation is then based on 13 cations, not just four or five.

(10) B. E. Conway, R. E. Verrall, and J. E. Desnoyers, *Trans. Faraday Soc.*, **62**, 2738 (1966); R. E. Verrall and B. E. Conway, *J. Phys. Chem.*, **70**, 3961 (1966).

An improvement in the precision of the extrapolation may be expected as more and better data become available. Some good partial molar volumes of secondary and tertiary alkylammonium bromides would be most useful to have. The calculation of van der Waals volumes is also subject to refinement. We need more reliable values for the bond lengths because the effect of a small variation in the C–N bond length is substantial. If we use 1.520 Å for this length, instead of 1.465, we obtain $V^{\ominus}(H^+) = -4.2 \pm 0.8$ ml mol^{-1}. The model of overlapping spheres used in calculating the van der Waals volume is admittedly a crude one. We might improve it by treating the atoms as pear-shaped.[7]

Acknowledgment. I thank Dr. Millero for allowing me to see his review[2] prior to its publication.

Complexes of Peroxy Radical with Transition Metal Ions

by A. Samuni* and Gideon Czapski

Department of Physical Chemistry, The Hebrew University, Jerusalem, Israel *(Received June 17, 1970)*

Several esr experiments have provided evidence for the existence of paramagnetic transients formed by HO_2 radical and metal ions such as Ti^{4+},[1-4] V^{5+},[5-8] Ce^{3+},[9] and Zr^{4+}.[5] Regarding Ti^{4+} [2] and V^{5+},[8] it was shown that peroxy complexes of the metal are involved in the formation of the peroxy–metal paramagnetic transient.

The study of these complexes was carried out mainly by esr spectroscopy of flowing mixtures of H_2O_2 and metal ions in a flow system.

In the primary step the metal ion reacts with an excess of H_2O_2, yielding HO_2 radicals according to either

$$Ce^{4+} + H_2O_2 \xrightarrow{k_1} Ce^{3+} + H^+ + HO_2 \quad (1)$$

or

$$M^{n+} + H_2O_2 \longrightarrow M^{(n+1)+} + OH^- + OH \quad (2)$$

followed by

$$OH + H_2O_2 \longrightarrow H_2O + HO_2 \quad (3)$$

(where M = Ti^{3+}, Fe^{2+}, V^{4+}).

The subsequent process involves the reaction between the HO_2 radical and the metal ion. In the present work we studied the esr spectra of the transients formed on mixing HO_2 radicals with solutions of U^{6+}, Th^{4+}, Mo^{6+}, and Zr^{4+}

The experiments were carried out using a flow system equipped with a double mixing cell; the experimental details were described elsewhere.[9] The HO_2 radicals were generated through reaction 1 in perchloric acid at the first mixing stage of the mixing cell and then after reaction 1 has been completed were mixed with the solutions of the metal ions at a second mixing stage. The final mixture flowed through the cavity of an esr spectrometer where the esr spectra were recorded.

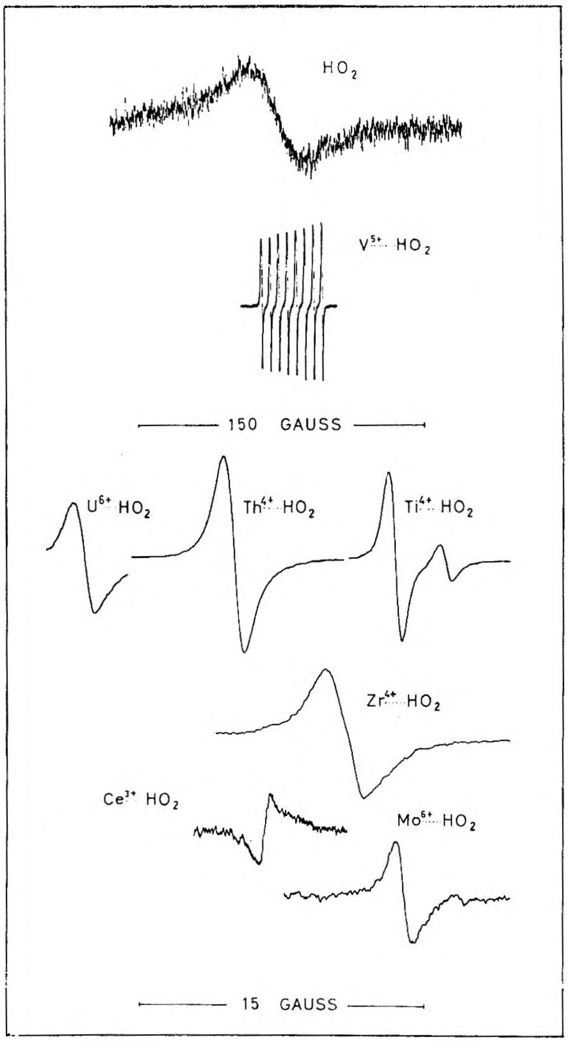

Figure 1. Esr spectra of M–HO_2 complexes: the esr signals in 0.1 *M* $HClO_4$, obtained on mixing HO_2 with the corresponding metal ions, compared with the free HO_2 radical.

The Esr Spectra of the HO_2–Metal Transients. The

* To whom correspondence should be addressed.

(1) W. T. Dixon and R. O. C. Norman, *Nature*, **196**, 891 (1962).
(2) V. H. Fischer, *Ber. Bunsenges Physik. Chem.*, **71**, 685 (1967).
(3) F. Sicilio, R. E. Florin, and L. A. Wall, *J. Phys. Chem.*, **72**, 3154 (1958).
(4) M. S. Bains, J. C. Arthur, and O. Hinojosa, *ibid.*, **72**, 2250 (1968).
(5) V. F. Shuvalov and N. M. Bazhin, *Zh. Strukt. Khim.*, **10**, 548 (1969).
(6) M. Setaka, Y. Kirino, T. Ozawa, and T. Kwan, *J. Catal.*, **15**, 209 (1969).
(7) M. S. Bains, J. C. Arthur, and O. Hinojosa, *J. Amer. Chem. Soc.*, **91**, 4673 (1969).
(8) A. Samuni and G. Czapski, *Israel J. Chem.*, **8**, 563 (1970).
(9) G. Czapski, H. Levanon, and A. Samuni, *ibid.*, **7**, 375 (1969).

esr spectra obtained from HO_2 reacting with U^{6+}, Th^{4+}, Zr^{4+}, Mo^{6+}, and those previously observed[1-8] from the reaction of HO_2 radical with Ce^{3+}, Ti^{4+}, and V^{5+} [1,8] are compared in Figure 1, while the magnetic parameters of the various signals are summarized in Table I.

Table I: Magnetic Parameters of the Esr Signals of HO_2 and $M-HO_2$ Complexes

Paramagnetic species	Line width, G	g Value
HO_2	27	2.0140
$V^{5+}-HO_2$[a]	0.74-0.66	2.0109
$Ti^{4+}-HO_2$[b]	0.7, 0.5	2.0140, 2.0120
$Ce^{3+}-HO_2$	1.3	2.0180
$Zr^{4+}-HO_2$	2.7	2.0158
$Th^{4+}-HO_2$	1.1	2.0190
$U^{6+}-HO_2$	1.2	2.0209
$Mo^{6+}-HO_2$	0.73	2.0140

[a] Eight lines from low to high field. [b] Pair of $Ti^{4+}-HO_2$ esr signals from low to high field.

The Precursors of the Paramagnetic Transients. Each of the metal ions which has been studied (Zr^{4+}, Th^{4+}, U^{6+}, Mo^{6+}) was in its higher normal oxidation state, *i.e.*, without an unpaired electron, and evidently neither the solution of the metal ion, nor the aged reaction mixture, gave rise to an esr signal. Moreover, no esr signal was observed on mixing the metal ion solution either with H_2O_2 or with Ce^{4+} ions (provided the metal ion solution did not contain H_2O_2). On the other hand, for a given $[HO_2]$, an increase of the concentration of the metal ion in a given range markedly enhanced the esr signal of the transient. When $[HO_2]$ itself was increased, the esr signal increased as well. These results suggest that both the HO_2 radical and the metal ion are requisite for the generation of the paramagnetic species which are responsible for the esr signals.

The Role of H_2O_2. The effect of the addition of H_2O_2 to the metal in solution was investigated in order to check whether a premixing of H_2O_2 with the metal is necessary. This would clarify the role of the peroxy-metal complex and that of the free metal ion in the formation of the paramagnetic transient with HO_2. In the case of Ti^{4+} [2-4] and V^{5+},[8] the H_2O_2 is requisite for the primary redox reaction as well as for the generation of a peroxy–metal complex which reacts with the HO_2 radical. (The free metal ions do not react with HO_2 to give a species observable by esr.)

In the case of the actinides (Th^{4+}, U^{6+}) the only effect of the addition of H_2O_2 up to 1 M to the metal ion solution (*i.e.*, the ratio $[H_2O_2]/[\text{metal}]$ was varied from 0 up to 1000) was an increase of about 70% in the signal intensity.

In the case of Mo^{6+} the signal intensity decreased on the addition of H_2O_2. The spectrum totally disappeared when $[H_2O_2]$ was greater than $[Mo^{6+}]$.

When H_2O_2 was added to 0.5 mM Zr^{4+} the signal decreased and totally disappeared at $[H_2O_2]/[Zr] = 4000$.

Thus we may conclude that peroxy complexes of Zr^{4+} and Mo^{6+} either do not react with HO_2 radical or, on reacting with HO_2, form a species not detectable by esr spectroscopy.

Regarding the two actinides, we may assume that either the same transient is formed by the interaction of HO_2 radical with both the metal ion and its peroxy complex or the two transients have identical esr spectra. Therefore, the possible reaction pathways might be

$$M + HO_2 \longrightarrow M-HO_2 \tag{4}$$

$$M-H_2O_2 + HO_2 \longrightarrow M-HO_2 + H_2O_2 \text{ or } M-H_2O_2-HO_2 \tag{5}$$

The slight enhancement of the signal when H_2O_2 was added might be explained by a greater scavenging efficiency of the peroxy–metal complex towards the HO_2 radical ($k_5 > k_4$).

Decay Kinetics of the Transient. The decay of the transients was followed in the esr cavity using the stopped-flow technique. We found for the transients formed by Zr^{4+}, Th^{4+}, and U^{6+} that the decay seemed to be nearly first order at high metal ion concentrations. Under these conditions the decay rate was independent on $[H_2O_2]$ and $[M]$ and increased slightly with $[H^+]$. At low $[M]$ the decay became faster and the order was neither first order nor pure second order.

The half-lifetimes of the HO_2 complexes with Zr^{4+}, Th^{4+}, and U^{6+} ($\sim 10^{-3}$ M) were similar to those observed for Ti^{4+} and V^{5+} [8] and were of the order of a few tenths of a second to several seconds.

Exchange of the Peroxy Group between Different Metal Ions. As described above, the HO_2 radical with various metal ions yields paramagnetic transients which might be denoted by $M-HO_2$. We studied the possibility of an exchange reaction between a peroxy–metal transient and another metal ion as given by

$$M-HO_2 + M' \rightleftharpoons M + M'-HO_2 \tag{6}$$

This was done by treating Ce^{4+} with a solution of $M + H_2O_2$ yielding $M-HO_2$ transient. This solution was mixed thereafter with a solution of M'. As a result the esr spectrum of $M'-HO_2$ appeared while the $M-HO_2$ signal correspondingly decreased. The same results were observed when the roles of M and M' were exchanged.

We studied reaction 6 in the following pairs of metal ions: $U^{6+}-Th^{4+}$, $Th^{4+}-Zr^{4+}$, $Zr^{4+}-U^{6+}$, $Th^{4+}-Ti^{4+}$, $U^{6+}-Ti^{4+}$, $V^{5+}-Ti^{4+}$, and found that reaction 6 occurs as well as its back-reaction.

Further studies on the formation rates and equilibrium constants of the $M-HO_2$ complexes as well as on the exchange rates and k_{eq} of reaction 6 are under investigation.

This kind of rather fast exchange of HO_2 among different metal ions may have an important role in similar reactions in biological systems.

Acknowledgment. We gratefully acknowledge the support of this research by the U. S. Atomic Energy Commission under Contract AT(30-1)-3753.

Dielectric Constant and Refractive Index of Weak Complexes in Solution. II[1a]

by M. E. Baur,* C. M. Knobler, D. A. Horsma, and P. Perez

Department of Chemistry,[1b] University of California, Los Angeles, California 90024 *(Received June 29, 1970)*

In a previous communication,[2] we reported the results of measurements of the molar polarization (P) and molar refraction (R) of benzene (B) and hexafluorobenzene (HFB) liquid mixtures over the entire composition range at 25°. One of the goals of that work was to obtain evidence bearing on the nature of the molecular complex believed to be present in that system.[3] The P of the mixtures studied was found to be additive to within experimental error; R showed a negative deviation from additivity well in excess of that typically found in mixtures of nonpolar species not exhibiting specific complexing effects. From these observations, we concluded that a significant concentration of B–HFB complex is present in the mixtures. The observed additivity in P is, however, incompatible with any important contribution of charge-transfer effects[4] to the stability of the complex, for the maximum dipole moment associated with this complex could not be more than about 0.1 D on the basis of our data. An alternative possibility is that the formation of the complex in the B–HFB system is to be attributed to electrostatic, induction and dispersion interactions. Recent theoretical studies[5,6] have indicated the importance of such interactions even in the benzene–halogen complexes, usually considered the archetype of charge-transfer species. Since our data could not be considered altogether conclusive, it seemed appropriate to extend the optical and dielectric measurements to liquid mixtures of HFB with the nonpolar methyl-substituted species *p*-xylene (X) and mesitylene (M), with which it is miscible in all proportions at somewhat elevated temperatures and with which it forms 1–1 solid solutions.[7] The donor strength for charge-transfer complex formation in the aromatic hydrocarbons is known to increase in the sequence B–X–M[6,8] and it might therefore be expected that charge-transfer effects with HFB, if any, would become apparent in mixtures of this species with X and M. In this note we report the results of such measurements.

Experimental Section

Details of the experimental methods have been previously described.[2] The benzene and hexafluorobenzene were the same materials used in the previous study; reagent grade *p*-xylene (Matheson Coleman and Bell) and research grade mesitylene (Phillips Petroleum) were distilled from over sodium just before use. Gas chromatographic analysis showed these latter materials to have a purity of 99.98 and 99.95%, respectively.

Refractive indices at 40° were measured at seven wavelengths for each mixture and the data were fitted to a three-term Cauchy dispersion formula by the method of least squares. The values of the constants n_∞, b, and c obtained by this procedure are listed in Table I. The dispersion relations fit each set of data with a standard deviation no greater than 0.0002, the estimated uncertainty of an individual refractive index measurement; the standard deviations listed for n_∞ have also been obtained from the analysis.

For the *p*-xylene and mesitylene mixtures, dielectric constants were measured for the pure components and three mixtures at 40°. No new data were obtained for the B–HFB system at 40°. However, in our previous paper[2] we reported dielectric measurements on this system at 10° intervals from 25 to 65°. Values of the molar polarization for B–HFB reported here have been obtained from these data by interpolation.

The molar volume of hexafluorobenzene was taken from the data of Counsell, *et al.*,[9] and the volumes of the hydrocarbons from the compilation by Timmermans.[10] These data for the pure components were combined with measurements of the excess volume[11] to obtain the molar volumes of the mixtures as given in Tables I and II.

* To whom correspondence should be addressed.

(1) (a) Supported in part by the National Institutes of Health, Public Health Service under Grant No. GM 11125. (b) Contribution No. 2645.

(2) M. E. Baur, D. A. Horsma, C. M. Knobler, and P. Perez, *J. Phys. Chem.*, **73**, 641 (1969).

(3) D. V. Fenby, I. A. McLure, and R. L. Scott, *ibid.*, **70**, 602 (1966).

(4) G. Briegleb, "Charge-Transfer Complexes," Springer-Verlag, 1962, Section III.

(5) M. W. Hanna, *J. Amer. Chem. Soc.*, **90**, 285 (1968).

(6) J. C. Lippert, M. W. Hanna, and P. J. Trotter, *ibid.*, **91**, 4035 (1969).

(7) W. A. Duncan and F. L. Swinton, *Trans. Faraday Soc.*, **62**, 1082 (1966); J. C. A. Boeyens and F. H. Herbstein, *J. Phys. Chem.*, **69**, 2153 (1965).

(8) M. Kroll, *J. Amer. Chem. Soc.*, **90**, 1097 (1968).

(9) J. F. Counsell, J. H. S. Green, J. L. Hales, and J. F. Martin, *Trans. Faraday Soc.*, **61**, 212 (1965).

(10) J. Timmermans, "Physico-Chemical Constants of Pure Organic Compounds," Elsevier Publishing Co., New York, N. Y., 1965.

(11) W. A. Duncan, J. P. Sheridan, and F. L. Swinton, *Trans. Faraday Soc.*, **62**, 1090 (1966).

Table I: Molar Refraction at Infinite Wavelength

$X_{C_6F_6}$	n_∞	$b \times 10^{-5}$ (Å^{-2})	$c \times 10^{-12}$ (Å^{-4})	$\bar{V}$ (cm^3/mol)	R_M^∞ (cm^3/mol)
		C_6H_6–C_6F_6, 40.10°			
0.0000	1.4675 ± 0.0012	6.32	3.1	91.09	25.30 ± 0.06
0.1728	1.4337 ± 0.0014	7.26	0.7	96.41	25.09
0.3683	1.4086 ± 0.0005	4.83	2.6	101.93	25.18
0.3794	1.4091 ± 0.0009	3.62	3.8	102.46	25.33 ± 0.05
0.4753	1.3946 ± 0.0013	5.44	1.0	104.85	25.11 ± 0.07
0.6466	1.3774 ± 0.0011	5.65	0.1	109.33	25.17 ± 0.07
0.7622	1.3713 ± 0.0016	4.02	1.8	112.28	25.47
1.0000	1.3546 ± 0.0009	3.89	1.3	118.32	25.76 ± 0.06
		C_8H_{10}–C_6H_6, 40.11°			
0.0000	1.4621 ± 0.0010	7.70	0.9	125.85	34.60 ± 0.06
0.1392	1.4472 ± 0.0005	5.55	2.8	124.89	33.37 ± 0.03
0.2858	1.4298 ± 0.0014	4.58	3.1	123.83	31.97
0.4444	1.4112 ± 0.0015	3.97	3.2	122.60	30.44 ± 0.10
0.7736	1.3771 ± 0.0014	3.26	2.6	120.06	27.61 ± 0.09
0.7761	1.3738 ± 0.0006	4.72	0.9	120.03	27.39
1.0000	1.3574 ± 0.0018	2.35	3.1	118.33	25.94 ± 0.11
		C_9H_{12}–C_6F_6, 40.19°			
0.0000	1.4677 ± 0.0008	7.02	1.7	144.68	39.36 ± 0.06
0.2069	1.4442 ± 0.0004	5.79	2.0	136.66	36.31 ± 0.03
0.2779	1.4385 ± 0.0010	4.15	3.7	134.94	35.45
0.4083	1.4275 ± 0.0015	2.37	5.3	131.80	33.87 ± 0.11
0.4371	1.4163 ± 0.0005	5.67	0.9	131.12	32.92
0.5709	1.4018 ± 0.0010	4.89	1.5	127.99	31.14 ± 0.07
0.7020	1.3901 ± 0.0016	3.23	3.0	125.02	29.63 ± 0.11
1.0000	1.3582 ± 0.0014	1.74	3.9	118.31	25.99 ± 0.09

Table II: Molar Polarization

$X_{C_6F_6}$	ϵ	$\bar{V}$ (cm^3/mol)	$P_M^{40°C}$ (cm^3/mol)
	C_6H_6–C_6F_6, 40.0°		
0.0000	2.275	89.41	26.72
0.2522	2.187	96.82	27.52
0.3817	2.152	100.33	27.90
0.4466	2.130	102.02	27.98
0.4850	2.127	103.01	28.22
0.6167	2.091	106.36	28.44
0.7419	2.066	109.46	28.76
0.8687	2.052	112.60	29.32
1.0000	2.029	115.79	29.68
	C_8H_{10}–C_6F_6, 40.0°		
0.0000	2.2402	125.72	36.78
0.2392	2.1816	124.09	25.06
0.5047	2.1169	122.06	33.11
0.7560	2.0542	120.15	31.24
1.0000	1.9922	118.31	29.41
	C_9H_{12}–C_6F_6, 40.0°		
0.0000	2.2580	141.67	41.86
0.2702	2.1959	135.04	38.48
0.4730	2.1452	131.26	35.98
0.8304	2.0431	122.15	31.51
1.0000	1.9922	118.31	29.41

Results

Values of R^∞, the molar refraction at infinite wavelength, are given in Table I for each of the three systems studied. They have been calculated from the infinite wavelength refractive index, n_∞, and the molar volume $\bar{V}$. The dielectric constants and molar polarizations for these systems are likewise given in Table II. From these data it is easily seen that for both the X–HFB and M–HFB mixtures, as for the B–HFB mixtures, P is additive to within experimental error over the entire concentration range, but as for the B–HFB mixtures, a sizable negative deviation in R is found for both of the new systems. Plots of P and R *vs.* concentration for the new systems are identical in general aspect with Figure 1 of ref 2 and are not included here.

These observations are best analyzed by considering the values for the quantity Δ defined in eq 13 of ref 2, the differential increment between P and R. As noted there, this quantity if interpreted in terms of the contribution of a complex to the low-frequency electric properties of a solution is given in lowest order by

$$\Delta = K_x\left(\frac{\mu_c^2}{3kT} + \alpha_c^a\right)\Big/(K_x + 1) \qquad (1)$$

where K_x is the mole fraction equilibrium constant for formation of the complex and μ_c and α_c^a are the dipole moment and (incremental) atomic polarizability of the complex, respectively. For HFB mole fraction equal to $^1/_2$, our results yield Δ(B–HFB) = 0.35, Δ(X–HFB) = 0.33 and Δ(M–HFB) = 0.38 at 40°. The experimental uncertainty in these values is ±0.05. Hence little significance can be ascribed to this small observed variation, and to within experimental error we conclude that Δ is constant throughout the series. Other tests for trends in the data for the three systems could be given, but would be less sensitive to changes than comparison of Δ values.

The pronounced departure from additivity in R provides positive evidence for the presence of a complex in both X–HFB and M–HFB mixtures. However, the analysis[2] of the maximum μ_c consistent with the data previously obtained for B–HFB mixtures also holds in an approximate way here. The dipole moments of the X–HFB and M–HFB complexes accordingly cannot be greater than 0.1–0.2 D. We cannot in practice make reliable direct estimates of K_x and μ_c separately from our data. Nevertheless, it is clear that either both these quantities remain sensibly constant through the series of mixtures studied or that an increase in one with ring methylation is largely compensated by a decrease in the other.

Some further considerations can be adduced. If one makes the physically plausible assumption that the entropy of formation of the complex is about the same throughout the series investigated here, then K_x is a measure of the heat of formation of the complex. If charge-transfer effects were to play a significant role in stabilizing the complex, then for given geometry K_x would be expected to increase with methylation of the benzene ring. However, such an increase in charge-transfer character would also entail an increase in μ_c,[4] behavior inconsistent with what is observed. This reinforces our conclusion that charge-transfer effects are of negligible importance for the formation of complexes in the systems studied here. The role of electrostatic, induction, and dispersion interactions in stabilizing complexes formed by methylated benzenes with the halogens and TCNE has recently been subjected to theoretical analysis,[5,6] and it was concluded that such interactions make contributions to the energy of formation of these complexes comparable in magnitude to that of charge transfer. The case of the B–TCNE complex is most relevant for comparison with the systems studied here; TCNE is a π electron system, like HFB, and is expected to have electrostatic and dispersion interaction parameters not significantly different from the latter. It should be noted that the principal contribution to stabilization of the B–TCNE complex from other than charge transfer appears to come from the electrostatic quadrupole–quadrupole interaction.[6] The magnitude of this interaction in the B–HFB complex should be comparable to that in the B–TCNE complex. Of particular interest is the result[6] that the electrostatic, induction, and dispersion interactions contribute approximately −9 kcal/mol to the heat of formation of the B–TCNE and X–TCNE complexes (the precise figure depending on the angle of orientation of TCNE in the complex) but only 0.11 and 0.14 D, respectively, to the dipole moments of these complexes. Thus, there exists an example of a system for which the computed electrostatic, induction, and dispersion interactions give a significant stabilization of the complex without producing a significant dipole moment. In view of the probable similarity in interaction parameters between the TCNE complexes and the complexes formed by benzene and its methylated homologs with HFB, it appears reasonable, therefore, to assert that the latter complexes are stabilized nearly exclusively by such noncharge-transfer interactions. Detailed theoretical calculations for the HFB complexes would be of help in making this conclusion precise and are being carried out.[12] We may also remark that the calculations on the B–TCNE and X–TCNE systems[6] indicate a net decrease in magnitude of the heat of formation of the complex in passing from B to X in consequence of the greater exchange repulsion energy of the complex formed from the latter species. A similar moderate decrease in heat of formation in the HFB complexes in passing from B to X, together with a small increase in the dipole moment of the complex, would be consistent with our data. No very strong conclusion on this point should be drawn, however, as it is evident that steric factors may play a more significant role in the case of the HFB complexes than in that of the TCNE complexes.

Finally, it should be noted that we previously found Δ(B–HFB) to be 0.55 at 25°.[2] If we assume that the decrease in this quantity to 0.35 at 40° reported here is entirely due to the temperature dependence of K_x, we obtain an estimate for the heat of formation of the B–HFB complex of −5 kcal/mol. This value is in reasonable agreement with an estimate obtained from measurements on B–HFB mixtures in the gas phase.[13]

(12) M. W. Hanna, private communication.

(13) E. M. Dantzler and C. M. Knobler, *J. Phys. Chem.*, **73**, 1602 (1969).

Field-Induced Ion Dissociation and Spontaneous Ion Decomposition in Field Ionization Mass Spectrometry

by James C. Tou

Chemical Physics Research Laboratory, The Dow Chemical Company, Midland, Michigan 48640 *(Received July 10, 1970)*

The fundamental mechanistic studies of field ionization mass spectrometry[1,2] and the great usefulness in

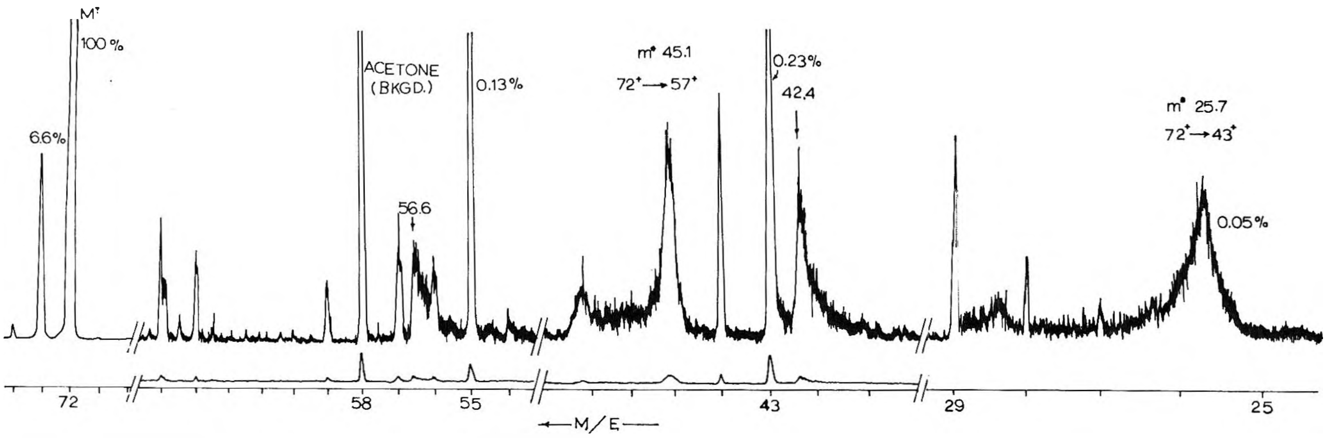

Figure 1. Field ionization mass spectrum of methyl ethyl ketone.

organic structure elucidation of the technique[3] have been reported in recent years. There are four different shapes of peaks observed in field ionization mass spectrum due to the ions generated from different processes.[1] (1) The normal symmetric peaks are due to molecular ions or fragment ions generated in an extremely short time ($\sim 10^{-14}$ to $\sim 10^{-12}$ sec) after the parent ions are formed. (2) The skew peaks at integer mass and with continuous tailing toward low mass are due to fragment ions formed along the ion path at various distances from the surface of the field emitter but with lower potential than the ion acceleration voltage. The ions contributing to the peak tailing are formed within $\sim 10^{-12}$ to $\sim 10^{-6}$ sec. (3) The noninteger diffuse peaks at $m^* = m_2^2/m_1$ are due to the ions produced from the spontaneous ion decomposition $m_1^+ \rightarrow m_2^+$ occurring in the field-free region between the source exit slit and the entrance slit of the magnet with transit time of $\sim 10^{-6}$ sec. (4) The skew molecular ion peak displaced from its integer mass, reported recently by Block,[2] is proved to be due to so-called remote ionization. The ionization takes place at a certain distance from the field emitter if the emitter voltage is very high.

Recently, we have observed displaced skew fragment ion peaks in our studies of 1-chloro-2-nitrosocycloalkanes[4] and dialkyl phthalates.[5] In the studies of the field ionization mass spectra of acetone, perdeuterated acetone and methylethyl ketone, we found that the displaced skew fragment ion peaks are always associated with the fragment ion generated from the following reaction

$$\mathrm{R{-}C({=}O^{+\cdot}){-}R'} \longrightarrow \mathrm{R{-}C{\equiv}O^+} + \cdot\mathrm{R'}$$

where the metastable ion is present. As a representative case, the field ionization mass spectrum of methyl ethyl ketone is shown in Figure 1. The two metastable ions corresponding to the above transition are detected at m/e 25.7 ($72^+ \rightarrow 43^+ + 29$) and 45.1 ($72^+ \rightarrow 57^+ + 15$). The fragment ions, m/e 43 and 57, with

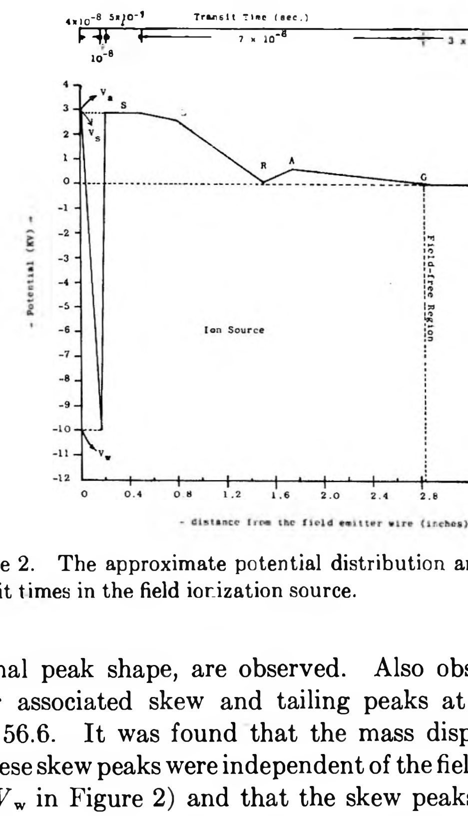

Figure 2. The approximate potential distribution and the transit times in the field ionization source.

normal peak shape, are observed. Also observed are their associated skew and tailing peaks at m/e 42.4 and 56.6. It was found that the mass displacements of these skew peaks were independent of the field strength (or V_w in Figure 2) and that the skew peaks were observed at times in the absence of their counterpart peaks with integer mass and normal symmetrical peak shape.[4,5] These displaced skew fragment ion peaks were proposed[4,5] to be due to the ions decomposed in the field-free region of a cylindrical focussing electrode (S) after leaving the high electric field. The approximate potential distribution in the field ionization source (Varian-Atlas CH4B mass spectrometer) is shown in Figure 2. The field emitter is a Wollaston wire with radius of about 1.5 μ. For an ion decomposition, m_1^+

(1) H. D. Beckey, H. Hey, K. Levsen, and G. Tenschert, *J. Mass Spectrom. Ion Phys.*, **2**, 101 (1969), and the references therein.
(2) J. Block, *Z. Physik. Chem.*, **64**, 199 (1969).
(3) G. G. Wanless and G. A. Glock, Jr., *Anal. Chem.*, **39**, 2 (1967).
(4) J. C. Tou and K. Y. Chang, *Org. Mass Spectrom.*, **3**, 1055 (1970).
(5) J. C. Tou, *Anal. Chem.*, **42**, 1381 (1970).

$\rightarrow m_2^{+}$, taking place in the field-free region of the cylindrical focussing electrode, S, the apparent mass, m_a, of the ions generated is related to the potential, V_s, applied to the electrode S by

$$V_s = \frac{m_1 m_a - m_2^2}{m_1 m_2 - m_2^2} V_a \qquad (1)$$

where V_a is the main ion acceleration voltage, 3 kV in our experiment. Any ion formed in the region, prior to and after the electrode S, with lower potential will contribute to the tailing of the peak toward lower mass ($<m_a$). Equation 1 was applied to the generation of ions giving the displaced skew peaks at m/e 42.4 and 56.6 from the spontaneous ion decompositions, $72^+ \rightarrow 43^+ + 29$ and $72^+ \rightarrow 57^+ + 15$ of methyl ethyl ketone. If these two ions are produced in electrode S, then the calculated V_s should be the same for the above two decomposition paths. The calculated results are 2896 V and 2899 V, and indeed confirm the previous proposal.

The transit times of the mass spectrometer were calculated for the molecular ion of methyl ethyl ketone, m/e 72, assuming V_s = 2900 V and linear potential distribution. The results are shown in Figure 2.

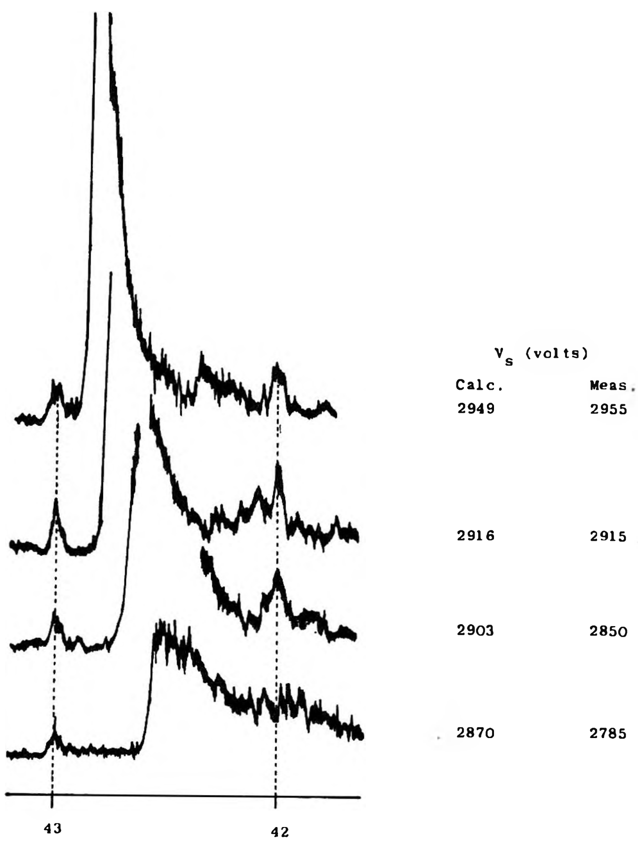

Figure 3. The V_s dependence of mass displacement for the spontaneous ion decomposition, $CH_3—C(=O^{+\cdot})—CH_3 \rightarrow CH_3—C{\equiv}O^+ + \cdot CH_3$.

It is obvious that the lifetime of the ions decomposing in the field-free region of the cylindrical focussing electrode, S, is about one order of magnitude shorter than that of the ions decomposing in the field-free region between the exit slit of the source and the entrance slit to the magnet.

The V_s dependence of the mass displacement of the skew peak, formed from $58^+ \rightarrow 43^+ + 15$ of acetone, is also investigated by keeping all other focussing potential invariable and the results are shown in Figure 3. Considering the expected strong fringing field effect and the change of the mass spectrometer focussing condition, the calculated results are good. The general trend of the V_s effect is clearly shown in Figure 3.

If the potential surface of the field-ionized molecule is distorted by the strong electric field to an extent that the internal energy of the molecular ion in a particular bond to be ruptured is above the dissociation limit, the dissociation will occur within one vibration. If it is below the dissociation limit, the dissociation through a quantum mechanical tunnelling effect might also occur with finite probability. After the excited molecular ions leave the high electric field, the rates of spontaneous decomposition of the molecular ion will be fully determined by the internal energy, the activation energy, and the unperturbed molecular ion parameters according to the QET theory of mass spectra.[6] These two distinct dissociation processes occurring in field ionization mass spectrometry are clearly demonstrated in this study of a peak at integer mass and with normal symmetrical shape, and its counterpart peak with mass displacement and skew peak shape.

Similar metastable ions were recently described which had been formed by electron impact in a similar focussing electrode in the ion source of the Hitachi RMH-2 mass spectrometer.[7]

Acknowledgment. The author wishes to express his sincere thanks to R. D. Beckrow for his careful experimental work.

(6) M. L. Vestal in "Fundamental Process in Radiation Chemistry," P. Ausloos, Ed., Wiley-Interscience, New York, N. Y., 1968, p 59.

(7) J. H. Beynon, W. E. Baitinger, J. W. Amy, and T. Komatsu, *J. Mass Spectrom. Ion Phys.*, 3, 47 (1969).

The Solid-State Photolysis of Tris(oxalato)cobalt(III) in a Host Lattice[1]

by Atul C. Sarma, Anne Fenerty, and Steven T. Spees[2]

Departments of Chemistry, University of Minnesota, Minneapolis, Minnesota 55455 and Michigan State University, East Lansing, Michigan 48823

(Received July 27, 1970)

The study of the photodecomposition of coordination compounds was initiated as early as 1917, when Vranek[3] found cobaltous oxalate, potassium oxalate, and CO_2 upon irradiating a solution of potassium cobaltioxalate. Most photodecomposition studies of the oxalato-metal systems have been investigated in solution.[4] While the data on solid-state photochemical reactions are limited, there have been a few recent studies.[5-7]

Here we report on the solid-state photolysis of the tris(oxalato)cobalt(III) ion which had been seeded in a transparent and photochemically inert single crystal lattice, $NaMg[Al(C_2O_4)_3]\cdot 9H_2O$. The spectroscopy of $Co(C_2O_4)_3^{3-}$ has been studied in this host lattice by Piper and Carlin.[8]

Two types of very thin crystal sections (of order 0.035 cm) were prepared from the mixed single crystal, *viz.*, (i) a section cleaved normal to the C_3 axis, termed the axial section, and (ii) a section with faces parallel to the C_3 axis, the orthoaxial section. Preparation of an orthoaxial section requires special care; uniform thin sections can be obtained by careful grinding, first with fine sandpaper and then with wet tissue paper. Polarization of incident light in any direction for an axial section produces the same spectrum. In the case of an orthoaxial section, there are two types of spectra. The spectrum recorded with light polarized normal to the C_3 axis is called π spectrum, and the spectrum with light polarized parallel to the C_3 axis, σ spectrum. The σ and axial spectra are identical. We obtain spectra which agree with those reported by Piper and Carlin.[8]

Spectra were obtained with a Cary Model 14 spectrophotometer. Three different light sources were used: (1) a 1000-W General Electric high-pressure mercury arc; (2) a 1000-W Hanovia xenon–mercury arc lamp; and (3) a helium–neon laser (6328 Å). Interference filters were used to select appropriate wavelengths with the first two sources. Light intensities were measured with a YSI Kettering Model 65 radiometer.

To determine the rate of photolysis, the optical density (D) at the maximum of each band was recorded as a function of time of irradiation. Plots of ln $[(D - D_\infty)/(D_0 - D_\infty)]$ *vs.* time gave reasonable straight lines over two to three half-lives. Quantum yields were calculated using eq 1

$$\phi = kc_0V/I_a \qquad (1)$$

where k (sec^{-1}) is the rate constant for the photochemical reaction, c_0 (M) is the initial concentration of complex, V (l.) is the volume of the crystal, and I_a (einstein sec^{-1}) is the absorbed light intensity. The results are shown in Table I along with comparable solution data and some recent results on pure $K_3[Co(C_2O_4)_3]\cdot 3H_2O$.

As might be expected, the quantum yields decrease in the solid state; at the beginning of the charge-transfer region they differ by nearly 10^2, and this difference increases to more than 10^3 at longer wavelengths. Although Spencer also finds the quantum yields are smaller in the solid state than in solution, his values are somewhat larger than we observe. In the dilute solid the radical produced by the homolytic fission of a cobalt–oxygen bond will have a much greater chance of recombination with Co(II). In fact, the recombination (or the oxidation of a reduced cobalt by some other species) can be followed spectrophotometrically. If the absorbance is measured immediately after the irradiation at 355–385 nm is stopped, the 420- and 610-nm peaks show a slight increase in intensity as a function of time as shown in Figure 1. The data give good first-order plots as shown in Figure 2 and summarized in Table II.

Table I: Quantum Yields for the Photodecomposition of Tris(oxalato)cobalt(III) Ion

State	λ, nm	$I_a \times 10^6$ einstein, sec^{-1}	ϕ	Reference
Solution	355–385	0.020	0.44	*a*
Solution	410	0.0085	0.24	*a*
Solution	590–650	2.32	8×10^{-4}	*b*
Solution	632.8	2.82	1.1×10^{-5}	*c*
Dilute solid	355–385	0.043	5.1×10^{-3}	*c*
Dilute solid	430	0.080	5×10^{-4}	*b*
Dilute solid	590–650	0.78	$<1 \times 10^{-5}$	*b*
Pure solid	366	~0.02	0.16	*d*
Pure solid	436		7.6×10^{-2}	*d*

[a] S. T. Spees and A. W. Adamson, *Inorg. Chem.*, **1**, 531 (1962). [b] N. C. Kneten, M.S. Thesis, University of Minnesota, 1967. [c] This work. [d] H. E. Spencer, *J. Phys. Chem.*, **73**, 2316 (1969).

Table II: Kinetics for Back Reaction to Product $Co(C_2O_4)_3^{3-}$

Irradiation time, min	$D_\infty - D_0$	k, sec^{-1}
30	0.016	1.86×10^{-3}
120	0.019	1.54×10^{-3}
240	0.017	8.67×10^{-4}

The rate constants exhibit a linear decrease with increasing irradiation time but the reason for this re-

(1) Abstracted from the M.S. thesis of A. C. S. (University of Minnesota) and A. F. (Michigan State University). Presented in part at the Eleventh International Conference on Coordination Chemistry, Haifa, Sept 1968.

(2) To whom correspondence should be addressed.

(3) J. Vranek, *Z. Elektrochem.*, **23**, 336 (1917).

(4) A. W. Adamson, W. L. Waltz, E. Zinato, D. W. Watts, P. D. Fleischaver, and R. D. Lindholm, *Chem. Rev.*, **68**, 541 (1968).

(5) W. W. Wendlandt and E. L. Simmons, *J. Inorg. Nucl. Chem.*, **28**, 2317, 2420 (1966).

(6) V. Balzani, R. Ballardini, N. Sabbatini, and L. Moggi, *Inorg. Chem.*, **7**, 1398 (1966).

(7) S. T. Spees, Jr., and P. Z. Petrak, *J. Inorg. Nucl. Chem.*, **32**, 1229 (1970).

(8) T. S. Piper and R. L. Carlin, *J. Chem. Phys.*, **35**, 1809 (1961).

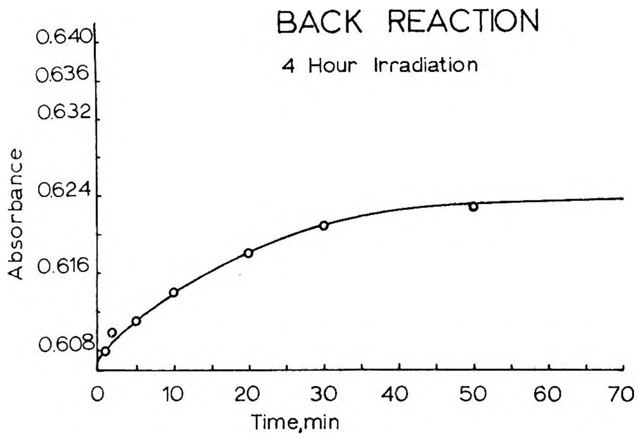

Figure 1. The increase in absorbance of the 610-nm peak in $Co(C_2O_4)_3^{3-}$ due to the thermal back reaction after a 4-hr irradiation with white light.

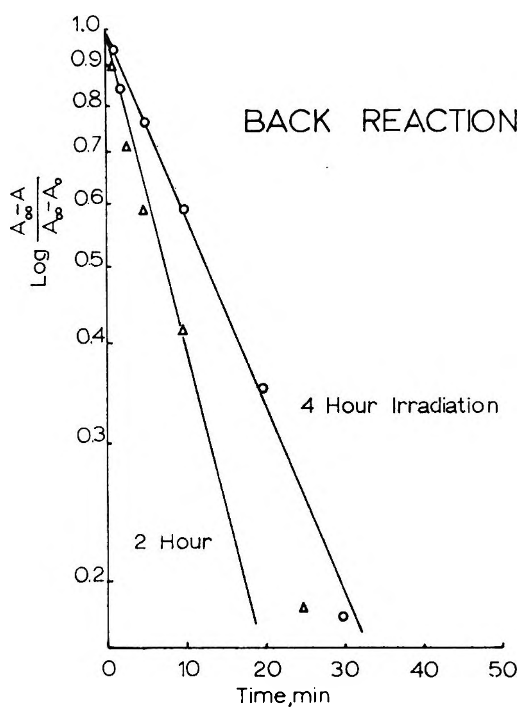

Figure 2. The first-order plot of the increase in absorbance of the 610-nm peak in $Co(C_2O_4)_3^{3-}$ due to the thermal back reaction after 2- and 4-hr irradiation with white light.

lationship is not known. The nearly constant value of $D_\infty - D_0$ strongly suggests a steady-state intermediate that can react to form products or the initial cobalt(III) complex.

Further evidence which supports the proposed intermediate is obtained from the uv absorption spectrum. A band at 320 nm[9] with high optical density grows in upon irradiation at 355–385 nm and, after short irradiation times, its intensity remains constant. We believe that the band is due to the radical intermediate, either the oxalate ion radical ($C_2O_4^-$) or the carbon dioxide ion radical (CO_2^-). Parker and Hatchard[10] reported an instantaneous rise in absorption at 313 nm when solutions of $Co(C_2O_4)_3^{3-}$ were flashed with krypton lamps. This was followed by a rapid fall in absorption followed by a slow fall in absorption. They suggested that the rapid reaction was due to a bimolecular reaction between the radical produced and a second Co(III) complex. The final slow step was supposed to be the dissociation of $Co(C_2O_4)_3^{4-}$. Recent work by Oncescu[11] on the mechanism for the decomposition of metal–oxalate complexes shows that in solution the radical must be $C_2O_4^-$. Her work is supported by calculations of Simon,[12] who shows that the enthalpy change for the reaction

$$C_2O_4^- \longrightarrow CO_2^- + CO_2 \qquad (2)$$

is about +27 kcal/mol. Therefore $C_2O_4^-$ would be expected to have a lifetime long enough to react with another $Co(C_2O_4)_3^{3-}$ ion rather than decompose to give CO_2^-. It would seem that in the solid state either (or both) might have lifetimes long enough to be responsible for the phenomena observed.

The band at 29×10^3 cm^{-1} reported for CO_2^- and discussed by Carrington and McLachlan[13] in regard to its esr spectrum[14,15] is at slightly lower energies than the band found here (31×10^3 cm^{-1}). The 31×10^3 cm^{-1} absorption is not due to either $C_2O_4^{2-}$ ($\sim 50 \times 10^3$ and 40×10^3 cm^{-1}) or $Al(C_2O_4)_3^{3-}$ (38.4×10^3 cm^{-1}). The absorption in the uv region for $Co(C_2O_4)_3^{3-}$ occurs at the same energy as the aluminum complex but with somewhat enhanced intensity. Work with frozen aqueous solutions (77°K) shows that the first radical seen in the photochemical decomposition is H and possibly the oxalate ion radical.[16,17] Warming produces secondary radicals, one of which is identified as CO_2^- (or possibly $CO_2H\cdot$). Esr studies are continuing in this laboratory to identify the radical(s) involved in the photodecomposition of $Co(C_2O_4)_3^{3-}$ in dilute single crystals.

(9) The wavelength of the band maximum depends somewhat on the wavelength of irradiation; it shifts to shorter wavelengths when 450-nm light is used. We have no explanation for this shift. The high optical density ($D \approx 2$) and broad bands ($\Delta_{1/2} \approx 10^4$ cm^{-1}) could be caused by more than one species with the proportion of various species dependent upon irradiating wavelength.

(10) C. A. Parker and C. G. Hatchard, *J. Phys. Chem.*, **63**, 22 (1959).

(11) T. Oncescu, *Rev. Roum. Chem.*, **15**, 209 (1970).

(12) Z. Simon, *ibid.*, **14**, 705 (1969).

(13) A. Carrington and A. D McLachlan, "Introduction to Magnetic Resonance," Harper and Row, New York, N Y., 1967.

(14) Incidently, Carrington and McLachlan discuss the esr spectrum of CO_2^- based upon a bent structure while the calculations of Simon suggest that the linear structure should be more stable. All interpretations of the esr data for CO_2^- assume a bent structure.[15]

(15) (a) D. W. Ovenall and D. H. Whiffen, *Mol. Phys.*, **4**, 135 (1962); (b) G. W. Chantry and D. H. Whiffen, *ibid.*, **5**, 189 (1962); (c) P. W. Atkins, N. Keen, and M. C. R. Symons, *J. Chem. Soc.*, 2873 (1962).

(16) (a) G. A. Shagisultanova, L. K. Neokladnova, and A. L. Poznyak, *Dokl. Akad. Nauk SSSR*, **162**, 1333 (1965); (b) A. L. Poznyak and G. A. Shagisultanova, *ibid.*, **173**, 227 (1967).

(17) D. R. Eaton and S. R. Suart, *J. Phys. Chem.*, **72**, 400 (1968).

COMMUNICATIONS TO THE EDITOR

Resolution of an "Inconsistency" in Recoil Tritium Reactions

Sir: A recent paper by J. W. Root and F. S. Rowland[1] dealing with recoil tritium reactions in methane–hydrogen systems comes to the disturbing conclusion that a discrepancy exists between the inferences that can be drawn from the various sets of data available. The inconsistency is not just the kind of modest quantitative misfit of kinetic theory parameters to be expected from the approximate nature of the assumptions generally used with this theory.[2,3] It is much more serious in that it appears to be a qualitative discrepancy.

In answering Root and Rowland's call for a resolution of this inconsistency, we quote their statement of the problem: "a qualitative inconsistency can now be seen in the respective requirements that (a) the energy ranges of hot reactions for CH_4 and CD_4 are approximately the same; (b) the ranges for CH_4 and D_2 are about the same; (c) H_2 reacts extensively at energies below the CD_4 threshold; and (d) D_2 reacts at a lower average energy than H_2."

We first examine the rigor of these statements. Statement (d) is based on the finding that in mixtures of H_2 and D_2 the product ratio HT/DT declines with dilution by noble gases.[4] The conclusion legitimately follows from the "energy shadowing effect."[2–4] According to this, dilution by an inert gas increases the relative number of hot atoms reaching the lower energy range and thus the relative yield of the lower energy product.[5] Hence it is possible to rank products according to their *mean energy* of formation. (These considerations may also be put in quantitative terms.[6])

Statement (a) is based on work by Chou[7] dealing with the behavior of yield ratios from CH_4–CD_4 mixtures upon rare-gas moderation. These experiments are of the same type as those on which statement (d) was based. Yet the conclusion reached goes further saying the *energy ranges* of hot reactions are about the same. No justification is given for this much more sweeping statement. (In principle it is possible to use higher order shadowing terms in the kinetic theory to obtain more information than just relative mean energies; in fact ratios of excitation functions could be evaluated. In practice experimental data available have nowhere near the precision required to make such an exercise remotely meaningful.) Statement (a) thus seems defensible only in a much more restricted version: (a′) *The relative mean energies of hot reactions of T with CH_4 and CD_4 are approximately the same.*

Statement (c) is based on variations in yield ratios from binary CD_4–H_2 mixtures of changing composition. This conclusion does not derive from the straightforward shadowing considerations applicable to data on dilution with inert moderators, but rather on model calculations of an unspecified nature.[1] In any case, statement (c) must almost certainly be correct (provided the word "extensively" is left undefined). We know this from previous data, which shows the threshold for reaction of atomic hydrogen with molecular hydrogen is much lower[8] than for tritium reaction with methane to form T-labeled methane.[9,10]

Statement (b) is based on the ratio of yields in CH_4–D_2 mixtures of varying composition.[11,12] As discussed above it is very doubtful that any meaningful conclusions on energy *ranges* can be justified on the basis of such data. In support of statement (b) there is cited a much earlier analysis of these experimental results.[3] In this there was used, as a working hypothesis, the simplest possible assumption on excitation functions for CH_4 and D_2, that they differed only by a constant factor.[13] It was pointed out that a resulting internal inconsistency (of about 30%) in parameters derived from the analysis was a measure of the incorrectness of the assumption.[13] Further, it was suggested that a model in which the energy ranges of the excitation functions were displaced would give better results.[13] How these conclusions could form a basis for statement (b) is puzzling.

It is not even obvious how data on yield ratios from mixtures of varying composition can lead to firm conclusions on relative *mean* energies of formation. While the effects on energy shadowing of moderation by an inert material are relatively simple to calculate, the effect of

(1) J. W. Root and F. S. Rowland, *J. Phys. Chem.*, **74**, 451 (1970).

(2) P. J. Estrup and R. Wolfgang, *J. Amer. Chem. Soc.*, **82**, 2665 (1960).

(3) R. Wolfgang, *J. Chem. Phys.*, **39**, 2983 (1963).

(4) D. Seewald, M. Gersh, and R. Wolfgang, *ibid.*, **45**, 3870 (1966).

(5) R. T. K. Baker, *J. Amer. Chem. Soc.*, **90**, 4473 (1968).

(6) R. T. K. Baker, M. Silbert, and R. Wolfgang, *J. Chem. Phys.*, **52**, 1120 (1970).

(7) C. C. Chou as quoted in ref 1.

(8) A. Kuppermann and J. M. White, *J. Chem. Phys.*, **44**, 4352 (1966).

(9) C. C. Chou and F. S. Rowland, *ibid.*, **50**, 2763 (1969).

(10) Statement (c) as given in ref 1 is somewhat ambiguous in that the meaning of "the CD_4 threshold" is not defined. We use it in the sense of the abstract[1] which states that "an appreciable amount of HT formation occurs below the threshold for CD_3T formation."

(11) J. W. Root and F. S. Rowland, *J. Chem. Phys.*, **38**, 2030 (1963).

(12) J. W. Root and F. S. Rowland, *ibid.*, **46**, 4299 (1967).

(13) Reference 3, p 2991.

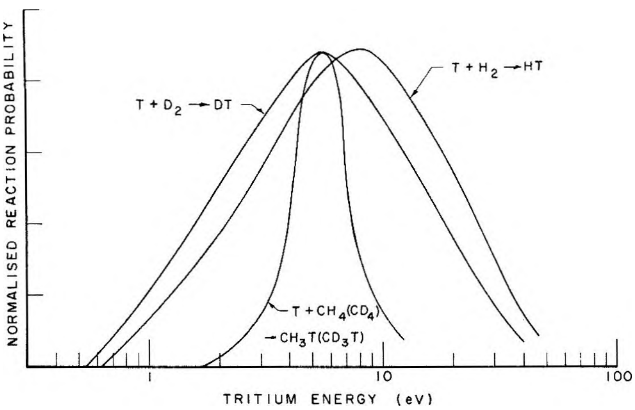

Figure 1. Relative reaction probabilities are plotted as function of logarithm of tritium atom energy. The $T + H_2$ and $T + D_2$ curves are based on theoretical estimates[14] consistent with experiment.[4] The $T + CH_4$ and $T + CD_4$ curves are hypothetical, but are consistent with and strongly constrained by experimental information[6,16,17] and calculations.[15] These excitation functions are mutually normalized. (Actual areas under such curves are given by experimental or theoretical reactivity integrals.)[4,16]

dilution by a second reagent is a much more complex matter. Only a much more restricted version of statement (b) would therefore seem defensible: (b′) *The mean energies at which hot tritium reacts with CH_4 and D_2 are probably not grossly disparate. There is no present justification for any conclusion on relative energy ranges for reactions in these systems.*

Figure 1 shows a set of excitation functions which are consistent with statements (c) and (d) and revised statements (a′) and (b′). Furthermore, these functions are not arbitrary, but are best estimates on the basis of independent information. Those for H_2 and D_2 are based on the calculation of Karplus, Porter, and Sharma[14] as confirmed by experiment.[4] Those for CH_4 and CD_4 are consistent (though not uniquely so) with calculations of Polanyi, *et al.*,[15] and experimental conclusions of Seewald,[16] Baker, *et al.*,[6] and Chou and Rowland.[17]

It thus appears that this qualitative discrepancy is an artifact which disappears upon elimination of unwarranted inferences. On the contrary, results from a wide variety of systems display satisfactory internal consistency.[18] While the intrinsic limitations of the kinetic theory[3] must ultimately lead to some deviation from experiment, the degree of reliability and precision of the data discussed here does not seem adequate to demonstrate the existence and extent of such deviations.

In this note we have attempted to show that, contrary to an earlier claim,[1] no discrepancy exists between qualitative inferences drawn from various sets of hot atom data, provided that the statements of these inferences are limited to what can be clearly justified. Professor Rowland in the accompanying comment[19] seems to accept our more conservative statement of the inferences in question.[20]

With the original purely qualitative discrepancy apparently resolved Rowland goes further.[19] Using the kinetic theory he attempts to evaluate quantitatively whether possible forms of excitation function of the relevant reactions are consistent with data on product ratios in unmoderated CD_4–H_2 systems. Such calculations should be capable of providing a meaningful estimate of the gap between model and reality in hot atom kinetics and are thus potentially valuable. Furthermore, the actual method of the calculation seems both simple and reasonable.

We agree fully with Rowland's conclusion as expressed in the title of his paper: the simple kinetic theory is inapplicable, or at least inaccurate, when applied to certain systems. The limitations of the simple kinetic theory introduced by the approximations which underlie it have been repeatedly emphasized in the past.[3,21] It has been specifically pointed out that it will be least accurate in systems of high reactivity,[3,21] such as the moderated CD_4–H_2 discussed by Rowland.

Nevertheless, we feel that Rowland's calculations provide little indication of the extent of these expected inaccuracies in the kinetic theory. Our reasons for this scepticism are twofold. (1) These calculations are based on the excitation function shown in Figure 1 of this paper. In addition, it is assumed that the excitation function for reaction $T + CH_4 \rightarrow HT + CH_3$ has the same form as that for the reaction $T + CH_4 \rightarrow CH_3T + H$.[22] However, there is reason to believe that the range over which the former process occurs extends to considerably higher energies.[15,16] If this is the case then the calculated product ratio indicated by the solid line in Figure 2 of ref 19 would show a significantly smaller decline with increasing CD_4 concentration. (2) The experimental product ratios were measured using oxygen as a scavenger. But it has been shown that in hydrogen systems O_2 does not effectively suppress the formation of HT by non-hot-atom mecha-

(14) M. Karplus, R. Porter, and R. Sharma, *J. Chem Phys.*, **45**, 3871 (1966).

(15) P. J. Kuntz, E. M. Nemeth, J. C. Polanyi, and W. H. Wong, *ibid.*, **52**, 4564 (1970).

(16) D. Seewald and R. Wolfgang, *ibid.*, **47**, 143 (1967).

(17) C. C. Chou and F. S. Rowland, *ibid.*, **50**, 2763 (1969).

(18) See for example, ref 16. Here I and α values derived from CH_4–D_2 mixtures are compared with those independently deduced from rare gas moderated CH_4 and moderated D_2. The agreement is good. A very similar situation obtains for CD_4–H_2.

(19) F. S. Rowland, *J. Phys. Chem.*, **74**, 4603 (1970).

(20) Professor Rowland does complain that the energy dependent reaction probabilities that are presented in Figure 1 of this paper do not accord well with criterion (b′). This complaint seems unwarranted. To the extent that (b′) is justified at all (and it is so vague as to be almost meaningless anyway) it refers to reaction of CH_4 to form all products: HT and CH_2T as well as CH_3T. Figure 1, however, shows only a possible excitation function for $T + CH_4 \rightarrow CH_3T + H$. Thus it can hardly be taken to imply that the mean energy of all reactions of hot tritium with CH_4 is "grossly disparate" from the reaction of T with H_2.

(21) *E.g.*, R. Wolfgang, *Progr. React. Kinet.*, **3**, 118 (1965); *Ann., Rev. Phys. Chem.*, **16**, 21 (1965).

(22) See ref 18, footnote 10.

nisms.[23] The relative amount of "spurious" HT produced is especially large when the concentration of H_2 is small.[23] Hence the rise in actual product ratios with CD_4 concentration as shown in Figure 2 ref 19, might be largely an artifact not reflecting direct hot reaction. It is thus doubtful whether these data are adequate for a quantitative comparison between theory and experiment at the level of precision required for the present purpose.

The probable effect of factors (1) and (2) would be to diminish, eliminate, or even reverse the direction of the apparent discrepancy between theory and experiment. Rowland's conclusion that the kinetic theory is likely to be inaccurate in systems of high reactivity is expected and has been predicted.[3,21] However, his calculations provide no reliable indication of the extent of any such inaccuracy in the CD_4–H_2 system.

Acknowledgement. This work was supported by the U. S. A.E.C. Discussions with D. J. Malcolme-Lawes are much appreciated.

(23) D. Seewald, Ph.D. Thesis, Yale University, 1967, p 74, ff.

DEPARTMENT OF CHEMISTRY RICHARD WOLFGANG
YALE UNIVERSITY
NEW HAVEN, CONNECTICUT 06520

RECEIVED APRIL 27, 1970

The Inapplicability of the Simple Kinetic Theory of Hot Reactions to Certain Binary Recoil Tritium Systems

Sir: In the recent paper by Root and Rowland,[1] the statement was made that "we have not been able to obtain even an approximately satisfactory set of reactivity integrals [for the kinetic theory of hot reactions][2-6] capable of reproducing the qualitative features of the experimental observations for all of the various binary pairs" (of CH_4, CD_4, H_2, D_2, and Ar), and the further conclusion was added that "we feel that no fit will be possible involving rather broad, structureless reactivity integrals."[1] The accompanying comment proposes a set of such structureless reactivity integrals, for which the claim is made that "results from a wide variety of experiments display an impressive internal consistency and agreement with theory."[7] The kinetic theory of hot reactions is expressed in quantitative terms, and the critical test for any such set of reactivity integrals is of course not their apparent satisfaction of one or another set of stated restraints, but rather their quantitative consistency with the pertinent experimental results. On the basis of the simple model calculations alluded to in ref 1 but not described therein, it is immediately apparent that this consistency is most

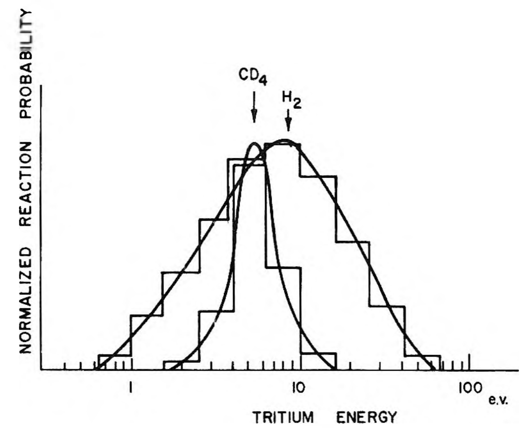

Figure 1. Normalized reaction probability curves. The smooth curves are proposed reactivity integrals (ref 7) for CD_4 and H_2. The step functions are the approximations used in the simple model calculations.

strained for this particular proposed set of reactivity integrals by the observations in binary mixtures of CD_4 and H_2, for which the experimental results were given in ref 1. The proposed CD_4 and H_2 reactivity integrals can be seen on visual inspection probably to violate criterion (c), that "H_2 reacts extensively at energies below the CD_4 threshold," the criterion originally generated by these CD_4-H_2 experimental data.[1] Accordingly, the agreement of these reactivity integrals is here compared through a simple model calculation with the available data for this binary system.

These model calculations have been carried out by the successive application of the Estrup–Wolfgang formulation of the hot yields from the kinetic theory of hot reactions,[2] $Y = 1 - \exp(-I/\alpha)$, to "blocks" of reactivity integral chosen to simulate the proposed integrals as shown in Figure 1. This simple Estrup–Wolfgang formula has been shown to provide excellent qualitative and reasonable quantitative agreement with the yields of hot reactions as obtained from detailed stochastic calculations.[8,9] The agreement in ratios of hot yields from competing processes is even better simulated in these comparisons than are the estimates of the total absolute yields. Moreover, the chief defects in calculations by this formula are most severe in hypothetical systems having very abrupt changes with energy of the

(1) J. W. Root and F. S. Rowland, *J. Phys. Chem.*, **74**, 451 (1970).
(2) P. J. Estrup and R. Wolfgang, *J. Amer. Chem. Soc.*, **82**, 2665 (1960).
(3) R. Wolfgang, *J. Chem. Phys.*, **39**, 2983 (1963).
(4) D. Seewald, M. Gersh, and R. Wolfgang, *ibid.*, **45**, 3870 (1966).
(5) R. T. K. Baker, *J. Amer. Chem. Soc.*, **90**, 4473 (1968).
(6) R. T. K. Baker, M. Silbert, and R. Wolfgang, *J. Chem. Phys.*, **52**, 1120 (1970).
(7) R. Wolfgang, *J. Phys. Chem.*, **74**, 4601 (1970).
(8) F. S. Rowland and P. Coulter, *Radiochim. Acta*, **2**, 163 (1964).
(9) Much more elaborate stochastic calculations have verified the general suitability of this formulation, if α can be considered to be energy independent. See, for example, R. M. Felder and M. D. Kostin, *J. Chem. Phys.*, **43**, 3082 (1965).

Table I: Acetylene-^{11}C Yields From Selected Alkanes and Benzene under Various Experimental Conditions

Run no.	System[a,b]	Dose, μA × sec	Relative yields,[c] % C_2H_2	C_2HD	C_2D_2	Absolute yield,[d] % of [illegible]
100–105	C_2H_6 + 4.5% O_2					29.6
36,38,39	C_2H_6–C_2D_6 + 4.5% O_2	100	50	6	44	
Ref 4d	C_3H_8 + 4.5% O_2					24.0
42,43,45	C_3H_8–C_3D_8 + 4.5% O_2	100	53	9	38	
Ref 4d	c-C_3H_6					52.7
1,6,7	c-C_3H_6–c-C_3D_6	100	45	18	37	
Ref 4d	c-C_3H_6 + 4.5% O_2					50.0
14	c-C_3H_6–c-C_3D_6 + 4.5% O_2	20	44	17	39	
46		100	45	14	41	
2		150	47	19	34	
8		375	46	17	37	
			45	17	38	
Ref 4c	c-C_3H_6 + 4.5% O_2 + 45.5% N_2					42.5
11	c-C_3H_6–c-C_3D_6 + 4.5% O_2 + 45.5% N_2	200	49	13	38	
13		400	53	10	37	
			51	11	38	
Ref 11	C_6H_6 (liq)					4.68
9,313	C_6H_6–C_6D_6	100	42	19	39	
20		200	39	21	40	
			41	20	39	
12	C_6H_6–C_6D_6 + 1.0% C_2 (HD)	100	39	21	40	
25		200	42	20	38	
			41	20	39	
21	C_6H_6–C_6D_6 + 2.5% C_2 (HD)	200	42	20	39	
24	C_6H_6–C_6D_6 + 5.0% C_2 (HD)	200	43	20	37	
25	C_6H_6–C_6D_6 + 1.0% C_2H_4	200	42	20	38	
10	C_6H_6–C_6D_6 + 4.5% O_2	100	44	17	39	
16	C_6H_6–C_6D_6 + 4.5% O_2 + 1.0% C_2 (HD)	100	43	15	42	
15,17		200	42	17	41	

[a] C_2 (HD) composed of 43.3% C_2H_2, 20.3% C_2HD, and 36.3% C_2D_2. [b] The isotopic composition of the compound used was as follows: C_2D_6, 99.6 atom %D, 98.3% d_6, 1.7% d_5; C_3D_8, 99.0 atom % D; c-C_3D_6, 99.24 atom % D, 95.44% d_6, 4.56% d_5; C_6D_6, 99.5 atom % D. [c] Relative yields of individual products are ± 2%. [d] Absolute yields: AD ≤ ±5.0%.

tonated and perdeuterated alkanes and benzene under varied experimental conditions are presented in Table I. In C_2H_6–C_2D_6 + 4.5% O_2 mixtures about 88% of the acetylene-^{11}C is formed by intramolecular pathways and is either $^{11}C_2H_2$ or $^{11}C_2D_2$. This result is in agreement with other workers (4g,5,6). However, the yield of $^{11}C_2HD$ (the observable intermolecular product) increases with structurally different substrates, and is 18% and 20% for neat mixtures of cyclopropane and benzene, respectively. It is apparent that radiolytic effects are not responsible for the isotopic distribution of the acetylene-^{11}C. The radiation dose, for a mixture of c-C_3H_6/c-C_3D_6 containing 4.5% O_2 scavenger, was varied from 1.7×10^{-3} to 6.5×10^{-2} eV·molecule^{-1}, and within experimental error, variations in the acetylene-^{11}C distributions were not observed.[9] Similarly, the relative distributions were unchanged, if 1.0% acetylene (composed of 43.3% C_2H_2, 20.3% C_2HD, and 36.3% C_2D_2) or 1.0% C_2H_4 was added as a radiation protection agent to C_6H_6–C_6D_6 systems prior to the proton irradiation. In Table II we have summarized the per cent of acetylene-^{11}C arising from intramolecular and intermolecular pathways in the various systems by using the amount of $^{11}C_2HD$ as an approximation of the intermolecularity. For example in a neat benzene mixture, the acetylene is 60% intramolecular and 40% intermolecular. However, if 4.5% O_2 scavenger is present in the benzene system the intermolecular acetylene is reduced from 40 to 34%. A similar effect was not observed for cyclopropane.

In one set of experiments a mixture of c-C_3H_6–c-C_3D_6 + 4.5% O_2 + 45.5% N_2 was subjected to 10.5-MeV protons to produce the $^{14}N(p, \alpha)^{11}C$ reaction. In this case the yield of $^{11}C_2HD$ was about 11%, (∴ ~22% intermolecular) compared to 17% (∴ ~34% intermolecular) when the $^{12}C(p, pn)^{11}C$ reaction was used, and N_2 was

(9) In a similar study with equimolar mixtures of methyl chloride-h_3 and -d_3, the radiation dose was varied over a 40-fold range and likewise variations in the acetylene-^{11}C distribution were not observed.

Table II: Summary of Per Cent of Total Acetylene-^{11}C Formed by Intramolecular and Intermolecular Mechanisms

System	Per cent[a] acetylene-^{11}C Intramolecular	Intermolecular
C_2H_6-C_2D_6 + 4.5% O_2	88	12
C_3H_8-C_3D_8 + 4.5% O_2	82	18
c-C_3H_8-C_3D_6	64	36
c-C_3H_6-c-C_3D_6 + 4.5% O_2	66	34
c-C_3H_6-c-C_3D_6 + 4.5% O_2 + 45.5% N_2	78	22
C_6H_6-C_6D_6	60	40
C_6H_6-C_6D_6 + 4.5% O_2	66	34

[a] The error is approximately ±4%. The data have not been corrected for isotope effects.

not present in the reaction vessel. The yield of $^{11}C_2HD$ is comparable to that reported by Ache and Wolf[5,6] for a large number of $N_2 + O_2 + C_nH_mF_x$-$C_nD_mF_x$ mixtures. Apparently the N_2 suppresses intermolecular mechanism that leads to acetylene-^{11}C formation.[10]

The formation of $^{11}C_2HD$ in these reaction systems cannot be accounted for solely by an intramolecular mechanism that restricts the only mode of formation of acetylene-^{11}C to energetic carbon-11 insertion reactions into CH bonds. The $^{11}C_2HD$ must be formed by other reactions involving precursors other than atomic carbon-11. The possible reaction schemes (with perprotonated alkane as an example of reactions of aromatics to be reported subsequently) that can lead to acetylene-^{11}C are shown in (1) to (3).

Insertion–decomposition

$R{-}CH_3 + {}^{11}C \longrightarrow$

$[R{-}CH_2{-}{}^{11}C{-}H]^* \longrightarrow H^{11}C{\equiv}CH$

$\longrightarrow$ [other decomposition products and fragments, *e.g.*, CH and C_2H] (1)

High energy stripping

$$R{-}CH_3 + {}^{11}C \longrightarrow \left.\begin{matrix} {}^{11}C_2 \\ \longrightarrow {}^{11}C_2H \\ \longrightarrow {}^{11}C_2H_2 \\ \longrightarrow {}^{11}CH \end{matrix}\right\} + \text{ fragmentation products} \quad (2)$$

Abstraction

$$\left.\begin{matrix} R{-}CH_3 + {}^{11}C_2 \longrightarrow {}^{11}C_2H \\ + {}^{11}C_2H \longrightarrow {}^{11}C_2H_2 \\ + {}^{11}C \longrightarrow {}^{11}CH \end{matrix}\right\} \text{ may lead to mixed acetylene-}^{11}C \quad (3)$$

$+ {}^{11}C_2 \longrightarrow {}^{11}C_2H_2$

one step leads to nonmixed acetylene-^{11}C

The insertion–decomposition model is consistent with an intramolecular mechanism and the high yields of $^{11}C_2H_2$ and $^{11}C_2D_2$.[4c,g,5,6,11,12] However, the stripping reactions leading to C_2 and C_2 hydrogen analogs, followed by hydrogen abstraction can account for the formation of $^{11}C_2HD$ as a hot reaction product, whereas the insertion–decomposition model is inadequate.[13,14]

Skell[12] has recently reported that C_2 can react with a variety of hydrocarbons to give acetylene by two different mechanisms. Singlet $C_2(X^1\Sigma_g^+)$ results in nonselective formation of acetylene, whereas triplet $C_2(X'^3\pi u)$ reacts by a radical mechanism. In matrix trapping of C_2 with CH_3CHO-CD_3CDO, CH_3COCH_3-CD_3COCD_3, and C_6H_6-C_6D_6 mixtures, Skell[12] reported 29, 25, and 18% intermolecularity, respectively, for acetylene production. It is interesting that the yields for C_2HD are of the magnitude we observed in our gas phase recoil-^{11}C experiments.[15] Pohlit[16] and Williams[11] have suggested the involvement of C_2H in the formation of phenylacetylene in the reactions of accelerated ^{14}C and recoil ^{11}C in solid and liquid benzene, respectively.[17]

We contend that one or more mechanisms other than insertion of ^{11}C into CH bonds and subsequent decomposition may lead to acetylene-^{11}C. The high-energy stripping and/or subsequent abstraction reactions leading to C_2 and C_2 analogs appear to be involved. The limitation of this study is that we cannot distinguish between the various pathways that may lead to intramolecular acetylene. Further studies using specifically labeled and substituted aromatics and alkanes are in

(10) Although there is a seeming discrepancy between the 11% $^{11}C_2HD$ reported for the nitrogen containing system reported here and the value of 5.7% reported earlier[5] two factors should be noted. The present work involved the use of more sophisticated data collection[8] and evaluation devices resulting in both higher precision and accuracy. This was coupled with a radiation damage study. Secondly in each instance of comparison the present results (based on oxygen scavenged systems only without the complication of a third reactant) show a systematic difference which *is real* and in which yields of $^{11}C_2HD$ are higher in each instance. We favor the present yields and stress that the differences in the reported $^{11}C_2HD$ yields do not alter the fundamental point that the intermolecular product is more abundant than previously supposed and its presence is not explained by eq 1.

(11) R. L. Williams and A. F. Voigt, *J. Phys. Chem.*, **73**, 2538 (1969).

(12) P. S. Skell, J. H. Plonka, and R. F. Harris, *Chem. Commun.*, 689 (1970).

(13) Clearly other reactions paths may also contribute to the formation of acetylene-C^{11}. CH reacts by insertion–decomposition reactions[2a,14] giving ethylene-^{11}C, and CH, could by alternate routes yield acetylene-^{11}C.

(14) (a) G. Stöcklin and A. P. Wolf, ref 7, pp 121–132; (b) R. M. Lambrecht and A. P. Wolf, unpublished results.

(15) The yield of intermolecular acetylene should decrease in condensed media because the deexcitation of intermediates is facilitated, thereby increasing the probability of formation of C_3, C_4, and higher hydrocarbon products. See ref 4a.

(16) A. Pohlit, T. H. Lin, W. Erwin, and R. M. Lemmon, *J. Amer. Chem. Soc.*, **91**, 5421 (1969).

(17) R. L. Williams has made a calculation that predicts that D atom pickup reactions by C_2H fragments result in a 6.5–9.5% yield of $^{11}C_2HD$ in a C_6H_6-C_6D_6 system. R. L. Williams, Ph.D. Thesis, Iowa State University, Ames, Iowa, 1970.

progress in efforts to define the intramolecular and intermolecular pathways.

(18) Osaka City University, Osaka, Japan.
* To whom correspondence should be addressed.

CHEMISTRY DEPARTMENT
BROOKHAVEN NATIONAL LABORATORY
UPTON, NEW YORK 11973

R. M. LAMBRECHT
N. FURUKAWA[18]
A. P. WOLF*

RECEIVED JULY 24, 1970

Micellar Effects on the Reactivity of the Hydrated Electron with Benzene[1]

Sir: Recent vigorous interest in the kinetics and mechanisms of organic reactions occurring in the presence of micelles has been prompted by recognized analogies between protein and micelle structures and between enzymatic and micellar catalysis.[2] To date, no attempts have been made to investigate the effects on radiation-induced processes by these species as possible models for more complex systems. Indeed, a recent report of an abrupt and marked increase in the yield of olefins in irradiated aqueous solutions of sodium linoleate as a function of solute concentration represents so far the only recognition of micellar effects in aqueous radiation chemistry.[3]

We have initiated a systematic investigation of the influence of micelles on rates of radiolytically generated radicals with a variety of substrates and wish to report a significant influence of micellar surfactants on the reactivity of the hydrated electron with solubilized benzene. Benzene was chosen because of its low solubility in water (2.4×10^{-2} M at 25.0°)[4] which causes a distribution favoring the micellar phase at high benzene concentration. Further, its low reactivity with e_{aq}^- (($k = 1.2 \pm 0.2$) 10^7 M^{-1} sec^{-1})[5] allows the measurement of electron decay in the microsecond region at benzene concentrations used. The choice of amphiphiles was dictated by systems for which detailed information concerning substrate–micelle interactions was available.[4,6] The surfactants used were: *cationic* hexadecyltrimethylammonium bromide (CTAB), $CH_3(CH_2)_{15}(CH_3)_3N^+Br^-$; *anionic* sodium dodecyl sulfate (NaLS), $CH_3(CH_2)_{11}SO_4^-Na^+$; and *nonionic* polyoxyethylene(15) nonylphenol (Igepal CO-730), $C_9H_{19}C_6H_4O(CH_2CH_2O)_{14}CH_2CH_2OH$. Purification of these surfactants has been described.[2] Half-lives of the hydrated electron in these micellar solutions have been determined by pulse radiolysis,[7] and the data are given in Table I. These low reactivities render it clearly possible to investigate electron scavenging by benzene in systems containing the high concentration of micellar surfactants necessary for solubilization. Table I also contains results of electron scavenging studies by benzene in the presence of micellar surfactants.

Table I: Hydrated Electron Attachment to Benzene in Charged and Uncharged Micellar Surfactant Solutions

10^3 [benzene], M	$t_{1/2}$ for e_{aq}^- decay, μsec	$10^6 k_{(e_{aq}^- + C_6H_6)}$ M^{-1}, sec^{-1a}
	Water	
1.50	41	11
20.0	2.6	13
	5×10^{-2} NaLS	
0	60	(0.23)[b]
5.0	14	9.6
10.0	9	7.5
20.0	5.6	6.1
30.0	4.1	5.6
40.0	3.6	4.8
50.0	2.9	4.7
	5×10^{-2} Igepal CO-730	
0	10.4	(1.3)[b]
5	7.2	5.9
10	5.6	5.7
15	4.6	5.6
20	3.9	5.5
40	2.6	5.0
60	1.5	6.5
	5×10^{-2} CTAB	
0	15	(0.92)[b]
2.0	4.6	52
4.0	2.0	75
10	0.8	78
15	0.7	63

[a] Calculated rate constant based on stoichiometric benzene concentrations; corrections have been applied for the decay of electron in water and in micellar solutions in the absence of benzene. [b] Electron attachment rates in micellar surfactants; these rates are considered to be upper limits.

In micellar NaLS solutions $k_{(e_{aq}^- + C_6H_6)}$ decreases substantially compared with that in water. This effect is most pronounced at concentrations of benzene at and above its solubility in water. With increasing benzene concentrations the half-life of e_{aq}^- approaches 2 μsec, the value obtained in aqueous saturated solutions of benzene in absence of micellar surfactants. It appears, therefore, that electron decay in these NaLS micellar solutions is essentially due to electron attachment by benzene in the aqueous bulk phase while that portion solubilized in the micelle is unreactive. Rehfeld has

(1) Supported in part by the U. S. Atomic Energy Commission.

(2) For a comprehensive review of micellar effects on the rates of organic reactions, see E. J. Fendler and J. H. Fendler, *Advan. Phys. Org. Chem.*, 8, 271 (1970).
(3) J. M. Gebicki and A. O. Allen, *J. Phys. Chem.*, 73, 2443 (1969).
(4) S. J. Rehfeld, *ibid.*, 74, 117 (1970).
(5) B. D. Michael and E. J. Hart, *ibid.*, 74, 2878 (1970), and references cited therein.
(6) J. C. Ericksson and G. Gillberg, *Acta Chem. Scand.*, 20, 2019 (1966).
(7) M. S. Matheson and L. M. Dorfman, "Pulse Radiolysis," The M.I.T. Press, Cambridge, Mass., 1969.

shown that benzene molecules lie well inside the hydrocarbon core of NaLS micelles.[4] The reduced reactivity of the benzene in this environment implies either a differential electron attachment rate in the two phases or that penetration of e_{aq}^- to the solubilized benzene is hindered by the outer structure of the micelle.

In micellar Igepal CO-730 surfactant solutions $k_{(e_{aq}^- + C_6H_6)}$ also decreases. This decrease is, however, manifested at a lower benzene concentration than that in NaLS micellar systems. Although the location of benzene in Igepal CO-730 micelles has not been elucidated, it is clear from our data that solubilization produces an environment unfavorable for electron attachment. The effects at a lower substrate concentration relative to those in the NaLS micelle may be interpreted in terms of a greater benzene–micelle binding constant in Igepal CO-730.

Conversely, rate enhancement, rather than retardation is observed in the presence of cationic micellar CTAB. Proton magnetic resonance investigations indicate that benzene is attached at the CTAB micelle–water interface.[6] Electrostatic interactions between the π-electron system of the benzene molecule and the net positive charge on the micelle surface seems likely to render benzene more susceptible to nucleophilic attack by the electron.

Values of k/ϵ from second-order decays of the transient electron adduct of benzene have been determined at 325 nm for several radical concentrations in water and in all three micellar solutions. These k/ϵ values were found in all three micellar surfactants observed to be substantially the same as that in water. Such second-order processes appear, therefore, to take place in the bulk phase of NaLS and Igepal CO-730. Since benzene is solubilized at the CTAB–H_2O interface, some radicals are inevitably formed from solubilized benzene. These processes evidently proceed at a rate very similar to that in the bulk phase. Further investigations of these systems and other radiation induced radicals with specifically solubilized substrates will be the subject of subsequent communication from our laboratories.

* To whom correspondence should be addressed.

Radiation Research Laboratories
Mellon Institute
Carnegie-Mellon University
Pittsburgh, Pennsylvania 15213

Janos H. Fendler
Larry K. Patterson*

Received September 21, 1970

ADDITIONS AND CORRECTIONS

1968, Volume 72

N. A. Matwiyoff and P. E. Darley: Direct Detection of the Hexaaquocobalt(II) Ion in Aqueous Solutions by Proton Magnetic Resonance Spectroscopy.

Page 2660. The following sentence should have been included in footnote 16: "For large P values, the chemical shifts in the rapid exchange limit were treated using the conventional equation for the weighted chemical shift: $\Delta\nu = P_f\Delta\nu_f + P_m\Delta\nu_m$."—N. A. Matwiyoff.

1969, Volume 73

Gilbert E. Janauer and Ira M. Turner: The Selectivity of a Polystyrenebenzyltrimethylammonium-Type Anion-Exchange Resin for Alkylsulfonates.

Page 2203. Please make the following addition to the Acknowledgment section: "Part of this work was also supported by the National Science Foundation under Grant No. GY-4534."—Gilbert E. Janauer.

Syed M. Ahmed: Studies of the Double Layer at Oxide-Solution Interface.

Page 3547. The positions of Γ_{H^+} and Γ_{OH^-} in eq 3 should be interchanged and the second derivative in eq 5 should have a negative sign.

Page 3553. Equations 10, 11, and 12 should read as follows.

$$-\Delta G°_{ap} = 2.303RT \log\left[\frac{\theta}{1-\theta}\frac{55.5}{a_{KNO_3}}\right] \quad (10)$$

$$-\Delta G°_{H^+} = RT \ln \frac{(a_{H^+})^f}{(a_{H^+})^i} = 2.303RT(pH_i - pH_f) \quad (11)$$

$$-\Delta G°_{K^+} = 2.303RT\left[\log\left(\frac{\theta}{1-\theta}\frac{55.5}{a_{KNO_3}}\right) + (pH_i - pH_f)\right] \quad (12)$$

S. M. Ahmed.

W. A. Senior and R. E. Verrall: Spectroscopic Evidence for the Mixture Model in HOD Solutions.

Page 4246. In Figure 2, the values of the ordinate, Optical density Y, should be: 0, 0.05, 0.10, and 0.15 instead of 0, 0.05, 1.0, and 1.5.

Page 4247. In Figure 3, the ordinate scale should be reduced by a factor of 10; *i.e.*, it should read $|\Delta Y| \times 10^1$.—Ronald E. Verrall.

1970, Volume 74

F. Baumgärtner and L. Finsterwalder: On the Transfer Mechanism of Uranium(VI) and Plutonium(IV) Nitrate in the System Nitric Acid-Water/Tributylphosphate-Dodecane.

Page 108. In the first line of the abstract, uranium(IV) should read uranium(VI).

Page 111. In the left-hand column, three lines above eq 5, the algebraic expression should read $kc(1 - \sigma N_{IFC})$.

Page 112. In the right-hand column, the third term $UO_2(NO_3)$ should read $UO_2(NO_3)_2TBP_2$.—F. Baumgartner.

Richard L. Redington: Internuclear Potential Energy Functions for Alkali Halide Molecules.

Page 182. In Table II, the correct value of $A_2 \times 10^{10}$ for LiI is 1.184, not 0.118. The correct value of $A_3 \times 10^{10}$ for KCl is 0.0815, not 0.815. Also, the value of $A_3 \times 10^{10}$ for RbBr is +0.0389, not −0.0389. The points for KI, RbI, and CsI were misplotted in Figure 2 and R_+ and R_- should be interchanged in eq 6.—Richard L. Redington.

J. F. Yan, F. A. Momany, R. Hoffman, and H. A. Scheraga: Energy Parameters in Polypeptides. II. Semiempirical Molecular Orbital Calculations for Model Peptides.

Page 421. In the legend to Figure 1, change "100" to "1000."

Page 426. In the footnotes of Table V, the correct footnotes should be: [e] The value of μ in ref 23 was obtained from microwave data. The values of μ given in footnote g of this table may be considered as experimental values since they were calculated from dielectric constants of vapors; the values from footnote h of this table and ref 40 are estimates from bond moments. [f] Reference 22. [g] R. M. Meighan and R. H. Cole, *J. Phys. Chem.*, **68**, 503 (1964). [h] W. D. Kumler and C. W. Porter, *J. Amer. Chem. Soc.*, **56**, 2549 (1934). [i] Reference 40.—H. A. Scheraga.

Norio Ise, Hideo Hirohara, Tetsuo Makino, Katsuhiko Takaya, and Masatoshi Nakayama: Ionic Polymerization under an Electric Field. XIII. Living Anionic Polymerization of Styrene in the Binary Mixtures of Benzene and Dimethoxyethane by the Three-State Mechanism.

Page 610. In the second line of the right-hand column, K_p''' should be k_p'''.—Norio Ise.

Z. A. Schelly, R. D. Farina, and E. M. Eyring: A Concentration-Jump Relaxation Method Study on the Kinetics of the Dimerization of the Tetrasodium Salt of Aqueous Cobalt(II)-4,4',4'',4'''-Tetrasulfophthalocyanine.

Page 619. Equations 3 and 4 should read

$$\tau^{-1} = {}_0k_{-1}\beta\left(1 + \frac{d\ln\beta}{d\ln C_D}\right) + 2{}_0k_1\alpha\left(2 + \frac{d\ln\alpha}{d\ln C_M}\right)C_M \quad (3)$$

$$\tau^{-1} = {}_0k_{-1} + 2{}_0k_1\alpha\left(2 + \frac{d\ln\alpha}{d\ln C_M}\right)C_M \quad (4)$$

rather than the published forms. Results and conclusions are unaffected. We thank Dr. J. M. Lang for calling our attention to this error.—Z. A. Schelly.

Michael Barfield: Angular Dependence of Long-Range Proton Hyperfine Coupling Constants in Aliphatic Radicals.

Page 622. Equations 6 and 7 should be corrected as follows.

$$Q_1(\alpha_S\alpha_S|1;1') = \sum_a c_{\alpha,a}{}^2Q_1(a_Sa_S|1;1') + \sum_b c_{\alpha,b}{}^2Q_1(b_{+1}b_{+1}|1,1') + \sum_{a,b}{}' c_{\alpha,ab}[2(-1)^{2S}\{S/(S+1)\}^{1/2}c_{\alpha,a}Q_1(0b_0|1;1') - 2^{1/2}\delta_{1,S}c_{\alpha,b}Q_1(0a_0|1;1')] + [1 - \{S(S+1)\}^{-1}]\sum_{a,b}{}' c_{\alpha,ab}{}^2Q_1(a_Sa_S|1;1') + [S+1]^{-1}\sum_{a,b}{}' c_{\alpha,ab}{}^2\,Q_1(b_{+1}b_{+1}|1,1') \quad (6)$$

$$Q_1(\alpha_{+1}\alpha_{+1}|1;1') = \sum_a c_{\alpha,a}{}^2 Q_1(a_{+1}a_{+1}|1;1') + \sum_b c_{\alpha,b}{}^2 Q_1(b_{+1}b_{+1}|1;1') + \sqrt{2}\sum_{a,b}{}' c_{\alpha,ab}[c_{\alpha,a}Q_1(0b_0|1,1') - c_{\alpha,b}Q_1(0a_0|1;1')] + \frac{1}{2}\sum_{a,b}{}' c_{\alpha,ab}{}^2[Q_1(a_{+1}a_{+1}|1,1') + Q_1(b_{+1}b_{+1}|1;1')] \quad (7)$$

Page 623. In the third line below eq 26, $f_{ji}{}^{r} = +1$. The calculated values in section III are not affected by these changes since they were based on the corrected form of eq 7.—MICHAEL BARFIELD.

J. N. Cooper: The Oxidation of Hypophosphorous Acid by Chromium(VI).

Page 956. The rate should have been defined in terms of the total, stoichiometric Cr(VI) concentration

$$\text{rate} = -\mathrm{d}[\mathrm{Cr(VI)}]/\mathrm{d}t$$

J. N. COOPER.

T. C. Werner and David M. Hercules: Charge-Transfer Effects on the Absorption and Fluorescence Spectra of Anthroic Acids.

Page 1033. In the last paragraph before the Discussion, the sentence beginning with, "This observation resulted . . . " should read: "This observation resulted from a trace of acid in the benzonitrile which shifted the acid–base equilibrium in favor of the molecular form."—DAVID M. HERCULES.

D. Patterson and A. K. Rastogi: The Surface Tension of Polyatomic Liquids and the Principle of Corresponding States.

Page 1069. In Figure 1, an error was made in calculating curve (a) for the (6, 12) model. The best fit is now with $M = 0.43$ instead of 0.35. The curve is, to within 1%, a straight line with intercepts of 0.107 and 0.124 at, respectively, $\alpha T = 0.2$ and 0.6.—DONALD PATTERSON.

R. E. James and F. Sicilio: Kinetics of Isopropyl Alcohol Radicals by Electron Spin Resonance–Flow Techniques.

Page 1168. We misinterpreted the notation used by Norman and West (ref 7) for the esr hyperfine coupling constants for the radical $\cdot CH_2CH(CH_3)OH$. Their values are in agreement with those reported by us.

Page 1169. Professor Norman points out that they did consider factors involved in the total reaction scheme. We regret any implication in our statements leading to an interpretation that such factors had not been considered.—FRED SICILIO.

R. Zahradník and P. Čársky: Conjugated Radicals. I. Introductory Remarks and Method of Calculation.

Page 1239. The matrix element $\langle {}^2\psi_{C\alpha}(i \rightarrow k)|\mathrm{H}|{}^4\psi_{C\alpha}(h \rightarrow l)\rangle$ (eq 40) should read

$$\langle {}^2\psi_{C\alpha}(i \rightarrow k)|\mathrm{H}|{}^2\psi_{C\alpha}(h \rightarrow l)\rangle = 2(hk|\mathrm{G}|li) - (hk|\mathrm{G}|il) + \delta_{hi}(mk|\mathrm{G}|lm) + \delta_{kl}(im|\mathrm{G}|mh)$$

$(k \neq l)$ or $(i \neq h)$

Our computer program has been free of this error; therefore the numerical results reported in the subsequent papers of this series are correct.—R. ZAHRADNÍK.

Julius G. Becsey, Gene E. Maddux, Nathaniel R. Jackson, and James A. Bierlein: Holography and Holographic Interferometry for Thermal Diffusion Studies in Solutions.

Page 1402. Equation 2 should read

$$\sum_{\text{all } i}[(\Delta P_{\text{obsd}}/\lambda)_i - (\Delta P_{\text{th}}/\lambda)_i - B]^2 \quad (2)$$

JULIUS G. BECSEY.

Thomas D. O'Sullivan and Norman O. Smith: The Solubility and Partial Molar Volume of Nitrogen and Methane in Water and in Aqueous Sodium Chloride from 50 to 125° and 100 to 600 Atm.

Page 1464. The first row of data in Table III should commence $10^{-5}k^*$, atm (not 10^5k^*, atm).—NORMAN O. SMITH.

Joseph J. Jasper, Marta Nakonecznyj, C. Stephen Swingly, and H. K. Livingston: Interfacial Tensions against Water of Some C_{10}–C_{15} Hydrocarbons with Aromatic or Cycloaliphatic Rings.

Page 1537. In the third line of the third paragraph of column 2, change 32.5 dyn/cm to 33.1 dyn/cm. In the second last line of footnote 10, change 0–0.5 to 0.1–0.6.—H. K. LIVINGSTON.

Richard P. Wendt and Mohammed Shamim: Isothermal Diffusion in the System Water–Magnesium Chloride–Sodium Chloride As Studied with the Rotating Diaphragm Cell.

Page 2778. Footnote *c* should be added to Table II to read, "More significant figures than are justified by the accuracy of the data are included in some entries in this table. See text for estimates of error in each entry."

Page 2779. In text, column 1, line 2, $\Delta C_{10} + \Delta C_{20}$ should read $\Delta C_1° + \Delta C_2°$.

Page 2781. Add footnote *b* to Tables VII, VIII, and IX, which should read exactly the same as footnote c added in this list of Errata to Table II. In Table VIII, in the first line of data headings, $\bar{C}_2$ should read $\bar{C}_1$; in column III, line 4, 0.67283 should read 0.067283.—RICHARD P. WENDT.

Kasimir Fajans: Polarizability of Alkali and Halide Ions, Especially Fluoride Ion.

Page 3408. The number in the third line below Table I should be 7.4, not 74.

Page 3409. The term in the fourth line of footnote 11a should read $(Q'_z)^8$ instead of $(Q'_z)^{.8}$.—KASIMIR FAJANS.

AUTHOR INDEX *to Volume 74, 1970*

SUBJECT INDEX *to Volume 74, 1970*[1]

LIST OF SUBJECT CLASSIFICATIONS

CHEMICAL THERMODYNAMICS

(1) Index prepared by Marian Henry and Margaret Knecht.

CHROMATOGRAPHY AND OTHER SEPARATION METHODS

COLLOIDS, DOUBLE LAYERS

CRYSTAL STRUCTURE, MOLECULAR STRUCTURE

ELECTRODE PROCESSES, POLAROGRAPHY

ELECTRONIC SPECTRA (ULTRAVIOLET AND VISIBLE)

FUSED SALTS

GAS PHASE KINETICS AND BEAMS

ION EXCHANGE

IONS IN AQUEOUS AND NONAQUEOUS SOLVENTS (TRANSPORT PHENOMENA)

IONS IN NONAQUEOUS AND MIXED SOLVENTS (THERMODYNAMICS)

IONS IN WATER (THERMODYNAMICS)

IRREVERSIBLE THERMODYNAMICS AND STATISTICAL MECHANICS

ISOTOPE EFFECTS

KINETIC THEORY OF GASES; COLLISIONS AND SCATTERING THEORY, ELECTRON IMPACT

MASS SPECTROSCOPY

MEMBRANES AND POROUS MEDIA (TRANSPORT)

NUCLEAR MAGNETIC RESONANCE

NUCLEAR QUADRUPOLE RESONANCE

OPTICAL ACTIVITY AND ROTATORY DISPERSION, CIRCULAR DICHROISM

PHOTOCHEMICAL KINETICS AND RADIOLYSIS

POLYELECTROLYTES

POLYMERS (OTHER THAN POLYELECTROLYTES)

QUANTUM MECHANICS

RELAXATION PHENOMENA (ULTRASONICS, DIELECTRIC RELAXATION, T-JUMP, VISCOELASTICITY)

SHOCK WAVES, EXPLOSIONS AND FLAMES

SOLID STATE DEFECT AND MATRIX ISOLATION SPECTROSCOPY

SOLID STATE REACTIONS (BULK)

SOLUTION KINETICS: IONIC REACTIONS

SOLUTION KINETICS: NONIONIC REACTIONS

SPECTROSCOPIC RELAXATION PHENOMENA (LINE BROADENING, INCOHERENT SCATTERING, FLASH PHOTOLYSIS, SPIN RELAXATION)

STATISTICAL MECHANICS

SURFACE ADSORPTION AND CATALYSIS; SURFACE CHEMISTRY

SURFACE SPECTROSCOPY; ATTENUATED TOTAL REFLECTANCE

THEORY AND CALCULATIONS (OTHER THAN QUANTUM MECHANICS)

THEORY OF LIQUIDS AND PHASE TRANSITIONS

THERMODYNAMICS OF LIQUID NONELECTROLYTE SYSTEMS

THERMODYNAMICS OF NONELECTROLYTES IN ELECTROLYTE SOLUTION AND TRANSPORT

THERMODYNAMICS AND TRANSPORT PHENOMENA AT HIGH PRESSURES AND/OR TEMPERATURES

THERMODYNAMICS AND TRANSPORT PHENOMENA IN SOLIDS, GLASSES, AND GELS

TRANSPORT IN LIQUID NONELECTROLYTE SYSTEMS

VIBRATIONAL AND ROTATIONAL SPECTRA (INFRARED, RAMAN, AND MICROWAVE)

WATER STRUCTURE AND HYDROGEN BONDS

X-RAYS AND ELECTRON DIFFRACTION

COMPOUND INDEX *to Volume 74, 1970*[1]

(1) Index prepared by Maxine Heinitz and Janja Husar.